Department of Civil Engineering

Concrete Materials and Structural Integrity Research Unit (CoMSIRU)

A dissertation submitted to the University of Cape Town

Performance of geopolymer concrete subjected to mineral acid corrosion and related to microbially-induced corrosion (MIC) of concrete in sewers.

Submitted by

Mandla Nhlanhla Dlamini

Supervised by:

Professor Mark Alexander

as partial fulfilment of:

Master of Science in Engineering

Declaration

I declare that this thesis is essentially my own work. I know the meaning of plagiarism and declare that all the work in presented, save for that which is properly acknowledged, is my own.

• I know that plagiarism is wrong. Plagiarism is to use another's work and to pretend that it is one's own.
• Each significant contribution to and quotation in this document from the work or works of other people has been attributed and has been cited and referenced.
• I have not allowed and will not allow anyone to copy this work with the intention of passing it as their own.
• This MSc dissertation has been submitted to the Turnitin module (or equivalent similarity and originality checking software) and I confirm that my supervisor has seen my report and any concerns revealed by such have been resolved with my supervisor.

Date 7 October 2020

Signature Signed by candidate

For my parents, Jabu and Tilly.

"For the growing good of the world is partly dependent on unhistoric acts; and that things are not so ill with you and me as they might have been, is half owing to the number who lived faithfully a hidden life, and rest in unvisited tombs."- George Elliot.

Abstract

Providing durable concrete sewer infrastructure requires knowledge related to the behaviour of concrete under the harsh conditions found in sewers. This is particularly important for buried sewer infrastructure such as concrete outfall sewer pipes, because they are typically difficult to inspect, repair and maintain. An important attribute of sewer infrastructure networks is the type of material used in sewer construction. In functional terms, design engineers evaluate materials according to their strength and durability. This study is primarily concerned with durability.

The most significant durability problem experienced in sewers is the microbially-induced corrosion (MIC) of concrete. MIC ultimately results in the production of sulfuric acid on the surface of the pipe leading to corrosion of the pipe. While this type of corrosion is intrinsically linked to the existence of a group of acid producing bacteria known as sulfur-oxidizing bacteria (SOB) hosted at the exposed surface of a sewer pipe, it is also exacerbated by physical phenomena such as erosion by flowing effluent. Thus, MIC can be characterised as a complex interplay of microbiological factors, physical effects, and the chemical reactions of sulfuric acid and concrete constituents.

Because sewer construction and rehabilitation projects are resource-intensive, rigorous methods for the comparison of competing materials are necessary. However, some aspects of concrete durability under MIC have not been developed extensively. Thus, gaps in understanding exist in aspects such as characterisation of the various MIC related exposure conditions found in sewers, the development accelerated performance-based testing, and calibrated service life models for concrete structures undergoing MIC.

While previous research findings have suggested that mineral acid performance tests do not adequately simulate the corrosive conditions in real sewers, it is argued that mineral acid performance can provide insight into the MIC durability performance of concrete if the limitations of test methods are understood. To understand these limitations, it is suggested that the MIC resistance of a material be broken down into unique resistance types (or components), wherein each resistance type is relatable to specific performance test(s). To this end, this study identified two MIC resistance components for evaluation, namely, kinetic resistance to dissolution and resistance by physical barriers emanating from corrosion products. These two MIC resistance components were then related to two performance acid tests, the dynamic acid test and the static acid test.

Findings from the mineral acid tests were used to compare the two identified MIC resistance components of geopolymers and comparing their resistance to that of Portland cement (PC) and calcium aluminate cement (CAC) concretes. Thus, concretes produced from Portland cement-dolomite aggregate, and calcium-aluminate cement-dolomite aggregate were used as controls in the experimental program.

The experimental program was comprised of two major parts, namely, material characterisation and performance testing. Because hardened concrete is constituted by hardened cement paste and aggregate components, these parts were characterised separately in order to understand the contribution of each component to acid-based deterioration. Material characterisation tests included x-ray fluorescence analysis, x-ray diffraction analysis and pH measurements of the milled hardened cement pastes and aggregates.

Performance testing was comprised of the "static acid test" and the "dynamic acid test", where the static test involved immersion of concrete specimens in an acidic solution and the dynamic acid test included both acid corrosion and the abrasion of rotating concrete specimens by brushing.

Hydrochloric acid (HCl) was used in both static tests and dynamic tests. Sulfuric acid (H_2SO_4) was used to test concretes with low calcium content in both the binder and aggregate components. This limitation was due in part to previous research which found that gypsum precipitation stifled the corrosion reaction in the dynamic sulfuric acid test when Portland and calcium aluminate cement paired with dolomite aggregate concretes were tested in sulfuric acid.

It was posited that the dominant exposure conditions at the crown and the effluent line of a sewer pipe undergoing MIC are "static biogenic corrosion" and "biogenic erosion-corrosion", respectively. Differentiating between these two forms exposure condition is important because previous research conducted in real sewers found that degradation at the effluent line is often much worse than degradation at the crown of the sewer pipe. Furthermore, results from this study show that high resistance under the static acid corrosion exposure condition cannot be extended to mean high resistance under the erosion-corrosion exposure condition for some concrete mixes. In this study, the static HCl test and the dynamic HCl test were used to measure the resistance of concrete mixes under the static corrosion exposure condition and erosion-corrosion exposure condition respectively.

However, concretes that exhibited high resistance to the erosion-corrosion exposure condition were consistent in exhibiting high resistance to the static corrosion exposure condition. This finding is consistent with the sequence of corrosion processes in MIC, wherein dissolution of the concrete components occurs before the precipitation of corrosion products. Therefore, it expected that high resistance in the dynamic acid test (i.e. resistance to dissolution) implies high resistance in the static test, which measures the combined resistance of dissolution and resistance emanating from corrosion products.

Both static and dynamic acid corrosion tests revealed that the geopolymer concretes tested in this study outperformed PC and CAC concretes. Results from the static HCl test showed that GP-ferro-quartz concrete, the most durable concrete specimen, provided a 69-fold improvement in resistance when compared to PC-dolomite mixes (control #1) and a 4.72-fold improvement in resistance when compared to CAC-dolomite mixes (control #2).

Results from the dynamic HCl test show that the GP-ferro-quartz mix provided a 180-fold increase in resistance when compared to the PC-dolomite mix and a 275-fold increase when compared to CAC-dolomite mix. The CAC-dolomite mix was found to have the lowest resistance to the erosive-corrosive exposure conditions of the dynamic HCl test. Thus, in terms of the concrete MIC resistance properties identified in this study, it is suggested that the CAC-dolomite mix had poor kinetic resistance to dissolution. However, under the static acid test (static corrosion exposure condition), the CAC-dolomite mix performed better than the PC-dolomite mix and GP-dolomite mix. CAC-dolomite concrete performed inferiorly only to the set of GP-siliceous-aggregate mixes in the static HCl test.

The difference in the performance of CAC-dolomite concrete performance between the static and dynamic test is largely attributed to the formation of alumina gel, an acid corrosion product of CAC hardened paste, which envelopes the concrete specimen and reduces the rate of surface corrosion in the static HCl test. However, under

the dynamic HCl test, the gel layer is brushed off the surface of the concrete specimen rendering it ineffective in protecting the concrete specimen from corrosion.

Previous research on the acid attack of concrete posits that the chemical make-up of concrete materials has a strong bearing on corrosion behaviour. To this end, various measures have been suggested such as the ratio of calcium to silicon (Ca/Si) in concrete. The approach utilised in this study was to calculate the "basicity value" which provides the ratio of major basic to acidic oxides found in the concrete.

XRF analysis of the hardened cement pastes and the 5 aggregate types used in the experiments enabled the calculation of basicity values. The combined basicity value for concrete specimens was determined by proportionally summing (according to mass) the basicity values of the aggregate and hardened cement paste parts.

A strongly correlated linear relationship between the basicity value of concrete and the corrosion rate from the dynamic HCl test was established. This empirical relationship warrants further investigation and verification, as it would, in principle provide a means to estimate the dissolution rate of concrete by calculating its basicity instead of undertaking laboratory acid tests.

Basicity was also found to be useful in determining the corrosion compatibility of binder type and aggregate types. It was found that the difference between the basicity value of hardened cement paste and the basicity value of the aggregate was useful in determining the type and extent of preferential corrosion of a concrete specimen tested under the dynamic HCl test. For ease of reading, this difference was called the "basicity differential". By visually assessing corroded concrete specimens from the dynamic HCl test, it is was possible to determine whether the hardened cement paste or aggregate component was preferentially corroded, and to gauge the extent of preferential corrosion visually.

GP-ferro-quartz and GP-granite concretes had the lowest levels of preferential corrosion which corresponded to their low basicity differential values. In contrast, CAC-dolomite concrete had the highest basicity discrepancy which corresponded visually to a high preferential corrosion of the hardened cement paste.

Mineralogical analysis via XRD, found that the hardened cement pastes of the three binder types consisted mainly of amorphous phases (>70%). The crystalline phase of the geopolymer hardened cement paste was mostly constituted by insoluble minerals such as mullite. This partially explains the higher corrosion resistance of geopolymer concretes. However, a more comprehensive explanation needs to include analysis of the amorphous phases, which fell outside the scope of this study.

SEM analysis of HCl corroded geopolymer hardened cement paste found that fly ash spheres embedded within the geopolymer matrix were preferentially corroded. This indicates that fly ash content negatively affected the rate of corrosion of the geopolymer hardened cement paste. Furthermore, SEM analysis showed that the geopolymer matrix surrounding the fly ash spheres was relatively intact.

Keywords:

Geopolymers, microbially-induced corrosion, mineral acid tests, fly ash, acid resistance.

Terminology

The student has opted for the American spelling of the word sulfur and its derivatives. Scientific literature refers to microbially-induced corrosion (MIC) and biogenic acid corrosion. These terms are used interchangeably and should be understood to have the same technical definition. Where the origin of acids is concerned the term biogenic is used in opposition to the word mineral, to indicate that the acid is a product of the microbial processes.

The terms geopolymer and alkali activated material are used interchangeably by some researchers in the literature. Strictly speaking, they each refer distinct binder systems. The author has attempted to ensure that these terms are not used interchangeably nor inappropriately.

The type of geopolymer cement used in the experimental study is a fly ash based geopolymer. Due to the wordiness of this identifier, the word geopolymer is used instead of fly ash based geopolymer in Chapter 1, 3, 4 and 5 of this study. The literature review chapter requires the use of the full term (fly ash based geopolymers) in order not to avoid confusion with geopolymer cements and concretes of a different composition found in the literature.

Definitions

Bacterio-static effect: A mechanism affecting the growth bacteria by interfering with bacterial protein production, DNA replication, or other aspects of bacterial cellular metabolism.

Biofilm: A biologically active layer on a surface or interface, consisting of a complex association of micro-organisms, microbial products, water and suspended solids.

Biogenic: Produced or formed by microorganisms.

Erosion-corrosion: An exposure condition where the chemical corrosion occurs simultaneously with on-going or cyclical erosion of particulates from the surface of concrete pipe.

Kinetic resistance: The tendency of a material (or state) which is not thermodynamically stable to change slowly.

Neutralization capacity: The quantity of acid hydrogen atoms necessary to neutralise a given quantity of material.

Static-corrosion: An exposure condition where chemical corrosion occurs without any physical weathering processes influencing the reactants or the products.

Sulfate reducing bacteria: Bacterial species that can perform anaerobic respiration using sulfur bearing compounds such as sulfate as a terminal electron acceptor.

Sulfide oxidizing bacteria: Bacterial species with the ability to oxidize of hydrogen sulfide, elemental sulfur, and thiosulfates to produce sulfuric acid.

Thermodynamic stability: Thermodynamic stability occurs when a system is in its lowest energy state, or in chemical equilibrium with its environment. This may be a dynamic equilibrium, where individual atoms or molecules change form, but their overall number in a particular form is conserved. This type of chemical thermodynamic equilibrium will persist indefinitely unless the system is changed.

Abbreviations

AAM	Alkali Activated Materials
ASTM	American Society for Testing and Materials
BOM	Biodegradable Organic Matter
CAC	Calcium Aluminate Cements
COD	Chemical Oxygen Demand
BOD	Biological Oxygen Demand
EPA	Environmental Protection Agency
MIC	Microbially-Induced Corrosion
PC	Portland Cement
PSD	Particle Size Distribution
SABS	South African Bureau of Standards
SANS	South African National Standard
SEM	Scanning Electron Microscopy
SOB	Sulfur-oxidizing Bacteria
SRB	Sulfate-reducing Bacteria
TEM	Transmission Electron Microscopy
VES	Virginia Experimental Sewer
XRD	X-ray Diffraction
XRF	X-ray Fluorescence Spectrometry
HCP	Hardened Cement Paste
UCS	Unconfined Compressive Strength
HDPE	High Density Polyethylene
PVC	Polyvinyl Chloride
BSI	British standards institute

Table of contents

List of figures

List of tables

1 Introduction

Sewer infrastructure is a critical component of the modern built environment. Much of this infrastructure is buried below ground, keeping it out sight from the public it serves.

This study focuses on sewer infrastructure constructed from concrete materials which are affected by a severe type of degradation known as biogenic acid corrosion or microbially-induced corrosion (MIC). Research has shown that this type of degradation is a major cause of premature sewer failures worldwide and is particularly severe in regions with warm climates (Greng 2018; Herrison and Saucier, 2015).

Microbially-induced corrosion (MIC) occurs when biogenic sulfuric acid reacts with concrete from sewer-system components such as pipes and manholes. Biogenic sulfuric acid exists as the result of a sequence processes driven chiefly, by two groups of bacteria known as sulfur reducing bacteria (SRB) and sulfur oxidizing bacteria (SOB).

Sulfur reduction by SRB is comprises of the conversion of solute sulfate into sulfide, and thereafter the liberation of hydrogen sulfide gas (H_2S). H_2S is a toxic gas that is deadly to humans if inhaled at high concentrations. This fact on its own makes biogenic H_2S generation a serious problem. However, with respect to MIC, H_2S is an intermediate biogenic product and as such, the details of H_2S generation does not form a significant part of this study.

The second biogenic process involves the conversion of H_2S into H_2SO_4 by SOB. H_2SO_4 is a strong acid, which completely dissociates in solution. Measurements in sewers affected by MIC have found high concentrations of acid, with pH values as low as 1 (Grengg 2018; Druga et al 2018).

The corrosive effect of strong acids on geopolymer concretes (GP), calcium aluminate cement (CAC) concrete and Portland Cement (PC) concretes is, therefore, the subject of this study.

1.1 Economic impact of MIC on concrete sewer infrastructure

Currently, the most widely used binder in concrete sewer infrastructure is Portland cement. Research into MIC of concrete in sewer environments has shown that Portland cement (PC) concretes often perform much worse than other competing sewer pipe materials in terms of biogenic acid resistance. The main alternative concrete binder in current use is calcium aluminate cement (CAC).

The cost of CAC often prohibits full replacement of PC, and therefore it is typically used as a lining on the inside of PC concrete pipes (Motsieloa 2012). Acid-resistant linings derived from organic polymers such as high-density polyethene (HDPE) are also an option used in lining the inside of concrete pipes, however, this too comes at a high cost.

Worldwide, the scale of the problem of MIC is immense. A study of German sewers revealed that 40% of concrete failures in German sewer systems can be attributed to MIC (Kaempfer and Berdnt 1999). The repair and rehabilitation costs for sewers undergoing MIC have been reported by researchers in different regions. A few notable repair and rehabilitation cost estimates are provided below:

- 456 million Euro required for the repair and rehabilitation of German sewers (Kaempfer and Berdnt 1999)
- 84.8 million Pounds required for the repair and rehabilitation of sewers in the United Kingdom (Gutierrez et al. 2010)
- 3.3 billion dollars required for the repair and rehabilitation of sewers in the United States of America for the year 2009 (Herrison and Saucier 2013)

Given the high costs involved in the construction and rehabilitation of sewers, sewer planners and designers need to pay careful attention to the various factors involved in sewerage system deterioration and the design options available to maximise its service life.

1.2 Complexity of sewer concrete deterioration due to MIC

The corrosion of sewers is a challenging area to study because it is influenced by numerous complex natural and man-made systems. A brief introduction to a few important systems that contribute to MIC are described in headings 1.2.1to 1.2.4 below.

1.2.1 The sulfur cycle

Sulfur is the 10th most abundant element on earth, and its compounds exist naturally in soils, water streams, flora, fauna, the atmosphere, and the oceans.

Where sewers are concerned, sulfate (SO_4^{2-}) is a sulfur compound that plays a key role in the process of biogenic sewer corrosion because sulfate is a necessary input for sulfur reduction by sulfur-reducing bacteria (SRB) in the production of sulfide (HS^-). This is in essence, the first of two important microbially-induced processes that lead to biogenic acid corrosion of sewer concrete. Therefore, the origins of sulfate (SO_4^{2-}) in the sewer are of interest to this study.

Sulfate originates from both man-made and natural sources. In nature, the main sources of sulfates are terrestrial and include sulfate bearing rock, soils, minerals and volcanic material (EPA, 2000).

Anthropogenic sources of sulfate originate from activities such as mining, mineral processing, agriculture, pulp processing, combustion of fossil fuels and refuse (Moreno et al. 2009). The sulfate content in effluent is also affected by potable water treatment, where the addition aluminium sulfate based coagulates have been found to increase the sulfate concentration in potable water significantly (Pikaar et al. 2014)

1.2.2 Hydraulic design of sewers

The hydraulic design of sewers influences biogenic acid corrosion because the type of hydraulic flow in the sewer has a bearing on two important waste-water states. Namely, anaerobic states and states where the release of hydrogen sulfide gas from solution occurs. Anaerobic conditions occur when the flow regime allows for the depletion of dissolved oxygen by micro-organisms in the effluent and is associated with supercritical effluent flows, while Release of hydrogen sulfide occurs under turbulent flows. Effluent flow may be controlled by careful design of hydraulic parameters such as the slope of the pipe, the internal diameter and the pipe material roughness (Chadwick et al. 2004). For instance, where the effluent has a high concentration of hydrogen sulfide in solution,

hydraulic design measures to minimise hydrogen sulfide Release include ensuring that the effluent flow is sub-critical, thereby minimising the amount of H_2S escaping from solution.

Similarly, hydraulic design measures can be taken to negate the occurrence of anaerobic conditions (which cause sulfur-reducing bacteria to metabolise sulfate) by ensuring that turbulent flows, which allow for sufficient re-aeration of the wastewater, are realised.

1.2.3 Influence of micro-bacteria in sewer corrosion

Two distinct groups of bacteria referred to as sulfur-reducing bacteria (SRB) and sulfur-oxidizing bacteria (SOB) are required for microbially-induced corrosion to occur. SRB, which exist in the submerged slimes layers of sewer pipes get their energy from reducing elemental sulfur or sulfate into hydrogen sulfide.

SOB, which exist in the exposed pipe surface, oxidize hydrogen sulfide gas produced by SRB to produce sulfuric acid. Both H_2S and sulfuric acid are considered to be harmful because H_2S gas can have serious or fatal effects if inhaled by humans at high concentrations, and sulfuric acid is a very strong acid that causes significant damage to concrete sewer infrastructure.

1.2.4 Material options for sewer pipe infrastructure

For civil engineers, a key consideration in the design of infrastructure is the type of material to use. Material-choice affects the capital and lifecycle cost of a sewer infrastructure project. Engineering designs frequently involve trade-offs between the level of safety, durability, strength, economy, and sustainability (De la Fuente et al. 2016).

Currently, concrete and plastics are the main material options for the construction of sewer networks. Structurally, the key difference between the two material groups is that concrete pipes are classified as rigid, and plastic pipes are classified as flexible. This difference relates to how loads from above the conduit are resisted. Flexible pipes rely on the bedding material for structural strength while rigid pipes are themselves loadbearing.

This makes flexible piping more vulnerable to damage by loading. As flexible pipe is buried and subjected to service loads, the vertical diameter of these pipe decreases, and the horizontal diameter increases. This increase in horizontal diameter is resisted by the soil at the sides of the pipe. Therefore, the bedding-materials must be of suitable strength to ensure that flexible pipes do not deflect excessively (USDI 1996). In general, flexible piping is of low mass and therefore requires less machinery and labour for transport, handling, and installation. Flexible pipes are typically manufactured from inert polymers such as HDPE or PVC, which makes them resistant to highly acid attack. This is a significant material advantage where sewer applications are concerned.

Concrete pipes are rigid and thus act as load-bearing structures which do not require structural assistance from the bedding material to resist loads. In addition, if a concrete pipe cracks while in service, the effect on its durability is not as serious as it would be with plastic pipes, because the steel reinforcement, if properly designed, limits crack openings to within an acceptable range. The weight of concrete pipe is notably higher in comparison to plastic systems, requiring more powerful means of transport and on- site handling (de la Fuente et al. 2016).

Given the challenges of the 21st century, which include the need for sustainable infrastructure and the mitigation of climate change, material selection methods for infrastructure need to include well-established engineering

parameters as well as parameters related to sustainability, such as embodied energy and the material's CO_2 emission. The embodied energy of a material is the sum of all the energy required to produce it, considered as if that energy was incorporated or 'embodied' in the product itself.

Generalised values for embodied energy and CO_2 emission should not be used for decision making when selecting materials in design, as these values can change significantly depending on local circumstances. However, it is useful to gauge the approximate range of embodied energies and carbon footprint values of competing materials used in sewer construction. Table 1-1 provides the embodied energies and carbon footprints of materials used in sewer concrete infrastructure such as reinforced concrete. The data shows us that organic polymer materials such as PVC and HDPE have high embodied energies and release greater amounts of carbon dioxide per kilogram of material produced.

Table 1-1: Embodied energy of selected materials (Tafesse and Abegas, 2019; Manjunatha et al. 2014; Dias and Pooliyadda, 2004, Scrivener 2014, Provis and van de Venter 2012, and, Hammond and Jones 2008)

Material	Embodied energy (MJ/kg)	Carbon footprint (kg of CO_2 /kg)
Portland Cement general	3.32-4.6	0.73-0.98
Geopolymer Cement (50 % waste input)	2.0-2.6	0.18-0.25*
Concrete (1:2: 4 mix)	0.95	0.035
Reinforced concrete (Portland)	2.8	0.2
High-density polyethylene (HDPE)	103	1.6
Polyvinyl Chloride (PVC)	70	1.9

**The carbon footprint of geopolymers is dependent on which industrial process the carbon dioxide is attributed. If the geopolymer cement incorporates a large proportion of material classified as waste (such as fly ash), then the carbon footprint emanating from the production of fly ash is not included in the carbon footprint of the geopolymer cement. Instead, the carbon footprint of the waste material is attributed to the primary reason for its production. In South Africa fly ash's carbon footprint is attributed to the generation of electricity in coal fired power stations.

With the increase in sewer construction material options now available, there is a need for methods by which these material options can be compared against each other on a rational basis. To this end, multi-criteria analysis such as the MIVES method have been developed. MIVES is a systems-engineering approach intended to objectively select the best solution for a complex problem (de la Fuente et al. 2016). This approach requires a clear description of the subject systems, its sub-systems, and boundaries. Secondly, it involves a system requirements tree, where the system requirements are listed, and weights of significance are apportioned to each requirement. Examples of system requirements include functionality, sustainability, economy and social effect. Table 1-2 provides an example of the requirements, criteria, indicators, and their respective weights for a MIVES analysis.

Table 1-2: Sewer system requirements described for use in MIVES analysis (de la Fuente et al. 2016)

Requirements	Criteria	Indicators
R1. Functional (11.1%)	C1. Pipe dysfunction (33.3%)	I1. Surface degradation (100%)
	C2. Joints dysfunction (33.3%)	I2. Problems in joints (100%)
	C3. Mechanical capacity (33.3%)	I3. Extra capacity (100%)
R2. Economic (33.3%)	C4. Cost (80%)	I4. Total cost (100%)
	C5. Execution time (20%)	I5. Time (100%)
R3. Environmental (33.3%)	C6. Emissions (20%)	I6. CO_2 emissions (100%)
	C7. Resources (60%)	I7. Prime materials (33.3%) I8. Water (33.3%) I9. Energy (33.3%)
	C8. Adaptations (20%)	I10. Sensitivity (100%)
R4. Social (22.2%)	C9. Labour safety (25%)	I11. Risk of accidents (100%)
	C10. Affectations (75%)	I12. Time (33.3%) I13. Pollution (33.3%) I14. Vulnerability (33.3%)

As can be observed from Table 1-2, a wide-ranging set of criteria are required to do a MIVES analysis, and durability data from research work such as the current study, may assist in quantifying only a single indicator out of the 14 required in Table 1-2 (surface degradation). However, this rigour is justified given the impact and importance of sewer infrastructure.

1.3 Geopolymer concrete: potential for sewer applications

Geopolymers are an emerging class of alumino-silicate based inorganic polymer binders (Davidovits, 2013). Geopolymer synthesis, which is the series of chemical reactions involved in the transformation of alumino-silicate precursor materials into inorganic polymers, was identified by Davidovits in 1973 when he produced a geopolymer material from metakaolin and sodium hydroxide (Davidovits, 2013). Geopolymers are in chemical structure and composition, distinct from Portland cements.

Researchers such as Grengg (2017), Bakharev (2005) and Druga (2018) suggest that geopolymers are promising construction materials that are suitable for corrosive environments due to properties such as low permeability, fine pore structure, and chemical stability in acidic solutions. The chemical stability of geopolymers under acidic conditions is primarily attributed to a lack of calcium bearing compounds which is the main cause of susceptibility to acid corrosion in Portland cement-based and calcium aluminate cement concretes (Grengg 2017).

Geopolymers may be produced using numerous raw materials and formulations (Davidovits 2013, Provis and van Deventer, 2017). Given the wide range of input material choices, and divergent scientific understanding of the

chemistry behind these materials, there has been some disagreement concerning the correct nomenclature and underlying chemistry of these materials (Provis and Van Deventer, 2017; Davidovits, 2013).

There has been a significant number of geopolymer, and alkali-activated cementitious materials developed in various parts of the world. Historically, prominent works include publications on the development of slag-based alkali-activated materials by Purdon and Glukhovsky in the years 1940 and 1965 respectively (Provis and van Deventer 2013). Davidovits (1973) described, what he termed a "geopolymer", as an inorganic polymer, constituted primarily of silicon, aluminium, and oxygen polymer chains. These initial works have served as the foundation for a multitude of formulations found in academic, commercial, and patent literature.

Unlike the Portland cement industry, little standardisation has been achieved with respect to geopolymer binders and alkali activated materials (Provis and Van Deventer, 2017). Geopolymer formulations have been developed to replace Portland cement concrete in many applications with varying success. Promising results have been reported in recent studies, suggesting geopolymer concretes possess acid resistance that is superior to Portland cement (Grengg, 2018; Bakharev, 2005).

Geopolymers utilise alumino-silicate rich pre-cursor materials as inputs (Davidovits, 2013). These precursor materials vary in alumino-silicate content and quality, with "purer" precursor materials such as metakaolin being used to produce cementitious materials with beneficial properties such as high-temperature stability (Davidovits, 2013).

Fly ash or pulverised fuel ash, is an alumino-silicate rich by-product of industrial processes such as coal-fired power generation. It is a particularly important material in South Africa because of its abundance, where electric power is primarily obtained from coal-fired power stations. Coal-fired power generation produces approximately 36 million tonnes of fly ash per annum, making it one of South Africa's most voluminous waste materials (Kruger, 1997). Currently, only 5-6% of this fly ash is reused by industry, mainly as an extender in Portland cement production (Reynolds-Clausen and Singh 2016).

Given the abundance of fly ash in South Africa, the impetus towards sustainable low carbon cements, and the need for acid-resistant concrete materials in sewers, a study on the performance of fly ash based geopolymers in acidic environments is warranted.

1.4 Testing concrete materials for resistance to microbially-induced corrosion

To the uninitiated, assessing the resistance of concrete to microbially-induced corrosion may only warrant a direct acid test, involving, for example, the immersion of concrete specimens in solution of sulfuric acid. However, early attempts at this method found large differences in concrete corrosion resistance between pure mineral H_2SO_4 testing and conditions where H_2SO_4 is produced microbially. It was therefore suggested that bacteria-concrete interaction may be the dominant factor influencing corrosion in the sewer environment (Monteny et al. 2000).

In brief, differences in Portland cement concrete resistance observed under mineral acid tests and microbially-induced corrosion are attributed to the interaction of bacteria, concrete and concrete corrosion products.

In a mineral acid test, when Portland cement concrete is attacked by H_2SO_4 to form gypsum, the gypsum forms a layer around the surface of the concrete specimen which acts as a barrier to further attack. Therefore, for corrosion to proceed, this layer must be penetrated by hydrogen ions. In the case of microbially produced H_2SO_4, researchers suggest that the corrosion interface (corroded layer) creates excellent conditions for the growth of sulfur-oxidizing bacteria. Due to the porosity of this layer, bacterial colonies are able to inhabit the corrosion layer and consequently generate H_2SO_4 very close to fresh concrete surfaces (Monteny et al. 2000; Grenng 2018)

However, this view is not unchallenged. Huber et al. (2016) compared corrosion caused by biogenic sulfuric acid and mineral sulfuric acid on Portland cement hydrated pastes and found that there was very little difference between the observed rates of corrosion between the two conditions.

There is currently little consensus on a test method to determine the resistance of concrete materials to microbially-induced corrosion (de Belie et al 2002). Numerous test methods of varying complexity have been developed by various researchers. The simplest methods measure the mass loss of materials exposed to acidic solutions. Tests such as the dynamic HCl Test add abrasion to acidic corrosion in a bid to mimic the erosive action of water at the effluent line (Fourie, 2007). The testing apparatus (TAP) for accelerated concrete deterioration exposes concrete specimens to brushing/abrasion and cyclic wetting in acidic medium and drying (De Belie et al. 2002).

Experience from tests such as the dynamic HCl test, has been that these tests may produce definite trends and results within 48 hours for Portland and calcium aluminate cement concretes. This makes this test suitable for obtaining rapid corrosion results (Alexander and Fourie, 2011). However, the dynamic HCl's usefulness for the problem of MIC has been questioned since some results by this method have been contradictory to results obtained in biogenic corrosion simulation tests and live sewer measurements.

More sophisticated MIC test methods aim to replicate selected biogenic processes. For instance, the Hamburg chamber produces H_2SO_4 by artificially creating an ideal environment for acid-producing bacteria (SOB) to thrive and produce biogenic H_2SO_4 on the surface of test specimens. Data from the Hamburg chamber has been shown to correspond well with measurements from real sewers in Germany and South Africa (Saucier and Kaitano 2018).

1.5 Research problem

The research problem is centred on two main concerns.

The first concern is related to durability design and is focused on whether simple mineral acid tests (static acid test and the dynamic acid test) can be used to extract useful data for applications where concrete is required to resist microbially-induced corrosion. A significant part of the mineral acid testing problem relates to varying the exposure conditions within the controlled mineral acid test by changing the acid type (hydrochloric and sulfuric acid) and introducing physical weathering (such as of brushing the concrete surface) to the corrosive conditions in the mineral acid test.

The second problem relates how fly ash based geopolymer concretes perform in comparison to traditional concretes used for sewer pipe production (Portland cement and calcium aluminate cement) under mineral acid testing. An important part of this problem involves varying the type of aggregate paired with the geopolymer binder to determine the most compatible aggregate type. Furthermore, there is a need to characterise the binder

and aggregate components of the subject concretes to understand how these characteristics affect corrosion behaviour.

1.6 Study objectives, approach, and scope

1.6.1 Objectives

The objectives of this study are:

1. To measure the performance of fly ash based geopolymer concretes under mineral acid attack in comparison to Portland cement and calcium aluminate cement concretes. Mineral acid testing refers to two acid test conditions, static conditions, where the acid attack is the only detrimental action on the concrete specimen, and dynamic conditions, where the concrete specimens are subjected to acid attack and brushing simultaneously. Hydrochloric acid and sulfuric acid are the two acid types used in the study.

2. To investigate the acid resistance compatibility of different aggregates types (of varying chemical and mineralogical composition) when paired with fly ash-based geopolymer cements, where compatibility is determined by measuring the performance of concrete specimens under static and dynamic mineral acid testing.

3. To characterise the chemical, mineralogical and morphological properties of the subject binders and aggregates and to determine what effect these properties have on the corrosion performance of geopolymer, Portland cement, and calcium aluminate cement concretes subjected to static and dynamic mineral acid tests.

4. To relate the corrosion performance of geopolymer cement, calcium aluminate cement and Portland cement concretes subjected to mineral acid testing to corrosion results obtained from live sewer experiments.

1.6.2 Approach to the problem of MIC and testing

A review of the literature was undertaken to understand the causes, mechanisms, and effects of MIC in concrete. Furthermore, a review of the test methods developed by researchers from different parts of the world was undertaken to understand the various concrete acid corrosion testing philosophies in existence.

PC and CAC cements have a long track record as concrete sewer materials and have been studied widely. Concretes made from these cements are used as experimental controls and are consequently used to benchmark the acid resistance performance of geopolymer concretes.

The most reliable method by which corrosion is assessed is by measurements in live sewer experiments or in complex sewer simulation rigs. An implication of testing materials under complex conditions such as a biogenic corrosion chamber or in real sewer corrosion measurements, is that the measured resistance is the combined product of multiple forms of resistance. Herrison and Saucier (2015) identified at least three MIC resistance mechanisms in CAC concrete listed below. These resistance mechanisms are described in detail in chapter 2 of this study.

1. Resistance by neutralisation capacity
2. Resistance by the bacterio-static effect (A materials ability to stifle the metabolism of detrimental bacterial species like sulfur-oxidizing bacteria).

3. Resistance by the formation of protective corrosion products (alumina gel).

However, a shortcoming of this approach is that it does not provide a ranking or proportioning of these resistance mechanisms in terms of their significance to overall resistance of concrete to MIC. It is reasonable to assume that these categories of resistance do not inhibit degradation to the same degree, therefore a systematic approach to quantifying these resistance types is required.

Furthermore, these categories of resistance are the product of more fundamental material properties. For instance, chemical stability could be the result a thermodynamic unfavorability corrosion reaction, or it could be the result of a thermodynamically favourable but slow corrosion reaction (relative to the service life of the concrete structure) or both. Therefore these chemical forms of resistance are best described by the thermodynamic and kinetic properties of the corrosion reactions.

However, a fundamental scientific approach is not feasible for a durability problem such as the MIC resistance of concrete, where the materials are highly variable, highly complex and not fully understood. Furthermore, the exposure conditions are also variable, complex, and are not amenable to precise characterisation. To address this complexity problem Alexander, Bentuur and Mindess (2017) state that the objective of durability design is to "predict long-term behaviour on the basis of short-term tests, in conjunction with predictive models that inevitably are simplifications of the real situation to which concrete will be subjected".

This study proposes that a materials resistance to MIC is divided into components or parts. The MIC resistance components of interest to this study are discussed in further detail in section 3.2.2 (Chapter 3). Table 1-3 provides a list of 7 suggested resistance components, ordered according to their corrosion phase and scientific category.

Table 1-3: Suggested MIC resistance components and categories

Corrosion phase	MIC resistance component	Scientific category
Reactants (Uncorroded concrete)	1. Thermodynamic unfavorability 2. Kinetic resistance* 3. Neutralisation capacity (NC)	Chemical
	4. Bacterio-static effect	Biological
	5. Permeability and porosity	Physical
Corrosion products (Precipitates and gels)	6. Bacterio-static effect	Biological
	7. Physical barrier *	Physical

*MIC resistance components evaluated in this study

1.6.2.1 Chemical material properties for corrosion resistance (including MIC)

Given that corrosion is a chemical process; it follows that the most important aspects of a materials corrosion resistance are chemical properties. A fully chemically resistant material is one which, when exposed to a strong acid such will result in a thermodynamically unfavourable reaction (under ambient temperature and pressure). However few material suitable for construction of sewer pipelines are suitable for this purpose. Instead the property that makes most materials durable under acidic conditions is due to the slow kinetics of the corrosion reaction (kinetic resistance to corrosion).

1.6.2.2 Biological material properties for MIC resistance

Since bacteria, hosted by the pipe are responsible for the production of sulfuric acid in the sewer, it follows that pipe materials that are toxic, or contain toxic agents, or produce corrosion products that are toxic to sulfur-oxidizing bacteria will reduce MIC to some degree. Given the complex microbiome of a corroding sewer pipe, which includes numerous species of bacteria and fungi, a widely accepted measure to quantify the MIC resistance afforded to concrete by the bacterio-static effect is yet to be identified.

1.6.2.3 Physical material properties for corrosion resistance

Sulfuric acid attack (including MIC) may be described as a surface phenomenon, in which damage occurs progressively from the outside to inside of concrete. Where the corrosion reaction produces insoluble precipitates, the precipitate's ability to form physical barrier that interferes (to some degree) with advancing corrosion is a physical corrosion resistance mechanism. Furthermore, dense concretes have been shown resist acid attack better than permeable and porous concretes (Motseiloa, 2012).

1.6.2.4 MIC resisting properties identified for evaluation in this study

Two components of MIC resistance were identified for evaluation in this study

- Resistance due to the slow kinetics of the corrosion reaction (dissolution phase) and,
- Resistance emanating from physical barriers formed by corrosion products such as gels and precipitates.

Evaluation of the other 5 MIC resistance components was not undertaken in this study.

1.6.2.5 Exposure conditions

With these types of resistance identified, an ideal approach would involve isolating and measuring each biogenic corrosion resistance mechanism separately in order to understand the proportional contribution of each mechanism to the total resistance of a concrete mix to MIC.

Furthermore, it is posited that the significance of individual MIC components to design is highly dependent on the environmental conditions to which concrete will be exposed. Two specific exposure conditions have been characterised in this study, namely; static biogenic corrosion and biogenic erosion corrosion. It is further posited that these exposure conditions are relatable to specific locations across the cross a partially filled sewer pipe subjected to MIC. In this study it is suggested that the dominant exposure condition at the crown of the pipe is static biogenic corrosion whereas the dominant exposure conditions at the effluent line is biogenic-erosion corrosion.

With these exposure conditions identified, static-corrosion resistance was measured through static immersion testing (static acid test) and erosion-corrosion resistance was assessed by exposing concrete specimens to brushing and acid attack simultaneously using the dynamic acid test apparatus devised by Fourie (2007).

Static corrosion testing and erosion-corrosion testing were mainly conducted using HCl instead of H_2SO_4 and thus the acid type used in the majority of the testing is not the acid type encountered in MIC. The use of HCl is a compromise measure necessitated by problems emanating the common ion effect which stalls the corrosion reaction when calcareous materials are tested in H_2SO_4 in the dynamic acid test. This effect was identified by Fourie (2007) when testing PC and CAC concrete in the dynamic hydrochloric acid test. However, where the

calcium content in the concrete was sufficiently low, an example is GP-Siliceous aggregate concrete mix, H_2SO_4 was also used in the dynamic acid test (erosion-corrosion testing). The other five forms of MIC resistances were not measured.

1.6.3 Scope

This study is intended to assess the behaviour of fly-ash based geopolymer concrete to mineral acid corrosion and erosion-corrosion. CAC and PC are used as controls in the experimental work. Five aggregate types are used in the production of concrete test specimens. These include, dolomite, dolerite, andesite, granite and ferro-quartz. Material characterisation of concrete, aggregate and hardened cement paste specimens were undertaken through scanning electron microscopy (SEM), X-ray diffraction (XRD), X-ray fluorescence (XRF), unconfined compressive strength (UCS) and pH measurement. Static acid corrosion and corrosion erosion performance testing of concrete specimens was undertaken using the static acid test and the dynamic acid resistance test, respectively.

1.6.4 Limitations

The complexity of MIC is difficult to replicate in the laboratory and thus laboratory based testing invariably involves reducing the test conditions to a manageable level of complexity. A brief description limitations of the experimental methods and materials are presented below.

1.6.4.1 Limitations in measuring resistance of concrete to MIC

While the primary problem this research attempts to investigate is the MIC of geopolymers for sewer applications, the approach adopted in this investigation does not involve simulation of the complex biosystems found in the sewer environment. Instead, the investigation sought to understand whether mineral acid tests could provide useful data for biogenic corrosion in sewers. With respect to this aspect, a major limitation was the use of hydrochloric acid instead of sulfuric acid as the acid used in testing corrosion resistance in the mineral acid tests. A detailed justification of this choice expanded upon in chapter 3.2 of this study.

1.6.4.2 Materials limitations

The concrete mixes (described in chapter 3.5.5) were not intended to be optimised mixes suitable for application in pre-cast concrete mixes for sewer applications. Instead, these mixes were designed enable comparison of the performance of competing concrete mixes (binder/aggregate combinations).

1.6.4.3 Materials characterisation limitations

The characterisation methods used in this study include, XRD, XRF, SEM, and pH measurement. While all the test mixes in their uncorroded state were characterised using these methods, SEM was conducted on corroded and un-corroded specimens or hardened cement pastes, corroded and un-corroded aggregates were not subjected to SEM analysis.

1.6.4.4 Performance testing limitations

While the MIC testing literature refers to numerous methods to the measurement of corrosion in concrete (loss in stiffness, mechanical strength, hydrogen ion consumption etc), the measurement of corrosion in this study was limited only to mass loss.

1.7 References

Chadwick, A., Morfett, J., Borthwick, M. 2004. “Hydraulics in civil and environmental engineering”. Fourth Edition, Spon Press. Taylor and Francis Group.

De Belie, N., Monteny, J, Taerwe L. 2002. “Apparatus for accelerated degradation testing of concrete specimens”. Materials and Structures vol 35.

De la Fuente, A., Pons, O., Josa, A., Aguado, A. 2016. “Multicriteria-decision making in the sustainability assessment of sewerage pipe systems”. UPC Barcelona Tech.

Dias, W.P.S, Pooliadda, S.P. 2004. “Quality-based energy contents and carbon coefficients for building materials: A systems approach”. Energy 29 (2004) 561–580

Fourie, C.W. 2007. “Acid resistance of sewer pipe concrete”. MSc Thesis. University of Cape Town. Cape Town, South Africa.

Gay, H., Meynet, T., Combani, J. 2016. “Local study of the corrosion kinetics of hardened Portland cement under acid attack”. Cement and concrete research.
Grengg, C., Mittermary, F., Ukrainczyk, N., Koraimann, G., Kienesberger, S., Dietzel, M. 2018. “Advances in concrete materials for sewer systems affected by microbially induced concrete corrosion: A review.”

Gutiérrez-Padilla, M.G.D., Bielefeldt, A., Ovtchinnikov, S., Hernandez, M., Silverstein, J., 2010. Biogenic sulfuric acid attack on different types of commercially produced concrete sewer pipes. Cem. Concr. Res. 40, 293–301. doi:10.1016/j.cemconres.2009.10.002

Hammond, G. P., Jones, C. I. 2008. “Embodied energy and carbon in construction materials”. Proceedings of the Institution of Civil Engineers - Energy, 161(2)

Huber, B., Hilbig, H., Mago, M., Drewes, J.E., Muller, E. 2016. “Comparative analysis of biogenic and chemical sulfuric acid attack on hardened cement paste using laser ablation-ICP-MS.” Cement and Concrete Research, 87

Manjunatha L.R., Anvekar, S.R, Sagari, S.S., Archana K. 2014. “An economic and embodied energy comparison of geo-polymer, blended cement and traditional concretes”. Journal of Civil Engineering Technology and Research Volume 1, Number 1 (2014), pp. [33-40]

Provis, L., van Deventer, S.J. 2009. “Geopolymers: Structure, Processing, properties and industrial applications”. Woodhead publishing in materials.

Saucier, F. Kaitano, T. 2018. “H_2S biogenic corrosion: “Why using calcium aluminate concrete and mortars to rehabilitate corroded sewer infrastructures”. IMESA

Taffese, W. Z, Abegaz, K. A. 2019. “Embodied energy and CO_2 emissions of widely used building materials: the Ethiopian context”

United States Department of the Interior (USDI). 1996. “Pipe Bedding and Backfill. Bureau of reclamation, technical service centre, Geotechnical services, Denver, Colorado”

2 Literature Review

2.1 Introduction

The microbially-induced corrosion of concrete in the sewer environment is a complex area of study, and so is the materials science behind geopolymer cements and concretes. Therefore, to present prior work logically, this literature review is made up of five parts. These parts are structured in the review as follows:

I. The causes of MIC in sewers,
II. Corrosion performance of concrete under MIC
III. Mitigation of MIC in concrete systems
IV. Geopolymer cements, and
V. Methods of assessing the resistance of cementitious materials to microbially-induced corrosion.

2.2 Causes of microbially-induced corrosion (MIC) in sewers

Prevention of microbially-induced corrosion (MIC) requires an appreciation of the underlying biological, chemical and physical processes that lead up to sulfuric acid corrosion of concrete in the sewer environment. Researchers have shown that MIC occurs as a result of a series of sequential biogenic processes which may broadly be categorized to include the following 2 stages:

a) biogenic sulfate reduction and H_2S release
b) biogenic sulfur oxidation:

These two biological processes occur in conjunction with physical and chemical changes to the sewer effluent, slimes layers and atmosphere. A study of these two broad biogenic processes follows.

2.2.1 Sulfate reduction, sulfides in solution and release of H_2S gas

The production of biogenic H_2S is the product of a multitude of natural and man-made systems. These systems are often enmeshed and dependent on each other in numerous ways. Biosystems are particularly complex because of the sheer number of inter-related organisms that exist in the sewer. Furthermore, biosystems are made even more complex by the fact that they adapt and change based on the prevailing circumstances.

Figure 2-1, gives a broad schematic representation some salient requirements for the generation of biogenic H_2S in the sewer environment to occur. These conditions or states, shown in the diagram are discussed further in the following subchapters.

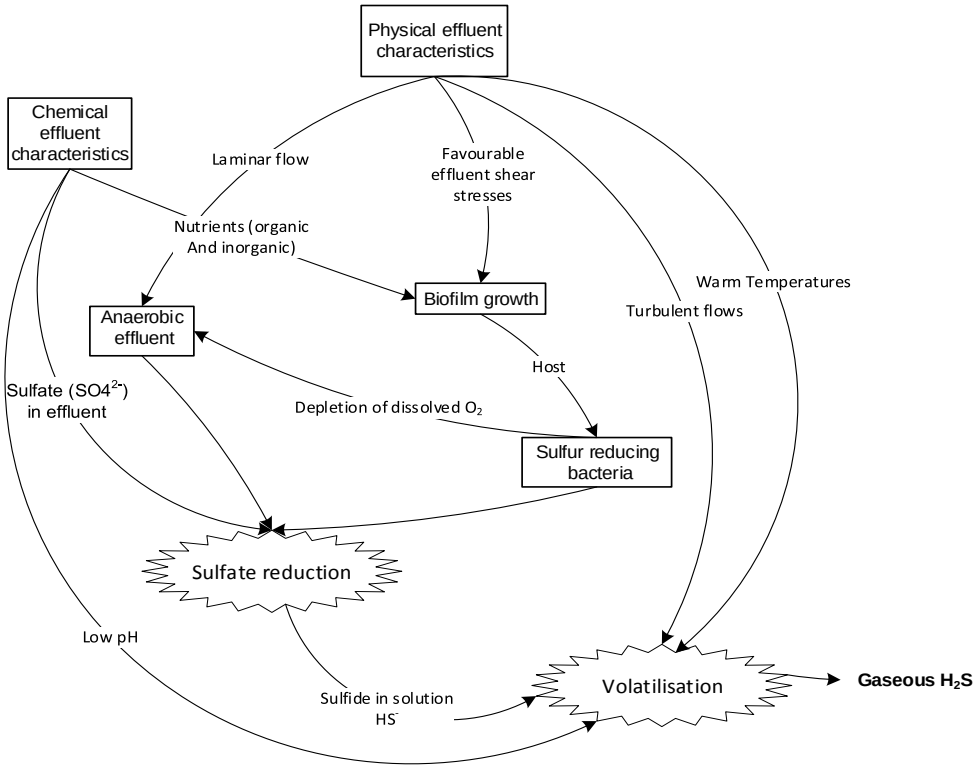

Figure 2-1: A schematic diagram of the conditions required for the release of Hydrogen sulfide gas in the sewer atmosphere

With this complexity in mind, a review of some of the factors involved in the process of biogenic H_2S generation is undertaken.

2.2.1.1 Origin and effect of sulfates

Sulfur is the most important chemical element in the process of MIC (Dong et al. 2017). Since sulfate is the sulfur compound involved in reduction by sulfur-reducing bacteria, it is necessary to investigate its sources

Sulfates are naturally occurring compounds originating from mineral deposits in soil, rocks and the combustion of sulfur-containing fuels (EPA, 2003). Major natural contributors of sulfate to the environment are sulfur released from erosion of natural minerals such as Evaporite, sulfide containing rocks and volcanoes (EPA, 2000).

While sulfate is found in nature, anthropogenic sulfate may be a significant fraction of sulfates found in sewer effluent, with 45% of river-borne sulfates being attributed to human activity (Moore, 1991). This point is further emphasised by Moreno et al. (2009), where they state that "a third of the sulfur reaching the environment is anthropogenic, and it is generated from industrial activities such as mining and mineral processing, agriculture, paper and pulp, combustion of fossil fuels and refuse. The mineral processing industries emit sulfur to the environment in the form of sulfate, sulfuric acid, hydrogen sulfide and SO_x gases."

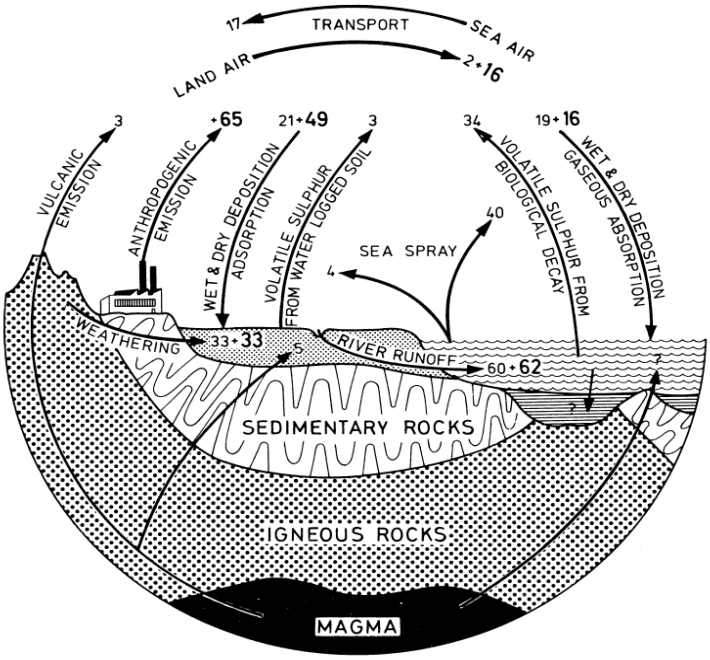

Figure 2-2: The sulfur cycle (Hallberg, 1976)

Figure 2-2 above, illustrates the sulfur cycle and the movement of sulfur through natural and man-made systems. Some researchers have argued that downstream problems (MIC and H_2S generation) associated with sulfur in the sewer system, can be mitigated significantly by limiting the amount of sulfate entered into the sewer system as a result of potable water treatment in water purification plants. A study across Australia, analysing the sources of sulfate (SO_4^{2-}) that end up in the sewer system found that aluminium sulfate addition during potable water production, contributed substantially to the sulfate load in sewers (Pikaar et al. 2014).

It should be noted that aluminium sulfate is one of the most economical coagulants in the treatment of raw water and is used widely throughout the world in water purification plants (Chaudhari and Sahu 2013). Pikaar et al. (2014) report that as much as 52% of the sulfate present in sewage in Queensland Australia was due to the addition of aluminium sulfate coagulant (Figure 2-3).

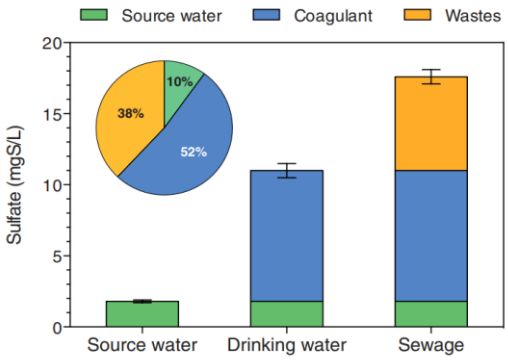

Figure 2-3: Sulfate concentrations in source water, drinking water and in sewage sampled in an Urban area in Queensland Australia (Pikaar et al. 2014)

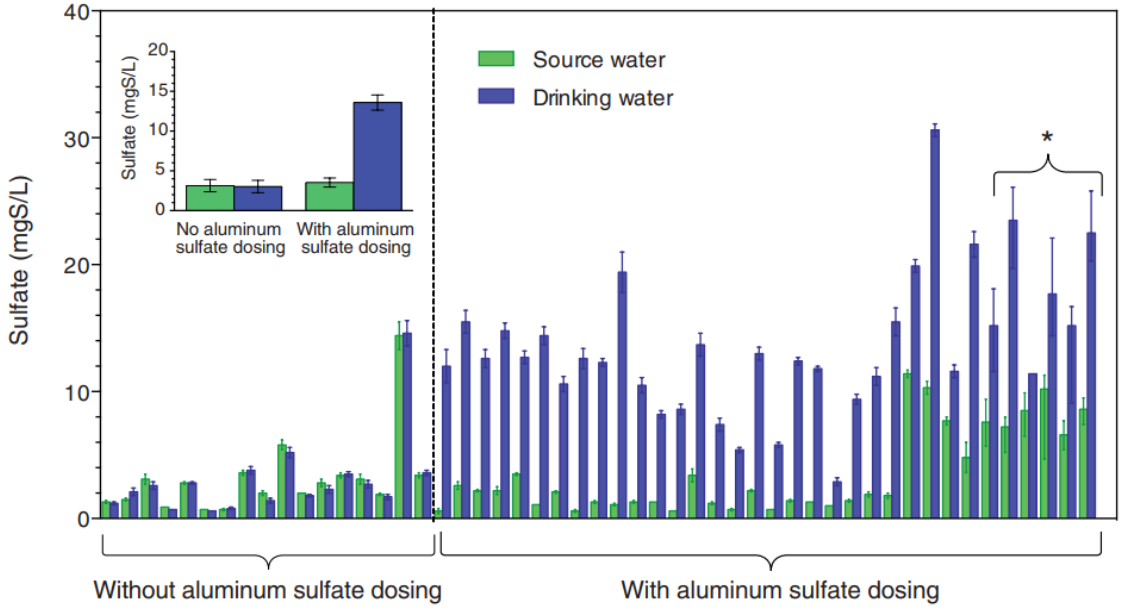

Figure 2-4: A comparison of sulfate in drinking water from water purification plants where aluminium sulfate coagulant is dosed and where aluminium sulfate is not used (Pikaar et al. 2014).

Figure 2-4 (Pikaar et al. 2014) indicates that sulfate concentrations in potable water depend on whether aluminium sulfate is used in water purification. Reducing the sulfate concentration in the effluent may, therefore, be a question of changing the type of coagulant used in water purification from aluminium sulfate to a non-sulfate bearing coagulant, such as ferric chloride or poly-aluminium chloride (Pikaar et al. 2014).

Figure 2-4, illustrates the observations made by Pikaar et al. (2014), where the difference in sulfate concentration in source water and potable water were compared in areas where aluminium sulfate dosing was undertaken versus where a non-sulfate bearing coagulant was used. These results show that aluminium sulfate dosing during water purification increased the sulfate concentration in drinking water by a factor of 3 or more.

Through the use of models that took into consideration the water sulfate concentration, hydraulic retention time, rising main fraction, and sewage temperature, Pikaar et al. (2014) suggest that significant sewer repair cost savings can be achieved by changing the type of coagulant to one that does not contain any sulfate.

While Pikaar et al. (2014) assert that their corrosion models indicate that higher sulfate concentrations in potable water result in higher biogenic corrosion rates in the sewer, in-situ measurements of corrosion in real sewers were not presented. It is therefore of interest to investigate whether sulfate concentration should be considered to be the main driver of MIC in the sewer environment.

The effect of sulfate concentration on H_2S production was studied by Nielsen and Hvitved-Jacobsen (1988). In laboratory biofilm reactor tests, SRB induced production of H_2S was used to determine what effect the sulfate concentration in the effluent had on the production of H_2S.

For biofilm thicknesses typically encountered in concrete sewers (100 µm), the sensitivity of sulfide flux to sulfate concentration was found to range between 0 mg and 2 mg of sulfate per litre (SO_4^2/l), after which the sulfide flux tapers off to a constant level with increasing sulfate concentration (Nielsen and Hvitved-Jacobsen, 1988). The

minimum value at which sulfate concentration effects no change in the sulfide flux is referred to as the limiting sulfate concentration (Hvitved-Jacobsen 1988).

The relationship between sulfide flux and sulfate concentration is shown in Figure 2-5. It must be noted that the many untreated source waters shown Figure 2-4 by Pikaar et al. (2014) have sulfate concentrations higher than 2 mg/litre. If it is to be accepted that sewer biofilm thicknesses are within the approximate range of 100 µm and that the limiting sulfate concentrations described by Nielsen and Hitved-Jacobsen (1988) apply, then high sulfate concentration cannot be said to be the driver of H_2S generation in the sewer.

The limiting sulfate concentration was found to be influenced by two parameters, the biofilm thickness and the organic composition of the effluent. Figure 2-6 shows that the limiting sulfate concentration increases as the biofilm gets thicker, and that the increase is dampened or amplified by effluent organic content, represented by the parameter K_{0f} .

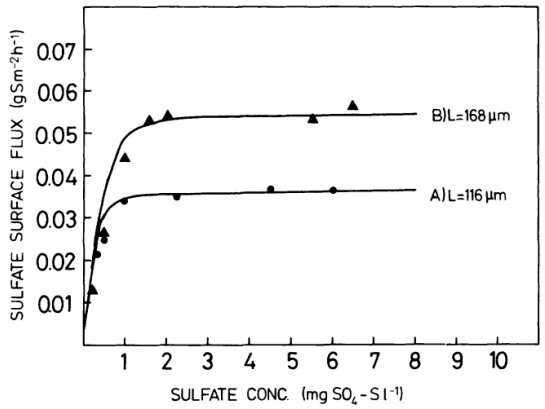

Figure 2-5: Sulfide* surface flux related to the concentration of sulfates (Nielsen and Hvitved-Jacobsen, 1988)

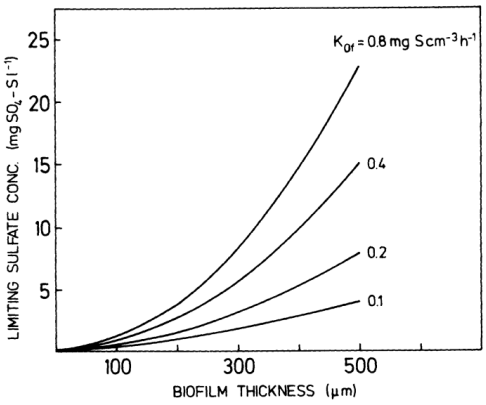

Figure 2-6: The influence of biofilm thickness on the limiting sulfate concentration (Nielsen and Hvitved-Jacobsen, 1988)

*The y-axis of this graph was incorrectly labelled by the original authors; it should read sulfide surface flux instead of sulfate surface flux.

2.2.1.2 Factors affecting biofilm growth

Figure 2-6, shows that biofilm thickness has a bearing on the limiting sulfate concentration, which in turn has a bearing on the amount of sulfide that can be generated by SRB. Biofilm is defined as "a structured community of microorganisms encapsulated within a self-developed polymeric matrix and adherent to a living or inert surface" (http://en.wikipedia.org, 2019).

Biofilms are important because they provide a condition where effluent residence time is longer which promotes the activity of SRB, given that SRB are slow-growing and can therefore cannot not generally establish a large population inside fast flowing wastewater. (Jensen, Biggs and Karunakaran 2016).

Biofilm thickness partly depends on the intensity of effluent flow which may remove some biomass due to the flow-induced shear stresses. This is because sewage stream generates shear stress of different values in different points of an active cross-section. The highest shear stress values are reached close to the pipe bottom and the lowest values are reached near the side walls close to the wastewater free surface. The abrasion forces caused by

solid suspension drag are also very important in biofilm removal. Biofilm resistance to removal may also be increased by fat settlement along the walls of sanitation pipe (Lagod et al. 2010).

While it is known that organic and inorganic nutrients play an important role in the formation of biofilms (EPA, 1974), there have been few studies quantifying the effects of inorganic nutrients on the biofilms and micro-organisms in sewers**.**

In studies focused on urine separation from wastewater effluent, Johnsson et al. (2000) measured the difference in the proportions of inorganic nutrients in wastewater and urine. It was discovered was that urine is responsible for 80% of the nitrogen and 55% of the phosphorous in household wastewater while only accounting for 1% of its volume (Johnsson et al. 2000). The main argument for the implementation of urine separation comes from the potential recovery of these valuable nutrients at their source, however, the fact that urine accounts for such a large proportion of nitrogen and phosphorous, urine separation may provide a way of depriving sewer biofilm of nutrition required to grow and host SRB. Little research has been related to this hypothesis. However, some researchers have made a few notable findings in the relationship between nutrients and biofilms in aquatic systems.

By studying selected wastewater streams and rivers in northern Utah (USA), Crawford (2013) reports that the BOD of wastewaters can be reduced by limiting the availability of inorganic nutrients. Biological oxygen demand (BOD) analysis is a measure of the biological activity in wastewater. It is also reported that biofilms are more abundant and denser in a nutrient-rich environment as it promotes the transition of bacterial cells from planktonic to biofilm state, while depletion of these nutrients causes detachment of biofilm cells from surfaces (Sehar and Naz, 2016).

The ability of biofilm to latch on to substrate is affected by the roughness of the substrate material (Sehar and Naz, 2016). It is understood that during the initial steps of colonization, surface roughness at nanoscale and microscale levels enhances the adhesion of bacteria to substrates by providing more surface area for cell attachment. Surface roughness also reduces the shear stresses on bacterial cells and communities present in flowing liquids at high flow rates, such as water pipes in industrial plants. Moreover, other factors such as charge, hydrophobicity and elasticity are also influential in microbial attachment (Sehar and Naz, 2016). Sehar and Naz (2016) report that divalent cations, such as Ca^{2+} are enablers of biofilm growth. Some studies have shown that the thickness of a biofilm can be enhanced by introducing more divalent cations which results in denser biofilms. Since Portland cement concretes are fundamentally calcium-rich systems

2.2.1.3 Reduction of sulfates by bacteria

Sulfur reducing bacteria (SRB) are organisms that exist in the biofilm that grows on the walls of sewer pipes (Gutierrez-Padilla et al. 2010). These bacteria typically oxidize sulfur compounds (sulfates and elemental sulfur) in the presence of dissolved oxygen in sewer effluent. Under anaerobic sewer conditions (no dissolved oxygen), sulfate (SO_4^{2-}) becomes the most thermodynamically efficient electron acceptor for SRB to use in place of dissolved oxygen. Sulfate-reducing bacteria obtain energy by metabolising organic compounds and/or molecular hydrogen (H_2) while reducing sulfate (SO_4^{-2}) to hydrogen sulfide (H_2S-HS) (Nielsen and Hvitved, 1998). *desulfovibrio* and *desulfotomaculum* are reported to be the dominant genera involved in sulfur reduction in the sewer environment (Gutierrez-Padilla et al. 2010). The sulfur reduction by SRB chemical reaction is shown in equation ((2-1) (Dec et al. 2016).

$$SO_4^{2-} + 2\ H^+ + 4\ H_2 \rightarrow H_2S + 4\ H_2O \quad (2\text{-}1)$$

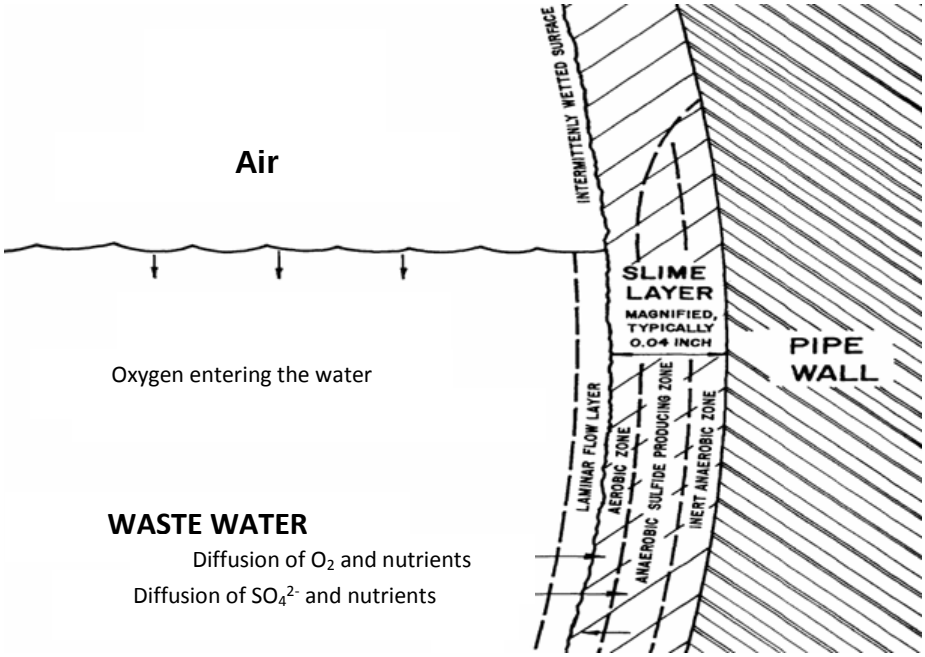

Figure 2-7: A depiction of the cross-section of the slime layer in a sewer pipe where sulfur reduction occurs (EPA, 1974)

The sewer temperature also influences how SRB oxidize sulfates to form sulfide in solution. Nielsen and Hvitved (1998) suggest that higher temperatures will increase the rate of oxygen consumption by sulfate-reducing bacteria leading to anaerobic conditions and subsequently the reduction of sulfates into sulfide. The production of sulfides (HS^-) by sulfur-reducing bacteria is more acute in rising sections of the sewer network, or in sections where the sewer runs full (Gutierrez-Padilla, 2010).

2.2.1.4 Effect of effluent pH and temperature on the formation of aqueous H_2S

The sewer effluent pH also affects the degree to which sulfide is produced. Rava (2008) states that H_2S is slightly soluble in mildly acidic solutions and that its solubility increases intensely as the pH decreases in value. Therefore, maintaining the pH of the wastewater at a pH between 8,0 and 8,5 is suggested as a measure to reduce the release of gaseous H_2S (Hagen and Hartung, 1997).

$$H_2S_{(aq)} \leftrightarrow HS^- + H^+ \qquad (2\text{-}2)$$

Aqueous hydrogen sulfide and sulfide in solution.

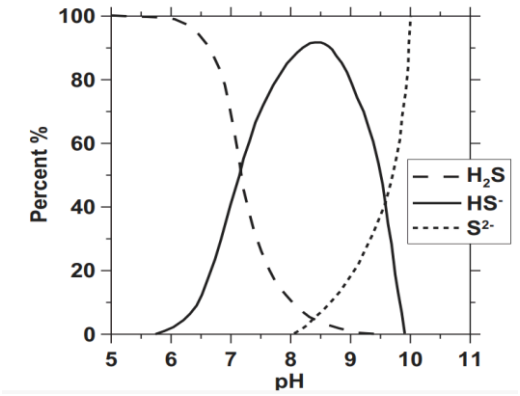

Figure 2-8: Effect of effluent pH on the prevalence of S^{-2}, HS^- and H_2S (House and Weiss, 2014)

The relationship between 3 species of sulfide in solution is shown in figure 7 (House and Weiss, 2014), indicating as Rava (2008) suggests, that H_2S is the dominant species as effluent becomes more acidic.

2.2.1.5 Release of gaseous H_2S from solution

Hydrogen sulfide is an intermediate product in the microbially-induced corrosion of concrete in sewers. However, the effects of the liberation of gaseous H_2S transcend the problem of sewer pipe corrosion. At low concentrations, H_2S may cause unpleasant odour and nasal irritation (1- 5 ppm), higher concentrations from 20-50 ppm may irritate the eyes and lungs, and concentrations above 250 ppm cause serious adverse health effects including death (Guidotti, 1996).

The liberation of H_2S gas from sulfide (HS^-) in solution occurs mainly in partially filled sections of the pipe network, and is due to an imbalance of H_2S in solution and H_2S in the sewer atmosphere (Goyns, 2013). In theory, H_2S will be liberated until equilibrium is reached between concentrations of H_2S gas in the sewer atmosphere and concentrations of HS^- in solution (Goyns, 2013).

Theoretically, the rate of mass transfer from the liquid phase to the gaseous phase can be calculated through the equation provided below (Yongsiri et al. 2004).

$$\frac{dC}{dt} = -K_L \frac{A}{V}(C - C_s) = -K_{La}(C - C_s) \qquad (2\text{-}3)$$

Where

C = concentration of the substance in the water phase (H_2S_{aq}) (g/m^3)

C_s= saturation concentration of the substance at equilibrium (g/m^3)

K_L= overall mass-transfer velocity (m/h)

A = interfacial area (m^2)

V = volume of the water phase (m^3)

K_{La}= overall mass-transfer coefficient

t = time (h)

$$S_g = kP_g \quad (2\text{-}4)$$

Henry's law

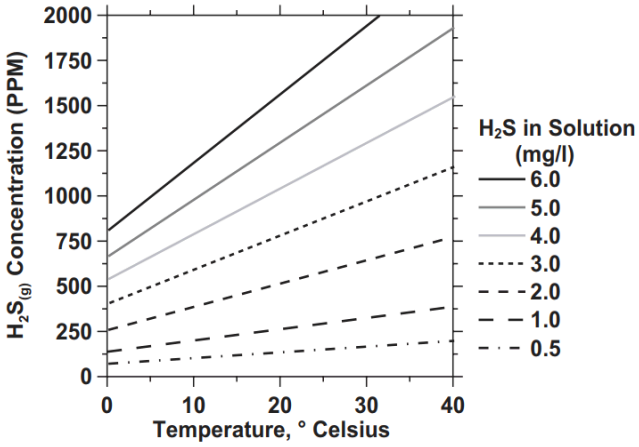

Figure 2-9: The effect of temperature on the volatilization of aqueous H_2S

House and Weiss go further (2014) in describing the theory of volatilization. In closed systems, H_2S phase change from solution to gas state is governed by "Henry's Law" (equation 3). A where S_g is the molar concentration of H_2S in its aqueous state, k is Henry's Law constant and P_g is the partial pressure of H_2S in the air over the solution (House and Weiss, 2014).

As can be deduced from Figure 2-9, which shows the relationship between the liberation of H_2S gas from solution and effluent temperature, an increase in temperature increases the amount of gaseous H_2S in the system.

The effect of temperature on the release of H_2S gas was observed by Alexander and Fourie (2011) where gaseous H_2S was observed to range between 110 PPM and 40 PPM between the warmest and coolest periods of the day respectively in the Virginia Experimental Sewer (VES) in South Africa.

2.2.1.6 Effect of effluent flow on the release of H_2S Gas

The stripping of H_2S from the effluent to the sewer atmosphere also affected by the type of effluent flow. Turbulent flows, which may occur where effluent velocities are high or where abrupt changes to the sewer geometric profile occur will cause significant increases in the liberation of hydrogen sulfide gas when compared to subcritical flows (Goyns, 2013).

A flowing fluid's turbulence can be assessed by calculating its Froude number. Subcritical flow is dominated by gravitational forces and behaves slowly or stably, and has a Froude number of less than one. Supercritical flow is dominated by inertial forces and behaves as rapid or unstable flow. The effect of varying the effluent speed and varying the Froude number on the liquid to gaseous phase mass transfer of H_2S was studied by Yongsiri et al. (2004).

The Froude number is a ratio of inertia to gravitational forces. The Froude number (Fr) is calculated by the formula:

$$Fr = \frac{u}{\sqrt{g d_m}} \quad (2\text{-}5)$$

Where u is the mean velocity (m/s), g is the gravitational acceleration (m/s^2), and d_m is the mean hydraulic depth (m).

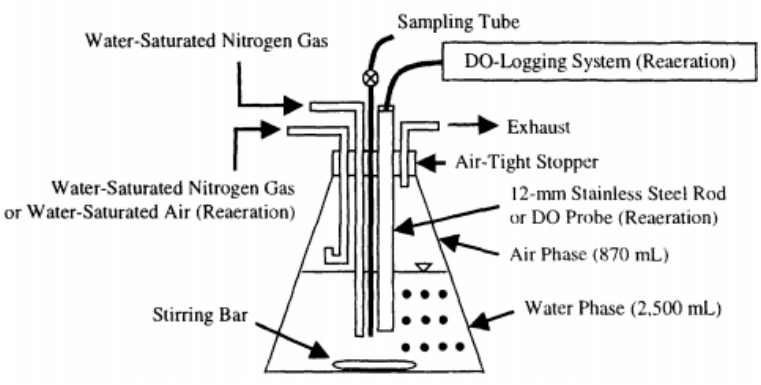

Figure 2-10: Rig setup for measurement of H_2S transfer from liquid to gaseous phase from the agitation of the liquid phase (Yongsiri et al. 2004).

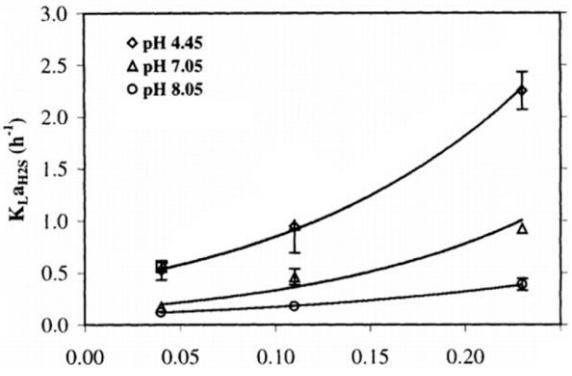

Figure 2-11: Overall mass transfer coefficient of H_2S (K_{LaH2s}(h^{-1}) compared to the liquid phase Froude number (Yongsiri et al. 2004)

To achieve varied velocities and Froude number values, Yongsire et al. (2004) stirred the sulfate-containing water phase in a vessel at three different speeds using a cylindrical magnetic bar that was 80 mm in length and 10 mm in diameter (Figure 2-10). Effluent velocity was measured using a digital anemometer. Thereafter, Yongsiri et al. (2004) plotted the calculated Froude number against the overall mass transfer coefficient (K_{LaH2s}). The relationship shown in Figure 2-11 shows that H_2S release increases exponentially with increasing turbulence, where their Froude number ranges between 0 and 0.2.

The effect of abrupt changes in pipeline vertical geometry on the release of H_2S was studied by Matias, Matos and Ferreira (2014). These changes are typically encountered where structures such as manholes and vertical drops are used. It was found that the turbulent flows at these abrupt geometric changes affected the quantity of H_2S gas liberated, and that the total amount of H_2S released from the bulk water increased with the drop height (Matias, Matos and Ferreira 2014). A laboratory experiment where dissolved sulfide (HS^-) bearing water was subjected to an abrupt drop in elevation was conducted to quantify the effect of elevation drops on the concentration of H_2S gas in the atmosphere.

Figure 2-12 shows the effect of varying drop height on the concentration of H_2S gas over time, where the dissolved sulfide (HS^-) concentration was kept constant at 5 mg/litre and the temperature was 24 degrees Celsius.

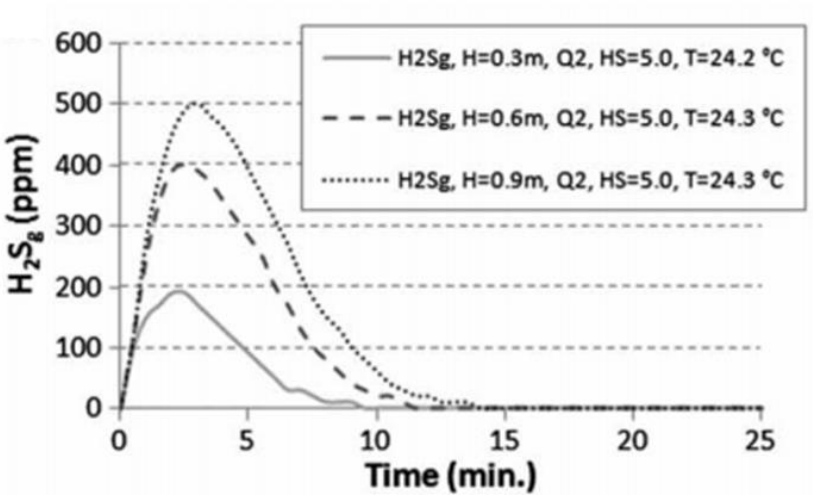

Figure 2-12: Effect of drop height on the concentration of $H_2S(g)$ (Matias, Matos and Ferreira 2014)

The results supported the hypothesis that H_2S phase change from liquid to gas is accelerated by turbulences induced by sharp changes in geometry.

The research work by Yongsiri et al. (2004) shows that under subcritical effluent flows, increasing turbulence leads to an exponential increase in volatilised H_2S, while Matias et al. (2014) under turbulent flows such as those experienced where sudden drops in elevation are encountered, increasing the drop in elevation increases the amount of H_2S volatilised.

2.2.2 Biogenic sulfur oxidation

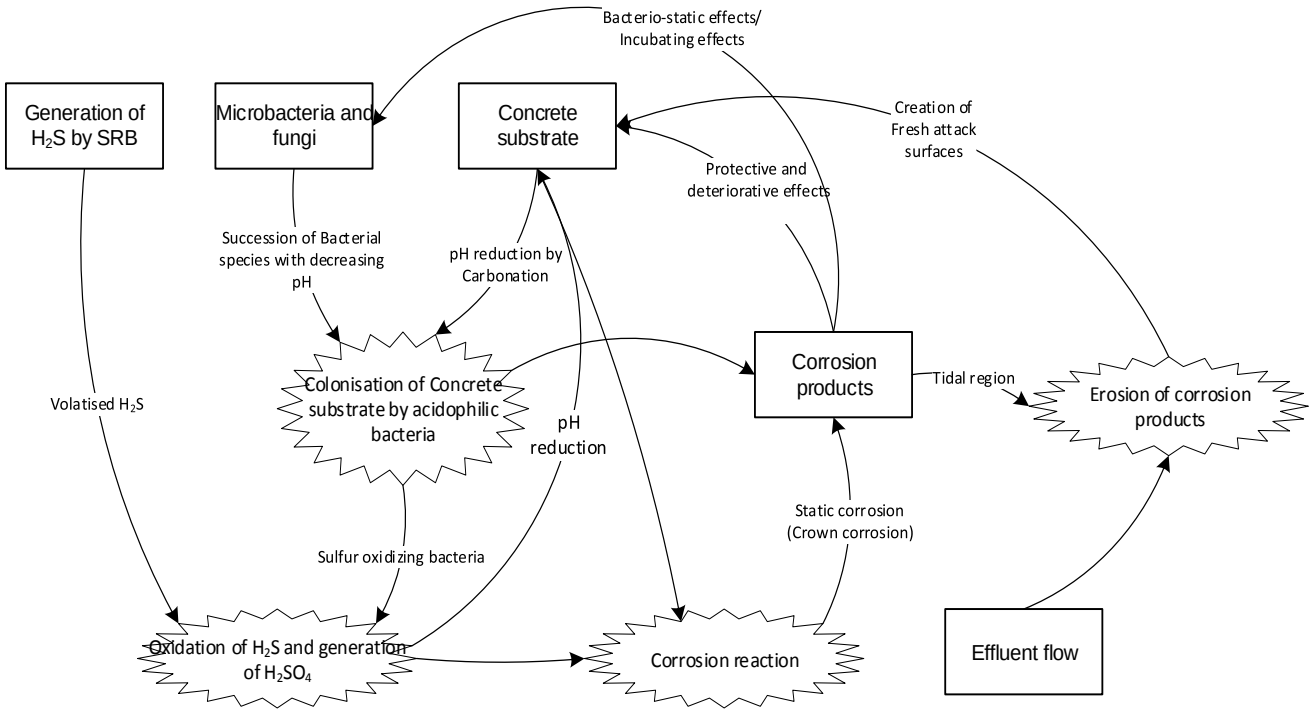

Figure 2-13: Conditions required for the production of biogenic sulfuric acid and the subsequent corrosion of concrete

The oxidation of H_2S by sulfur oxidizing bacteria and the subsequent corrosion of concrete in the sewer environment is a process that is affected by numerous complex and intertwined systems. Figure 2-13, shows a few important system categories and the form in which they are linked.

Concrete is one of the most affordable and available construction materials on earth. It, therefore, follows that bulk infrastructures such as dams, paving works, sewer networks and other infrastructure a built using this material. Newly cast Portland cement concrete is hostile to most organisms because of its high pH (12-13). However, in the sewer, this ideal state doesn't last long as the concrete is susceptible to mechanisms and forms of degradation that reduce its pH over time. The humidity in the sewer provides ideal conditions for bacterial colonisation. Bacteria study on the film of moisture on the concrete surface in the sewer atmosphere was found contain species of sulfur-oxidizing bacteria (Yamanaka et al. 2002). This was attributable to the ability of the sulfur-oxidizing bacteria to grow in the thin water layer which contained hydrogen sulfide and covered the piece even when the surface pH of concrete was 12–13.

Carbonation is a form of degradation and it occurs when calcium hydroxide (CaOH), which is a product of cement's hydration reaction reacts with carbon dioxide in the presence of water to form calcium carbonate ($CaCO_3$). Carbonation is a slow process and occurs in a front. Figure 2-14, adapted from Chang and Chen (2006) shows the relationship between the degree of carbonation and the pH of concrete. The high pH of concrete is also neutralised by the formation of weak acids such as sulfurous acid (H_2SO_3) which is the result of H_2S gas and moisture in the sewer atmosphere also reduces the pH as it reacts with concrete hydration products such as calcium hydroxide (Gutierrez-Padilla et al. 2010).

The effect caused by carbonation is much more rapid where MIC is experienced, because the sewer biofilm is found on the surface of the pipe, where it measures between 0.3 and 0.3 1 mm in thickness (House and Weiss, 2014).

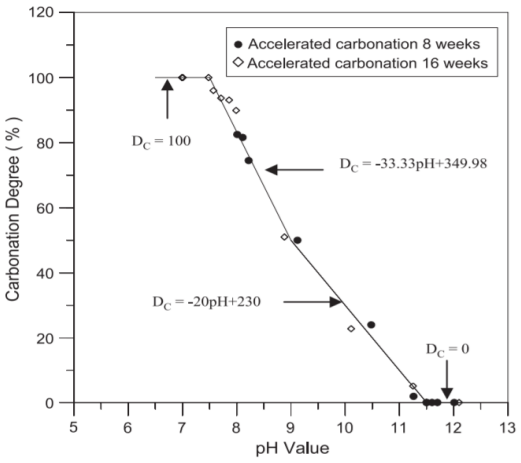

Figure 2-14: Relationship between pH value and carbonation (Chang and Chen, 2006)

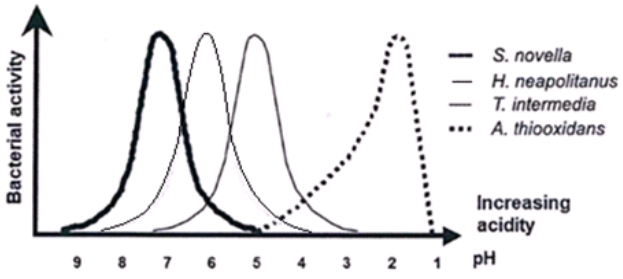

Figure 2-15: The successive growth of 4 species of Sulfur reducing Bacteria in the sewer environment, adapted from Saucier and Herrison (2016)

Of concern to the durability of concrete in sewer network is a set of bacteria referred to as sulfur oxidizing bacteria (SOB). Much like sulfur-reducing bacteria (SRB) discussed earlier, these bacteria use sulfur compounds (S, H_2S, H_2SO_3) as an input in their metabolic processes (Okabe et al. 2006).

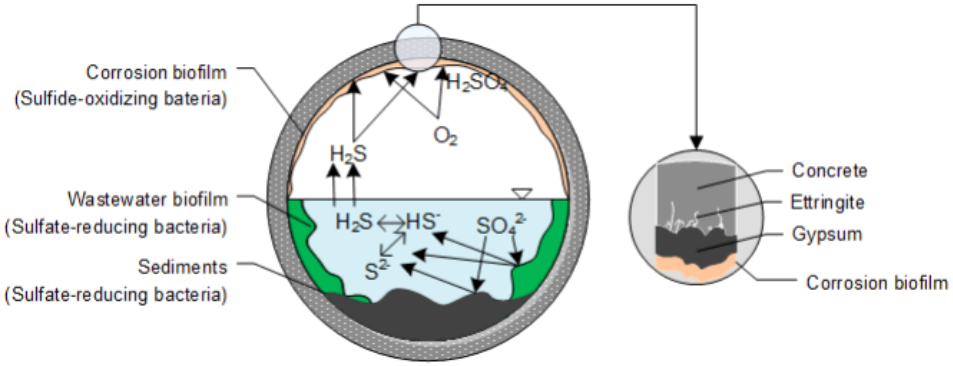

Figure 2-16: Sulfur reducing and sulfur oxidizing bacteria, corrosion of the pipe and ettringite induced cracking.

The sewer is a complex environment, and is a host to many bacteria, fungi and other micro-organisms with complex interrelationships. In a study of Japanese sewers, Okabe et al. (2006) found that over 50% of the biofilm community found in sewer pipes was heterotrophic bacteria other than SOB.

While the bacterial ecosystem may not be fully characterised, studies have shown that as the pH of the concrete pipe reduces, successive species of sulfur-oxidizing bacteria (from neutrophilic to acidophilic) which thrive at decreasing pH levels begin to colonise the pipe. The most detrimental bacterial species in the microbially-induced corrosion process is *acidithiobacillus thiooxidans*, which exists from pH 4 to 1 (Saucier and Herrison, 2016). Selected sulfur oxidizing bacteria studied by Saucier and Herrison (2016) are shown in Figure 2-15.

Sulfur-oxidizing Bacteria such *acidithiobacillus thiooxidans* convert H_2S gas in the presence of water to form sulfuric acid.

$$H_2S + 2O_2 \rightarrow H_2SO_4 \qquad (2\text{-}6)$$

Equation 2-7: Oxidation of H_2S by sulfur-oxidizing bacteria, (Dec et al. 2016).

Research undertaken in Japan by Okabe et al. (2006), analysed various bacterial species that exist in the sewer environment. Their objective was to understand the process of bacterial colonisation and acquire quantitative data of the populations of microbial communities which induce corrosion in concrete by using several 16s RNA gene-based molecular techniques. From the results of the study which was conducted over one year, the data indicated that the MIC process can be divided into three stages:

a) Initial moderate lowering of pH

During this stage, it was found that the pH decrease was not solely due to carbonation and weak acids such as sulfurous acid. A diverse range of bacteria, which include heterotrophic, halotolerant and neutrophilic bacteria were present on the concrete surface. It is suggested that these pioneer microorganisms may have a great impact

on the pH decrease and the establishment of suitable growth environments for the follow sulfur-oxidizing bacteria (Okabe et al. 2006).

b) The continued decrease in pH with the appearance of a succession of neutrophilic sulfur-oxidizing bacteria (SOB)

During this phase, the microbial populations increase significantly, and a succession of neutrophilic bacteria emerge. At this stage, very little mass loss of the concrete is observed. Okabe et al. (2006) found that the dominant SOB species succeeded in the following sequence: t*hiothrix spp*., t*hiobacillus plubophilus*, t*hiomonas spp*., and *halothiobacillus neapolitanus*. Okabe et al. (2006) suggest that these species of bacteria are likely to be the first producers of sulfuric acid in the MIC process, and this results in a further decrease in the pH of the concrete.

c) The emergence of acidophilic sulfur-oxidizing bacteria (SOB) and the development of sever concrete corrosion.

This stage of bacterial succession is characterised by a low pH of around 2, and severe mass loss of the concrete. In a Japanese sewer study, a*cidithiobacillus thiooxidans* was the most dominant microbially species. Previous work found that 5 t*hiobacillus* species (*T. thioparus, T. novellus, T. neapolitanus, T. intermdius, and T. thiooxidans*) play important roles in the oxidation of H_2S, however, Okabe et al. (2006), using 16s RNA gene-based methods could not detect the presence of some of the species which are frequently cited in sewer studies, these included *T. thioparus* and *T. novellus* (Okabe et al. 2006).

Cayford et al. (2012) investigated MICC communities in two corroding concrete sewers in Sydney Australia and found a*cidiphilium spp*. and *mycobacterium spp.* to be the most dominant acidophilic microbial groups across the 10 samples examined. In contrast, *acidithiobacillus spp*. was prominent in only one sample and made up less than 3 per cent of the populations in the other sewers.

These studies show that this aspect of the MIC process is highly variable, and that the range of bacteria and fungi inhabiting the sewer is not fully characterised.

2.3 Corrosion of concrete by biogenic sulfuric acid

2.3.1 Corrosion reactions in Portland cement concrete

Once biogenic sulfuric acid has been generated, the nature of the interaction between acid and the concrete substrate becomes important. Studies on this aspect of MIC have primarily focused on biogenic corrosion of Portland cement concretes. Of particular importance is what effect the corroded layer shown in Figure 2-17 has on the corrosion rate of concrete pipe.

The most soluble hydration compound in hardened Portland cement paste is Portlandite (CaOH). The reaction between sulfuric acid and Portlandite produces gypsum and water.

$$H_2SO_4 + Ca(OH)_2 \rightarrow CaSO_4 + 2\ H_2O \qquad (2\text{-}8)$$

Where carbonation of concrete has occurred, sulfuric acid reacts with calcium carbonate (calcite) to form gypsum and carbon dioxide and water.

$$H_2SO_4 + CaCO_3 \rightarrow CaSO_4 + CO_2 + H_2O \quad (2\text{-}9)$$

While calcium silicate hydrates (C-S-H) are less soluble than Portlandite and calcite, they are also susceptible to decalcification by sulfuric acid, where the reaction produces gypsum, $Si(OH)_4$ and water (Kiliswa, 2014,)

$$H_2SO_4 + CaO.SiO_2.2\,H_2O \rightarrow CaSO_4 + Si(OH)_4 + H_2O \quad (2\text{-}10$$

While the acid-base reactions producing gypsum decalcify the hardened cement matrix, a severe deterioration mechanism occurs when gypsum reacts with unreacted C_3A to produce ettringite.

$$3\,CaSO_4 + 3CaO.Al_2O_3.6\,H_2O + 26\,H_2O \rightarrow 3.CaO.Al_2O_3.3\,CaSO_4.32\,H_2O \quad (2\text{-}11)$$

Ettringite is detrimental to the concrete matrix because it develops long and slender crystals which pushi against the rigid hardened concrete matrix causing internal stresses within the concrete matrix. In corroding concretes, where the strength has been already been compromised by acid attack, ettringite formation exacerbates corrosion.

2.3.2 Concrete-biogenic acid interaction

The proposed models of acid production at the surface of a corroding concrete pipe range from fairly simple to highly complex (see Figure 2-17 and Figure 2-18). Sun (2015) stratifies the point of biogenic corrosion into 3 layers, a liquid layer, the corrosion layer and the intact concrete layer. Figure 2-17 from Sun (2015) seems to indicate acid diffusion as a factor in the corrosion model, however in Portland cement concretes, it should be noted that the rate of acid attack is orders of magnitude faster than diffusion (Alexander 2020, personal communication, 29 June).

A fundamental issue in MIC models, is where biogenic acid is produced in relation to the identified strata shown in Figure 2-17. Monteny et al. (2000) state that the corrosion layer (composed mainly of gypsum ($CaSO_4$)) resulting from the corrosion of Portland cement concretes is also a site of biogenic acid production.

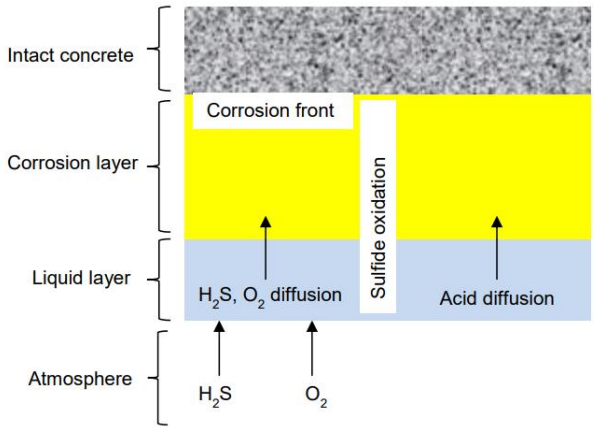

Figure 2-17: Conceptual model for the process of biogenic acid corrosion of concrete (Sun 2015).

By placing Portland concrete specimens in a sewer undergoing severe MIC for 12 months, Grengg (2017) investigated the corroding surfaces of specimens using advanced analytical techniques. These techniques include elemental mapping, microbiome analysis, X-ray diffraction and hydro-chemical analysis of the pore fluids.

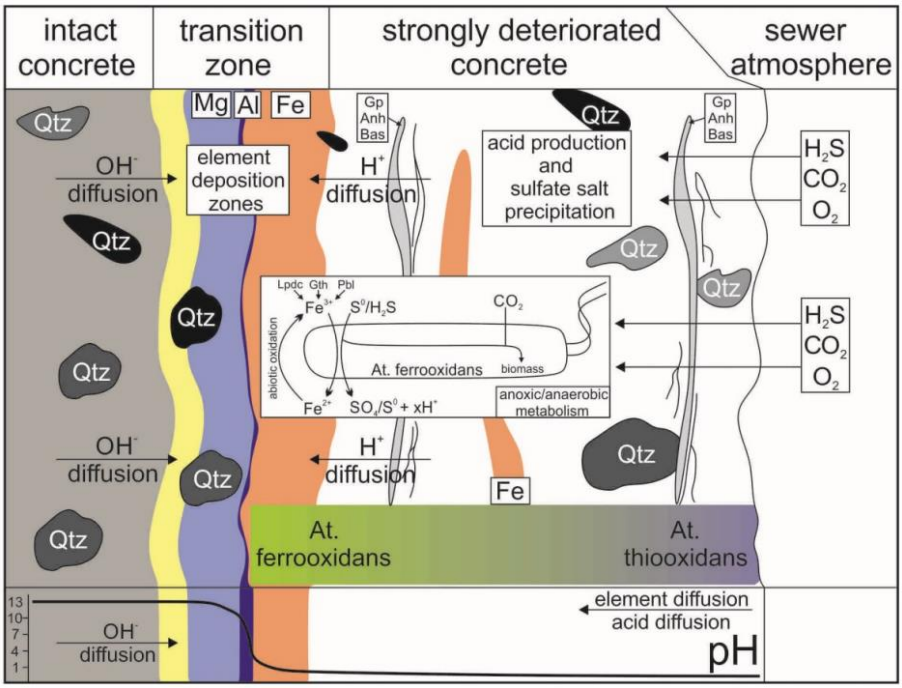

Figure 2-18: pH and diffusion-controlled corrosion model (Grengg, 2017)

Using data collected from the aforementioned analysis, Grengg (2017) proposed a corrosion model for Portland cement concrete which includes biological, hydro-chemical and mineralogical factors. Like Sun's (2015) model, the corrosion interface is stratified into intact (un-corroded) concrete, a transition layer and a layer of strongly deteriorated concrete.

In terms of chemical interaction, the model suggests that hydroxyl ions (OH^-) diffuse from intact concrete towards the transition zone. Similarly, hydrogen ions (H^+) diffuse from the corroded zone (location of acid production) towards the transition zone. This model proposes that acid-producing microorganisms are not limited to the pipe/atmosphere interface, but they are distributed throughout the corrosion layer of the concrete. A*cidithiobacillus ferrooxidans* was found near the reaction front, while *acidithiobacillus thiooxidans* closer to the surface of the specimen (Figure 2-18). An important finding is that the transition zone (TZ) between non-corroded and strongly affected concrete is characterized by an extreme drop in pH from 13 to below 1 characterised by a reaction front of around 1 mm (Grengg, 2017).

It must be stated that the models proposed by Sun (2015) and Grengg (2017) do not consider the effects of effluent abrasion (shear stresses) on the corroding surfaces which are experienced near the tidal line in cases where the sewer should run full or in cases where the sewer is exposed to cleaning and maintenance actions such as water jetting.

2.4 Mitigation of microbially-induced corrosion.

There are multitudes of products and methods by which MIC can be mitigated reported in commercial and academic literature. However, it is more useful to understand where in the path of processes leading up to MIC for these measures take effect. A simplified illustration of the necessary sequence of MIC processes is provided in Figure 2-19.

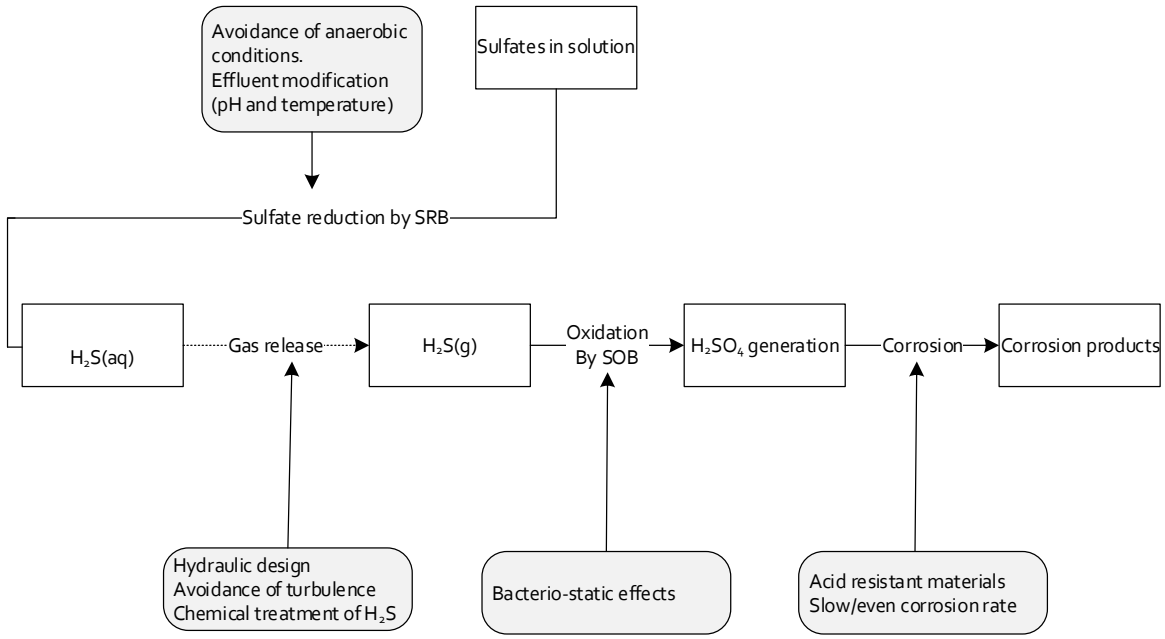

Figure 2-19: The sequence of critical processes leading to MIC

Ideally, measures to stop MIC should be at the beginning of the sequence of processes and are mainly related to the mitigation of H_2S generation and release in the sewer. Pipe material solutions can only address corrosion and thus the problem of H_2S generation remains. A brief description of a few common approaches for the mitigation of the essential sequence of processes (Figure 2-19) leading up to MIC are provided in the following sub-chapter.

2.4.1 Inhibiting biogenic sulfide generation

2.4.1.1 Hydraulic design measures

The hydraulic design of sewer pipelines can be used to limit the amount of sulfide generated in the sewer. By controlling effluent flow, the conditions that lead to anaerobic effluent and sulfate reduction can be reduced substantially. A discussion on the hydraulic parameters that lead to sulfide generation follows:

2.4.1.1.1 Slope and pipeline length

Pomeroy and Parkhurst (1977) state that the slope of the pipe is the key criterion in designing a wastewater collection system to avoid sulfide generation. Sewers designed with long runs at minimum slope are prone to sulfide generation due to long residence times, poor oxygen transfer. and deposition of solids. The relationship between the average sulfide concentrations (mg/l) in several sewers was compared and it was found that sewers with small slopes and long distances had high concentrations of sulfide (Figure 2-20).

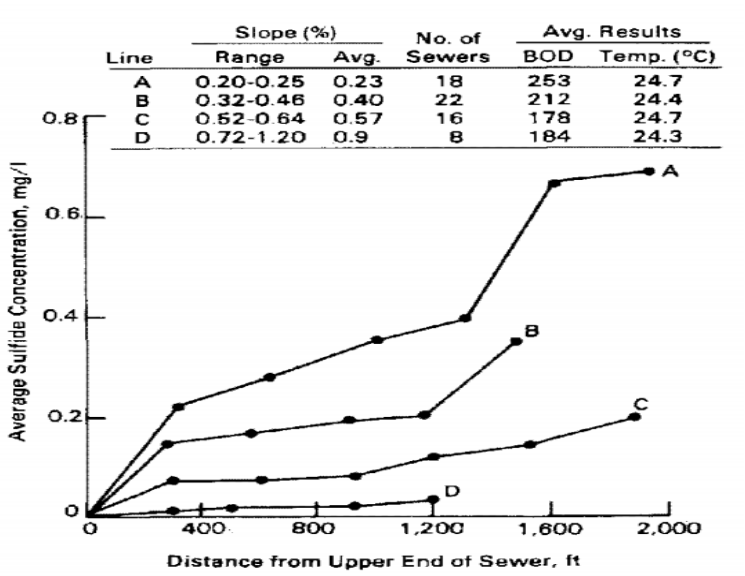

Figure 2-20: Sulfide concentration in effluent according to the slope and distance of pipeline (Pomeroy and Parkhurst, 1977)

Therefore, to avoid sulfide generation, design should aim at minimising retention times, making sewer sections as short as practicable, and designing for the effluent velocities that will allow for air entrainment (Goyns, 2013).

2.4.1.1.2 Drop structures and junctions

Drop structures can result in the wastewater stream picking up substantial amounts of oxygen, helping to maintain aerobic conditions and preventing sulfide generation (Pomeroy and Parkhurst, 1977). However, an important proviso, is that effluent must have low concentrations of sulfide. This is because, where sulfide concentrations are high, drops and falls accelerate the liberation of H_2S gas and thus create H_2S emissions and MIC problems. Therefore, the use of drop structures in the mitigation of sulfide emission and MIC relies on a high level of confidence that the effluent will have low sulfide concentration.

2.4.2 Inhibiting H_2S liberation from effluent

2.4.2.1.1 Chemical treatment to limit H_2S liberation

Where H_2S has already been generated, there are several chemical methods by which H_2S can be treated. These methods are mainly utilised in industrial applications such as natural gas extraction where H_2S is considered a contaminant (Rava, 2008).

Figure 2-21 shows chemical control options available to limit H_2S release in the sewer (Zhang et al. 2008). These options are categorised into two main approaches, inhibiting the generation of H_2S and secondly the elimination of H_2S already formed by SRB.

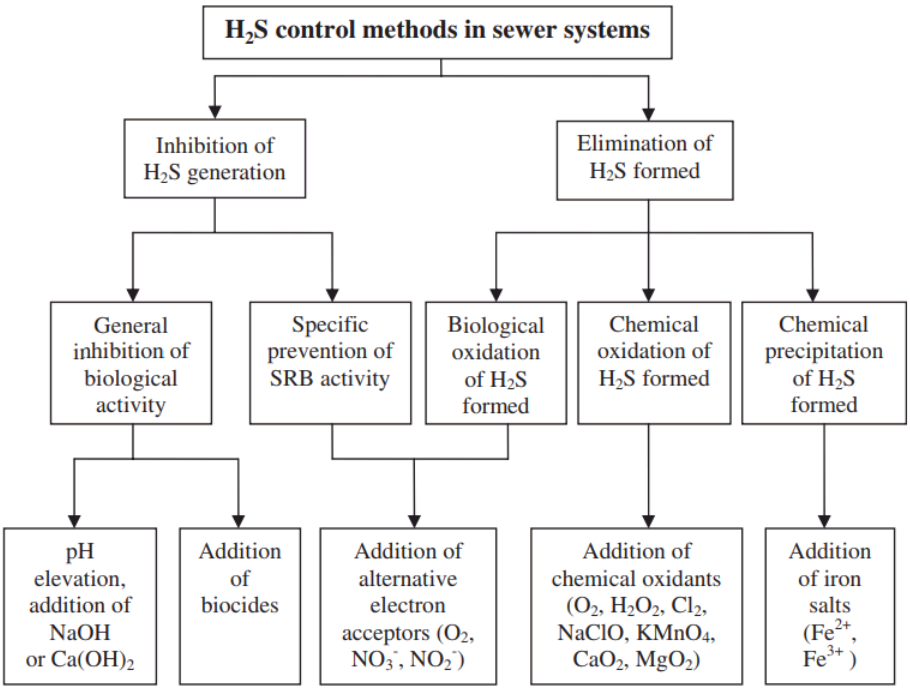

Figure 2-21: Chemical control of H_2S in sewer systems (adapted from Zhang et al. 2008).

While Zhang et al. (2008) list biological oxidation through the addition of alternative electron acceptors such as nitrate, these methods are not well established with regards to mitigating MIC in concrete sewer infrastructure. This is exemplified research by Mohanakrishnan et al. (2009), who foud that nitrate addition to sewers had no inhibitory effects on SRB activity and did not alter the major SRB populations in sewer biofilm

Rava (2008) states of the most common chemical dosing options available for the removal of hydrogen sulfide are H_2S scavenging, H_2S chemical oxidation and H_2S precipitation chemicals.

H_2S scavenging is a process that involves spraying specially design chemicals into H_2S contaminated air or gas. Chemicals used as scavengers are glyoxal or glyoxal in combination with glutaraldehyde or formaldehyde. Chemical oxidation of H_2S in solution is possible through the addition of the following compounds, chlorine, hydrogen peroxide, potassium permanganate, ozone, and chlorine dioxide. Precipitation of H_2S by metal salts such as ferrous and ferric sulfate, ferric chloride, aluminium sulfate, zinc chloride, ferrous chloride and magnesium oxide (Rava, 2013).

A cost analysis of using ferric sulfate to precipitate H_2S was undertaken in the City of San Antonio, Texas where A 21.4 km sewer line was dosed with ferric sulfate to eliminate H_2S. The reaction between ferric sulfate and H_2S rapidly produces black iron sulfide precipitate and sulfuric acid.

$$FeSO_4 + H_2S \rightarrow FeS + H_2SO_4 \quad (2\text{-}12)$$

The economic assessment by Recio-Oviedo et al. (2011) conducted for the year 2011 found that treating hydrogen sulfide build-up in the San Antonio sewer line by reacting it with ferric sulfate would cost the city $ 32 219 per kilometre each year. Given the extensive distances covered by sewer lines and the high recurring costs involved in chemical dosing, it is not widely used in the control of MIC (Zhang et al. 2008).

2.4.2.1.2 Hydraulic measures to limit H_2S liberation

Under condition where sulfide build-up is unavoidable, the design objective becomes to limit the likelihood of H_2S gas being liberated. A practical approach is to design the sewer to flow full, thus ensuring there is no gaseous atmosphere for H_2S gas to be released to. This is achieved by using the smallest practical pipe diameter (Goyns, 2013). However, this approach is not always possible, especially in the case of new sewers, where the sewer capacity has to be adequate projected future effluent volumes.

As stated by Matias, Matos and Ferreira (2014), Goyns (2013) and Yongsiri et al. (2004) turbulent flows of septic effluent are associated with higher rates of H_2S gas liberation. Therefore, the minimisation of turbulence in septic effluent is important. The highest amount of turbulence is anticipated at junctions and drop structures. Pomeroy and Parkhurst (1977) state the turbulent flows are found often found at junctions. Therefore the features that should be avoided in the design of junctions are:

- Abrupt changes in grade between upstream and downstream sewer lines.
- Large differences in velocity between two or more upstream sewer lines entering the same manhole.
- Acute angles between upstream and downstream lines.
- Large changes in flow between two or more upstream sewer lines that may be caused by upstream pumping or daily flow variation between different sewer service areas.

2.4.3 Inhibiting sulfur-oxidizing bacteria

2.4.3.1 Effect of Heavy metals on sulfur-oxidizing bacteria

In the USA, during the mid to late 1980s, a noticeable increase in the number of premature pipeline failures resulting from the production of H_2S were observed. Reporting on this change Nixon (1997) stated, "gaseous H_2S levels have generally risen in most wastewater treatment plants since 1980 from less than 10 ppm to as high as several hundred ppm. In conjunction with this, surface pH values are now commonly measured to be in the 1.0 range. In order of magnitude, this means that sulfuric acid concentrations have risen from 1 to 1.5% solutions to as high as 5 to 7%."A proposed reason for this increase relates to the implementation of the clean water act of 1980 which imposed limits on the levels of heavy metal ions discharged into the sewer by industry (Nixon 1997; Cabrera et al. 2006).

Since heavy metal ions are thought to heavy a toxic effect on bacteria (Gutierrez-Padilla et al. 2010), some researchers have suggested that heavy metal ions such as copper should be dosed into concrete mixes during the manufacture of sewer pipes (Druga et al. 2018; Caicedo-Ramirez 2018).

An assessment of the effectiveness of heavy metals was conducted by Alexander and Fourie (2011) in the Virginia experimental sewer. The assessment which formed part of the second phase of the VES research project, included the testing of concrete specimens dosed with a silver-zinc-copper biocide. The concrete core specimens were placed just above the maximum tidal/flow line and were monitored for changes in surface pH and mass at 5 and 17 months. The specimens dosed with heavy metal exhibited slightly lower mass loss (5.92%) than the control specimen (6.3%) after 17 months of exposure to the sewer atmosphere (Alexander and Fourie, 2011).

Caicedo-Ramirez (2018) attempted to understand the bacteria inhibiting effects of heavy metals on *A.thiobacillus Thiooxidans* in the sewer through the partial replacement of fine aggregates in concrete by sorbent materials, such

as granular activated carbon, dosed with heavy metals like copper, cobalt and zinc. The amount of heavy metal-laden sorbent dosed into the concrete at the mixing stage was reported as a percentage of the fine aggregate replacement. The range of replacement was between 2% and 10% of fine aggregate. This study found that there was little benefit in dosing heavy metal ions into concrete at low (2-5%) fine aggregate replacement values. Furthermore, higher replacement of sorbent laden aggregate produced mild reductions biogenic corrosion.

2.4.3.2 Concretes with bacteria-inhibiting corrosion products and protective corrosion products.

Inhibiting, or stifling the growth of sulfur-oxidizing bacteria is still the subject of much research. Bacteriostatic properties of the pipe material are now considered to be an important parameter in the selection of sewage pipes. Saucier and Herrison (2015) report that pipes manufactured using calcium aluminate cement (CAC) as a binder have superior bacteria inhibiting properties when compared to Portland cement (PC) concrete. Herrison and Saucier suggest (2015) that three mechanisms of resistance are active where calcium aluminate cement concrete is subject to attack by acids, these are:

a) An acid neutralisation capacity that is 40% higher than Portland cement.
b) The formation of an Alumina gel (AH_x), which serves as a barrier against acid attack and;
c) The decomposition of the Alumina gel liberates of aluminium ions which have a toxic effect on acid-producing bacteria.

Work by Letourneux and Scrivener (1999), revealed that the neutralisation capacity of CAC is higher than Portland cements at lower pH (under acidic conditions), while at higher pH values (basic conditions) Portland cement exhibits a higher neutralisation capacity (Figure 2-22).

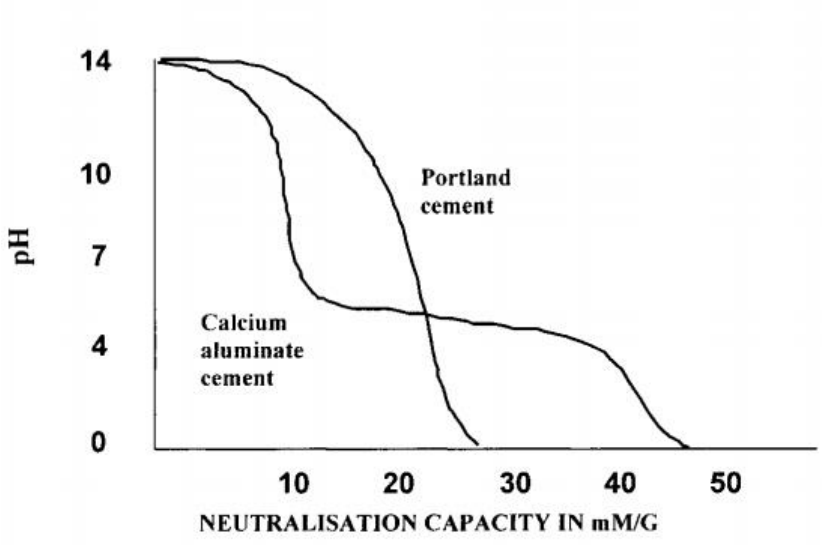

Figure 2-22: Neutralisation capacity vs pH of acidic solution (Letourneux and Scrivener, 1999)

It is suggested that when the pH of CAC based concrete pipes reaches between pH 3 to pH 4, the alumina gel corrosion product, becomes unstable which causes the release of aluminium ions. Saucier and Herrison (2015) state that once the concentration of aluminium ions reaches 300-500 ppm level within the biofilm on the surface

of the pipe, a bacteriostatic effect is observed on the bacteria's metabolism, effectively stopping the activity of sulfur-oxidizing bacteria (SOB).

Furthermore the high MIC resistance of calcium aluminates cement concretes compared to that of Portland cement concretes can be attributed not only to the absence of calcium hydroxide and the presence of more stable calcium aluminate hydrates, but also to the formation of aluminium hydroxide (AHx) in the course of acidic corrosion which encapsulates and protects the hydrates (Allahverdi and Skvára, 2000).

As reported by previous studies (Monteny et al. 2000; De Belie et al. 2004; O'Connell et al. 2010), an accelerated bio-deterioration test cannot rely on a simple immersion test in an acidic solution and requires live sewer testing or a fully representative laboratory simulation of microbially-induced corrosion such as the Hamburg breeding chamber. In tests that confirmed the superior performance of calcium aluminate cements in the Hamburg chamber, Ehrich et al. (1999) state "the good performance of CAC mortars in the biological simulation experiment was therefore based on a combination of their high neutralisation capacity and the reduced amount of biogenic sulfuric acid attacking the material."

The superior durability of calcium aluminate cement's subjected MIC was observed in the Virginia experimental sewer (VES) where data collected showed that the combination of calcium aluminate cement with dolomitic aggregate was four times more resistant to biogenic acid attack than using a Portland cement with dolomitic aggregate, and at least 10 times as resistant as using a Portland cement and siliceous aggregate (Goyns, 2013).

2.4.4 Cements and aggregates with compatible acid solubility

An approach to mitigating the effects of biogenic attack is by using calcareous aggregate in concrete. The use of calcareous aggregates, such as dolomite as a sacrificial aggregate in sewer concrete was influenced by the observed effects of using aggregates that are acid resistant. It was found that sewer pipes with siliceous aggregate suffered rapid and severe disintegration, this occurred when because siliceous aggregate did not contribute to neutralising acid attack, and thus the cement binder was rapidly depleted resulting in early structural failure and aggregate fallout. (Goyns, 2013).

Figure 2-23: A sewer undergoing MIC and preferential corrosion of the binder (Teplý et al. 2018)

In South Africa, acid solubility of concrete is currently assessed by using SANS 677:2010's "Method for determining the amount of material in calcareous aggregate concrete that is insoluble in hydrochloric acid". This method assesses the acid solubility of cured concrete of known mix proportions by:

a) Crushing hardened concrete to a size fraction smaller than 150 microns, oven drying it at 100 degrees Celsius for 2 hours and cooling to room temperature in a desiccator.
b) Mixing the <150mm fraction of crushed concrete with 200ml of water and slowly adding 25-30mL of concentrated hydrochloric acid and allowing the mixture to boil for 5-10 minutes. A constant volume is maintained by adding distilled water, thereafter the solution is allowed to digest for an hour at a temperature just below boiling.
c) The contents are then filtered and material that remains after filtration is oven-dried at 100 -110 degrees Celsius.

This test aims to determine the percentage of insoluble matter (m/m) % in the concrete mix.

Appendix B of SANS 677:2010 specifies, with the aim of mitigation of biogenic corrosion, that the following should be stated where necessary:

a) Whether pipes must have a low content of material insoluble in hydrochloric acid and the percentage of insoluble if less than 25%.
b) Whether or not the pipes should be manufactured using dolomitic aggregate, sulfate resisting cement or any other special material; and
c) The thickness of a sacrificial layer for the specified alkalinity.

Because calcareous aggregates have acid solubility comparable to Portland cement paste, corrosion is therefore uniform and gradual, thereby increasing the service life of the pipe. Calcium aluminate cement is often used instead of Portland cement because it has three purported resistance properties against biogenic sulfuric attack. These properties are stated to include; higher neutralisation capacity, formation of a protective alumina gel layer and bacterio-static properties (Saucier and Herrison, 2013).

2.4.5 Provision of a sacrificial lining

The design of high Portland cement concretes for MIC can be conducted using the life factor method (LFM). Originally developed by Pomeroy and Parkhurst (1977), this method uses formulae that employ the concept of equivalent calcium carbonate ($CaCO_3$) or "alkalinity" to estimate the corrosion rate in concrete sewer mixes, where the rate of corrosion and alkalinity are inversely proportional. The formula used in calculating is:

$$c = 11.4k \frac{\phi_{sw}}{A} \quad (2\text{-}13)$$

Where c = annual corrosion rate (mm/year), k = acid efficiency factor and Φ_{sw} is the rate at which H_2S is absorbed into the exposed sewer pipe and A is the alkalinity. By multiplying the annual corrosion rate (c) by the required service life, this method provides the designer with the ability to calculate the thickness of a pipe lining required to keep the pipe serviceable for the duration of its service life.

Kiliswa and Alexander (2016) observed that alkalinity (equivalent $CaCO_3$) as used in the life factor method, on its own was not a sufficient parameter for the accurate prediction of corrosion in all cementitious systems, and

that the method could be improved by including parameters which take account of calcium hydroxide (CH) content, Alumina gel (AH_3), FeOH, the Al/Ca ratio and the Fe/Ca ratio of the hardened cement pastes.

Long term data has been collected on the durability of various concrete mix combinations by researchers at the Virginia sewer experiment which sections of pipe and specimens of concrete are exposed to biogenic corrosion. Specimens which included calcium aluminate cements, Portland Cements, Fly Ash and GGBS blends of Portland cement were used with both siliceous and calcareous aggregate. Corrosion data collected in the VES is particularly valuable because it can be compared to values corrosion rates calculated from methods such as the LFM.

2.4.6 Acid-resistant material alternatives for sewer applications

2.4.6.1 PVC and HDPE pipe

The use of acid-resistant material such as organic polymer-based materials in sewage may seem like an obvious solution to avoid degradation of sewer infrastructure. Acid-resistant pipe such as high-density-poly-ethylene (HDPE) pipe are available as pipe structures and as pipe linings. However, organic polymer linings are expensive and not easily justified on all sewer pipe sizes (Goyns, 2013).

The major disadvantage of PVC or HDPE pipe stems from their high cost, which prohibits their use as rigid pipe because of the requirement for a thick pipe sections. Instead PVC and HDPE are classified as flexible , which means their structural resistance relies on the bedding material. Furthermore, because material making up the pipe is relatively thin, these pipes are vulnerable to denting, buckling, and excessive deflection (Kuliczkowska and Zwierzchowska 2016).

2.4.6.2 Polymer modified concrete

While organic polymer materials have long been known to possess high acid resistance, the inclusion of organic polymers in concrete to improve its corrosion resistance has essentially taken three forms; partial aggregate (filler) replacement, polymer impregnation where a low viscosity polymer is impregnated into the porous structure hardened concrete, and full replacement of Portland cement by a polymer matrix (Pacheco-Torgal and Jalali, 2009).

These 3 types of polymer modified concrete were subjected to sulfuric acid resistance tests by Pacheco-Torgal and Jalali (2009). It was found that concrete with polymer addition (as aggregate) during the mixing phase provided a minor beneficial effect on the durability and acid resistance of concrete pipes. Concrete with polymer impregnation performs better than concrete without polymer addition. The use of polymer impregnation process enhances the chemical resistance of hardened concrete. Jalali (2009) found that polymer impregnation was economically viable, especially for smaller diameters and that full replacement of Portland cement by organic polymer was successful in producing an acid-resistant concrete (where siliceous aggregate was used).

2.5 Methods of assessing acid resistance of cementitious materials subjected to sewer corrosion

There are numerous laboratory tests intended to assess the resistance of various concretes to acid attack. Given that a fully representative simulation of MIC in the laboratory is very complex, researchers have had to design

tests that focus on specific aspects of sewer corrosion. This section of this study aims to review some common methods used in practice and research

2.5.1 Mineral acid testing: Static immersion testing

Continuous immersion tests are the simplest acid resistance tests. Testing involves placing concrete specimens inside an acidic solution and maintaining the pH over a specified period. Immersion tests such as those conducted on fly ash-based geopolymers by Song et al. (2005) involved submerging concrete cubes in 10% sulfuric acid and measuring various mass loss over 8 weeks where the acid was maintained at a constant level and the acidic solution was completely replaced weekly.

As is seen in work by Bakharev (2005) Song et al. (2005) and Bernal and Provis (2014), much of the testing of geopolymer concrete subjected to acid testing has been conducted by this method. However, there is a general acceptance that where concrete materials intended for use in the sewer environment are concerned, the value of mineral acid testing is limited (Monteny et al. 2000, Kiliswa 2016). This is because of large differences found between purely chemical tests with H_2SO_4 and tests involving microbially produced H_2SO_4.

It is widely accepted that the activity of the bacteria is affected by the substrate material, which in turn affects the amount of sulfuric acid formed (Monteny et al. 2000). In PC binder systems, gypsum and ettringite are the main corrosion products. These insoluble corrosion products form a soft and pulpy layer is formed on the eroded surface.

In mineral sulfuric acid tests, the gypsum layer enveloping the concrete specimen acts as a barrier, which limits the exposure of un-corroded concrete surfaces to corrosion. However, in the sewer environment, the gypsum layer creates good conditions for the growth of the bacteria (Monteny et al. 2000). The growth of bacteria within the gypsum layer means that SOB produce acid near the un-corroded concrete surfaces, which invalidates the casts doubt on the efficacy of the gypsum precipitate layer serving as a barrier to biogenic corrosion.

2.5.2 Mineral acid testing: the dynamic HCl resistance test

Gu et al. (2018) suggest that the key characteristics of biogenic acid corrosion test outside of fully representative simulations of the sewer environment should be brushing, wetting, and drying cycles and the use of a strong acid**.**

The dynamic HCl resistance test developed at the University of Cape Town was intended to test the performance of concrete for use in sewers typically containing sacrificial aggregates such as dolomite. The test required the production of cylindrical concrete test specimens measuring 150 mm in length and 80 mm in diameter, compacted by mechanical means, using dry concrete mixes to simulate industrial pipe manufacturing processes (Alexander et al. 2013). These cylindrical specimens were placed in an acid rig (chamber), rotated at 16 revolutions per minute (rpm) on rubberised rollers and subjected to brushing by PVC bristles while immersed in hydrochloric acid with a pH of 1 (Figure 2-24).

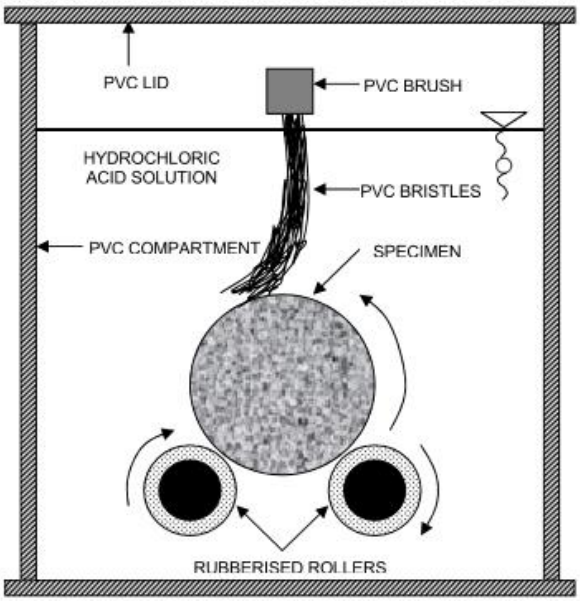

Figure 2-24: A cross-section of the dynamic HCl rig (Alexander and Fourie, 2009)

The use of hydrochloric acid (HCl) instead of sulfuric acid (H_2SO_4) was necessitated by precipitating gypsum, which results from the reaction between sulfuric acid and the compounds of hydrated Portland cements. Fourie (2007) found that a soft calcium sulfate ($CaSO_4$) layer is formed around the concrete specimen forming a barrier around the concrete that prevents further acid attack to some degree. However, the primary reason why the sulfuric acid corrosion trials in the dynamic acid test were unsuccessful was because the acidic solution became saturated with calcium sulfate within 2 hours of immersion. Due to the ongoing precipitation and saturation of calcium sulfate hydrogen ion consumption was virtually stalled within 30 hours of immersion due to the common ion effect (Kiliswa, 2016).

$$H_2SO_{4\,(aq)} + Ca(OH)_2 \rightarrow CaSO_{4\,(precipitate)} + 2\,H_2O_{\,(aq)} \qquad (2\text{-}14)$$

To understand the common ion effect it is useful to refer to the sulfuric acid Portlandite corrosion reaction which produces gypsum and water (2-14). Given that gypsum is a precipitate, and exists in solid form, either suspended in the solution or settling to the bottom of the solution, if this precipitate is not removed from the solution then the reaction will proceed until the equilibrium between soluble and precipitating gypsum is reached. As corrosion proceeds and the solution cannot bear more gypsum precipitation gypsum tends to exist in ionic form (Ca^{2+} + SO_4^{2-}). However the dissolution of Portlandite into Ca^{2+} and OH^- is retarded by Ca^{2+} already in solution through a phenomenon known as the common ion effect. It is suggested by Alexander and Fourie (2011) that in the sewer environment, the gypsum layer would ordinarily be removed by the action of flowing water at the waterline.

Hydrochloric acid has the advantage of producing soluble salts such as calcium chloride while fully disassociating in solution. While this test which does not involve a bacterial component and thus cannot be used to assess any bacterio-static effect that the concrete may exhibit it may be used to determine the compatibility of various cement and aggregate combinations under acid attack. A detailed description of this test is provided in Chapter 3.

Despite the name given to the test, the type of acid need not be limited to hydrochloric acid, if the products of acid attack of a material are do not produce salts that have an obstructive effect on the test.

2.5.2.1 Notable findings from the dynamic HCl test

Fourie (2007) and Motsieloa (2012) conducted studies on the behaviour of sets varying Portland and calcium aluminate cement-based concretes to the dynamic HCl test. Fourie (2007) measured the mass loss (Figure 2-25) and the hydrogen ion consumption (Figure 2-26) of combinations of Portland cement and calcium aluminate cement with dolomitic calcareous aggregates (Olifantsfontein dolomite, Blackheath dolomite and Alag aggregate).

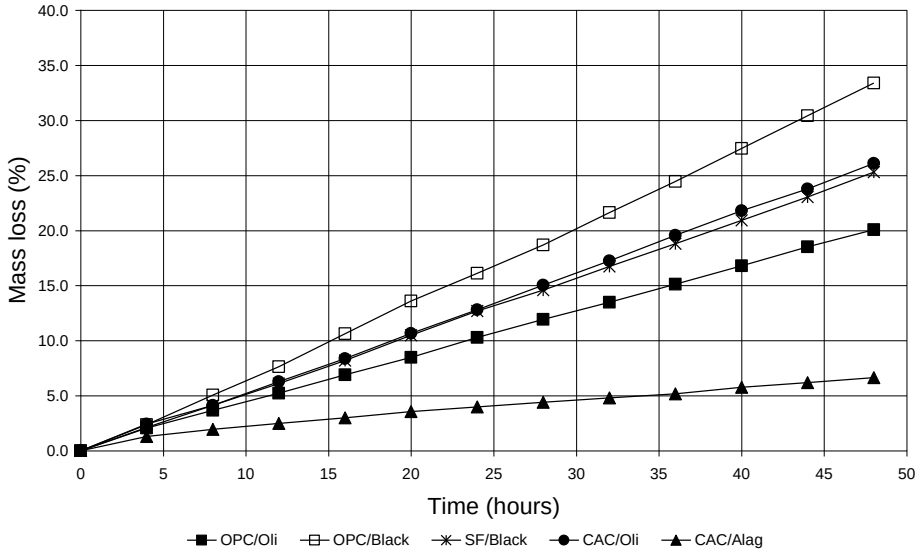

Figure 2-25: Mass loss with time in the dynamic HCl test (Fourie, 2007)

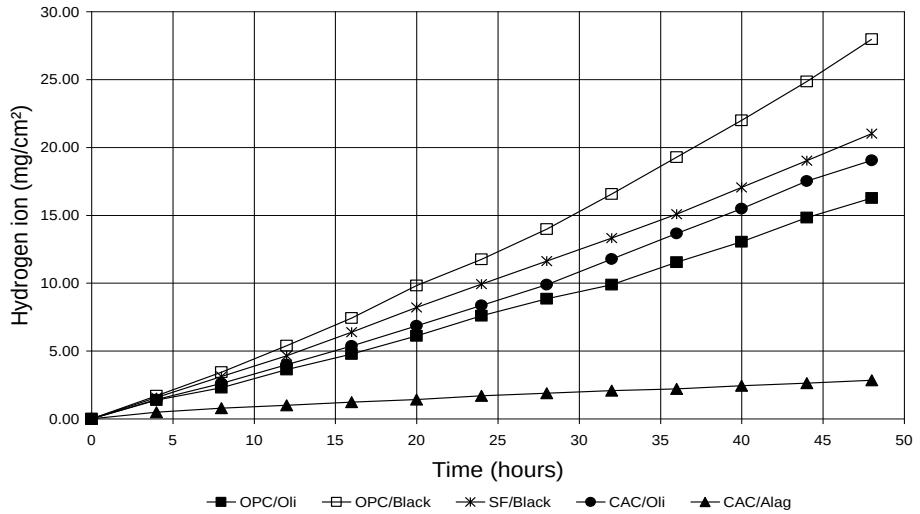

Figure 2-26: Hydrogen ion consumption with time in the dynamic HCl test (Fourie, 2007)

Hydrogen ion consumption and mass loss data produced by Fourie's (2007) tests indicate that a CAC/Alag concrete is the most resilient concrete combination. This result agrees with data collected from live sewer experiments such as the Virginia sewer experiment (VES) where CAC concretes were shown to have lower rates of corrosion in the live sewer. However, a result that does not correspond well with live-sewer measurements is

found when CAC and OPC cements paired with dolomitic aggregate (Olifantsfontein) are compared. Fourie's (2007) test results show that both mass loss and hydrogen ion consumption, are higher for CAC/Oli-dolomite concrete than for OPC/Oli-dolomite concrete. Fourie's (2007) findings were verified by testing undertaken by Motsieloa (2012), where it was confirmed that CAC systems had higher mass losses (Figure 2-27) and higher hydrogen ion consumptions (Figure 2-28) when tested under the dynamic HCl test where the same aggregate was used for both mixes.

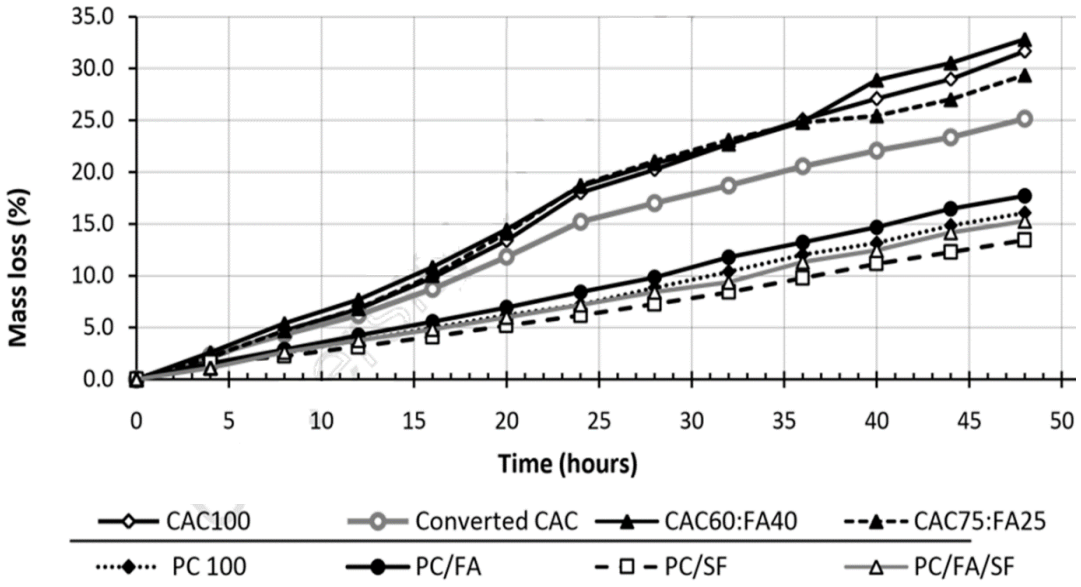

Figure 2-27: Mass loss of CAC and Portland cement systems using Olifantsfontein dolomite subjected to the dynamic HCl test (Motsieloa, 2012)

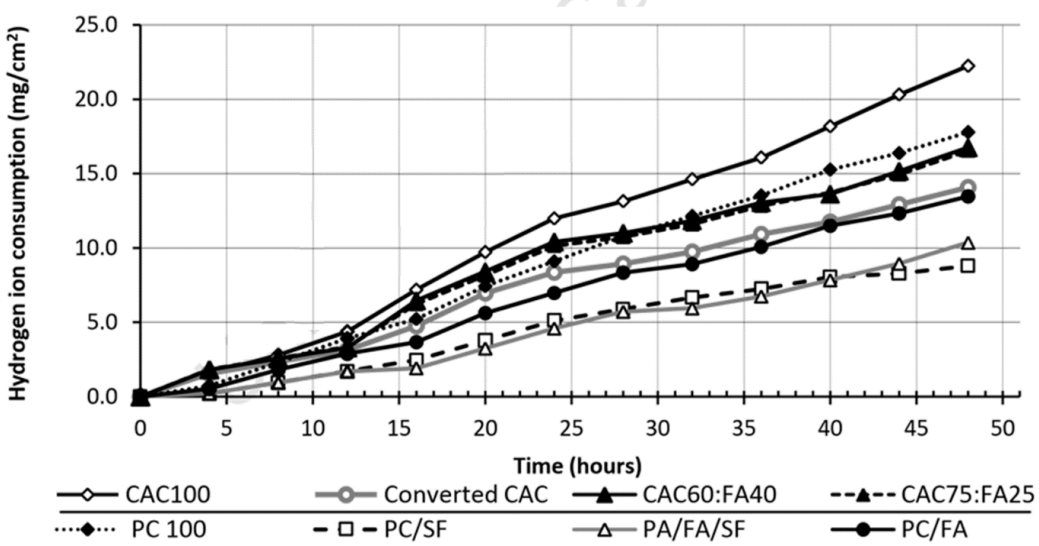

Figure 2-28: Hydrogen ion consumption of CAC-dolomite and Portland-dolomite cement systems subjected to the dynamic HCl test (Motsieloa, 2012)

A noteworthy finding from the studies conducted by Fourie (2007) and Motsieloa (2012) is that the CAC (un-converted) concrete specimens exhibited a higher hydrogen ion consumption than the Portland cement concrete

specimens (where aggregate type was common). If the findings by Fourie(2007) and Motsieloa (2012) are considered together with findings by Herrison and Saucier(2015) and Letourneux and Scrivener (1999) (discussed in section 2.4.3.2), then the higher hydrogen consumption by CAC concretes appear unexpected. This is because Letourneux and Scrivener (1999), and Herrison and Saucier (2015) both measured 40% or higher neutralisation capacity for CAC concretes when compared to Portland cement concretes in highly acidic solutions (pH 1).

A possible explanation to the higher consumption of hydrogen ions by CAC concretes may be that the kinetics of the two reactions are not equivalent, and the rate of the CAC-dolomite corrosion reaction was faster than the rate of the PC-dolomite corrosion reaction in Fourie (2007) and Motsieloa's (2012) experiments. In the dynamic hydrochloric acid test, the acidic solution's pH was maintained at 1 by replenishing the acid, therefore, a faster CAC-HCl reaction may have led to higher mass loss, higher hydrogen ion consumption and a higher requirement for the replenishment of HCl to the acidic solution compared to PC-dolomite corrosion over the duration of each test.

However, to determine the neutralisation capacity, there would be a need to account for both the hydrogen ion consumption and the total mass of the proportion of concrete that is fully neutralised, bearing in mind that mass loss and neutralised mass are not necessarily equal.

The dynamic HCl testing, as conducted by Fourie (2007) and Motsieloa (2012) did not completely consume the reactants in the concrete specimen because the test is not configured to corrode the entire specimen. Instead, the acid consumed as much material as the kinetics of corrosion reactions would allow within the test's duration. Therefore, it is suggested that the dynamic HCl test, may provide useful insight into the kinetics of concrete corrosion reactions instead of insight into the neutralisation capacity of concrete in acid. In other words, the mass loss rate and hydrogen ion consumption rate measured in this test indicate the speed at which corrosion occurs.

2.5.3 Mineral acid testing: Testing Apparatus for accelerated concrete degradation (TAP)

Effluent volumes are not constant during the daily operation of the sewer, furthermore, weather and climate which influence the humidity and temperature in the sewer are also variable. These uncontrollable factors have a bearing on the production of H_2S. However, it is plausible to infer that acid concrete corrosion in the sewer environment occurs in wetting and drying cycles. This is especially applicable to concrete located along the tidal region of the sewer pipe's cross-section. Thus, the effect of these cycles also needs to be considered for a better understanding of MIC.

The accelerated degradation test method developed at the University of Ghent, includes wetting and drying cycles by partly submerging cylindrical concrete specimens in acid while rotating the specimens at 1 rotation per hour. This test is configured such that a third of the specimen's outer circumference is always submerged in the acidic solution. Wetting and drying is accompanied by the application of brushing to simulate the abrasive effects of effluent flow. Table 2-1adapted from De Belie et al. (2002) relates the specific test principle to the deterioration mechanism in the sewer environment.

Table 2-1: Principle tested in the TAP test and its corresponding real sewer co ndition.

TAP principle	Sewer environment condition
Cyclic immersion in acidic medium	Wetting/drying by fluctuation of the wastewater level+
Drying in air	Dry weather situation with low wastewater levels
Abrasion by brushing	High flow rates because of high loading or rain, abrasion by flowing water and turbulence.

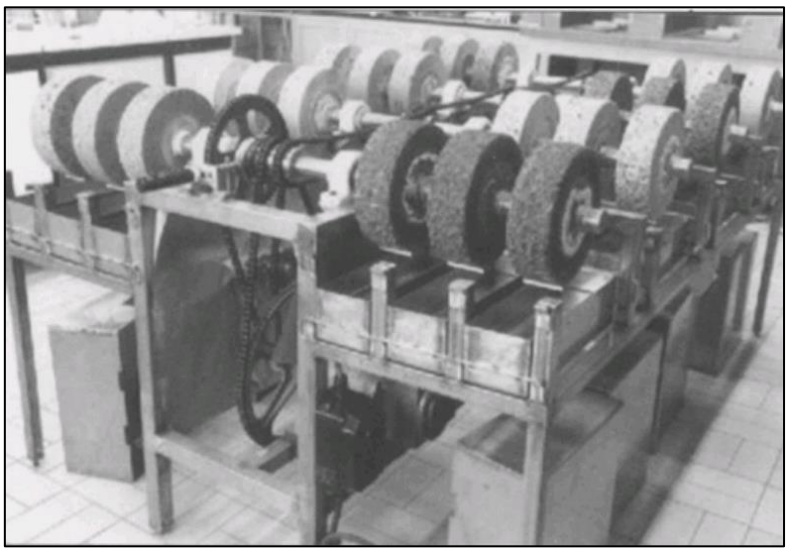

Figure 2-29: TAP testing rig (De Belie et al. 2002)

As the concrete cylinders are subjected to attack cycles (brushing, acid immersion and drying), measurements of the cylinder's radius are taken through the use of laser sensors. Through the use of data logging equipment and computer software, accurate measurement of changes in the radius and roughness of concrete specimens can be made.

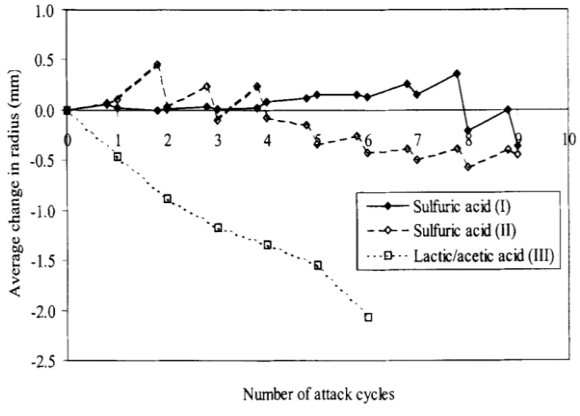

Figure 2-30: Change in radius vs the number of attack cycles (De Belie et al. 2002)

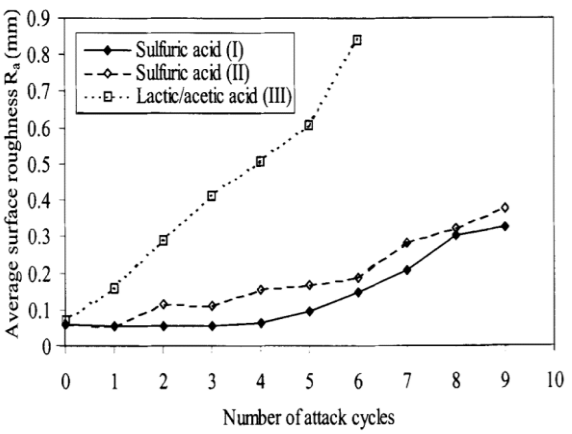

Figure 2-31: Average surface roughness vs the number of attack cycles (De Belie et al. 2002)

Figure 2-30 and Figure 2-31, show the results of a high sulfate resistant (HSR) Portland cement concrete mix (I and III) and HSR concrete mix with 30 kg/m^3 silica fume added to the mix (II) subjected to sulfuric acid and lactic acid.

2.5.4 Biogenic acid testing: The Hamburg chamber test (Fraunhofer Umsicht H_2S biogenic corrosion test)

An accelerated test, adequately simulating sewer conditions would be an ideal method to evaluate materials for sewer design. The Hamburg Chamber is purported to provide reliable results after one year of testing of testing and is used to assess various cementitious materials for use in concrete sewers (Saucier and Kaitano, 2018).

This test involves placing specimens in a chamber set to 98% relative humidity where the temperature is maintained at 30^o C. A variety of bacteria found sewers including species of sulfur-oxidizing bacteria and H_2S are deposited into the chamber along with nutrient solution to enable the biogenic production of sulfuric acid. This configuration is shown schematically in Figure 2-32 (Herrison and Saucier, 2015; Alexander, 2013). A biofilm is formed around the concrete specimens as the bacteria colonise the surfaces of the concrete test specimens.

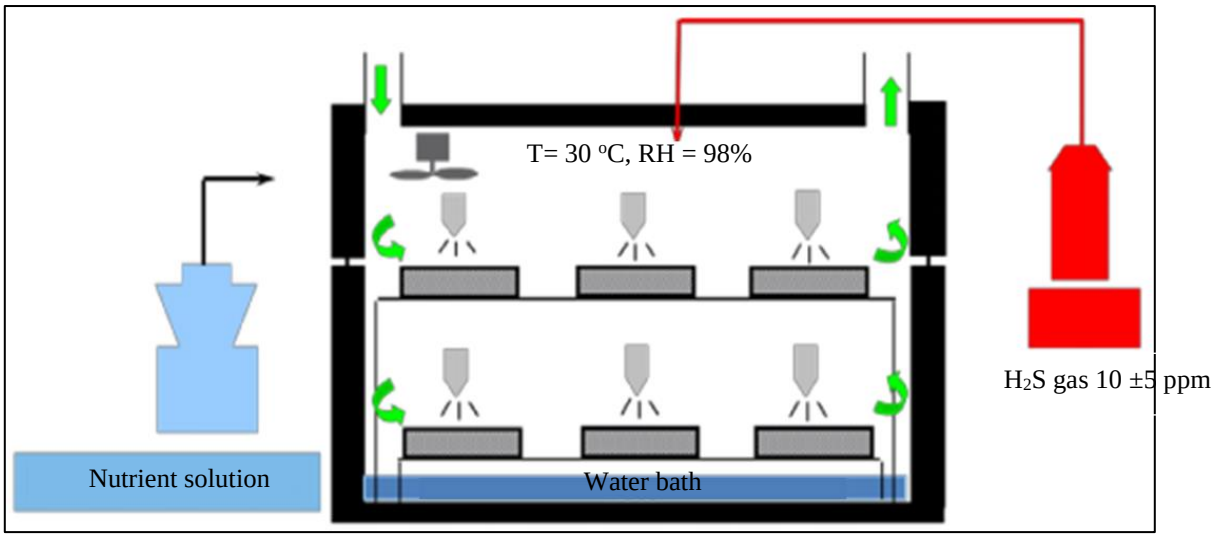

Figure 2-32: Fraunhofer UMISICHT H_2S biogenic corrosion test model (Herrison and Saucier, 2015)

Results from specimens subjected to the Hamburg chamber test for one year were compared to concrete specimens exposed in a live corroding sewer in the Hamburg area. The results data was correlated and it was calculated that one year in the Hamburg chamber was comparable to 24 years of exposure in the live reference sewer (Herrison and Saucier, 2015).

This test allows for specimen mass and surface pH to be monitored over the 12-month testing period. Evidence of the reliability of the Hamburg chamber is seen the tests results of various cement blends and calcium aluminate cements which are consistent with live sewer corrosion measurements at the Virginia experimental sewer (Alexander, 2013).

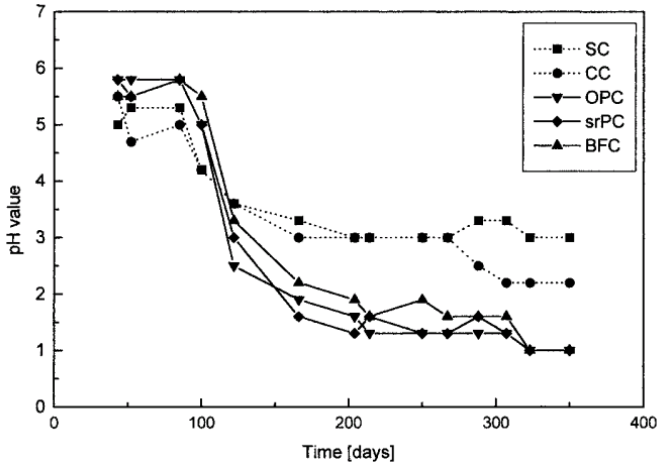

Figure 2-33: Progression of superficial pH on cementitious mortars in the Hamburg chamber test

Surface pH measurements of concrete specimens in the Hamburg chamber are used to explain the bacterio-static effect that is characteristic of calcium aluminate mortars. Tests results showed that the initial reduction in pH of Portland cements and calcium aluminate cements were relatively similar, however at about pH 4, the pH of CAC levelled off while Portland cement mortars continued to experience pH reductions to pH 1. The pH profile of calcium Aluminate cements at pH 3 coincides with the level at which $Al(OH)_3$ becomes soluble and the concentration of aluminium ions, which have a toxic effect on bacteria, increases (Herrison and Saucier, 2015).

2.5.5 Biogenic acid testing: Accelerated test for biodeterioration of cementitious materials

This test developed at Université de Toulouse, INSTA (Institut national des sciences appliquées de Toulouse) is more widely known as the BAC-test (Bacteria-Acid-Concrete test). However, in order to remain consistent with the cited work, the name of the test is cited as reported by Lavigne (2015).

This laboratory tested developed, by Lavigne et al. (2015) consists of inoculating the inner surface of cementitious linings in pipe products with a highly diverse microbial consortium (sourced from activated sludge collected from a sewage treatment plant) and in trickling a feeding solution, containing a reduced sulfur source over the inoculated surface. These conditions are ideal for sulfur oxidation by SOB, which results in acid-attack by biogenic sulfuric acid on the cementitious substrate.

Table 2-2: Principle tested in the TAP test and its corresponding real sewer condition.

Test principle	**Sewer environment condition being simulated**
Thermostated pipe segments with BSFC or CAC linings.	Sacrificial lining of concrete and metallic pipes using.
Activated sludge consortium inoculation	Sewer micro-bacteria (including SOB) colonisation of pipe
Reduced sulfur source (thiosulfate)	H_2S
Nutrients feeding	Nutrients available in biofilm and effluent
Aerated feeding	Release of gases in the sewer environment

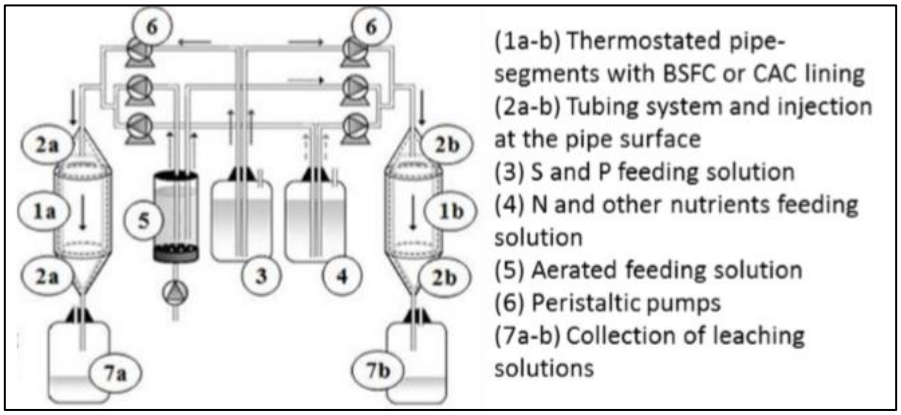

Figure 2-34: Accelerated test for bio-deterioration set up (Lavigne et al. 2015).

Test results are obtained by analysing the leaching solutions collected from below the pipe after the feeding solution has been trickled onto the surface of the pipe. By measuring the cumulative concentration of the hydrogen (H^+) and sulfate (SO_4^{2-}), the production of biogenic sulfuric acid is verifiable. These measurements may also be used to identify whether the cementitious material being tested is a favourable host to sulfur-oxidizing bacteria or whether bacterio-static material properties inhibit the production of sulfuric acid.

Measuring the concentration of calcium in the effluent indicates the severity of corrosion in calcium-rich binder systems such as PC mortars and CAC mortars. Using this test set-up, the researchers (Lavigne et al. 2015) make some important observations relating to the biogenic corrosion of CAC and a CEM III extended with GGBS in a study that lasted 120 days.

Lavigne et al. (2015) found that sulfate concentrations in the leaching solutions of both CAC and CEMII mortars showed an intensification of the kinetics of corrosion occurring in two distinct stages. The first stage (0-50 days) shows a parabolic increase in the sulfate concentration while stage (50-117d, matching pH≈ 3.5), the sulfate production was almost linear where the rate of sulfate production is used as a measure.

Where the leaching solutions were analysed for cumulative sulfate concentration, cumulate hydrogen ion concentration, and pH, no significant differences in trends were observed between the CAC lining and the CEM III linings.

However, where cumulative calcium concentration was measured, the CAC lining exhibited a significantly lower concentration of calcium than the CEM III (labelled as BFSC in a to d in Figure 2-35).

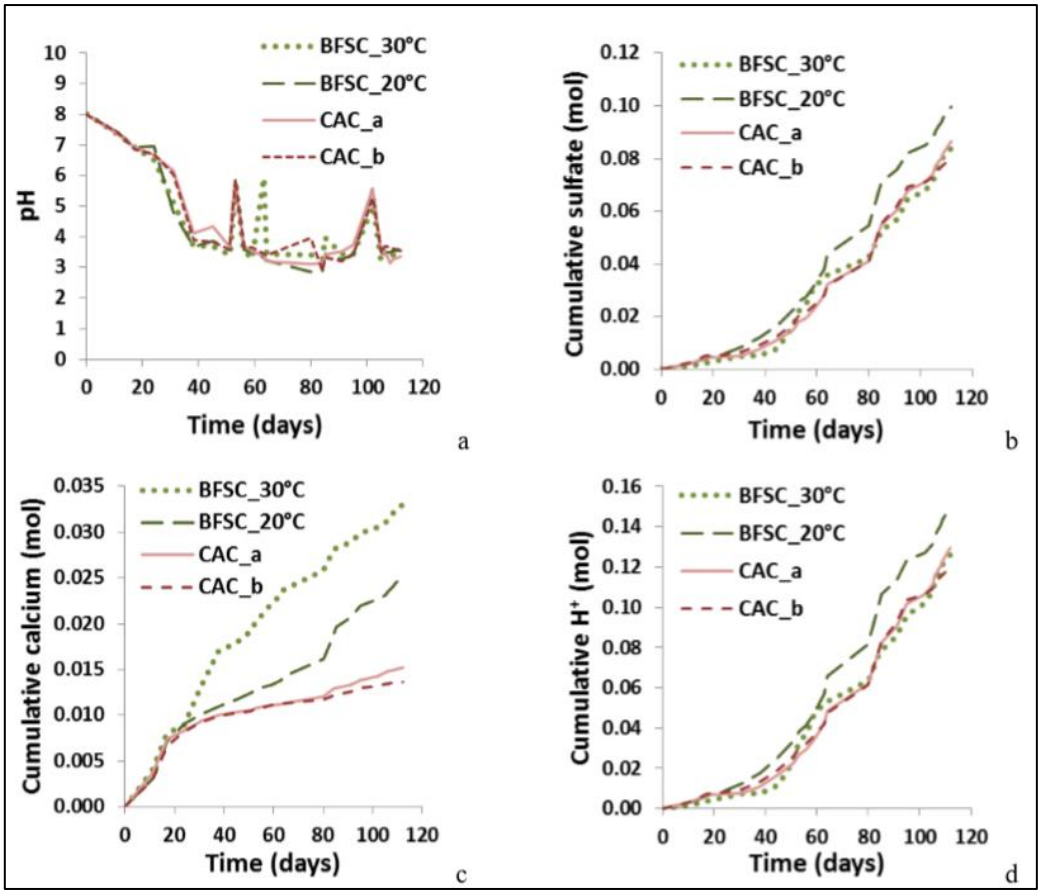

Figure 2-35: Evolution of a) pH, b) cumulative sulfate, c) calcium and d) H+ of the leaching solution according to time (Lavigne et al. 2015)

Leaching solution measurements were coupled with SEM and EDS analysis of the cementitious coatings after 120 days in the accelerated corrosion test. It was found that the chemical and microstructural evolutions of the cementitious linings were representative of those observed in a sewer environment, this included observations of gypsum at the surface and ettringite in the depth of the deteriorated lining in the test specimens.

While not mentioned by Lavigne et al. (2015), the data shown in Figure 2-35, does not indicate that CAC systems have a stifling effect on acid-producing bacteria even when the pH of the leaching solution was lower than 4. Figure 2-35-a shows that after 40 days of testing, for the most part, the pH of the leaching solution in both systems ranges between 3 and 4. If the bacterio-static effect as described by Herrison and Saucier (2013) holds, then the metabolic activity of SOB colonising the CAC mortar should be stifled and result in a reduction in sulfuric acid production. Therefore, an appreciable reduction of sulfate ions in the leaching solution should be observable when compared to the CEM III system. This expected difference is not observable in the data.

2.5.6 The Virginia experimental sewer (VES)

This live sewer, situated in the town of Virginia in the Free State province of South Africa, was built in 1988 and commissioned in 1989. Where pipe materials are concerned, the purpose of this experiment was to compare the performance of various pipe materials over time in a real sewer (Kiliswa, 2016). This sewer experiment was not limited to pipe material performance and valuable data on the sewer environment was also collected. The

experimental work has been in conducted in phases, with 3 phases of the research having been completed at this time.

2.5.6.1 Phase I

Phase I, which ran from 1988-1995 involved monitoring selected sewer pipe materials. Three categories of pipe were chosen, cementitious pipe, protected (lined) cementitious pipes and HDPE. Of interest to this review is the set of pipes manufactured from cementitious materials. They included concrete mixes of: Portland cement paired with siliceous aggregate (PC/Sil), Portland cement paired with calcareous aggregate (PC/Dol), calcium aluminate cement paired with siliceous aggregate (CAC/Sil) and an asbestos fibre cement composite mix.

Over the 7 years that the experiment ran, measurements of the pipe wall thickness revealed that; PC/Sil concrete pipes had lost up to 43% of their wall thickness, PC/Dol concrete pipes had concrete losses of up to 21% of their wall thickness, Asbestos-cement pipes lost up to 25% of their wall thickness, and CAC/Sil concrete pipe had section thickness losses of up to 14%. (Kiliswa, 2016).

2.5.6.2 Phase II

Phase II research, which ran from 1995 to 2003 attempted to do more than monitor results from the live sewer, but also to relate data in the sewer to a suitable laboratory test.

A new set of concrete core specimens (dia = 80mm, length = 150 mm) was placed in an IM (inlet manhole) at the sewer, just above the maximum effluent (tidal) line using plastic holders and monitored over time. The core specimens were all cementitious materials consisting of the following combinations of cement and aggregates (i) PC-dolomite (ii) blended PC/Silica fume-dolomite (iii) CAC with both Alag and dolomite aggregate and (iv) PC-dolomite with biocides such as silver copper and zinc.

Figure 2-36: Core specimens placed in the VES during phase II (Alexander and Fourie, 2011)

The results of this work showed that in the crown of the sewer, calcium aluminate cements were significantly superior to Portland cements. CAC outperformed PC concretes by a factor of 4 where high-quality dolomitic aggregates were used (Table 2-3).

Table 2-3: pH and mass loss of core specimens exposed to the sewer atmosphere over 17 months (Alexander and Fourie, 2011).

Mix Combination	Binder %	pH	Mass loss (%)
PC/SIL	14	-	4,14
PC/DOL -low quality	16	2,4	4,71
PC/DOL-high quality	18	1,44	6,3
PC (90%)/SF (10%) /DOL 2	16	2,4	4,72
PC/Ag-Zn-Cu (1%)/Dol 3	18	1,45	5,92
PC/SIL	23	6,7	6,09
PC/DOL-high quality	23	6,7	2,46
CAC/DOL -high quality	23	6,7	0,35
CAC/ALAG	23	7,14	0

2.5.6.3 Phase III

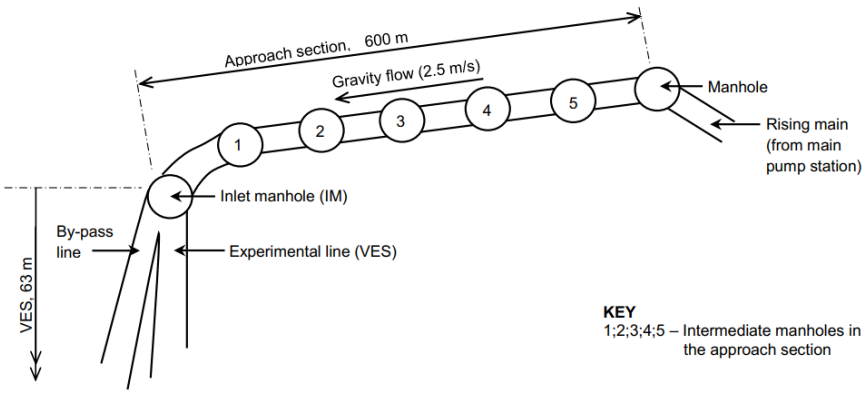

Figure 2-37: A schematic plan view of the Virginia Sewer (Kiliswa, 2016)

This initially involved placing short pipe lengths (900 mm diameter by 300 mm length) of various composition along a sewer line where microbially-induced corrosion was likely to occur (Figure 2-38). The top 120° of each pipe was cut to form 'lids', so that they were removable. The removable 'lids' enabled observations and corrosion data such as the mass loss on the lids to be collected (Kiliswa, 2016).

Figure 2-38: Lid removed for inspection at the VES (Kiliswa, 2016)

Figure 2-39: Series of pipe sections installed at the VES (Kiliswa, 2016)

The types of concretes tested in in this phase were classified by binder (cements) and aggregate type. Two binders, Portland cement and calcium aluminate cement were used while dolomitic and siliceous sand and stone were selected as aggregates. Mix designs of the various combinations are presented in figure 38 adapted from Kiliswa (2016).

The live sewer experiment has been of immense value in providing evidence for and against various claims about materials subjected to microbially-induced corrosion (MIC). Since the experiment has been running for more than 30 years it has been suggested that the "material factor", in the life factor method equation be derived from data obtained from the Virginia sewer (Goyns, 2013).

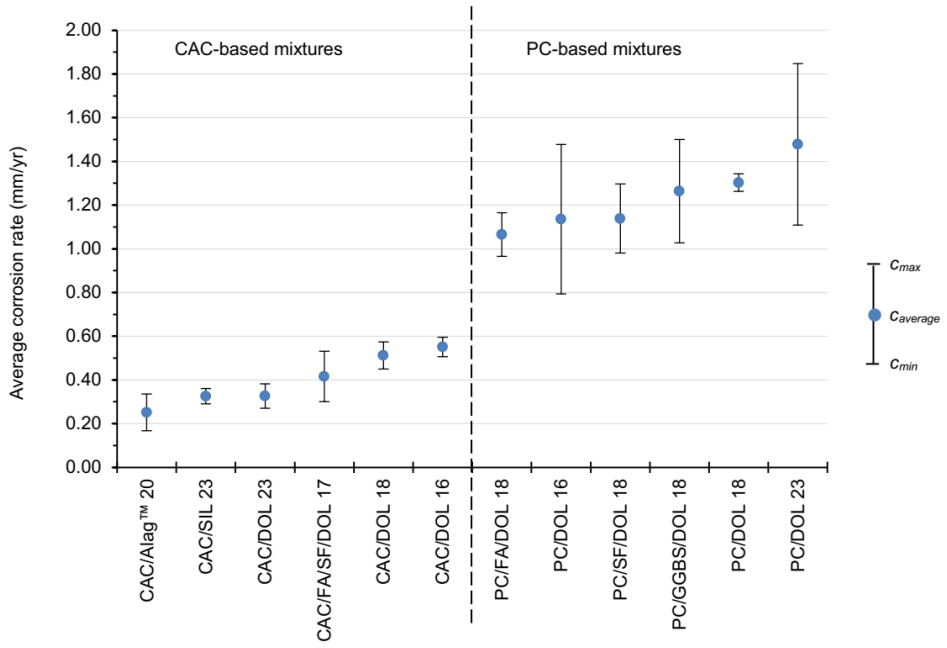

Figure 2-40: Manholes i, ii & iii: relationship binder content & estimated annual section loss of lids -over 6 year period from November 2008 to November 2014 samples in the sewer for 10 years (Kiliswa, 2016)

The most prominent finding of the live sewer experiment was the superior performance of calcium aluminate cements over Portland cements. Figure 2-40, provides a summary of the performance of the concrete mixes. The graph ranks the performance (in terms of loss in pipe thickness per annum) of the mixes from left to right in increasing order. As can be seen, CAC mixes outperformed Portland cement mixes by a significant margin, even in cases where calcium aluminate cements were paired with siliceous aggregates, CAC mixes performed better than Portland cement mixes with dolomite mixes (Figure 2-40). Goyns (2013) reports that PC/DOL mixes did not perform as well as anticipated because of the differential in solubility between the Portland cement binder and the dolomitic aggregate, which resulted in aggregate fall out.

Apart from comparing and ranking the performance of concrete mixes subjected to MIC, work from the VES can be used to determine the value of inputs to design codes such as the life factor method. Goyns (2013), states that the VES provides a reliable basis by which the material factor (MF) used in the life factor method can be extended to concrete mixes not utilising Portland cement.

2.6 Geopolymers and Alkali Activated Cements

A fundamental investigation of cement chemistry and material science is typically beyond the scope of the work of civil engineers. However, since differences are to be found in the literature concerning the underlying chemistry and terminology of geopolymers or alkali-activated materials, it is important to justify the selected of terminology and fundamental chemical model accepted in this work.

The two popular terms used in literature are geopolymers and alkali activated materials (AAM). Using these terms interchangeably is not advisable because there are divergent understandings of the chemistry of these materials (Provis and van Deventer, 2017). It is therefore important to review their respective definitions.

2.6.1 Geopolymers defined

Davidovits (2013,2017), who proposed the name geopolymers, suggested that geopolymers are ceramic-like inorganic polymers produced at low temperature, generally below 100^{o}C, consisting of chains of Mineral Molecules linked with covalent bonds, characterised by a well-defined size and molecular structure.

An alternative definition is provided by Provis et al. (2018) who suggest that geopolymers are a subgroup of alkali-activated materials (AAM's) that are characterised by low calcium content and exhibit a highly coordinated alumino-silicate binding phase. While this definition is not in conflict with the definition of geopolymers, Davidovits (2018) takes exception to AAM as an umbrella term because the chemistry of all AAM systems do not necessarily involve the formation of inorganic polymers.

A chemical model for geopolymers was suggested by Davidovits (2008) that involved geopolymer synthesis in either one of two routes, an alkaline environment or an acidic environment. Alkaline-based geopolymers have enjoyed the majority of scientific study while acid-based geopolymers have not received as much attention from researchers and have consequently not been developed as well.

The chemical character of geopolymers has been the subject of numerous studies. The basic building blocks of a geopolymer material are described by as 3-dimensional oligomer species (Silicon-oxo-Aluminate). Davidovits' chemical model describes the arrangement of silicon, oxygen, aluminium and alkali-metal ions in polymer structures in relation to the ratio of Silica (SiO_2) to Alumina (Al_2O_3) (Figure 2-47).

Alkali based geopolymers are the product of two sequential reaction steps (Davidovits, 2017):

1. Alkalination: where alumino-Silicate precursor materials are exposed to alkali metal hydroxides and results in the formation of "Oligomer" chemical species.
2. Oligomer poly-condensation: reaction where the Alkali metal hydroxide species react with the various oligomer species to form geopolymer molecular chains and water.

Other researchers such as Van Jaarsveld and van Deventer (2002) describe the formation of geopolymers in three main steps:

1. Dissolution with the formation of mobile precursors through the complex action of hydroxide ions.
2. Partial orientation of mobile precursors as well as the partial internal restructuring of the alkali poly-silicates and;

3. Re-precipitation where the whole system hardens to form an inorganic polymeric structure.

2.6.2 Alkali activated material (AAM) defined

Alkali activated material (AAM) is the broadest classification, encompassing essentially any binder system, derived from the reaction of an Alkali Metal Source and a dissolved silicate powder. (Provis et al. 2017).

Unlike geopolymers, AAM's are suggested to consist of gel-like structures which are in at least one mode of alkali activation (where the materials activated are high in calcium and silicon), not dissimilar to Portland cement C-S-H gels in that they form a calcium-aluminate-silicate-hydrate (C-A-S-H) gel systems (Palomo et al. 2014).

This gel is described as a three-dimensional inorganic alkaline polymer gel known as N-A-S-H (geopolymer) (Palomo et al. 2014). The formation of N-A-S-H gel is reported to be a fairly complex process which would include a series of stages that Palomo et al. (2014) summarise as follows:

- When the source of aluminosilicate comes into contact with an alkaline solution it dissolves into several species, primarily silica and alumina monomers.
- These monomers interact to form dimers, which in turn react with other monomers to form trimers, tetramers and so on.
- When the solution reaches saturation, an Al-rich, metastable N-A-S-H gel precipitates (called Gel 1) as an intermediate reaction product.
- As the reaction progresses, more Si-O groups in the source of aluminosilicate dissolve, raising the silicon concentration in the reaction medium and its proportion in the N-A-S-H gel (Gel 2).

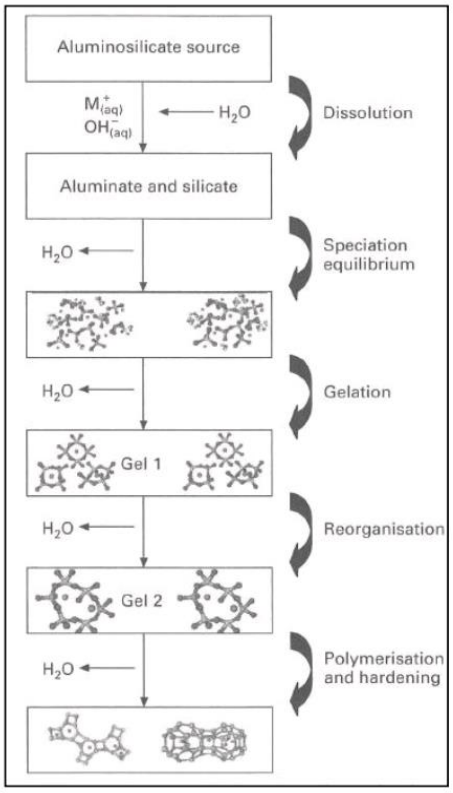

Figure 2-41: Chemical model for alkali activation as presented by Provis and van Deventer (2012).

However, these three steps can overlap with each other and occur almost simultaneously, thus making it difficult to isolate and examine each of them separately 1999 (Palomo et al. 1999).

This is in contrast to the theory of geopolymers which begin with the formation of oligomers which subsequently form polymers in alkaline milieu. Alkali activated materials are described as gels, which are materials with an indefinite amorphous compound with no known dimension (Provis et al. 2017).

There are differences in the understanding of these materials, and consequently, a widely accepted theoretical model of alkali-activated and geopolymer materials is yet to be achieved. What is clear from the literature is that AAM's refer to a significantly larger range of materials which typically form gels, whereas geopolymers refer to a narrow range of alumino-silicate based inorganic polymer materials.

2.6.3 Chemical character of geopolymers

An important consideration when referring a specific geopolymer is the nature of the raw materials used in producing the cements. Davidovits (2013) refers to groupings of geopolymer cement materials which are classified according to their starting raw-materials:

- Rock-forming minerals, alumina-silicates
- Amorphous silica
- And industrial by-products such as alumina-silicate rich coal fly ash and slag

These starting raw materials react may react in two different geopolymer synthesis routes:

2.6.3.1 Synthesis in alkaline medium

This is the most common form of geopolymer synthesis and typically involves the use of alkali metal hydroxides such as sodium hydroxide (NaOH). This work, except for the short description of acid-based geopolymers in the following subheading, will refer to geopolymers formed in an alkali medium as geopolymers.

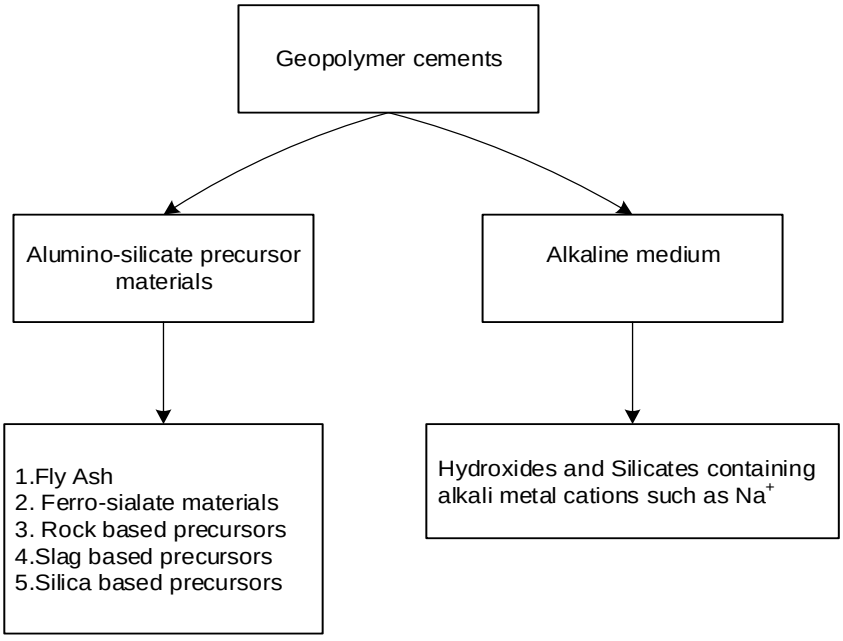

Figure 2-42: Alkali based geopolymer raw materials (Davidovits, 2013)

To understand geo-polymerisation in an alkali medium, it is apt to utilise the example of a geopolymer with a well-understood structure. A metakaolin based geopolymer that was synthesised by Davidovits in 1973. Meta-kaolin is an anhydrous form of the clay mineral kaolin achieved through heat treatment typically at temperatures below 800 degrees Celsius resulting in the calcination (de-hydroxilation) of the chemical structure of kaolin is shown in figure 16.

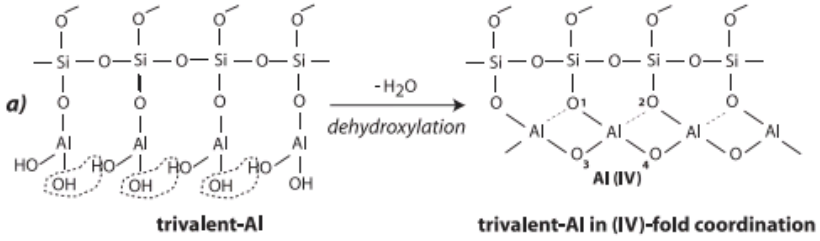

Figure 2-43: Dehydroxylation of kaolin to form metakaolin

Of significance, in this process is that while the aluminium atoms remain trivalent, they become tetra-co-ordinated when kaolin is calcined to form metakaolin. This chemical structure shown in figure 16 shows Al covalently bonded to 3 oxygen atoms with a pseudo bond to a fourth oxygen atom.

Once in this tetra-coordinated trivalent form, aluminium under the process of alkalination becomes tetravalent (Figure 2-44).

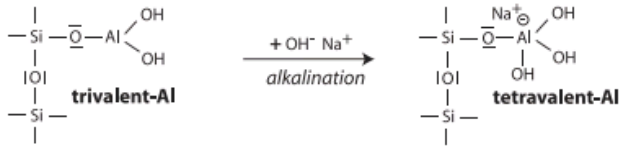

Figure 2-44: The effect of alkalination on metakaolin

Alkalination refers to the exposure of alumino-silicate precursors to alkali-metal hydroxides. When metakaolin is exposed to sodium hydroxide it forms a compound known as ortho-sialate (Figure 2-45). The term sialate is an abbreviated form for silicon-oxo-aluminate and is represented by the chemical structure in figure 19.

Sialate is a fundamental building block of geopolymers and is classified as an oligomer. Oligomers until recently were only hypothetical pieces to the puzzle of geopolymer synthesis, but were still used to explain subsequent geopolymer polycondensation reactions. The existence of oligomers was verified by North and Swaddle (2000) using NMR spectroscopy, where it was shown that the polycondensation reaction of the oligo-sialate species (figure 18, diagram #1) was occurring at a timescale of approximately 100 milliseconds (Davidovits, 2017).

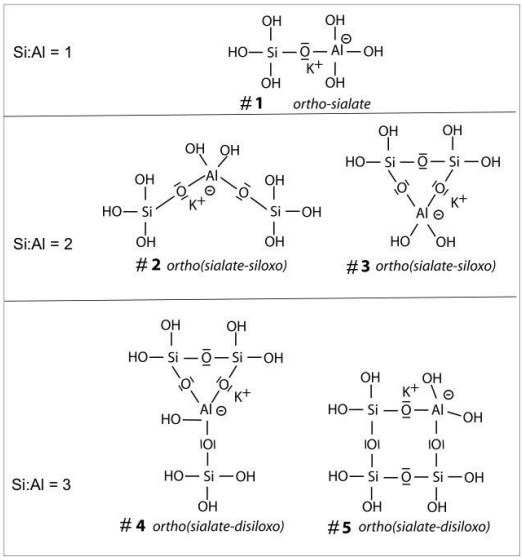

Figure 2-45: Oligomer Species suggested by Davidovits (1973), and identified by North and Swaddle (2000)

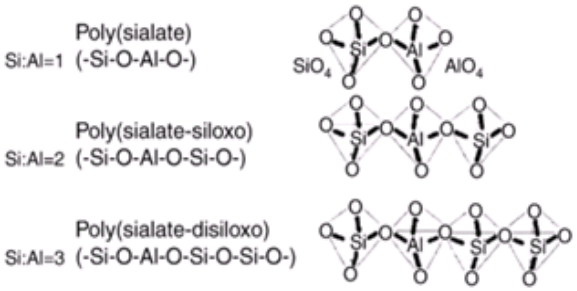

Figure 2-46: Geopolymers are characterised by molecular groups and categorised by their Si:Al (SiO_2:Al_2O_3) ratio (Davidovits, 2013)

Once Metakaolin has been "alkalinated" and oligomer species are formed, a polycondensation reaction, involving alkali metal-hydroxide occurs which produces a geopolymer ((Na, K)-poly-sialate, (Na, K)-poly-sialate-siloxo) and water (Figure 2-46).

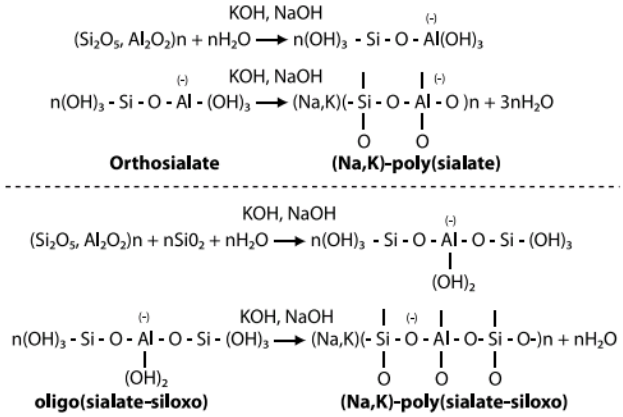

Figure 2-47: Geopolymer polycondensation of ortho-sialate and oligo(sialate-siloxo) species.

The chemistry of other geopolymer precursor materials such as fly ash is likely to be much more complex than the relatively pure geopolymer synthesis of metakaolin. The most investigated materials for use in geopolymers are largely industrial solid waste materials with a widespread of properties. Geopolymer synthesis of these materials is dependent on the properties of these raw materials which vary from source to source. The properties of fly ash, for instance, are dependent on the type of coal burned and the temperatures at which the coal fire power stations operate (Soto et al. 2013).

However, the chemical reactions that lead to the formation of metakaolin based geopolymers, it's chemical composition and structure may very well be useful in understanding how other geopolymers are affected by acid attack.

2.6.3.2 Synthesis in acidic medium

This mode of geopolymer synthesis is not as common and has received comparatively less research and development. Daviodvits (2013) demonstrated acid-based geopolymer synthesis through the use of phosphoric acid and organic carboxylic acids. Acid-based geopolymers are not considered in this study.

2.6.4 Nanostructure of geopolymers

Geopolymers at the atomic level form chains of alumina-silicate materials which agglomerate into identifiable macromolecules. Davidovits (2013) states that geopolymer microstructure is made up of geopolymer micelles, were a micelle is a macromolecule with a measurable size and molecular weight. Kriven et al. (2003) investigated the microstructure fully reacted K-poly(sialate) geopolymers using transmission electron microscopy (TEM) and scanning electron microscopy (SEM), it was found that the K-poly (Sialate) geopolymer consisted of nanoparticles that range between 5 and 15 Nanometres.

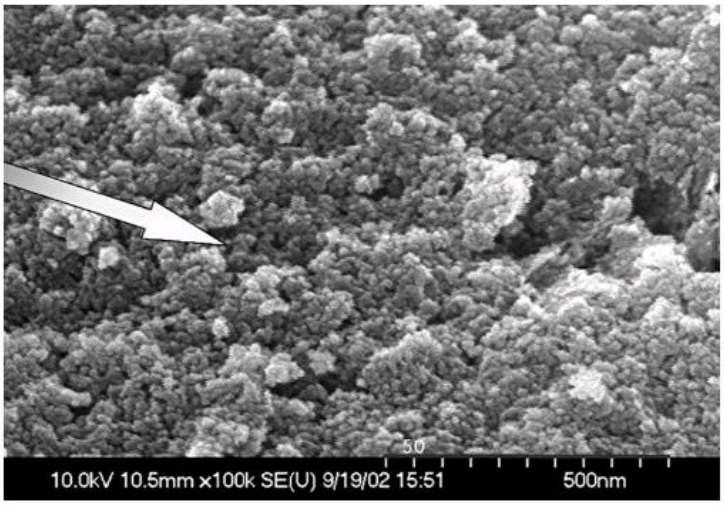

Figure 2-48: Scanning Electron Microscopy image of geopolymer micelles (Kriven et al. 2003).

The discovery of geopolymer micelles has not been restricted to metakaolin based geopolymers, Sindhunata et al. (2006) found similar geopolymer micelles in the microstructure of a fly ash based geopolymer, through the use of scanning and transmission electron microscopy (SEM and TEM). A characteristic of the microstructure of geopolymers is the size of micelles, which measure between 5 and 20 nanometres, and their connected structure which forms nano-channels and pores (Davidovits, 2017).

2.6.5 Fly ash based geopolymers

Fly ash based geopolymers cements are likely to be a viable alternative Portland and calcium aluminate cements because of the abundance of fly ash and it's relatively low cost as a raw material. Since fly ash comes about as a by-product of coal combustion, it can be highly variable as it is inherently heterogeneous consisting of both crystalline and amorphous phases each with unique reactivity in the concrete environment (Chancey et al. 2010).

In the South African context, fly ash is a bulk material which mainly comes from the combustion of coal at coal-fired power stations. The total output of fly ash from coal-fired electricity generation is estimated to be about 36 million tonnes per annum, making it one of the most voluminous waste materials produced in the country (Reynolds-Clausen and Singh 2016). However, about 78% of the ash is currently unavailable for reuse because it is used for the treatment of water/effluent from Eskom's operations, thus reducing the available amount 5 million tonnes per annum.

The majority of all recycled fly ash is used in the blending of Portland cements and thus its standardisation has been geared towards its utility in cement. SANS 50 450: Fly ash for concrete (2012), defines fly ash as a fine powder material mainly consisting of spherical glassy particles, derived from the burning of pulverised coal, with or without combustion materials, which has pozzolanic properties and consist essentially of Silica (SiO_2) and alumina (Al_2O_3).

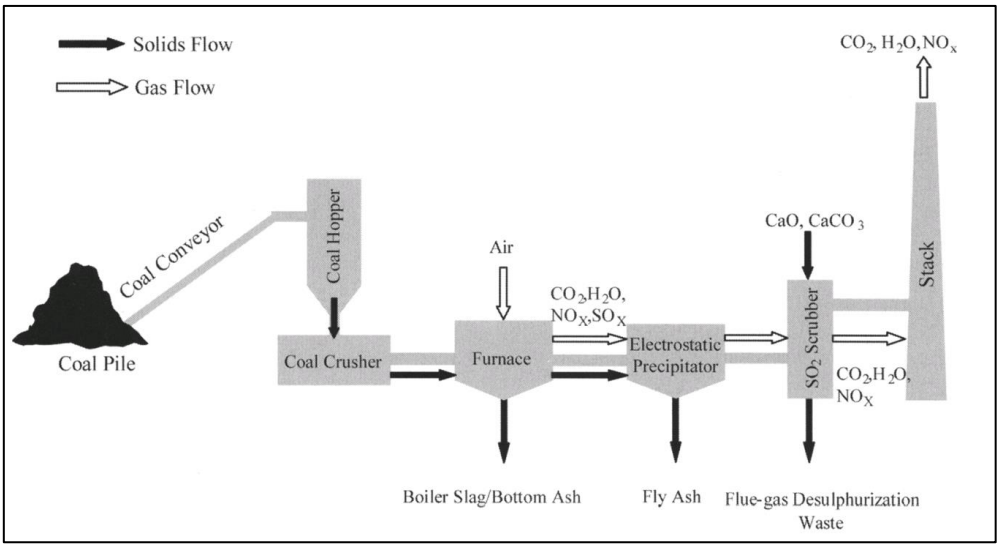

Figure 2-49: Production of fly ash coal-fired power station (adapted from Tishmak and burns 2016)

This definition may fall short for geopolymer cements since they do not require any pozzolanic properties from fly ash because geopolymer synthesis does not rely on chemical reactions with cement hydration products to form compounds possessing cementitious properties.

2.6.5.1 Classification of fly ash

Internationally, the standard ash classification most referred to in research is ASTM 618, which makes a distinction between high and low calcium fly ashes. Low calcium fly ash (Class C) is characterised as having less than 5% Calcium oxide while high calcium fly ash (Class C) has more than 5% calcium oxide by mass of fly ash.

South Africa's fly ash suppliers categorise their fly ashes using the SANS 50450 standard: "Fly ash for concrete" which categorises ashes according to fly ash particle size properties.

SANS 50 450 designates:

- Category N: the fineness shall not exceed 40 % by mass, and it shall not vary by more than ± 10 percentage points from the declared value.
- Category S: the fineness shall not exceed 12 % by mass. The ± 10 percentage points fineness variation limits are not applicable.

Where fineness of fly ash is expressed as the mass proportion in per cent of the ash passing through a 0,045 mm mesh sieve.

2.6.5.2 Fly ash as a geopolymer precursor material

The suitability of fly ash as a geopolymer precursor stems from its alumina-silicate rich composition. The most abundant chemical compounds in fly ash are SiO_2 and Al_2O_3, which are key ingredients for the formation of oligomers and their subsequent poly-condensation reactions.

Table 2-4: Chemical composition of fly ash (Tishmak and Burns, 2016)

Chemical Component	Fly Ash (wt%)	Bottom ash (wt%)
SiO_2	45.5-57	20-60
Al_2O_3	18-33.7	10-35
Fe_2O_3	6.85-16	5-35
CaO	2.8-10	1-20
MgO	1-5.5	0.3-4
SO_3	0.75-3.3	0.1-12

Besides the requirement for an alumina-silicate rich material, the amenability of fly ash to geopolymer synthesis is also determined by its amorphous (glassy) phase content. The amorphous phase of fly ash is defined as a phase lacking the range order of crystals. Davidovits (2013) states that reactivity of fly ash in turn determined by the operating temperatures at which coal is burned in the boiler.

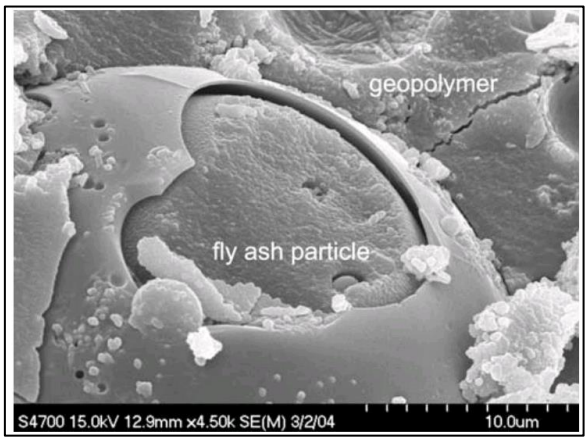

Figure 2-50: Interface between geopolymer micelle matrix and a fly ash particle (Skvara et al. 2006)

2.6.6 Carbon footprint of fly ash based geopolymer concretes

With greater emphasis being placed on the effects human beings have on the climate, the idea that carbon dioxide emissions have a strong bearing to earth's climate and in particular, it's warming, has gained wide acceptance amongst scientists. Before any attempt can be made to assign carbon footprint values to geopolymers or alkali-activated cements, some context is necessary.

The proprietary nature of many geopolymer formulations at the current time ensures that the constituents and proportions of these materials are not openly published. This requirement for secrecy, and the wide array of raw materials utilised in geopolymer cements makes accurate general calculations of the footprint of geopolymers impossible.

Raw materials, such as alkali silicates and metal hydroxides are, at the current time, sourced mainly from a few industrialised countries in the world. For instance, alkali silicates are mainly sourced from the USA, China, India and the UK (Davidovits 2015). Therefore, the determination of a geopolymer's carbon footprint, has to include a transport emissions component which is dependent on the location at which the geopolymer is constituted (Turner and Collins 2013).

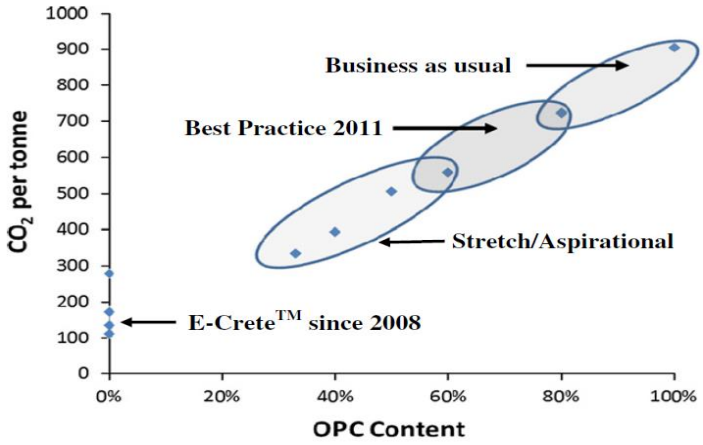

Figure 2-51: Carbon emissions per tonne of cementitious materials produced (Provis and van Deventer 2012)

Figure 2-51 shows a carbon footprint comparison of OPC cement and a commercially available geopolymer cement (E-Crete™) undertaken by the Australian CSIRO and the University of Melbourne. It was found that fly ash-based geopolymers enabled a 5-fold energy efficiency improvement and an 80% reduction in CO_2 emissions when compared to CEM 1 Portland cement. These improvements in energy efficiency and CO_2 reduction are attributed to the fact that high temperature calcining is not needed for geopolymer production, thereby saving on energy and the unwelcome release of CO_2 emanating from the chemical reactions involved in the calcination of limestone (Smith, Hargroves and Desha 2016).

Scrivener (2014) casts doubt on the sustainability of both AAM's and geopolymers, stating that these materials offer at best, a slight reduction in the carbon footprint when compared to Portland cement, and that they are less desirable than Portland cements with respect to other environmental impact categories. A key concern for Scrivener (2014) is that the geopolymer pre-cursor materials are the same materials used as supplementary

cementitious materials (e.g. fly ash) and these are available in relatively low quantities when compared to cement clinker.

Scrivener's (2014) analysis emanates partly from work undertaken by Harbert et al. (2011), whose own analysis was based on European conditions. In the European context, Harbert et al. (2011) concluded that "when the production of fly ashes and granulated blast furnace slags is taken into account during the life cycle assessment (using either an economic or a mass allocation procedure), it appears that geopolymer concrete has a similar impact on global warming to standard concrete".

However, the methods used to get to these findings are worth some scrutiny. The differentiating factor, when compared to South African conditions, would be that Harbert et al.'s (2011) method allocated the entire CO_2 footprint of fly ash geopolymer cement. While this may be suitable for the European situation, it is not as applicable in South Africa, where the primary driver of fly ash production is the generation of electric power. As reported by Reynolds-Clausen and Singh (2016), fly ash production from power generation exceeds 36 million tonnes per annum. This value far exceeds the annual production capacity of cement clinker in South Africa, which was reported in 2018 to stand at 21 million tonnes per annum (Arp et al. 2018). Furthermore, fly ash produced by Eskom is classified as waste by the South African government's Department of Environmental Affairs, which classifies waste materials according to SANS 10234:2019: "Globally harmonized System of classification and labelling of chemicals (GHS)."

Therefore in cases where fly ash (a waste whose generation is primarily due to power generation) is used as an ingredient for geopolymer binders, the embodied energy and carbon footprint of the ash should be attributed to the process of coal fired power generation and not to the manufacture of fly ash based geopolymer cements. If this principle is accepted then then the analysis by Provis and van Deventer (2012) shown in Figure 2-51 holds true.

2.6.7 Carbonation of fly ash based geopolymer concretes

Carbonation is responsible for an initial lowering of the pH in Portland cement concrete which stimulates microbially-induced corrosion, making it possible for a succession of sulfur-oxidizing bacteria to colonise the pipe (Ismail et al. 1993). Therefore, it may be worthwhile to understand the effect of carbonation on geopolymers as well.

Provis and Winnefeld (2018), exposed alkali-activated materials to accelerated carbonation found that these binders were also susceptible to carbonation. Measurements of the initial (uncarbonated) pH of low calcium fly ash based geopolymer concretes was found to range between 11-11.5 (Khan et al. 2016). Compared to the uncarbonated pH of Portland cement which typically exceeds 12.5, because the pH is a logarithmic scale, geopolymers exhibit substantially lower alkalinity in their un-carbonated state than Portland cement. (Khan et al. 2018; Provis and Winnefield 2018).

The products of carbonation were studied by Khan et al. (2016), were low calcium fly ash based geopolymer concretes were subjected to carbonation in an accelerated carbonation chamber where the concentration of CO_2 gas was varied between 1% and 3% over 1 to 6 weeks. The temperature and humidity in the chamber were kept at 23^{o}C and 55% respectively.

Khan et al. (2016) analysed carbonated geopolymer pastes using X-Ray diffraction. Their study found that in fly ash based geopolymers the primary carbonation reaction products, were mineral phases of sodium carbonate (Na_2CO_3). These phases consisted of soluble salts which were easily readily out with the effect of increasing the porosity of the affected concrete. The two major phases of sodium carbonate identified were natron ($Na_2CO_3 \cdot 10H_2O$) and nahcolite ($NaHCO_3$).

Given the wide range of mix designs applicable to alkali-activated materials and geopolymers (Pasupathy et al. 2016) found carbonation rate of geopolymer concretes highly depends on the mix design of materials. In particular, fly ash-based alkali-activated materials activated using sodium silicate showed poor resistance against carbonation compared to Portland cement concrete. Bakharev et al. (2001) studied the carbonation behaviour of alkali-activated slag concrete where it was found that alkali-activated concretes were more susceptible to carbonation than ordinary Portland cement concretes.

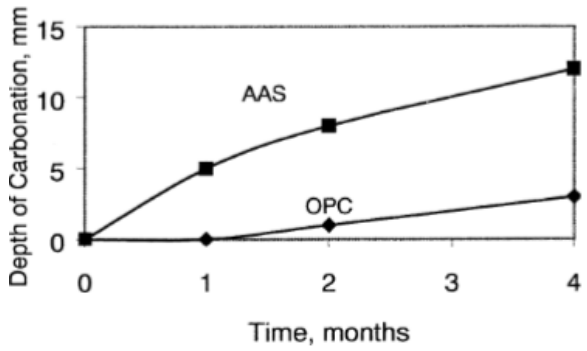

Depth of carbonation in Alkali activated slag cements and OPC concretes exposed to an atmosphere containing 20% CO_2, 70% relative humidity (Bakharev 2001)

Findings by Criado et al. (2005) suggest that the degree to which alkali-activated precursor materials and geopolymers have reacted or polymerised has a bearing on the carbonation resistance of these materials. Their investigation found that curing conditions play a significant role in the carbonation of geopolymers at an early age. Furthermore, carbonation of geopolymers at early age affects the strength development geopolymers, were well cured geopolymer concretes exhibit higher strengths than poorly cured carbonated concretes. Criago et al. (2019) describe the ideal curing regime as one where specimens are not exposed to high humidity and atmospheric carbon dioxide.

2.6.8 Acid resistance of geopolymer cements and concretes

2.6.8.1 Mineral acid effect on pastes

Fly Ash based geopolymers are cementitious materials which utilise pulverised fuel ash (PFA) or fly ash as the alumina-silicate precursor source. Van Deventer et al. (2012) assessed the composition of alkali-activated cement (AAC) pastes using scanning electron microscopy (SEM) and energy-dispersive-x-ray spectroscopy (EDS).

A ternary binder composition chart for low calcium geopolymers, high calcium geopolymers, Portland cement, fly ash and ground granulated blast furnace slag was plotted. The ternary plot shows that low calcium geopolymers are mainly constituted by alumina (Al_2O_3) and silica (SiO_2).

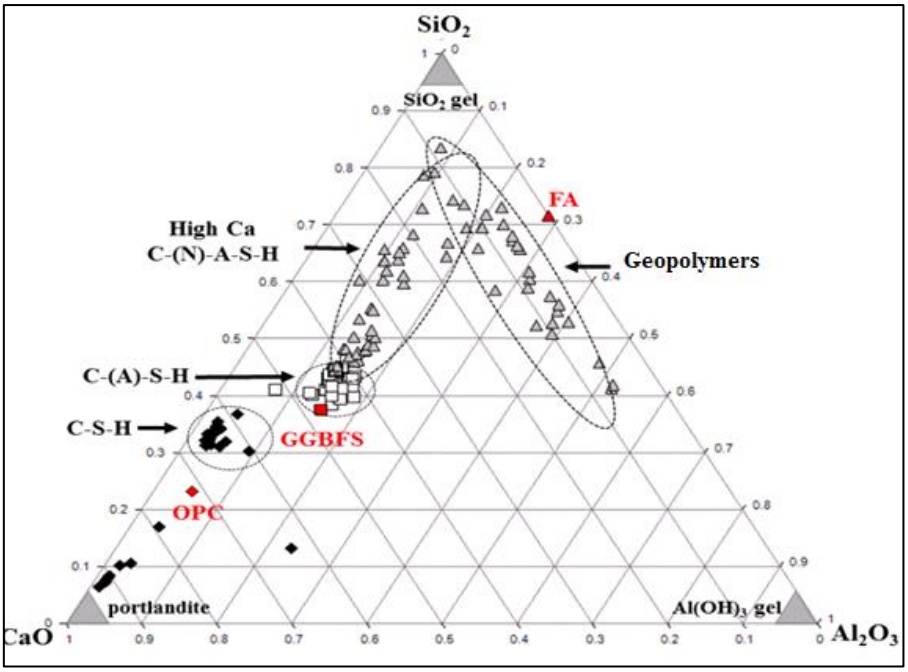

Figure 2-52: Ternary plot of binder gel compositions measured by SEM-EDX after 28 days of curing of OPC, and AAC (geopolymer) pastes (van Deventer et al. 2012)

While the calcium content in Portland cements is high and cements hydration product susceptibility to acids is well understood, an advantage of geopolymers is that they may be produced with materials that have low calcium content (Figure 2-53). The resistance of geopolymer cements to mineral acid tests has received a fair amount of study. However, a fact that must be re-iterated is that geopolymer and alkali activated cement formulations are not standardized as yet, and thus, any insight from the literature relates to the specific materials tested in the cited studies.

Bakharev (2005) investigated the durability of geopolymer materials manufactured using a class F fly ash (FA) and alkaline activators when exposed to 5% solutions of acetic and sulfuric acids.

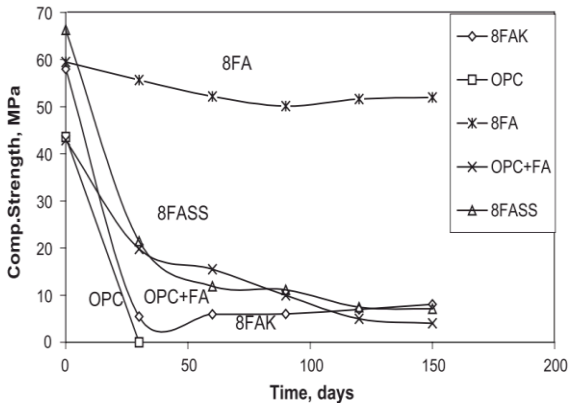

Figure 2-53: Effect of immersion in 5% sulfuric acid on the compressive strength of geopolymer concrete and Portland cement concrete.

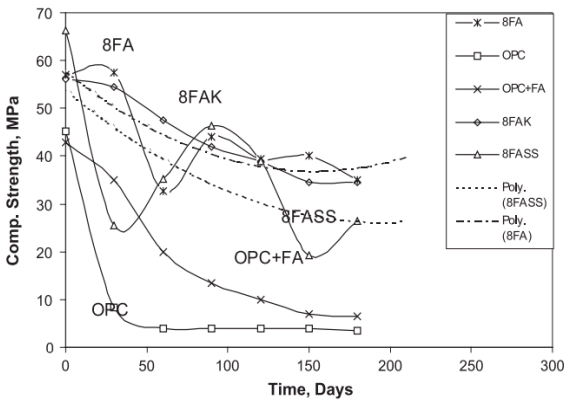

Figure 2-54: Effect of immersion in 5% sulfuric acid on the compressive strength of geopolymer concrete and Portland cement concrete.

This study demonstrated the mechanical integrity of geopolymer cement pastes exposed to acids were diminished at lower rates than Portland cement and Portland/fly ash cement blends. Portland cement samples were shown to be completely deteriorated in the first month of the test and PC + FA samples had 77% strength loss and were severely deteriorated.

Song et al. (2005) also conducted continuous immersion tests on geopolymer and Portland concrete specimens. Residual compressive strength and mass loss measurements were conducted over a course of 65 days. This test showed that the Portland cement concrete specimens had lost more than 50 percent of their mass by the 28th day of immersion while the fly ash based geopolymer specimens had lost only 3% of their mass at 56 days (Song et al. 2005).

Figure 2-55: Appearance of concrete specimens exposed to 10% sulfuric acid immersion for up to 56 days (Left: Portland cement concrete specimen, Middle and right geopolymer cement specimens). (Song et al. 2005)

Bakharev (2005) concluded that alkali-activated slag and fly ash materials exhibited better acid resistance than Portland cement, retaining 75% of their original strength after 150 days of exposure to 5% concentrations of acetic acid whereas Portland cement concrete specimens lost all their compressive strengths within 40 hours. Higher stability of alkali-activated binders (geopolymers) under acetic acid attack was attributed to lower initial permeability, higher alkalinity of the pore solution, and a low CaO/SiO_2 ratio in the alkali activated fly ash system (Bernal and Provis, 2014).

2.6.8.2 Geopolymer chemical reactions with acids

The effect of acids on geopolymers is dependent on the acid strength and may involve the following chemical reactions (Grengg et al. 2018).

- An ion exchange between the penetrating acid protons (H^+) and the charge compensation cations of the geopolymer network.
- Dissolution of tetrahedral Al from the alumina-silicate framework by breaking of Si-O-Si bonds and formation of water as a by-product resulting in an increase in solution pH
- Crystallisation of zeolites (a large group of minerals consisting of hydrated alumino-silicates of sodium, potassium, calcium, and barium).

Bakharev (2005) attributes deterioration of geopolymers in acidic milieu to the depolymerisation of alumino-silicate polymers, liberation of silicic acid, replacement of Na^+ and/or K^+ cations by hydrogen (H^+) or hydronium ion ($H_3O^{+)}$ and the de-alumination of the geopolymer structure. It is also connected to precipitation of siliceous polymers and zeolites, which in some cases lead to a significant loss of strength (Bakharev 2005).

Table 2-5: Acid-Base reactions, compounds dissolved and precipitates formed (Adapted from Grengg et al. 2018).

Acid-Base Reactions	**Binder types**		
	Ordinary Portland cement	**Calcium aluminate cement**	**Low Ca-geopolymers**
Dissolution	Unreacted cement;	CAH_{10}	Unreacted precursors
	$Ca(OH)_2$	C_2AH_8	Na+/K+
	Ca from C-S-H gel;	C_3AH_6	Al and Si from GP gel/framework
	Al-Fe-hydrates	AH_x	
	$CaCO_3$	Fe-hydrates	
Precipitation	$CaCO_3$;	$CaCO_3$	Carbonates
	S^o	AH_x	Sulfate salts
	Sulfate Salts	Sulfate Salts	Zeolites
		S^o	S^o

A proposed explanation for the acid resistance of geopolymers is the formation of a highly siliceous framework that is relatively hard but brittle, which follows the dissolution of aluminium from the geopolymer framework replaced by Si. This siliceous layer could effectively inhibit the process of corrosion by acting as a barrier to the transport of acid protons as well as dissolved constituents (Grengg et al. 2018).

Fundamental chemical studies on the effect of acids on geopolymers are minimal, some researchers believe that the degree of intrinsic ordering of the geopolymer gel has a strong bearing on the durability of geopolymer cements and their resistance to acid attack (Grengg et al. 2018, Bakharev 2005).

A key concern in concrete durability is the nature of the chemical products resulting from chemical attack, little is reported concerning volume change and solubility of the corrosion products formed by the reaction of sulfuric acid and geopolymer concretes.

2.6.8.3 Influence of aggregate type on the resistance of geopolymer concretes

While geopolymers pastes are reported to exhibit higher resistance to acid attack, to optimise the durability of geopolymer concrete, an approach to selecting a suitable aggregate should also be sought.

Alexander and Mindess (2005) state that the advantage of selecting a compatible aggregate is due to the acid attack being spread over both the aggregate and cement paste phases. This principle has been successfully implemented where calcium-rich binder systems such as Portland cements and calcium aluminate cements have been paired with calcareous aggregates.

However, results from the Virginia experimental sewer (VES) show that this compatibility is seldom optimal. Goyns (2013) reports that while OPC concrete using dolomitic aggregate performs better than OPC concrete using siliceous aggregate, it is not as effective as the theory based on the alkalinity value of the concrete as given in the literature on the LFM predicts. This is because the acid-solubility of dolomite is significantly less than that of

cement and hence there is a difference in their corrosion rates due to the relative rates of acid solubility resulting in some aggregate fallout".

Given that siliceous aggregates such as quartzite are known to be virtually immune to acid attack (Alexander and Mindess 2005), research on the compatibility of various geopolymer binders with both calcareous and siliceous aggregates of varying solubility. Little study has sought to apply the same principle to geopolymers and alkali-activated cements.

2.6.8.4 Effect of geopolymers on biofilm growth in the sewer environment

A study by Druga et al. (2018) assessed the affinity of sewer micro-organisms to various cementitious substrates. Four types of mortar specimens were submerged in the effluent from the clarifier of a waste-water treatment plant for 35 days. The mortar specimens were prepared using a Metakaolin-based geopolymer, a Metakaolin-based geopolymer doped with copper, Portland cement and a calcium aluminate cement.

This affinity would be assessed through the measurement of the following microbial activity indicators:

- Protein concentration via the use of the "Total Protein Kit" (Sigma-Aladrich kit, Missouri, USA) and serum almumin for the standard calibration curve.
- Bacterial respiration via the use of the Oxitop Control ® system. Each specimen with biofilm on its surface was immersed in special 200mL vessels containing artificial, oxygen saturated wastewater, to which acetate and ammonium sulfate were added as a substrate. Thereafter the oxygen uptake was measured indirectly by tracking the pressure decrease in the headspace of the device for 12 hours.

After 35 days of immersion in the effluent, the mortars were removed and subjected to protein concentration, bacterial respiration measurements and scanning electron microscopy.

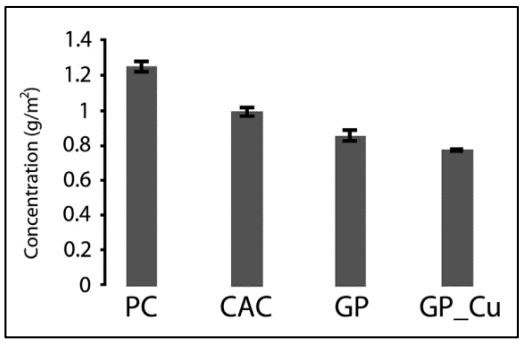

Figure 2-56: Protein concentrations on the surface of mortars studies by Druga et al. (2018)

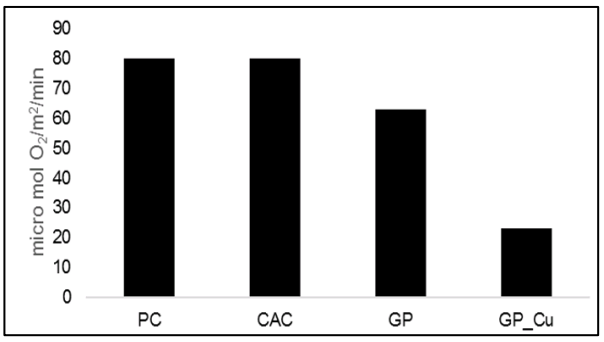

Figure 2-57: Bacterial respiration as measured by Druga et al. (2018) on the surfaces of mortars.

Both bio-receptivity tests (protein concentration and bacterial respiration) indicate that geopolymer mortars were less hospitable to sewer micro-organisms than Portland cement and calcium aluminate cements (Druga et al. 2018). While not providing a comprehensive picture this recent study is one of the very first published attempts to assess the affinity of sewer micro-organisms to geopolymers.

2.7 Discussion and conclusions

This review has considered the problem of MIC in sewers from four vantage points, they include; (i) the causes of MIC, (ii) methods of mitigating MIC, (iii) methods of assessing acid resistance of sewer pipe materials to MIC and (iv) geopolymers and their potential as acid-resistant cementitious materials for use in sewers.

2.7.1 Causes of MIC

If it were possible to eliminate sulfur from the sewage system, MIC could be avoided at its source. Sulfur and its compounds, particularly sulfate, which is at the genesis of the process of MIC, are naturally occurring in rocks, soil, and natural watercourses. Sulfate is also deposited into the sewer network by various man-made systems.

Research by Pikaar et al. (2014) suggests that a significant portion of sulfate found in effluent emanates from aluminium sulfate used in the treatment of water in purification plants, and that by substituting sulfate bearing coagulant chemicals for alternative coagulants, the problem of H_2S in sewer systems could be drastically reduced, and by extension so would MIC.

However. Pikaar et al.'s (2014) research did not relate sulfate concentration to actual corrosion data from sewers, instead, a mathematical model was used to estimate corrosion rates sewers where source water treatment included the use of aluminium sulfate coagulant and where alternative coagulants were used. The use of mathematical models instead of real sewer data or experimental data brings the integrity of the findings into question because findings are highly dependent on the quality of the models used.

The first biogenic process occurs when sulfate is reduced to form sulfide in solution by SRB. This process is strongly influenced by complex natural and man-made systems namely; sewer atmospheric conditions, sewer hydraulics and effluent characteristics.

The second biogenic process relates to sulfur oxidation. The critical path of processes involves; (i) the initial moderate lowering of substrate pH, (ii) the continued decrease in pH with the appearance of a succession of neutrophilic SOB and (iii) the emergence of acidophilic SOB, the oxidation of H_2S gas into H_2SO_4 and the development of severe concrete corrosion (Okabe et al. 2016)

The sewer biome is known to be highly complex and the composition of micro-organism populations in the sewer environment seem to vary significantly from location to location. Okabe et al. (2016) only found 2 (*T. thioparus and T. novellus*) species of sulfur-reducing bacteria in a sewer in Japan whereas studies from elsewhere suggest that 5 species of sulfate-reducing bacteria are responsible for the oxidation of sulfate into sulfide. The same can be said about SOB, as Cayford et al. (2012) discovered that a*cidithiobacillus* species was missing in the majority of corroding sewers in their Australian study. The results from that study showed that t*hiobacillus* species were prominent in only one sample and made up less than 3 per cent of the populations in the other sewers.

The complexity of the sewer system at the biological level also raises numerous unanswered questions regarding the effects of reducing the amount of inorganic nutrients from various sources including urine on sewer micro-organisms.

This part of MIC is very complex. As shown in the literature, generalisations on the composition of micro bacteria in sewers, both SRB and SOB are likely to fall short of reality.

2.7.2 Methods of mitigating MIC

The approaches to dealing with the problem of MIC reviewed in this study can be summarised in the following methods.

1. Reducing the quantities of sulfates and organic nutrients in sewer effluent (Pikaar et al. 2014, Johnnson 2000). Treatment of sewer effluent to avoid the production of H_2S, either through exterminating sulfur-reducing bacteria (SRB) or by reacting sulfides in solution with chemicals that produce precipitates. (Zhang et al. 2008, Gutierrez-Padilla et al. 2010, Rava 2013).
2. Avoiding unnecessary depletion of dissolved oxygen by designing for effluent flow regimes that allow for aeration of the effluent. Where sulfide build-up is unavoidable (e.g. in rising mains) designs that minimise opportunities for H_2S to be released into the sewer atmosphere are recommended (Goyns, 2013).
3. Where gaseous H_2S has been released, solutions to biogenic corrosion may include inhibiting the production of biogenic sulfuric acid through dosing chemicals toxic to bacteria into site of biogenic acid production (Rava 2013) or using pipe materials with toxic effects on sulfur-oxidizing bacteria (Saucier and Herrison 2015).
4. Where sulfur oxidation is in effect and biogenic sulfuric acid is generated, the use of fully acid-resistant materials, such as organic polymer materials (HDPE, PVC etc) or concretes with bacteria inhibiting properties are available. Where cost and performance need to be balanced, the use of aggregates and cements with compatible rates of corrosion, which ensure even corrosion between aggregate and paste phases of the sacrificial lining in the concrete pipe (Alexander and Fourie 2011, Goyns 2013).

The approaches listed in points one and two are interventions which may not only have a bearing on the sewer longevity but on broader environmental concerns associated with the sulfur cycle, such as reducing dangerous H_2S levels along sewer pipelines and the exploitation of valuable components of effluent waste as described by Johnnson (2000).

If material-based solutions are favoured, evidence from various tests have shown that CAC concretes have outperformed PC concretes in resistance to biogenic acid attack where specimens have been exposed to corrosion in the sewer atmosphere. This has been observed in sewer simulation studies utilising the Hamburg chamber and in live sewer measurements such as the Virginia experimental sewer (Goyns 2004, Kiliswa 2016, Alexander et al. 2013).

The three forms of MIC resistance for CAC concretes are stated as; a higher neutralisation capacity (40% greater than Portland cement), the formation of a protective alumina gel (AH_3) layer and finally the liberation of bacteria-toxic aluminium ions at a pH lower than 4 (Herrison and Saucier 2015).

However, CAC concretes present an interesting puzzle because the protective contributions the 2nd and 3rd barriers to corrosion have not been assessed on their own. This has implications for conditions where one or more of the

barriers to corrosion are not applicable such as in abrasive conditions, where the protective alumina gel may be removed from the surface of the concrete.

2.7.3 Methods of assessing acid resistance in concrete sewer pipe materials

Attempts at understanding the effects of MIC on concrete materials have been ongoing for decades. The approaches to testing materials for corrosion in the sewer environment have differed significantly, and as such, there is no international standard or consensus as yet on the most appropriate accelerated laboratory test for MIC.

The six methods reviewed in this assessment are diverse. Their usefulness is dependent on an understanding of the causes and mechanisms discussed in chapter 2.2 of this report.

Test method	Damage mechanisms	Sewer condition simulated
Static immersion tests	Static mineral acid attack	Corrosion at the crown of the sewer
Dynamic hydrochloric/sulfuric acid test	Mineral acid attack and abrasion	Corrosion at the effluent line
Testing apparatus for accelerated concrete degradation	Mineral acid attack, abrasion and wetting and drying cycles.	Corrosion at the effluent line
Accelerated test for bio-deterioration of cementitious materials	Static biogenic acid attack	Corrosion at the crown of the sewer pipe
Fraunhofer-Umsicht H_2S Biogenic acid test	Static biogenic acid attack in the sewer atmosphere	Corrosion at the crown of the sewer
Virginia sewer experiment (Measurement up to now)	Static biogenic acid attack in the sewer atmosphere	Not a simulation****

2.7.4 Geopolymers and their potential as acid resistant materials for sewer applications

Until recently, viable binder options in concrete systems have been limited to PC and CAC systems. Over the past 3 decades, geopolymers and alkali-activated cements have received significant research attention and there is currently a lot of interest in the use of geopolymers as an alternative to Portland cements because of their stated benefits which include, a lower carbon footprint and the re-use of industrial wastes such as fly ash (van Deventer et al. 2012; Davidovits 2013; Druga et al. 2018).

Of relevance to the problem of MIC is that geopolymers have been shown under preliminary but limited testing to exhibit both high resistance to mineral acid corrosion and some level of bacterial inhibition (Grengg et al. 2017; Druga et al. 2018; Bakharev 2005).

A gap in current geopolymer research relates to the behaviour of geopolymer concrete subjected to acid attack where aggregate type has been varied. For biogenic corrosion mitigation, calcareous aggregate is recommended

for PC and CAC systems, however, the compatibility of GP cement with calcareous and siliceous aggregates has not been studied in sufficient detail.

Furthermore, geopolymers and alkali-activated materials may be constituted using a wide range of input materials (including fly ash, boiler ashes, rice husk ashes, metallurgical slags and clays) and the varied approaches in research and development, there has been very little standardisation of these materials (Davidovits 2013).

This is due, in part to the proprietary nature of many geopolymer research and development projects. There has also been disagreement in the scientific community around the correct terminology and the fundamental chemistry of these materials. Noting these complexities, this study has used the terminology suggested by Davidovits and the chemistry described "geopolymer Chemistry and Applications" (Davidovits 2008).

2.8 References

Alexander, M., Bentur, A., Mindess, S. 2018. "Durability of Concrete: Design and Construction". CRC Press, Taylor and Francis Group.

Alexander, M., Bertron, A., De Belie, N. 2013. "Performance of Cement-Based Materials in Aggressive Aqueous Environment: RILEM-State of the Art Report TC 211"

Alexander, M., Fourie, C.W. 2011. Performance of sewer pipe concrete mixtures with Portland and calcium aluminate cements subject to mineral and biogenic acid attack. Materials and Structures. Volume 44.

Alexander, M., Mindess, S. 2005. "Aggregates in Concrete (Modern concrete technology)". CRC Press.

Allahverdi, A. Skvara, F. 2000. "Acidic corrosion of hydrated cement-based materials: Part 2. -Kinetics of the phenomenon and mathematical models". Ceramics Silikaty.

Arbi, K., Nedeljkovic, M., Zuo, Y., and Ye, G. 2016. "A Review on the Durability of Alkali-Activated Fly Ash/Slag Systems: 2 Advances, Issues, and Perspectives". Industrial and Engineering Chemistry Research.

Ariffin M.A.M, Bhutta, M.A.R, Hussin, M.W., Tahri M.M., 2013. "Sulfuric acid resistance of blended ash geopolymer concrete. Construction and Building Materials 43.

Arp, R., Bole-Rentel, T., Jakuja, N. 2018. "Greenhouse gas emissions reduction options for the South African cement sector". WWF Technical report-ZA.

Bakharev T., 2005. "Resistance of geopolymer materials to acid attack". Cement and Concrete Research 35, pp 658-670

Bernal, S. A.; Provis, J. L. 2014. Durability of Alkali-Activated Materials: Progress and Perspectives. J. Am. Ceram. Soc. 997, 997.

Cabrera, G., Perez, R., Gomez, J.M, Abalos, A., Cantero, D. 2006. "Toxic effects of dissolved heavy metals on Desulfovibrio vulgaris and Desulfovibrio sp. Strains". Journal of Hazardous Materials A135.

Caicedo-Ramirez, A. 2018. Antimicrobial aggregates for the in-situ control of Microbially induced concrete". PhD dissertation University of Colorado, Boulder.

Cayford, B. I., Dennis, P. G., Keller, J., Tyson, G. W., and Bond, P. L. (2012). High-throughput amplicon sequencing reveals distinct communities within a corroding concrete sewer system. Appl. Environ. Microbiol. 78, 7160–7162. doi: 10.1128/AEM.01582-12

Chancey. R. T., Stutzman, P., Juenger, M.C.G, Fowler, D.W. 2010. "Comprehensive phase characterization of crystalline and amorphous phases of a Class F fly ash". Cement and Concrete Research 40, pp 146–156

Crawford, J.L.2013. “Effects of Inorganic Nutrients and Dissolved Organic Carbon on Oxygen Demand in Select Rivers in Northern Utah” MSc Thesis, Department of Watershed Science, Utah State University.

Criado, M., Palomo, A., Fernandez-Jimenez, A. 2005. “Activation of fly ashes. Part 1: Effect of curing conditions on the carbonation of the reaction products”. Eduardo Torroja Institute (CSIC), Madrid Spain. Fuel 84.

Davidovits, J. 2008. “Geopolymer Chemistry and Applications.” Saint Quentin, France: Geopolymer Institute.

Davidovits, J. 2017. Geopolymers: Ceramic-Like Inorganic Polymers. Journal of Ceramic Science and Technology.

Davidovits, J. 2018. “Why Alkali-Activated Materials are not Geopolymers”. Accessed, 25 February 2019<.https://www.geopolymer.org/faq/alkali-activated-materials-geopolymers>

De Belie, N., Monteny, J, Taerwe L. 2002. “Apparatus for accelerated degradation testing of concrete specimens”. Materials and Structures vol 35.

Dec W., Cwalina, B., Michalska, J., Merdkuda, D. 2015. Growth of Acidithiobacillus Thiooxidans Biofilm on Glass, Concrete and Stoneware. Solid State Phenomena Vol 2207 pp286-289.

Dong, Q., Shi, H. and Liu Y.2017. “Microbially Character Related Sulfur Cycle under Dynamic Environmental Factors Based on the Microbially Population Analysis in Sewerage System”. Frontiers in Microbiology.

Druga, M., Ukrainczyk, N., Weise, K., Lackner, S. 2018. “Interaction between wastewater microorganisms and geopolymer on cementitious materials: Biofilm characterization and deterioration characteristics of mortars”. International Biodeterioration & Biodegradation, Volume 134.

Ehrich, S., Helard, L., Letourneux, R., Willocq,J., Bock, B. 1999. “Biogenic and chemical sulfuric acid corrosion of mortars”. Materials in Civil Engineering.

Feng Rao, Qi Liu. 2015. “Geopolymerization and its potential application in mine tailings consolidation: A Review”. Mineral Processing & Extractive Metall. Rev., 36: 399–409.

Fourie, C.W. 2007. “Acid resistance of sewer pipe concrete”. MSc Thesis. University of Cape Town. Cape Town, South Africa.

Government Regulation Gazette no No.9801 vol 566. 2012. Republic of South Africa.

Goyns, A. M. 2003. Virginia sewer rehabilitation: Progress Report 1. Pretoria: Concrete Manufacturers Association.

Goyns, A. M. 2004. Virginia sewer rehabilitation: Progress Report 2. Pretoria: Concrete Manufacturers Association.

Goyns, A. M. 2013. Design manual for concrete pipe outfall sewers. Midrand: Concrete Manufacturers Association.

Gregg C. 2017. “Microbially induced acid corrosion in sewer environments”. Doctoral thesis submitted to Graz University of Technology.

Grengg, C., Mittermary, F., Ukrainczyk, N., Koraimann, G., Kienesberger, S., Dietzel, M. 2018. “Advances in concrete materials for sewer systems affected by microbially induced concrete corrosion: A review.”

Guidotti T.L. 1996. “Hydrogen Sulfide”. Occupational Medicine Vol. 46, No. 5. pp. 367-371.1996

Gutiérrez-Padilla, M.G.D., Bielefeldt, A., Ovtchinnikov, S., Hernandez, M., Silverstein, J., 2010. Biogenic sulfuric acid attack on different types of commercially produced concrete sewer pipes. Cem. Concr. Res. 40, 293–301. doi:10.1016/j.cemconres.2009.10.002

Habert, G., d'Espinose de Lacaillerie, J.B., Roussel, N. 2011. "An environmental evaluation of geopolymer based concrete production: reviewing current research trends". Journal for Cleaner Production 19.

Halberg, R.O., 1976. "A global sulfur cycle based on a preindustrial steady state of the pedosphere" Nitrogen, Phosphorus and Sulfur - Global Cycles. SCOPE Report 7. Ecol. Bull. (Stockholm) 22:89-134.

Herrison, J., Minerbe, M., van Hullebusch, E.D., Chassadent, T. 2017. "Influence of the binder on the behaviour of mortars exposed to H_2S in sewer networks: a long-term durability study". Materials and Structures 50.

Herrison. J., Saucier. F. 2015. Use of calcium aluminate cements in H_2S biogenic environment. Institute of Concrete Technology. 2015-2016 Yearbook.

House, M. W., Weiss, W., J. 2014. "Review of Microbially Induced Corrosion and comments on needs related to testing procedures". 4th International Conference on the Durability of Concrete Structures.

Hvitved-Jacobsen, T., Vollertsen, J., 2002. "The sewer as a bioreactor- a dry weather approach." Water Sci. Thechnol. 45, 11-24

Hvitved-Jacobsen, T., Vollertsen, J., Nielsen, A.H., 2013. "Sewer Processes: Microbially and Chemical Process Engineering of Sewer Networks. CRC Press, Boca Raton."

Ismail, N., Nonaka, T., Noda, S., Mori, T. 1993. "Effect of carbonation on microbial corrosion of concretes". Journal of construction management and engineering.

Jensen, H., Biggs, C.A. and Karunakaran, E. 2016. "The importance of sewer biofilms." WIREs Water, 3: 487-494. doi:10.1002/wat2.1144

Jiang, G., Keating, A., Corrie, S., O'halloran, K., Nguyen, L., and Yuan, Z. 2013. Dosing free nitrous acid for sulfide control in sewers: results of field trials in Australia. Water Res. 47, 4331–4339.

Johansson, M. 2001. Urine separation–closing the nutrient cycle. Final report on the R&D project: source-separated human urine–a future source of fertilizer for agriculture in the Stockholm region, Stockholm Water Company

Johnsson H, Vinnera˚s B, Ho¨glund C, Stenstro¨m TA, Dalhammar G, Kirchmann H. 2000. "Ka¨llsorterad human urin i kretslopp (Recycling source separated human urine, in Swedish)". VA-Forskrapport. VAV AB, Stockholm, Sweden

Kaempfer W., Berndt, M. 1999. Estimation of Service Life of Concrete Pipes in Sewer. 8th Conf. Durability and Building Material Components 1, 36-45.

Kiliswa, M. W. 2016. "Composition and microstructure of concrete mixtures subjected to biogenic acid corrosion and their role in corrosion prediction of concrete outfall sewers." PhD thesis, University of Cape Town.

Kriven, W.M., Bell, J., Gordon, M. 2003. "Microstructure and micro-chemistry of fully-reacted geopolymers and geopolymer matrix composites". Ceram. Trans.,153, 227 – 250.

Kruger, R. 1997. Fly Ash Beneficiation in South Africa: Creating new opportunities in the market place. Fuel 76(8) 777-779.

Kuliczkowska, E., Zwierzchowska, A. 2016. "A qualitative analysis of early defects present in PVC-U sewers but not observed in rigid pipes"

Lagod, G., Sobczuk, H., Suchorab, Z., Widomski, M.K. 2010. "Biofilm in gravitational sewer systems and its influence on wastewater biodegradation". Ecological chemistry and engineering. Vol 17.

Lavigne, M., P., Bertron, A., Patapy, C., Lefebvre, X., Paul, E. 2015. "Accelerated test design for biodeterioration of cementitious materials and products in sewer environments". Matériaux & Techniques 103.

Letourneux, R., Scirvener, K. 1999. "The resistance of calcium aluminate cements to acid corrosion in wastewater applications". Lafarge, France.

Letourneux, R., Scrivener, K. 1999. High performance concretes from calcium aluminate cements. Cement and Concrete Research, 29, 8, 1215-1223

Lu, L., Visintin, P., Bennet, T. 2018. "Evaluation of accelerated degradation test methods for cementitious composites subject to sulfuric acid attack; application to conventional and alkali-activated concretes."

Monteny, J., Vincke, E., Beeldens, A., Taewre, L., Van Germet, D. 2000. "Chemical, microbiological, and in situ test methods for biogenic sulfuric acid corrosion of concrete". Cement and Concrete Research 30.

Moreno, P., Aral, H., Vecchio-Sadus, A. 2009. "Environmental impact and toxicology of sulfate". CSIRO Minerals, Clayton South, Victoria 3169, Australia

Motsieloa, N. 2012. "Acid resistance of sewer pipe concrete." MSc thesis, University of Cape Town.

Nielsen P. H., Hvitved-Jacobsen T.1988. "Effect of sulfate and organic matter on the hydrogen sulfide formation in biofilms filled sanitary sewers".

Nielsen, A.H., Raunkjaer, K., Hvitved-Jacobsen, T., 1998. "Sulfide production and wastewater quality in pressure mains." Water Sci. Technol. 37, 97-104.

Nixon, R. 1997. "Future material selection guidelines for coatings on concrete for exposure to changing conditions in large municipal wastewater collection treatment systems," No. 379,Corrosion 97, NACE International .

North, M.R., Swaddle, T.W. 2000. "Kinetics of silicate exchange in alkaline aluminosilicate solutions, inorganic chemistry, 39.

Okabe S., Odagiri M., Ito T., Satoh H., 2007. "Succession of Sulfur-Oxidizing Bacteria in the Microbially Community on Corroding Concrete in Sewer Systems." Applied and Environmental Microbiology 971-980.

Palomo A, Grutzeck MW, Blanco MT. 1999. "Alkali-activated fly ashes, a cement for the future." Cem Concr Res ;29:1323–9

Palomo. A., Krivenko. P., Garcia-Lodeiro I., Kavalerova E., Maltseva, O., Frenandez-Jimenez A. 2014. "A review on alkaline activation: new analytical perspectives". Materiales De Construccion vol 64.

Park, K., Lee, H., Phelan, S., Liyanaarachchi, S., Marleeni, N., Navartna, D., Jegatheesan V., Shu, L. "Mitigation strategies of hydrogen sulfide emission in sewer networks- A review" 2014. "Mitigation strategies of hydrogen sulfide emission in sewer networks- A review". International biodeterioration and biodegradation. 251-261.

Pikaar I., Sharma, K.R., Hu, S., Gernjak, W., Kelly, J., Yan, Z. 2014. Reducing sewer corrosion through integrated urban water management.

Pomeroy, R.D., Parkhurst, J.D. 1977. The forecasting of sulphide buildup rates in sewers. Progress in Water Technology, Vol. 9.

Provis J.L. and van Deventer J.S.J. 2009. "Geopolymers Structure, processing, properties and industrial applications. CRC Press."

Provis, J.L., van Deventer, J.S.J. .2017. "Report on Alkali-Activated Materials (State of the Art Report)" RILEM Technical Committee.

Rava, E. 2008. “Management of Hydrogen Sulfide generation at Kraft Paper Mill”. MSc Thesis. Faculty of Engineering, Built Environment and Information Technology, University of Pretoria.

Recio Oviedo, E., Johnson, D., Shipley, H. 2011. “Evaluation of hydrogen sulfide concentration and control in a sewer system”. Environmental Technology. Vol. 33.

Reynolds-Clausen K., Singh, N. 2016. Eskom’s revised ash strategy and Implementation Progress.http://nla.org.za/webfiles/conferences/2016/Manuscripts.

Sahu,O. P., Chaudhari, P. K. 2013 “Review on Chemical treatment of Industrial Waste Water” Journal of Applied Science in Environmental Management. Volume: 17 (2) 241-257

Scrivener, K.L. 2014. “Options for future cements”. The Indian Concrete Journal

Sehar, S., Naz, I. 2016. “Role of the Biofilms in Wastewater Treatment”. DOI: 10.5772/63499.

Sindhunata, van Deventer, J.SJ., Lukey, G.C., Xu, H. 2006. Effect of curing temperature and silicate concentration on fly-ash based geopolymerisation. Industrial Engineering and Chemistry Research, 45.

Skvara, F., Jike, T., Kopecky, L. 2006. “Geopolymer materials based on fly ash.”

Smith, M.H., Hargroves, K., J., Desha, C. J. K. 2009. “Factor 5 in eco-cement: Zeobond Pty Ltd”. Ecos Magazine, June-July, 2009. Volume 149. Viewed 15 January 2020. <http://www.ecosmagazine.com/?paper=EC149p21>

Song, X.J, Marosszeky, M., Brungs, M., Munn, R. 2005. “Durability of fly ash based geopolymer concrete against sulfuric acid attack”. 10DMC International Conference on Durability of Building Materials and Components.

Soto, F., Dhakai, M., Kupwade-Patil, K., Daniela, S. 2013. “Examination of precursors in Fly Ash for development of an engineered geopolymer concrete”.

South African Bureau of Standards. 2010. “SANS 677: Concrete non-pressure pipes.”

South African Bureau of Standards. 2014. “SANS 50450-1: Fly ash for concrete Part 1: Definition, specifications and conformity criteria.”

Sudthanom, J., Zaidi, S. 2011. “To Analyze The Relationship between BOD, Nitrogen and Phosphorous Contents at Constant Dissolved Oxygen Concentration In Municipal Wastewater Treatment.” Masters Thesis: School of Sustainable Development of Society and Technology, Malardalen University, Sweden.

Teplý, B., Rovnaníková, M., Řoutil, L., & Schejbal, R. 2018. “Time-Variant Performance of Concrete Sewer Pipes Undergoing Biogenic Sulfuric Acid Degradation”. Journal of Pipeline Systems Engineering and Practice, 9(4), 04018013. doi:10.1061/(asce)ps.1949-1204.0000327

U.S. Environmental Protection Agency Office of Water (EPA). 2003. “Drinking Water Advisory: Consumer Acceptability Advice and Health Effects Analysis on Sulfate”

Van Deventer, J.S.J., Provis, J.L., Duxson, P. 2012. “Technical and commercial progress in the adoption of geopolymer cement”. Minerals Engineering 29.

Van Jaarsveld, J. G. S., J. S. J. van Deventer, G.C. Lukey.2002. "The effect of composition and temperature on the properties of fly ash and kaolinite based geopolymers." Chemical Engineering Journal 89(1-3): 63-73.

Yongsiri, C., Vollertsen, J., Rasmussen, M., Hvived-Jacobsen, T. 2004. “Air-water transfer of hydrogen-sulfide: Ana approach for application in sewer networks”. Water Environment Research, Vol. 76.

Zhang, L., De Schryver, P., De Gusseme, B., De Muynk, W., Boon, M., Vestrate, W. 2008. Chemical and biological technologies for hydrogen sulfide emission control in sewer systems: A review.

3 Research Methodology

3.1 Introduction

This study attempted to achieve the four broad objectives listed in chapter 1.6.1 and briefly restated below.

1. To measure the performance of fly ash based geopolymer concretes under mineral acid attack in comparison to PC and CAC concretes.
2. To investigate the acid resistance compatibility of different aggregates types (of varying chemical and mineralogical composition) paired with fly ash-based geopolymer cements, where compatibility is determined by assessing the performance of concrete specimens under static and dynamic mineral acid testing.
3. To characterise the chemical, mineralogical and morphological properties of the subject binders and aggregates and to determine what effect these properties have on the corrosion performance of GP, PC, and CAC concretes subjected to static and dynamic mineral acid tests.
4. To relate the corrosion performance of geopolymer cement, calcium aluminate cement and Portland cement concretes subjected to mineral acid testing to corrosion results obtained from live sewer experiments.

While fly ash-based geopolymer concrete is the main subject material, Portland cement concretes and calcium aluminate cement concretes are also subjected to characterisation and performance testing. In the context of this work, PC and CAC concretes were intended to be control specimens and as such, were subjected to the same testing as fly ash-based geopolymer concrete.

MIC is a durability problem experienced in sewer structures, therefore a section of this chapter is devoted to justifying the applicability of mineral acid performance tests according to concrete durability design theory (see headings 3.2 and 3.3). Given the complexity that comes about from the numerous variables involved (binder type, aggregate type, acid type, mineral acid test, characterisation test etc), it was not feasible to include all possible test configurations in the experimental programme. Therefore, there is also a section devoted to justifying the selected combinations of materials and tests (see heading 3.3). The rest of this chapter is focused on describing the materials and methods used for characterisation and testing.

3.2 Durability design: exposure conditions and resistance to MIC

"Durability is the ability of a material or structure to withstand the service conditions for which it is designed over a prolonged period without unacceptable deterioration" (Alexander, Bentur and Mindess, 2017).

Civil engineering design typically involves a quantification of the loading applied to a structure as well as a quantification of a structure's capacity to resist loading. If the structure is to be deemed safe or fit for purpose, its

resistance capacity should exceed the expected loading. This is a well-established principle that is used in numerous design codes.

However, in traditional structural engineering, loading and resistance have been characterised mainly in terms of structural mechanics, with less attention given to environmental loading and durability. Thus, there is now also a need for durability-based design methods.

To this end, Alexander, Bentuur and Mindess (2017) state that the objective of durability design is to "predict long-term behaviour on the basis of short-term tests, in conjunction with predictive models that inevitably are simplifications of the real situation to which concrete will be subjected".

Since the methods used in this experimental programme are intended to be of use to durability design, it is therefore useful to separate durability design into two parts, environmental loading, and resistance capacity. The first part relates to the environmental loading (or exposure condition), where MIC is concerned, it is related to the production of H_2SO_4 by sulfur-oxidizing bacteria (including the complex processes leading up to it) and other damaging effects that occur simultaneously in the sewer environment. Therefore, there is a need to characterise exposure conditions where MIC needs to be designed for.

The second part is the resistance capacity of a material which is a quantity related to the durability of concrete under MIC (MIC resistance). Therefore, there is a need to establish what MIC resistance means, when considered in terms of the definition of durability suggested by Alexander, Bentur and Mindess (2017).

3.2.1 MIC exposure condition

Sulfuric acid corrosion in the sewer is likely to be exacerbated by physical weathering actions found in the sewer. This is confirmed numerous studies, where the most severe corrosion was found along the effluent line, where both corrosion and erosion are likely to occur (Kiliswa, 2016). Figure 3-1 lists some exposure conditions and the scenarios in which they are found in the sewer.

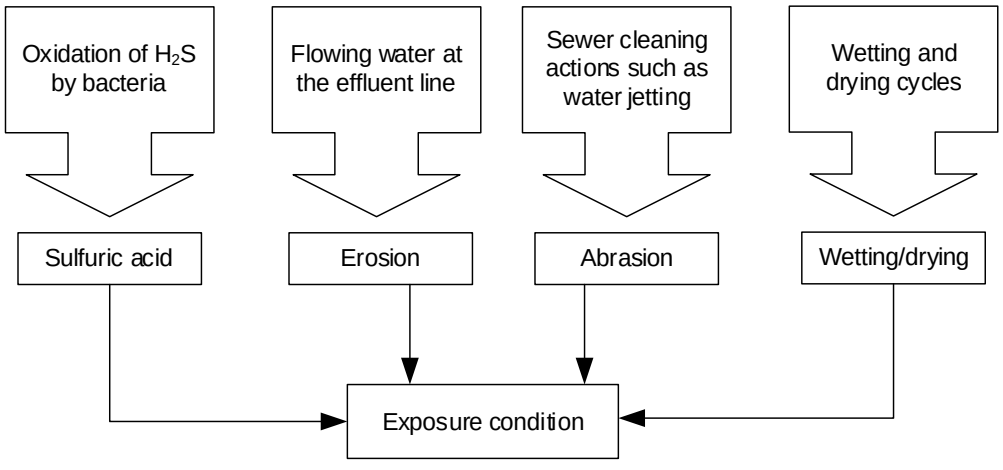

Figure 3-1: Exposure conditions for sewer concrete subjected to MIC

The formation of H_2SO_4 has already been treated in chapter 2 of this study. Physical weathering actions are typically not a concern for concrete not undergoing acid corrosion, however, corrosion has a severe effect on physical properties of concrete, making the concrete more vulnerable to weathering effects. Fourie (2007) stated

that concrete near the effluent line would be subjected to both acid and stresses emanating from flowing water (erosion). Wetting and drying cycles are also experienced by concrete along the effluent line (De Belie et al. 2002). Furthermore, since sewers often get clogged, maintenance actions may expose the corroding concrete abrasive conditions. Cant and Trew (1992) state that the water pressures generated during sewer-jetting (cleaning and unblocking) may be as high as 35 MPa. Therefore, it is important to design for the worst likely combination of corrosion and physical weathering for sewer structures. Thus, the behaviour of various concrete mixes under these combinations should be understood by the designer.

3.2.1.1 Sewer pipe exposure conditions

In a partially filled gravitational sewer pipe, the nature of corrosion has been shown two differ in two specific regions along its cross-section (see Figure 3-2). In this study, the corrosive conditions at the crown of the sewer pipe are generally not accompanied by physical weathering, this exposure condition is thus described as “static acid corrosion”.

However, corrosive conditions at the tidal line, where effluent flow stresses are present do have an erosion component. The conditions at the effluent line are thus described in this study as being erosive-corrosive. It is important to state that the tidal region has been found to exhibit the highest corrosion in MIC studies of concrete in real sewers (Kiliswa 2016).

It is suggested that using the dynamic acid test enables the effects of acid corrosion and erosion to be measured together. However, it is useful to be able to isolate the effect of corrosion from the combined effect of erosion-corrosion. Therefore, static acid testing performance (static corrosion) is compared to dynamic acid testing performance (erosion-corrosion) and the difference in performance is related to the abrasive effects in the dynamic acid test.

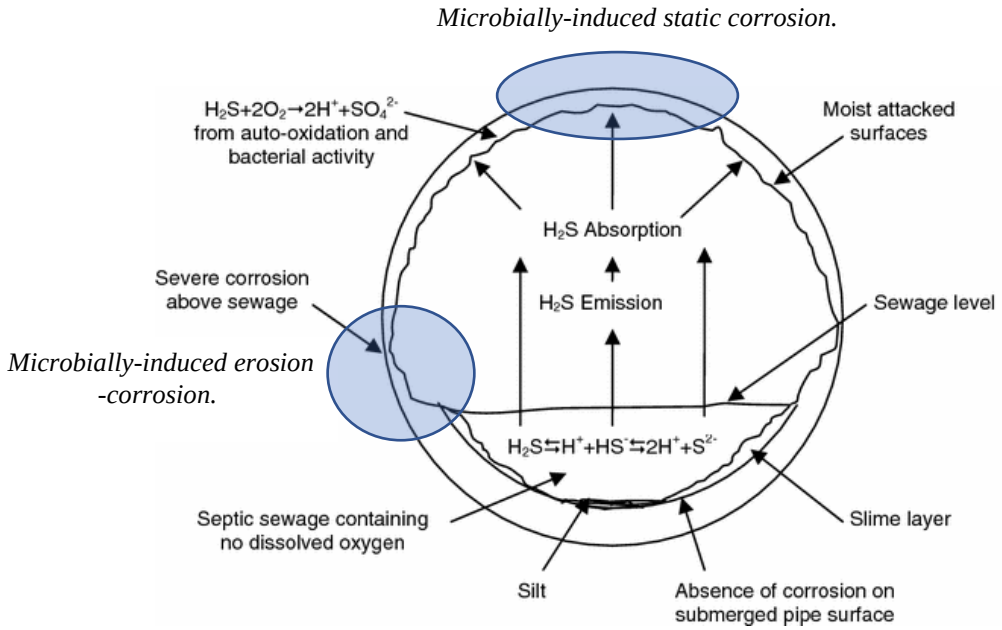

Figure 3-2: Exposure conditions at a sewer pipe section. Adapted from Alexander and Fourie (2011).

3.2.2 MIC resistance of concrete

Characterising and quantifying the MIC resistance of concrete is a complex endeavour. Firstly, because concrete possesses numerous forms of resistance, and secondly because concrete, is itself, a heterogeneous material, made up of numerous sub-components, each of which, react uniquely with acids.

3.2.2.1 Complexity due to concrete possessing numerous and diverse forms of MIC resistance

If, only the ability of the concrete to resist biogenic acid is considered, it is useful to distinguish between the different forms (or mechanisms) of MIC resistance a specific material possesses. Table 3-1 shows 7 suggested forms of resistance to MIC identified and investigated by other investigators.

According to the scheme shown in Table 3-1, corrosion resistance is categorised according to whether it originates from virgin concrete or from the products of corrosion. Furthermore, the MIC resistance mechanisms may fall into chemical, biological, or physical categories. These differences in the form of resistance make quantifying the total MIC resistance of concrete a difficult task.

Table 3-1: Forms of MIC resistance

Source of resistance	MIC resistance component	Example and reference
Reactants (virgin concrete)	1. Thermodynamically unfavourable (chemical property)	A chemical (corrosion) reaction with a positive value for the resulting free-energy (ΔGrx) change.
	2. Kinetic resistance (chemical property)	PVC and HDPE are thermodynamically unstable under sulfuric acid attack, however they decompose at a slow, or negligible rate, making them relatively inert if taken in the context of typical service life durations in sewer infrastructure (Goyns, 2013).
	3. Neutralisation capacity (NC) (chemical property)	CAC (provides 40% increase in neutralisation capacity when compared to PC). (Saucier and Kaitano 2018). N
	4. Bacterio-static effect (biological property)	Use of heavy metals (e.g. copper, zinc) dosed into concrete (Druga et al. 2018)
	5. Permeability and porosity (physical property)	Use of concrete with low permeability (Motsieloa, 2012).
Corrosion products (precipitates and gels)	6. Bacterio-static effect (biological property)	Aluminium ions released from the decomposition of alumina gel (a corrosion product) at pH values lower than 4 have a toxic effect on SOB. (Herrison and Saucier 2015)
	7. Physical barrier (physical property)	Alumina gel hydrate provides a physical barrier to further acid corrosion by encapsulating (Herrison and Suacier 2015). Precipitated gypsum may provide some protection to corrosion (Huber et al. 2016)

3.2.2.2 Complexity of corrosion due to concrete being a composite material

While the microbial processes leading the production of corrosion in the sewer are complex, they result in a well understood chemical compound, sulfuric acid. Concrete, on the other hand, is significantly more complex. This complexity is brought about by the fact that concrete is not a homogenous substance but a composite material made up of aggregate and contained in a hydrated/hardened cement paste matrix. Furthermore, both aggregate and paste are themselves, heterogeneous in terms of chemical composition and mineralogy.

Natural aggregates are made up of rock-forming minerals, this makes amenable to characterisation qualitatively and quantitatively by x-ray diffractive methods. However for Portland cement hydration products, characterisation

has hampered by the absence of long-range order, preventing detailed structural studies by diffraction techniques (Richardson et al. 2010).

Given that acids will react differently with the numerous crystalline and amorphous phases in both hardened cement paste and aggregate, a comprehensive understanding of concrete corrosion would require an understanding of the corrosion reactions each compound.

It must be noted that a comprehensive understanding of hardened cement pastes for concrete binders has not yet been achieved. For instance, in Portland cements, calcium-silicate-hydrates make up the bulk (60%+) of cement hydration products, and yet this phase is not well understood (Kiliswa, 2016). However, the reactions of the crystalline phases of hydrated Portland cement and sulfuric acid are better understood. Xiao provided a list of Portland cement hydrate reactions with sulfuric acid and their thermodynamic constants (Table 3-2).

Table 3-2: Sulfuric acid-concrete corrosion reactions with thermodynamic constants (Xiao 2016)

Reactants		**Corrosion products**	**ΔG_m**	**logK**
H_2SO_4(aq) + CaOH (Portlandite)	→	$CaSO_4 + 2H_2O$	-208	36.6
$2CaO.SiO_2 + {}_2H_2SO_4 + 4.H_2O$	→	$2CaSO_4.2H_2O + Si(OH)_4$	-168	29.6
$(3CaO.SiO2) +3 H_2SO_4 + 5H_2O$	→	$2CaSO_4.2H_2O + Si(OH)_4$	-453	79.5
$CaCO_3 + H_2SO_4+H_2O$:	→	$CaSO_4 + H_2O + CO_2$	-136	28.9
$(3CaO.2SiO_2.3H_2O) + 3H_2SO_4+4H_2O$	→	$2(CaSO_42H_2O) + Si(OH)_4$	-172	30.2
$(2CaO.SiO_2.1.167H_2O) + 2H_2SO_4+2.833H_2O$	→	$2(CaSO_4.2H_2O) + Si(OH)_4$	-165	28.9

Furthermore, corrosion of concrete includes the effects of corrosion products on the concrete itself. A damaging effect is the formation of secondary ettringite from gypsum originating from the initial sulfuric acid-Portlandite reaction.

Table 3-3: Corrosion products reactions with hydrated cement paste compounds

Corrosion product		Hardened cement paste (compounds/minerals)		Secondary products
$CaSO_4$	+	$3CaO.Al_2O_3.6 H_2O +26 H_2O$	→	$3.CaO.Al_2O_3.3 CaSO_4.32 H_2O$

Thus, it may be posited that the MIC of concrete consists of a set of chemical reactions, between the compounds in virgin concrete and sulfuric acid, each with different chemical properties, occurring simultaneously. It may further be stated that the negative effects of corrosion products such as secondary ttringite formation during PC concrete corrosion form are an indirect component of microbially-induced corrosion.

3.2.2.3 MIC resistance according to the life factor method (LFM)

A well-recognised method is the life factor method (LFM), which is used to predict the rate of sulphide (S) generation in the sewage, H_2S flux from the sewage surface, and the annual corrosion rate (influenced by the concrete's alkalinity) due to biogenic H_2SO_4 attack in PC-based concrete sewer pipes (Kiliswa 2016; EPA 1985).

Since this method is used to describe both the environmental loading under MIC (H_2S flux) and resistance capacity of concrete (annual corrosion rate) which it bases on a parameter called "alkalinity" ($CaCO_3$ per g concrete material).

However, the LFM does have significant limitations. A key limitation of this method is that it is accurate only for certain Portland cement-based mixes. The performance of alternative binders such as PC based systems with calcareous aggregates and calcium aluminate cement (CAC) based systems varied from the LFM predictions (Kiliswa, Alexander and Beushausen 2015).

Furthermore the "alkalinity" parameter used by the LFM to determine a concretes capacity to resist acid attack, is related to neutralisation capacity, which is an important chemical property for corrosion resistance, however, it does not take into account the kinetics of the corrosion reaction, nor does it take into account numerous other MIC resisting properties of concrete such as, the bacterio-static effect and the protective barriers caused by corrosion products.

3.2.2.4 MIC resistance according to thermodynamic stability

Since corrosion is a chemical phenomenon, it follows that the most important material properties to consider are chemical and should be amenable to analysis on a theoretical basis.

Table 3-2 shows a few chemical reactions between compounds in Portland HCP and sulfuric acid. Xiao (2016) calculated the thermodynamic constants associated with each reaction. A comparison of the ΔG (free energy) shows that there are significant variations if these reactions are compared.

Xiao et al. (2016) states that Gibbs free energy changes (ΔG) the six reactions presented above are negative, and the logarithmic values of the reactions' equilibrium constants (log K) are greater all than 5, indicating that these reactions go to completion. However, these reactions do not represent all sulfuric acid reactions because hydrated Portland cement paste has not fully been characterised.

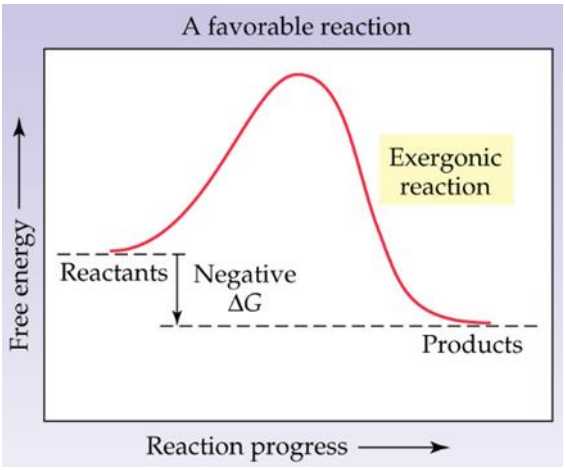

Figure 3-3: Thermodynamically favourable reaction (negative ΔG)

It is reasonable to assume that the aggregated thermodynamic properties of each binder type when subjected to acid attack differ to some extent when compared to another binder type. Due to the complexity of cementitious materials, this part of corrosion resistance in cementitious materials and concrete is yet to be fully understood, however understanding the corrosion resistance according to thermodynamic stability is of great importance.

3.2.2.5 Reaction kinetics

While thermodynamics can tell us if a reaction will go to completion and the relative proportions of products to reactants in a closed system, the kinetics of the reaction are also of great importance to concrete durability. Gay et al. (2016) suggest that the kinetics of acid corrosion in cementitious should be divided into two processes, namely, dissolution and precipitation.

By using digital holographic interferometry techniques to assess to the pure surface reaction rate between Portland hydrated cement paste and 3 acid types (HCl, H_2SO_4, and HNO_3), Gay et al. (2016) were able to discriminate between the dissolution and precipitation stages of the corrosion of hydrated Portland cement pastes. A significant finding in the study was that Portland cement paste in pure aqueous solutions of hydrochloric, nitric, and sulfuric acids at pH 2 dissolved at a similar rate of approximately 1 $mg/m^2/s$ (Gay et al. 2016). This finding is significant because dissolution represents the first step in corrosion damage. In corrosion reactions where insoluble precipitates are not produced the rate of dissolution may very well control the rate of degredation. Furthermore, the rate dissolution may also control degradation in exposure conditions where corrosion products are continuously transported away from the site of corrosion. Concerning the precipitation reactions, there is a gap in the literature on the kinetics of precipitation from biogenic corrosion reactions in concrete.

3.3 Relating mineral acid tests to MIC exposure conditions

It may be taken as self-evident that high resistance to mineral acid corrosion also indicates inertness to microbially-induced corrosion. This principle is already in practice where PVC and HDPE pipes are used as sewer conduits or as protective linings in concrete pipes. However, economical construction materials such as Portland cement concrete have relatively low resistance to acid corrosion. Furthermore, the interactions of cementitious materials with acids, bacteria, and physical weathering simultaneously (as is expected in sewer conditions) are extremely complex and this is the cause of conflicting results obtained from laboratory tests and live sewers.

If these complexities in determining the acid resistance of concrete are considered in terms of the ideas expressed by Alexander, Bentuur and Mindess (2017), then simplifications of the real situation to which concrete will be subjected can be used to determine concrete durability are necessary. However, it is suggested that these simplifications are related in some way to specific components of MIC in real sewer conditions and secondly to fundamental understanding of corrosion, which includes, thermodynamics and the kinetics of chemical reactions.

The ultimate goal this research hopes to contribute to is the use performance tests as a means to assessing the resistance capacity of concrete to MIC in much the same way the unconfined compressive strength performance test is used as an input parameter in determining the capacity of a concrete structure's mechanical resistance capacity. The performance testing approach is beneficial because it enables the resistance capacity to be established regardless of the type of material being tested. Furthermore it allows for quality monitoring at the time of construction or at a specific point in time during the service life of the structure.

Some nuances need to be considered when acid resistance is related to the durability of concrete structures undergoing MIC. Often, acid resistance in this context, relates to the ability of a material to meet its serviceability requirements under acid attack for the duration of a structure's service life. As discussed in chapter 2 of this study,

researchers such as Monteny et al. (2000) and Kiliswa (2016) have stated that pure mineral acid testing does not provide results which are relatable to MIC in the sewer environment.

It is suggested that this dismissal should not be taken as an absolute truth. Instead, it should be stated that mineral acid tests on their own are not sufficient to predict the behaviour of concrete under biogenic acid attack. Furthermore, it is postulated that mineral acid-based performance test can be used to assess specific components of MIC resistance in concrete. These components of acid resistance are related to the acid-resisting properties of cementitious materials referred to in Table 3-1.

This study uses mineral acid tests to assess the resistance of concretes to two exposure conditions, static acid corrosion and erosion-corrosion, which are discussed in section 3.6.3 of this dissertation.

Concerning the relatability of microbially-induced corrosion of Portland cement concretes in the sewer environment to the corrosion of PC concretes under mineral acid testing, two opposing views expressed in the literature are of interest. These views are related primarily to the effects of gypsum precipitation on degradation caused by MIC.

One hypothesis is that the gypsum layer forms a porous, moist, pulpy layer, which provides conditions in which SOB will thrive and produce H_2SO_4 within the precipitate layer, thereby bypassing any physical protection the gypsum precipitate layer would provide (Monteny et al. 2000). This view is supported to some extent by a live sewer study conducted by Grengg (2017) (see Figure 2-18), where it was found that species of sulfur-oxidizing bacteria (*A.thiobacillus ferro-oxidans*) were present within the corrosion layer, close to the corrosion front, indicating that acid was possibly being produced near fresh attack surfaces.

The opposing hypothesis is that gypsum formation will retard biogenic corrosion to some extent by forming a protective physical barrier which limits the amount of sulfuric acid in contact with fresh attack surfaces on the concrete. This hypothesis is supported by work conducted by Huber et al. (2016) after they conducted a comparative analysis of laboratory-produced biogenic and mineral sulfuric acid attack on hardened cement pastes. Huber et al. (2016) concluded that there were no obvious differences in the corrosion resistance of Portland hardened cement paste subjected to biogenic and mineral sulfuric acid. Furthermore, Huber et al. (2016) concluded that thick corrosion layers (1.8 -2.0 mm) do not support microbial growth and that this is likely due to oxygen and transport limitations.

The approach employed by this study is more in line with the hypothesis made by Monteney et al. (2000). However an important compromise made in the static acid test where, HCl was used instead of H_2SO_4. If the MIC of concrete model suggested by Grengg (2017) and illustrated in Figure 2-18 is considered, it may be suggested that the use of HCl (which produces soluble calcium salts) in a static immersion test may better simulate the 1 mm thick corrosion reaction front found in the gypsum corrosion layer in sewers. In essence similarity here is that both conditions are unencumbered by the formation of protective precipitating salts (in the case of PC and CAC concretes). Lastly, the pH of the biogenic corrosion front as measured by Grengg (2017) and the pH of mineral HCl acid tests conducted in this study are both 1. This indicates that at the attack surface both scenarios have the same order of H^+ ion concentration.

H_2SO_4 could have been used in the static acid test ascertain the robustness of Hubert's (2016) hypothesis. However, this was not done, and it is an acknowledged limitation to this study the implications of which are provided under 3.7.2 of this chapter.

To justify the use of HCl for the dynamic acid test, it is suggested that if the fact that H_2SO_4 and HCl both fully ionise in solution is considered together with Gay et al.'s (2016) finding that the dissolution reactions in cementitious materials are independent of acid type so long as the pH of the solution remains constant, then the use of HCl instead of H_2SO_4 is allowable as long as the corrosion process being assessed is the rate of dissolution of concrete in acidic solution.

It is not suggested that the dynamic HCl test is useful for measuring corrosion parameters related to precipitation stage of corrosion because the rate of the precipitation reactions depend strongly on the type of acid involved in corrosion (Gay et al. 2016).

This hypothesis was assessed by testing geopolymer-siliceous aggregate concretes using both HCl and H_2SO_4 in the dynamic acid test. Calcium-rich concretes such CAC and PC, and concretes containing dolomite aggregates were only tested using HCl, to avoid the common ion effect, which as reported by Fourie (2007) stalls the corrosion reaction when H_2SO_4 was used. For sulfuric acid to be used in the dynamic acid test would require a test that could remove gypsum and other solid precipitates from the acidic solution before the acidic solution becomes saturated.

3.3.1.1 Relating kinetic resistance (to corrosion reactions) to the dynamic acid test

The dynamic acid test used in this study (see headings 2.5.2 and 3.6.3.1) consists of both brushing (abrasion) and acid attack, this test has been used previously to measure the rate of corrosion through mass loss and hydrogen ion consumption over time (Fourie 2007, Motsieloa 2012).

Of significance is the finding by Gay et al. (2016), that dissolution precedes precipitation and that the rate of dissolution and precipitation may differ significantly. The term dissolution describes a class of processes wherein a solid is dissolved in a liquid, with the solid forming the minor component of the mixture, known as the solute, and the liquid forming the major component, or the solvent (Seager et al. 2018).

It is therefore plausible to suggest that concrete specimens undergoing both acid attack (dissolution and precipitation) and brushing (abrasion) will experience corrosion rates controlled by the rate of dissolution of the solute. This is because dissolution, in effect means that compounds in the solute have become unbound to the rest of the solid phase and now form part of the solution. If the dissolved ions do not form precipitates rapidly, then the physical effects of brushing (abrasion) may transport these ions away from the corroding surface. Furthermore, brushing (abrasion) may have the effect of breaking any adhesion or bonding between corrosion precipitates and the undissolved solute material (concrete). It is important to note that the brushing action in the dynamic acid test is unlikely to damage sound or un-corroded concrete because the PVC bristles from the brush are significantly softer than standard strength concrete, secondly, the bristles are flexible which means they will deform when brushed against sound concrete. Therefore abrasion in this context, refers to brushing or removal of corrosion products and corroding material with significantly diminished mechanical strength.

Abrasion may also enhance aggregate particle pop-outs in concrete which adds to the removal of material from the surface of the corroded layer. The quantity of material loss is dependent on the severity of abrasion and the strength of the surface material. Continuous removal of the precipitate layer and dissolved ions would mean that the rate of corrosion is determined by the kinetics of dissolution. Therefore, it is suggested that the dynamic acid test (H_2SO_4/HCl) could be used to index the rate of dissolution of various concretes undergoing acid attack.

3.3.1.2 Relating precipitate barriers to the static HCl test

The type of acid used in the static test is HCl whereas H_2SO_4 is the acid type responsible for MIC. This shortcoming is acknowledged and should be the subject of further study. However, using HCl does provide some comparative benefit due to the use of HCl in the dynamic test for PC, CAC and GP concrete mixes paired with calcareous aggregates. Furthermore, corrosion products of MIC such as alumina hydrate gel (AH_3), which have been suggested to provide physical barrier protection to concrete undergoing MIC (Herrison and Saucier 2015) are common to both H_2SO_4 and HCl in the corrosion CAC concretes. Therefore, the value of this test to MIC, is limited to the protective effects formed by precipitate products which are common to both H_2SO_4 and HCl corrosion reactions.

3.4 Testing strategy

To investigate the corrosion resistance behaviour of GP concretes, a twofold strategy was employed. The first strategy involves investigating the properties of the subject aggregates, hardened cement pastes (HCP's) and the second strategy involves subjecting concrete specimens to mineral acid performance testing and measuring their performance.

With regards to material characterisation, this study treated concrete as a composite material consisting of hardened cement paste (HCP) and aggregate and the characterisation of these two parts was undertaken separately. Geopolymers are binder materials, therefore most of the characterisation has been conducted on the HCP component of the concretes. Hardened cement paste characterisation included, X-Ray diffraction (XRD, XRF, SEM (before and after corrosion) and pH. Characterisation of the five aggregate types included XRD and XRF analysis, because corrosion is a chemical reaction and thus understanding the chemical composition and mineralogy of the aggregates was important.

Accelerated performance testing is currently not widely used to evaluate the durability of concrete to MIC. Performance testing involved two types of corrosion tests, static corrosion testing and dynamic corrosion testing. Compressive strength testing was undertaken to measure the structural capacity of the concretes.

Figure 3-4 provides an overview of the components the experimental programme. Material characterisation involved characterisation of sound (un-corroded) hardened/hardened cement pastes and aggregates via scanning electron microscopy (SEM), x-ray diffraction (XRD), x-ray fluorescence and pH measurements according to the arrows shown in Figure 3-4. Furthermore, a limited set of corroded concrete specimens taken from specimens that were subjected to dynamic acid tests were also analysed via SEM. Performance involved subjecting cured concrete specimens were subjected to two types of corrosion performance testing (static and dynamic acid test) and compressive strength testing (Figure 3-4).

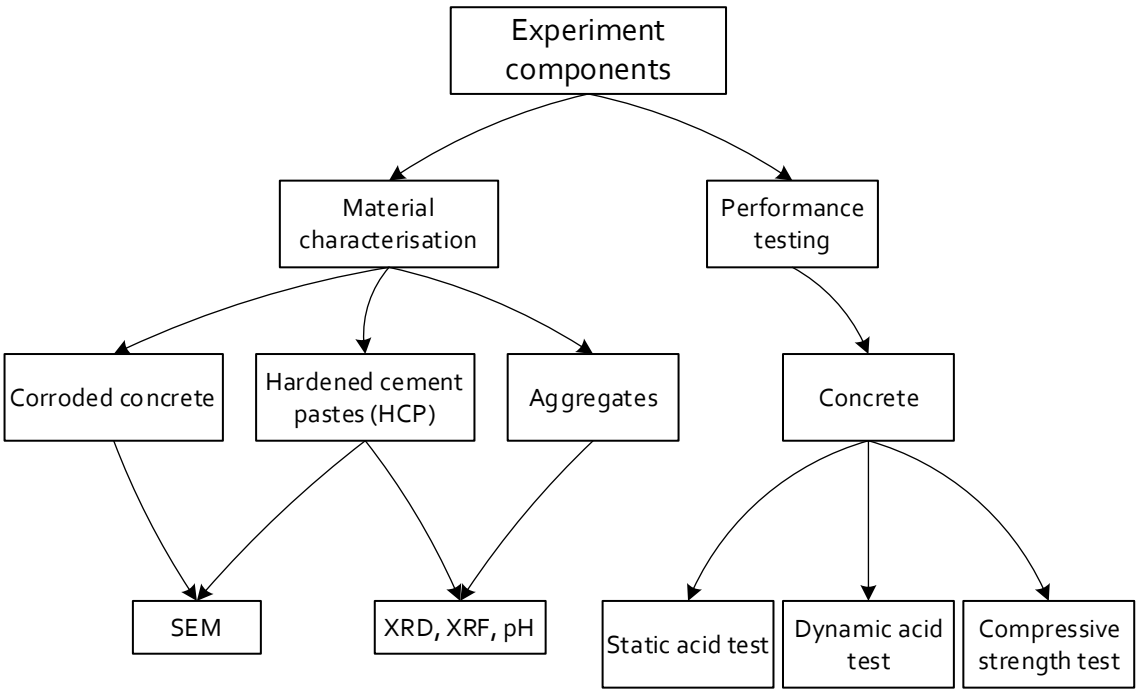

Figure 3-4: A schematic representation of the experimental programme showing the components of material characterisation and performance testing.

Detail of the particular form of the test specimens used to in the characterisation is provided in Table 3-4. XRD, XRF and pH testing required the specimens to be milled while SEM used particulates chipped off from the surface of corroded and un-corroded concrete specimens (from the dynamic acid test).

Table 3-4: Test type, material type and specimen description used for material characterisation.

Type of test	**Material tested**	**Description of test specimens**	**Reference method**
X-Ray fluorescence (XRF)	Hardened cement pastes Aggregates	Milled powder	Fusion technique.
X-Ray diffraction (XRF)	Hardened cement pastes Aggregates	Milled powder	Phases identified using X'Pert Highscore plus software
Scanning electron microscopy (SEM)	Hardened cement pastes Corroded concrete specimens	Chips fractured from concrete specimens	Non-standard,
pH	Hardened cement pastes Aggregates	Milled powder	Non-standard, method similar to Kiliswa (2016)

Table 3-5 relates the type of performance test to; exposure condition (see 3.2.1), the MIC resistance component being tested, the type of test specimen, and method or standard used in testing. Greater detail of each performance test is provided in section 3.6 of this chapter.

Table 3-5: Test type, performance measure and specimen description used in performance testing.

Performance test	Sewer (MIC) exposure condition	MIC resistance component tested	Description of test specimens	Reference method
Static acid test	Static biogenic corrosion	Corrosion product protection	50 mm concrete cube specimens	Non-standard
Dynamic acid test	Erosion-corrosion	Kinetics of concrete corrosion	78 mm diameter by 150 mm long cylindrical concrete specimens	Non-standard Fourie (2007)
Compressive strength	Mechanical loading	N/A	100 mm concrete cubes	SANS 5863: Compressive strength of concrete

3.5 Materials

3.5.1 Binders

The origin and density properties of Portland cement, calcium aluminate cement and geopolymer cement that were used in the experimental work are described in Table 3-6. Of significance is that the relative density of the fly-ash based geopolymer cement used in this study is significantly lower than the relative density of calcium aluminate cement and Portland cement. The geopolymer paste's low density has implications for the design of concrete mixes because the volumetric proportions of paste in each mix will differ substantially if the mix designs are designed to have equivalent binder proportions in terms of mass.

Table 3-6: Binders used in this study

Cement type and origin	Relative density	Loose bulk density (kg/m^3)
CEM I, 52.5 R, Portland cement from PPC	3.1	1260 kg/m^3
Cement Fondu-calcium aluminate cement (Brand: Imerys)	3.3	1370 kg/m^3
Fly ash-based geopolymer cement developed by CSIR Smart Places.	2.5	1020 kg/m^3

3.5.2 Aggregates

Five types of aggregate were collected to for use in the concrete mixes. Four aggregate types were sourced from Afrisam's ® quarries located in Gauteng, South Africa. Dolomite aggregate was sourced from Lyttleton quarry ® in Centurion, Gauteng. Because this study characterised aggregates and pastes separately, no blending of aggregates from different sources or types was permitted. Therefore, for the purpose of mix design, both fine (crusher sand) and coarse fractions (stone) from were collected from each quarry. The quarry (source) and the relative density of each aggregate type is shown in Table 3-7. The relative density of the aggregate's ranges between 2.6 and 3.0.

Table 3-7: Aggregate type and source

Aggregate	Source quarry	Relative density
Dolomite	Olifantsfontein	2.86
Ferro-quartz	Ferro (Pretoria)	2.6
Andesite	Eikenhof	2.94
Dolerite	Rooikraal	3.0
Granite	Roodekrans	2.67

The grading curves of all the fine aggregates (crusher sands) and coarse aggregates are shown in Figure 3-5 and Figure 3-6 respectively. Grading data for each aggregate type and size classification is provided in Appendix C: Aggregate grading data.

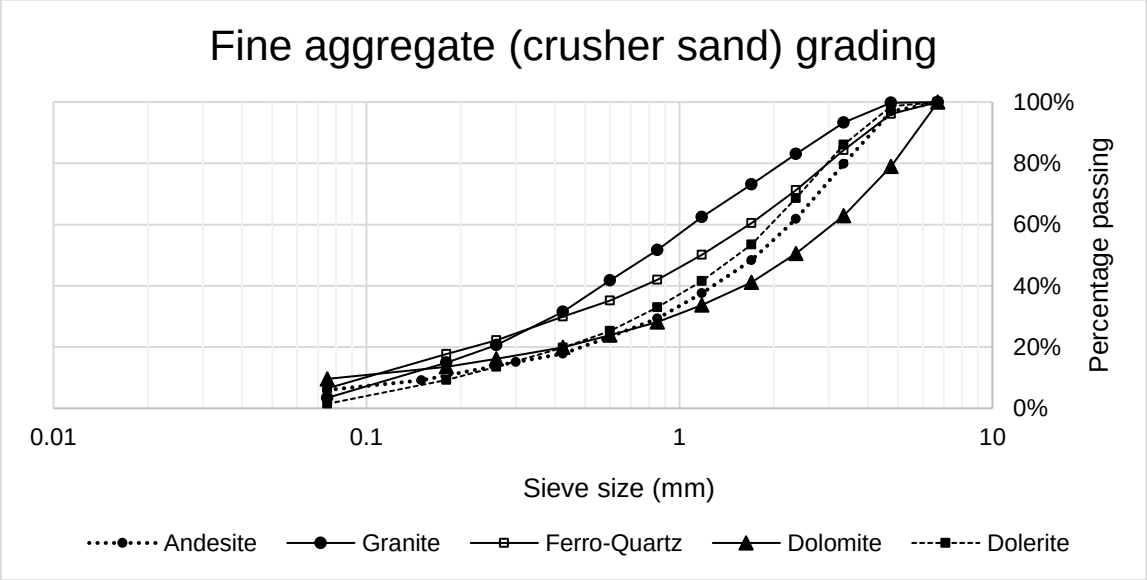

Figure 3-5: Grading of crusher sands

Fineness modulus (FM) values were calculated according to SANS 3001-PR5:2011 for the crusher sands are provided in Table 3-8. The calculated fineness moduli ranged from 2.4-3.9, with granite aggregate being the finest (FM = 2.88) and dolomite aggregate (3.9) being the coarsest crusher sand. The gradings of the crushed stone were relatively similar (Figure 3-6).

Table 3-8: Fineness moduli of the crusher sands

FM-Ranking	Aggregate type	Fineness modulus (FM)
1	Dolerite	2.42
2	Granite	2.88
3	Ferro-quartz	3.2
4	Andesite	3.69
5	Dolomite	3.9

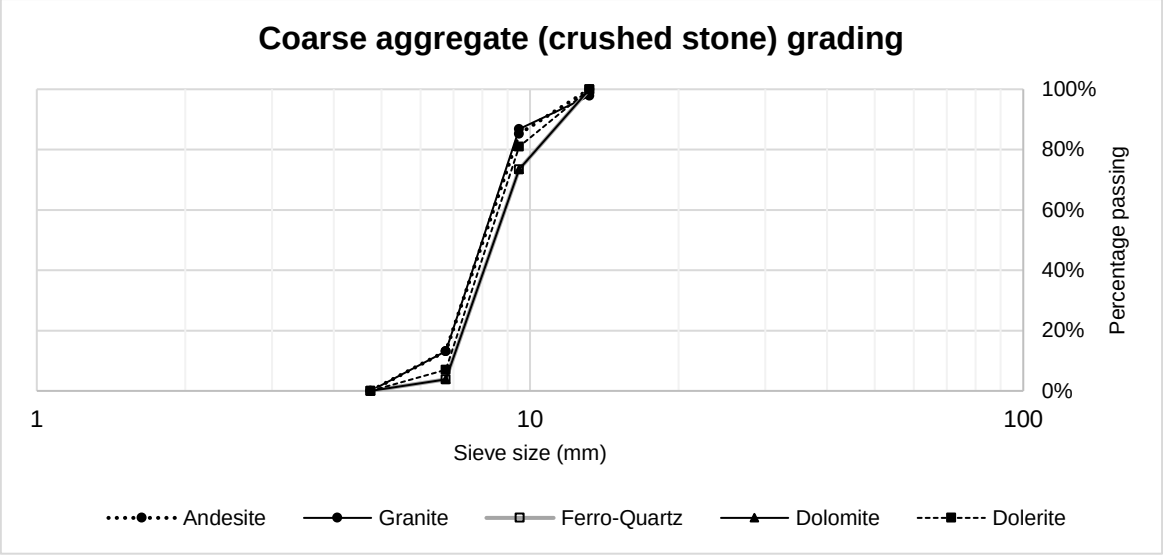

Figure 3-6: Grading curve coarse aggregate (stone)

3.5.3 Cement-aggregate combinations

Previous work by Fourie (2007) provided interesting results on the corrosion resistance of PC and CAC concretes paired with different qualities dolomitic aggregate when tested under the dynamic hydrochloric acid test wherein the quality of dolomite was found to influence the corrosion rate when the binder type was kept constant. This finding indicates that classifying aggregates into calcareous or siliceous groups may not be sufficient for estimating the corrosion resistance of concrete.

Therefore, the approach used in this study was to use aggregates of varying mineralogy and pair them with geopolymer binders in concrete mixes. Where sufficient understanding of the corrosion performance of aggregate-binder pairs is well understood, these combinations have not been considered, such as combinations of CAC or PC binders with siliceous aggregates. These combinations are known to have very poor acid resistance because of the preferential corrosion of the binder component. GP binder was paired with both siliceous and calcareous aggregates.

3.5.4 Mixes combinations tested

This study sought to make up concretes suitable for comparison with previous work while being available for purchase in the general market. Common aggregates used within the Gauteng region were selected to find the binder/aggregate pair with the highest acid resistance.

Considered in this study are three binder types (PC, CAC and GP) and two major groupings of aggregates (siliceous and calcareous). However, selecting the aggregates solely along the basis of calcium content may not be sufficient where geopolymer cements are concerned. Therefore, 4 siliceous aggregates types of varying mineralogy available in the Gauteng region were selected to pair with geopolymer cement for acid resistance testing. Furthermore, two mineral acid testing regimes (static and dynamic) were undertaken wherein two types of strong acid were used (hydrochloric and sulfuric acid).

This combination of binder type (3), aggregate type (5), mineral test type (2), and acid type (2) creates a large number of possible combinations (60) for testing. It was therefore necessary to reduce these possible combinations in a rational manner, where data from only the most useful combinations of aggregate, binder, test regime and acid type would be collected.

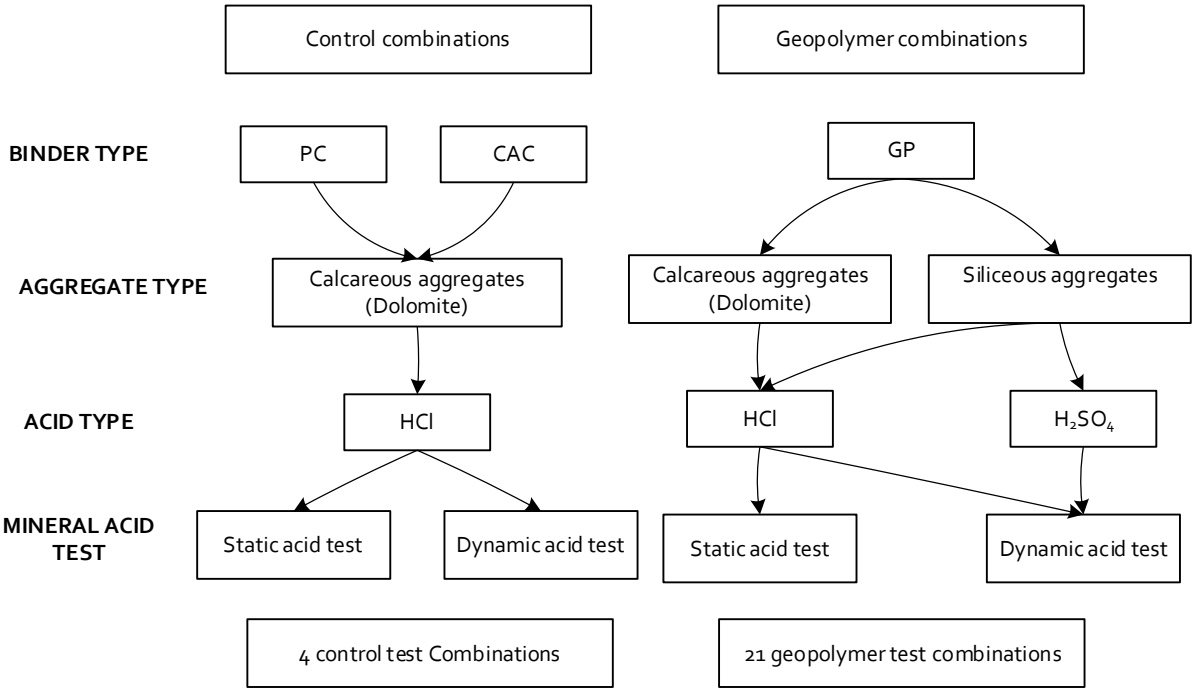

Figure 3-7: Schematic representation of the selected concrete mix, acid type, and test type combinations tested in this study

3.5.4.1 Control combinations

The control group of samples were PC and CAC cements paired with calcareous dolomitic aggregate. These pairs were tested under both static and dynamic tests using only hydrochloric acid. The rationale behind only using hydrochloric acid, as mentioned by Alexander and Fourie (2011), is that these calcium-based systems produce insoluble gypsum which saturates the acidic medium and effectively stifles attack on the specimens through the common ion effect.

3.5.4.2 Test combinations

This group of specimens includes geopolymer cement paired with either calcareous aggregate or siliceous aggregate. Where siliceous aggregates were used, specimens were exposed to both hydrochloric acid and sulfuric acid under both dynamic testing and static testing (CSIR, 1959).

3.5.4.3 Redundant combinations

Redundant combination included specimens which were tested in previous work and exhibited low resistances in laboratory tests and the sewer environment (CSIR 1959, Fourie 2007, Motsieloa 2012). This group of mixes included combinations of PC and CAC with siliceous aggregates. This group was not considered in this study.

3.5.5 Mix designs

To have a meaningful basis for comparison of the concretes considered in this study, the proportions of binder (cement), fine aggregate (crusher sand) and coarse aggregate (stone) were kept constant for the control specimens (PC and CAC) at the proportions provided in Table 3-9 for specimens intended for dynamic acid testing and Table 3-10 for specimens intended for static acid testing.

The mix designs shown below are adaptations based on previous mixes prepared for evaluation in the VES as reported by Goyns (2013) and Kiliswa (2016). Of significance is that these mixes deliberately had relatively high binder contents by mass (23%) because the binders were of primary concern to that study.

Table 3-9: Mix design of control specimens used in dynamic acid tests and mechanical strength testing

Concrete mix component	Mix proportion as a percentage of total mass	Mix Ratio (by mass)
CAC/PC	23%	1
Fine aggregate (sand)	33%	1.43
Coarse aggregate (stone)	44%	1.92
Ratio of fine to coarse aggregate by mass	43:57	
Water-cement ratio	0.35	

Specimens prepared for static tests in this study did not include coarse aggregate because the 50 mm mould size used to cast the concrete cubes was limiting. However, the same binder to aggregate ratio was maintained.

Table 3-10: Concrete mix design of control specimens used in static acid tests

Concrete mix component	Mix proportion as a percentage of total mass	Mix Ratio (by mass)
CAC/PC	23%	1
Fine aggregate (sand)	77 %	3.35
Water-cement ratio	0.37	

Since corrosion occurs on an attack surface in sewer concrete, it follows that comparing acid resistance of mix designs where the mix proportions of competing systems are equivalent by mass, is less suitable than a mix design based on volume. This is especially important if there is significant variation in the relative densities of HCP and/or aggregate.

Ideally, if competing concrete binder systems are to be compared, the proportions of the binder of competing systems by area on the attack surface should be relatively similar. It follows that mix proportions should be volumetrically comparable.

Since the relative densities of fly ash-based geopolymer concrete is significantly (by at least 25%) lower than PC and CAC (see Table 3-6) the mass proportion of fly ash based geopolymer was reduced to ensure that the of the binders was approximately equal to the CAC and PC binders. Therefore, the binder mass in the GP specimens was specified to be 75% of the mass of the GP and PC concretes. The mass proportion of GP binder thus was adjusted to 17% while the coarse and fine fractions of aggregate were adjusted upwards while keeping the coarse/fine aggregate proportions constant.

Table 3-11: Mix design of geopolymer concrete specimens used in dynamic acid tests and mechanical strength testing

Concrete mix component	**Mix proportion as a percentage of total mass**	**Mass Mix Ratio (by mass)**
Fly ash based geopolymer	17%	1
Fine aggregate (sand)	35.5%	2.1
Coarse aggregate (stone)	47.5%	2.79
Ratio of fine to coarse aggregate by mass	43:47	
Geopolymer liquids to geopolymer solids ratio	0.35	

As with the control (CAC and PC) mixes, GP concretes prepared for static tests did not include coarse aggregate because the 50 mm mould size was limiting.

Table 3-12: Mix design of geopolymer concrete specimens used in static acid tests

Concrete mix component	**Mix proportion as a percentage of total mass**	**Mass Mix Ratio**
Fly ash based geopolymer	17%	1
Fine aggregate (sand)	83 %	4.89
Geopolymer solids to geopolymer liquids ratio (Analogous to water-cement ratio)	0.37	

The grading of the combined fine/coarse aggregates proportioned at the ratio 43/57 are shown in Figure 3-8.

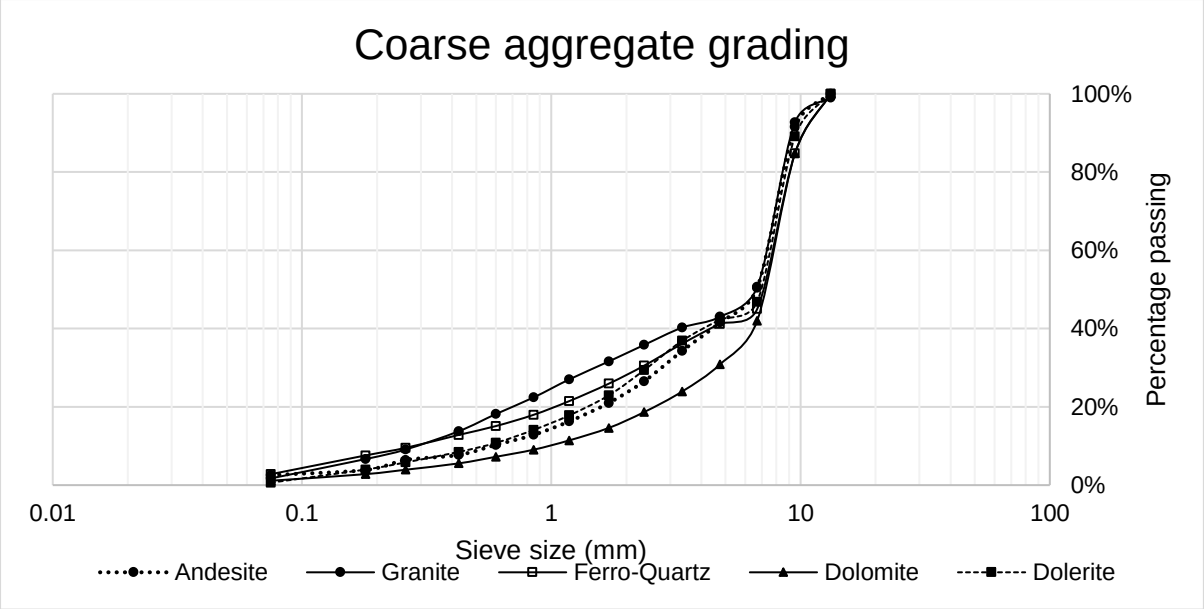

Figure 3-8: Combined grading of coarse and fine aggregate fractions used for the concrete mixes

According to the fineness modulus calculation, granite had the finest aggregate (4.65) grading for concrete mixes intended for the dynamic HCl/H_2SO_4 test, while the dolomite (5.28) aggregate mix had the coarsest grading.

Table 3-13: Fineness modulus of aggregates used in mixes

FM-Rank	Aggregate type	Fineness modulus
1	Granite	4.65
2	Ferro-quartz	4.79
3	Dolerite	4.95
4	Andesite	4.99
5	Dolomite	5.28

3.5.6 Acids

Acid corrosion (including biogenic corrosion) consists of an acid-base reaction which produces a salt. Sulfuric acid completely dissociates in water to form H^+ and SO_4^{2-} which makes it a strong acid. Studies from the sewer environment show us that the pH in these environments can be as low as pH 1 (Grengg 2017, Monteny et al. 2000).

When Portland cement paste, calcium aluminate cement paste and calcareous aggregates are exposed to sulfuric acid, the reaction produces calcium sulfate, an insoluble salt which precipitates from the acidic solution. While using sulfuric to test Portland concretes and calcium aluminate concretes, Alexander and Fourie (2011) observed that the acidic solution became saturated within hours with calcium sulfate which effectively halted corrosion making the test untenable.

Thus, it was decided, that the performance tests be primarily conducted using hydrochloric acid because the products of its reaction with Portland are soluble. Since geopolymers are predominantly alumino-silicate materials with much lower levels of calcium than Portland and calcium aluminate systems, acid testing of geopolymer

concretes utilising non-calcareous aggregates was conducted using both sulfuric acid and hydrochloric acid, while PC and CAC concrete and geopolymer concretes using calcareous aggregates were tested in only hydrochloric acid.

3.6 Methods

This section describes the methods used in sample preparation, characterisation, and performance testing.

3.6.1 Specimen preparation

3.6.1.1 Specimen preparation for dynamic acid tests

Since sewer pipes are the primary application for concrete in this study, an attempt to simulate the method by which concrete is produced in industry was utilised, wherein dry-mixes are subjected to high compaction . Fourie (2007) and Motsieloa (2012) produced dry mixes of concrete, cast and compacted using a specially designed mould and compaction procedure. The process was meant to simulate how sewer pipes are manufactured in practice. The casting and compaction procedure used in this study borrows from Fourie (2007) with changes made only in the compaction method and coring of the specimen.

3.6.1.1.1 Mixing

Concrete was mixed in a 5-litre Matest mixer. The following procedure was followed.

Figure 3-9: Matest mixer used for mixing the concretes

- The mixing bowl was filled with 2.5 kg of combined aggregate and cement and locked onto the Matest mixer.
- The mixer was turned on to low speed and water or liquid binder was added to the mix.
- The concrete was mixed for 3 minutes and discharged into the mould for compaction.

These steps were repeated for each sample until approximately 7 kg of material was available for the moulding and compaction. Because of the volumetric capacity of the mixing bowl, these sub-batches (2.5 kg) were mixed and combined together to fill the moulds.

3.6.1.2 Compaction and de-moulding procedure

The method by which specimens were compacted was adapted from the compaction procedure specified in TMH 1, method A7- "The determination of the maximum dry density and optimum moisture content of gravel, soil and sand".

A 152 mm diameter, 152 mm length steel mould with a perforated detachable baseplate was used to contain the concrete during compaction. A 150 mm round sheet of filter paper was placed on the base plate to prevent the concrete from sticking to the plate.

The mould was filled incrementally with layers equalling approximately 30 mm dry mix concrete. A total of 5 layers was required to load the mould for each specimen.

The surface of the concrete was levelled by hand by pressing down on it, and subsequently tamped with 11 blows with a 4.5 kg tamper for each compacted layer. The tamper, which was dropped from a height of 457 mm, is configured to distribute blows evenly over the surface of the layer being compacted. The total compaction effort, measured in blows, equalled 55 blows for each concrete specimen. The concrete specimens were allowed to set for 60 minutes and extracted from the steel moulds, through the use of a hydraulic press.

Figure 3-10: Compaction of concrete dry mix using TMH 1 A7 compaction device

3.6.1.2.1 Curing

1 hour after compaction, all types of concrete specimens were placed in a sealed plastic bag, and then placed in an oven at 60^{o}C for 4 hours. The purpose of the sealed bag was to maintain a relatively constant humidity while specimens were cured in the oven. Thereafter, the geopolymer specimens were cured in sealed bags for 28 days at 23 ^{o}C. Portland and calcium aluminate cement concretes were cured in curing baths at 23 ^{o}C for 28 days before testing in the dynamic acid test.

3.6.1.2.2 Coring

A deviation from the method of manufacture used by Fourie (2017) and Motsieloa (2012) was that the test specimens used were cored out of a larger concrete cylinder instead of being cast into a cylindrical mould of the

required specimen dimensions. A core barrel with a 78 mm internal bore was used to produce concrete specimens for testing.

Figure 3-11: 78 mm diameter test specimens were cored from larger 152 diameter cylinders after 28 days of curing.

3.6.1.3 Specimen preparation for static acid tests

Specimens produced for static acid tests were cast in 50 mm cube moulds. Unlike the larger cylindrical specimens produced for dynamic acid testing, the mix design for static tests does not include coarse aggregate. The relatively small mould size (50 mm cube) made compaction of concrete mixes, where coarse aggregate was used, impractical. Therefore, only binder and fine aggregates were used to produce the concrete specimens. Compaction was achieved by hand, using a tamping rod. For these specimens tamping was conducted in layers of 25 mm. Each of the two layers were tamped 10 times.

3.6.1.4 Specimens for compressive strength testing

Specimens for compressive strength testing were cast in 100 mm cube moulds. Mix proportions provided in Table 3-9 and Table 3-11 were used for the concrete specimens. Because of the dryness of the concrete mixes, compaction of these specimens was achieved by hand, using a tamping rod. The concrete was compacted in 3 layers, where each layer was tamped 20 times or more. Hand tamping was used because the 100 mm mould for the compressive strength tests were not compatible with the TMH 1 A7 compaction device shown in Figure 3-10. Given that the compaction methods used for the preparation of concrete specimens in the dynamic acid test differ, it is plausible to assume that the degree of compaction will differ somewhat. However, the purpose of the compressive strength testing was to compare the performance of geopolymer concretes that if the control specimens (Portland cement and calcium aluminate cements).

3.6.1.5 Specimen preparation for SEM testing

The changes in morphology due to corrosion were investigated via SEM at high magnification. To get a picture of the effects of acid attack at that scale, SEM images were taken before and after the specimens had been subjected to corrosion. To obtain the specimens approximately 5 grams of paste was chipped from the surface of GP, PC and CAC concrete cylinders before and after subjecting them to the dynamic acid tests. Care was taken to ensure that the particles collected, consisted of pastes or were aggregates coated in hardened paste. The chipped

pastes were then sputter coated in carbon in order to avoid them from charging when subjected to the electron beam in the SEM.

3.6.2 Material characterisation

3.6.2.1 X-Ray fluorescence (XRF)

X-Ray fluorescence (XRF) spectroscopy can be used to identify elements (and compounds by means of computation from the elemental analysis) in test specimens both quantitatively and qualitatively (Reinhold Schlotz and Uhlig 2006; Oyedotun 2017). X-ray fluorescence is a specialised technique, a full description of which falls outside of the scope of this study. However, a brief description of the method is warranted.

The measurement principle used in x-ray fluorescence analysis is based on the behaviour of chemical elements, when bombarded by an electron beam which causes them to emit characteristic X-ray radiation which can then be related to the element's atomic number. An element's characteristic radiation emission thus provides the basis for identifying chemical elements within a specimen (Schlotz and Uhlig 2006). X-ray detection is achieved through suitable detector materials, which experience pulses whose strengths are proportional to the energy of the respective x-ray quanta produced by the effect of X-rays (Schlotz and Uhlig 2006).

3.6.2.2 X-ray diffraction (XRD)

Concerning their intrinsic ordering, solid-phase materials can be classified as single crystals, polycrystals or amorphous (Ceramic society of Japan, 2012).

- A crystal is a material which possess long-range order because it is composed of atoms arranged in a regular ordered pattern in three dimensions. This periodic arrangement, known as the crystal structure, extends over distances much larger than the interatomic separation.
- A polycrystalline material consists of many small single-crystal regions (called grains) separated by grain boundaries. The grains on either side of the grain boundary are misoriented relative to each other. The grains in a polycrystalline material can have different shapes and sizes.
- In amorphous (glassy) materials the atoms are not arranged in a regular periodic manner.

X-ray diffraction (XRD) is a powerful technique for the study of crystalline materials (Scrivener et al. 2004). The working principle of XRD, known as Bragg diffraction, occurs when radiation with a wavelength comparable to the atomic spacing of the crystalline lattice, undergoes constructive interference. Constructive interference occurs when the maxima of two or more waves add up together so that that the resulting wave has an amplitude equal to the sum of the individual amplitudes (Bunaciu et al. 2014).

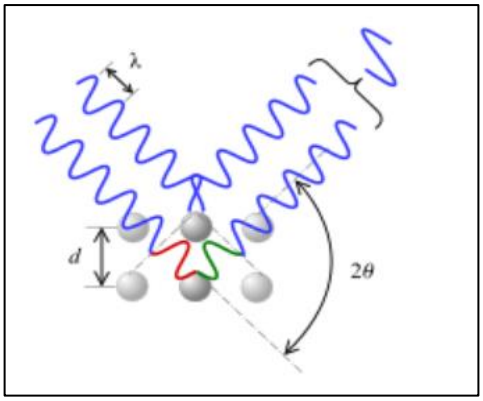

Figure 3-12: Principle of Bragg diffraction ("Bragg's Law", 2019)

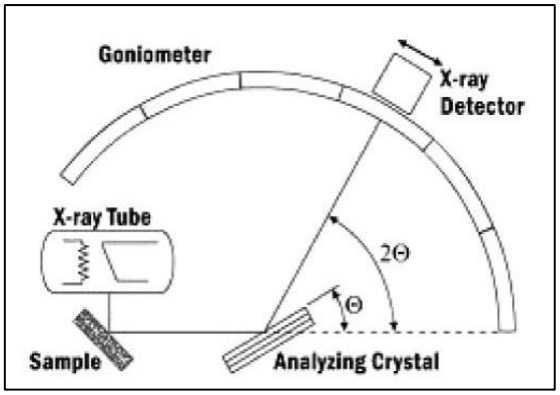

Figure 3-13: A schematic diagram showing the arrangement of elements in a diffractometer system (Bunaciu et al. 2014)

The interaction of the incident rays with the sample produces constructive interference (and a diffracted ray) when the conditions satisfy Bragg's law:

$$n\lambda = 2dsin\theta$$

Where;

λ is the wavelength
n is an integer
d is the lattice spacing and,
θ is the diffraction angle.

In the experimental setup, X-rays are generated by a cathode ray tube, filtered to produce monochromatic radiation (constant wavelength), running in parallel and concentrated in the direction of the sample. These rays are subsequently diffracted by the sample (Figure 3-13).

These diffracted X-rays are then detected, processed, and counted. By scanning the sample through a range of 2θ angles, all possible diffraction directions of the lattice should be attained due to the random orientation of the powdered material. Conversion of the diffraction peaks to d-spacings allows identification of a crystalline material. Typically, this is achieved by comparison of d-spacings with standard reference patterns (Bunaciu et al. 2014)

In this study, XRD was used for two purposes. Firstly, it was used to identify the relative proportions of crystalline and amorphous phases within the hardened cement pastes, and secondly it was to characterise the mineralogy of the crystalline phases identified. The prepared materials were analysed with a Malvern Panalytical Aeris diffractometer with PIXcel detector and fixed slits with Fe filtered Co-Kά radiation. The phases were identified using X'Pert Highscore plus software.

3.6.2.3 Scanning electron microscopy (SEM)

Scanning electron microscopy is used in the imaging of materials at magnifications as high as 300 000 times of the actual size, thus allowing the material to be seen at the micro and nano-scale.

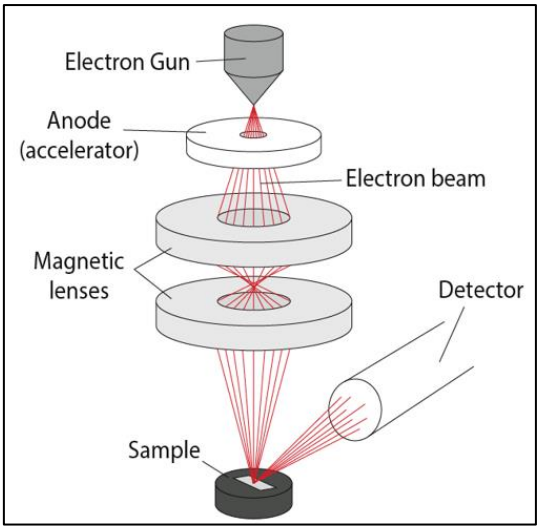

Figure 3-14: A schematic representation of the components of a scanning electron microscope (Vernon-Parry 2000)

In summary, the working principle of scanning electron microscopy is that accelerated electrons shot from an electron-gun carrying significant amounts of kinetic energy colliding with a specimen can be used to extract topographical information of a small area on the specimen (Figure 3-14).

Energy is dissipated when the incident electrons are decelerated in the solid sample creating a variety of signals which include, secondary electrons, backscattered electrons and electron beam induced current (Vernon-Parry, 2000). Secondary electrons are electrons that escape from the atoms on the specimen by mainly being knocked out of their orbits by incident electrons shot from the electron gun. These secondary electrons will then collide with the detector equipment which is then used to provide high-resolution spatial images since they can only escape from a very shallow, near-surface layer of material (Vernon-Parry 2000).

The preparation of specimens for may be conducted several ways. Scrivener (2004) recommends the use of flat polished sections because they are representative of a continuous plane in the concrete specimen. This enables a section view of the concrete specimen, which allows for the identification of paste/aggregate interfaces, and mineral phases of the hardened cement paste.

Another method is to conduct SEM on a fracture surface, which essentially reveals the flaw path from which the specimen being imaged is broken off. Since this study is interested in the effect of corrosion at the surface of geopolymer concreter specimens, polishing the surface would change the morphology of the corroded surface. Therefore, to assess the differences in microstructure before and after acid corrosion, the approach used is to scan and image fractured paste particles. A JEOL JSM-7500F, field emission scanning electron microscope was used for this purpose.

3.6.2.4 Determination of the pH of acidic solutions

pH is a measure of hydrogen ion concentration of a solution, mathematically stated as:

$$pH = -\log_{10}[H^+]$$

The pH scale ordinarily ranges from 1 to 14. Aqueous solutions at 25°C with a pH less than 7 are defined as acidic, while those with a pH greater than 7 are defined as basic or alkaline. pH measurements in this study were taken using a portable pH meter (Hanna-HI9811-5). The effective use of a pH meter requires some understanding of the measurement principle. pH meters such as the Hanna-HI9811-5 have a probe with two electrodes (Figure 3-15) that enable the determination of pH when submerged into a solution. A description of the electrodes follows:

A glass electrode that consists a pH-sensitive special glass membrane (approx. 0.1 mm thick) which contains an internal standard acidity solution (typically 0.1 N HCl) and an internal reference electrode (Ag/AgCl salt-covered wire electrode) and an external reference electrode (Ag/AgCl).

The pH-sensitive glass membrane has a special property that allows it to absorb or release hydrogen protons, depending on the nature of the solution it is in contact with. The associated chemical reaction occurring at the surface of the glass membrane reported by Karastogianni et al. (2016) is as follows:

$$Si\text{-}O^- + H_3O^+ <=> Si\text{-}O\text{-}H + H_2O \quad (3\text{-}1)$$

When in operation, both electrodes are immersed in the solution being tested. This produces a complete circuit. Hydrogen ions in the test solution exchange for other positively charged ions on the speciality glass bulb electrode, creating an electrochemical potential across the pH-sensitive glass electrode and the external electrode (Karastogianni et al. 2016).

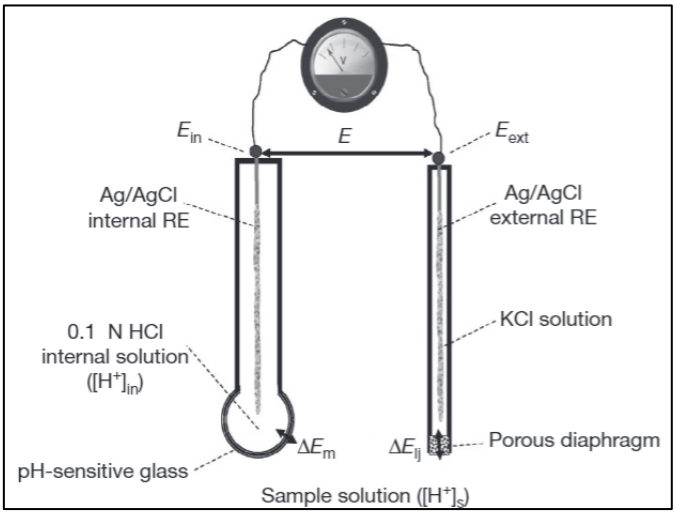

Figure 3-15: Schematic representation of a pH meter (Karastogianni et al. 2016)

The potential difference between the electrodes is amplified and converted to a pH reading by the electronic meter. To get an accurate idea of the pH in the test solution, pH meters need to be calibrated against standard buffer solutions which are normally accurate to 2 decimal places pH. The standard buffer solutions used in this study were solutions of pH 4, 7 and 10.

Before each reading, the pH meter had to be calibrated by adjusting the pH when placed in the buffer solutions to its correct pH. All three buffer solutions (pH 4, pH7 and pH 10) were used to calibrate the meter before each reading.

3.6.2.5 Determination of pH of cement pastes and aggregates components

Hardened cement pastes and aggregates were milled to prepare the specimens of pH measurements. The process followed involved placing 4 g of milled powder into 100 ml of distilled water in a plastic container. Measurement of pH in this way was undertaken to compare the surface pH of un-corroded specimens of PC, CAC and PC hardened cement pastes as well to compare the surface pH of the 5 aggregates. The digital pH meter (Hanna) used in the current study was then calibrated using standard buffer solutions before taking the pH measurements.

3.6.3 Corrosion performance testing

Corrosion performance is measured under two conditions, dynamic acidic conditions and static conditions. Descriptions of these two test conditions follow.

3.6.3.1 Static acid test

Mineral acid attack under static conditions involved placing 50 mm concrete cubes in hydrochloric acid bath. The pH was maintained between 1 and 1.1 by adding concentrated acid into the PVC bucket while measuring the pH using a calibrated pH meter. Furthermore, the acid was fully replaced every 24 hours.

The concrete cube specimens were first placed in water for 4 hours and their saturated surface dry mass was recorded together with their dimensions. Four cubes of the same type are placed into 5 Litres of acid (HCl) solution of pH 1.

Four concrete specimens of each mix design were placed in a container and submerged in 5 litres of pH 1 acid solution. Therefore, the total initial surface area subjected to acid attack for each specimen was 150 cm^2, and the total initial surface area of concrete specimens within a bucket containing 5 litres of pH 1 acid was 600 cm^2. The ratio of initial surface area to the volume of pH 1 acidic solution is 0.12 m^2/m^3 ($600cm^2/5000cm^3$).

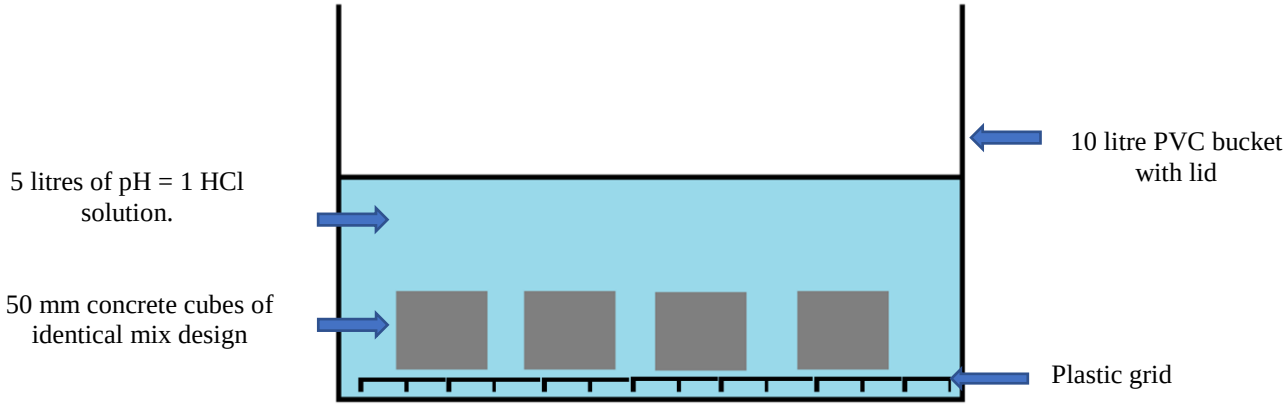

Figure 3-16: Static test configuration

This experimental arrangement provides a relatively low surface area per unit volume of acid solution. In comparison, Xiao et al. (2016) when conducting a sulfuric acid immersion test on concrete specimens placed 12 cylindrical concrete specimens contained in a 60-litre vessel. The corroding concrete surface to acidic solution ration used in Xiao et al.'s (2016) study was calculated to be 0.16 m^2/m^3.

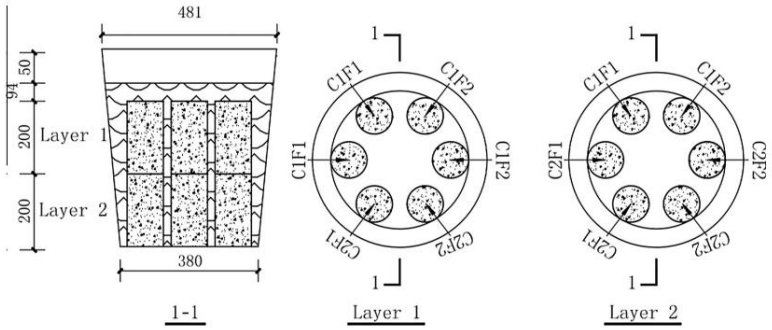

Figure 3-17: Immersion test configuration used by Xiao et al. (2016)

Care was taken during the mass measurement process not to unintentionally abrade the specimens as this test was meant to measure the material removed from the specimen without disturbing any protective precipitates or gels that were formed during corrosion. The mass of specimens was recorded every 6-8 hours for the duration of the experiment which ranged from 300 to 800 hours for various specimens.

Three specimens of each mix design were placed in a container with a hydrochloric acid solution maintained at pH 1. The mass evolution of the specimens was monitored by measuring each specimen's mass individually and then taking the average of the three readings as the representative reading.

3.6.3.2 Dynamic acid test

The most relevant previous work related to this test method was undertaken by Fourie (2007) and Motsieloa (2012). Originally developed by Fourie (2007) at the University of Cape Town, this test has been identified to assess the kinetic resistance to dissolution of Portland, calcium aluminate and geopolymer concrete produced in this study. As discussed in section 3.2 of this chapter, concrete's kinetic resistance (to dissolution) is important where the exposure condition involves both erosion and corrosion (erosion-corrosion).

This test involves subjecting concrete specimens to both acid attack and abrasion simultaneously, making it a very aggressive test on concretes. This test is typically conducted over 48 hours, however clear trends and satisfactory results were achieved for most specimens within 24 hours in this study as well as previous studies (Fourie 2007, Motsieloa 2012). .

A compartment was filled with approximately 50 ℓ of a hydrochloric or sulfuric acid solution (pH=1). Cored cylindrical concrete specimens (78 mm diameter × 125 mm) were firstly pre-saturated with tap water for four hours. Thereafter they were immersed in the acid tank and rotated at approximately 16 revolutions per minute over rubberised rollers driven by rubber pulleys connected to an electric motor (Figure 3-18). A PVC brush is lowered onto the surface of the specimen to dislodge any loose erodible material forming at the surface of the specimen.

Measurements of the mass of the specimen were measured every 2 hours and a pH of between 1.0 and 1.1 was maintained for the duration of the test. The acid solution was renewed daily (24 h) for specimen tests that were conducted for durations longer than 24 hours.

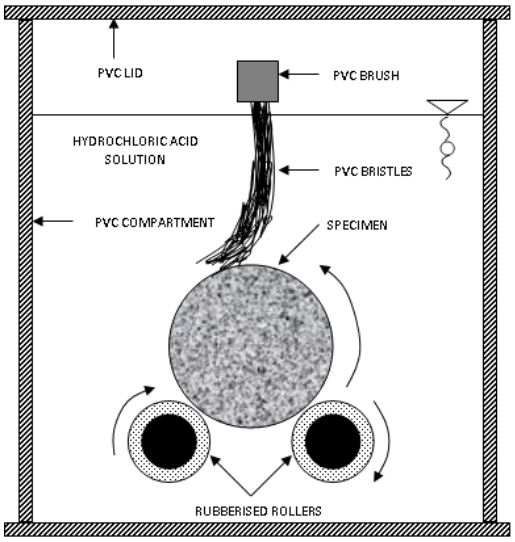

Figure 3-18: Dynamic acid test rig (Fourie 2007)

3.6.4 Compressive strength (UCS) testing

Two strength requirements for sewer pipe were considered in this study. Firstly, due to sewer pipe manufacturing requirements, adequate compressive strength is required for handling newly cast concrete pipe after a 4-hour steam curing period. Secondly, during a pipe's service-life, adequate strength is required to resist dead and live loads in service. Therefore, the compressive strength of concrete specimens was measured after four hours of humidity-controlled oven curing and after 28 days of conventional curing.

Pipe manufacturers state that this production process typically allows for the concrete pipe to be de-moulded immediately after curing which enables the mould to be reused (van Burick, personal communications 2019). The required concrete strength at de-moulding is 15 MPa.

Furthermore, adequate concrete strengths are required for structural capacity during its service. Concrete strength measurements were conducted 28 days after casting. 100 mm cubes produced for compressive strength testing were tested under axial compression as per SANS 5863 (2006).

3.7 Assumptions and limitations

While this study is aimed at assessing the potential of geopolymer concretes for sewer applications, it is acknowledged that the sewer is a complex environment and replication of its complex systems is not within the scope of this work nor the capability of the researcher.

3.7.1 Components of MIC resistance evaluated

A key assumption is that the resistance of concrete subjected to MIC can be separated into the parts listed in Table 3-1. While dealing with the proposed parts of corrosion is easier, simplifications are still necessary for the practicality of the experimental work. No attempt is made to simulate biogenic acid production.

Only two of the MIC listed in Table 3-1 resistance components are evaluated. The first is related to kinetic resistance, where only the dissolution rate is accounted for. The test selected to evaluate the kinetic resistance

component of MIC resistance of concrete is the dynamic acid (HCl/H_2SO_4) test. The second MIC resistance component evaluated is physical barrier resistance emanating from corrosion precipitates. As mentioned in heading 3.3.1.2, this study used only HCl for the static acid test whereas it would have been of interest to conduct the test using both acid types. However, the protective gels and precipitates that form the HCl corrosion reaction are evaluated. It is suggested corrosion precipitate gels such as AH_3 occur in both H_2SO and HCl corrosion.

Table 3-14: Relating corrosion product, test method and the relate sewer exposure condition

MIC corrosion component	Performance test used t	Related sewer exposure condition
Kinetic resistance (to dissolution)	Dynamic acid test	Static corrosion
Physical corrosion barrier formed by corrosion products (precipitates and gels)	Static acid test	Erosion corrosion

3.7.2 Limitations in acid performance tests

Two significant simplifications are acknowledged in the performance-testing methodology used in this study. The first limitation is that the severity of corrosion was only measured in terms of mass loss of the concrete specimens. Other researchers, in addition to mass loss, have used hydrogen ion consumption (Fourie 2007, Motsieloa, 2012), compressive strength (Bakharev, 2004) and the dynamic modulus of elasticity (Xiao) to assess concretes resistance to corrosion. The second significant simplification relates to the use of hydrochloric acid instead of sulfuric acid in the static acid test, and where calcium-rich systems are tested in the dynamic acid test.

3.7.3 Limitations in characterisation methods

The primary material characterisation methods (XRD and XRF) are highly developed and sophisticated methods. The purpose of using these methods to characterise materials in this study was to obtain a reasonable measure of the elemental and mineralogical character of the hardened cement pastes and aggregates. These results are not intended to be definitive and thus some degree of error should be allowed for in a reading these results.

3.8 References

Alexander, M., Bentur, A., Mindess, S. 2017. “Durability of concrete design and construction”. CRC Presse. Taylor and Francis group.

Bragg’s Law .2019. Wikipedia. Available at: <https://en.wikipedia.org/wiki/Bragg%27s_law > (Accessed: 15 December 2019).

Bunaciu, A., Udristioiu, A.G., Aboul-Ennin, H.Y. 2014. “X-Ray Diffraction: Instrumentation and Applications” Critical Reviews in Analytical Chemistry (2015) 45, 289–299.

Cant, J., & Trew, J. .1998. “High-Pressure Water Jetting: Avoiding Damage to Sewers. Water and Environment Journal”, 12(4), 265–267.

Council for Scientific and Industrial Research. 1959. “Corrosion of concrete sewers. Pretoria”: CSIR. Series DR12.

Fourie, C.W. 2007. “Acid resistance of sewer pipe concrete”. MSc Thesis. University of Cape Town. Cape Town, South Africa.

Gay, H., Meynet, T., Combani, J. 2016. “Local study of the corrosion kinetics of hardened Portland cement under acid attack”. Cement and concrete research.

Goyns, A. M. 2013. Design manual for concrete pipe outfall sewers. Midrand: Concrete Manufacturers Association.

Grengg, C., Mittermary, F., Ukrainczyk, N., Koraimann, G., Kienesberger, S., Dietzel, M. 2017. “Advances in concrete materials for sewer systems affected by microbially induced concrete corrosion: A review.”

Huber, B., Hilbig, H., Mago, M., Drewes, J.E., Muller, E. 2016. “Comparative analysis of biogenic and chemical sulfuric acid attack on hardened cement paste using laser ablation-ICP-MS.” Cement and Concrete Research, 87

Jensen, W., B. 2015. “The importance of kinetic metastability: some common everyday examples”. Journal of Chemical Education 92 (4), 649-654

Kaech, A. 2014. “An introduction to electron microscopy instrumentation, imaging and preparation”. Centre for microscopy and image analysis. University of Zurich

Karastogianni, S., Girousi, S., Sotiropoulos, S. 2016. “pH: Principles and measurement”. Aristotle University of Tessaloniki, Greece.

Mohammed, A., Abdullah, A. 2018. “Scanning electron microscopy (SEM): a review”. Proceedings of 2018 international conference on hydraulics and pneumatics”.

Monteny, J., Vincke, E., Beeldens, A., Taewre, L., Van Germet, D. 2000. “Chemical, microbiological, and in situ test methods for biogenic sulfuric acid corrosion of concrete”. Cement and Concrete Research 30.

Motsieloa, N. 2013. “Acid resistance of sewer pipe concrete”. MSc (Eng) dissertation. University of Cape Town, Cape Town.

Oyedotun, T., Temitope, D. 2017. “X-ray fluorescence (XRF) in the investigation of the composition of earth materials: a review and overview”. Geology, Ecology and Landscapes, volume 2.

Richardson, I. G., Skibsted, J., Black, L., & Kirkpatrick, R. J. (2010). “Characterisation of cement hydrate phases by TEM, NMR and Raman spectroscopy”. Advances in Cement Research, 22(4), 233–248.

SABS. 2006. “SANS 5861-3:2006: Concrete tests, Part 3: Making and curing of test specimens”.

SABS. 2006. “SANS 5863:2006: Compressive strength of hardened concrete”.

Schlotz, R, Uhlig, S. 2006. “Introduction to X-Ray Fluorescence (XRF)”. Bruker advanced X-Ray solutions.

Scrivener, K.L. 2004. “Backscattered electron imaging of cementitious microstructures: understanding and quantification”. Cement and Concrete Composites. 26(8): 935 – 945.

Seager, R.J., Acevedo, A.J., Spill, F. 2018. “Solid dissolution in a fluid solvent is characterized by the interplay of surface area-dependent diffusion and physical fragmentation”.

The Ceramic Society of Japan. 2012. Classification of Ceramics. In: Advanced Ceramic Technologies & Products. Springer, Tokyo

Vernon-Parry, K, D. 2000. “Scanning electron microscopy: an introduction”.

Xiao, J., Qu, W., Li, W, Zhu, P. 2016. “Investigation on effect of aggregate on three non-destructive testing properties of concrete subjected to sulfuric acid attack” Construction and building materials 115, 489-495.

4 Results and Discussion

4.1 Introduction

This chapter presents results from material characterisation and corrosion performance testing of geopolymer concretes, calcium aluminate cement concrete and Portland cement concrete. The first part of this chapter is concerned with the characterisation of hardened cement pastes (HCP) and the characterisation of calcareous and siliceous aggregates used in concrete specimens subjected to corrosion testing.

Chemical characterisation performed by x-ray diffraction (XRD) and x-ray fluorescence (XRF) was used to investigate the relationship between chemical composition and mineralogy of corrosion PC concretes, CAC concretes and GP concretes. Scanning electron microscopy provided visual evidence of deterioration (via corrosion) at high magnification, which is useful for assessing corrosion in the microstructure of concrete.

The second part of this chapter is concerned with the performance of the concretes under acid conditions. As discussed in Chapter 3.2, it is suggested that these acid tests should be related to a MIC exposure condition and the MIC resistance component of the concrete. Figure 4-1 illustrates this proposed relationship schematically.

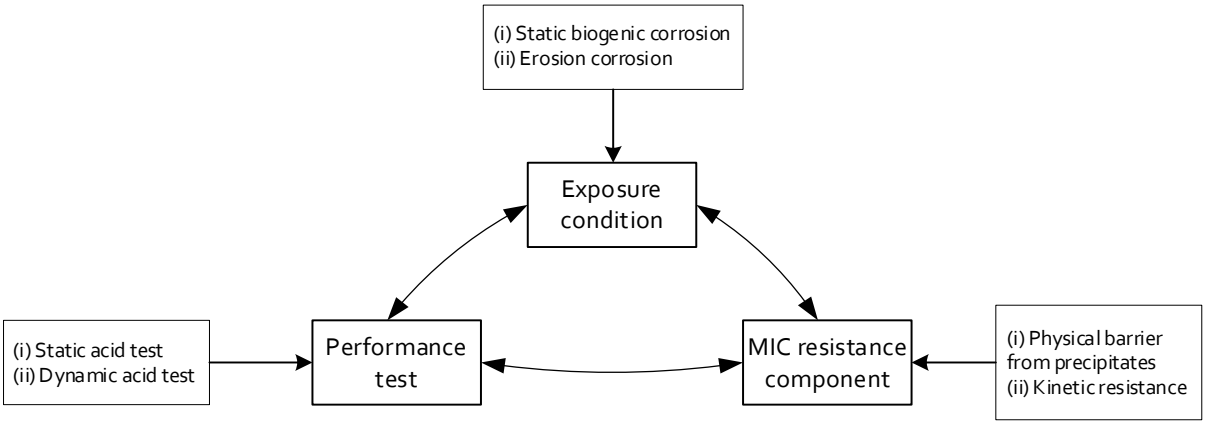

Figure 4-1: Mineral acid performance tests related to exposure condition and the MIC resistance component

The third part of this chapter is concerned with the analysis of the results obtained from material characterisation and mineral acid testing.

4.2 Material characterisation

Material characterisation results are presented for both HCPs and aggregates. The types of analysis used are XRF, XRD. SEM and pH measurements (of milled HCP and aggregates).

4.2.1 X-ray fluorescence (XRF)

4.2.1.1 XRF of hardened cement pastes

Elemental analysis of the composition of the three hardened cement pastes shows that Portland hydrated cement paste is composed of calcium oxide (53%) and silica (17.7%). Calcium aluminate HCP is composed of

approximately equal amounts of alumina (32.75%), and calcium oxide (32.9%). The main constituents of geopolymer HCP are silica (44%) and alumina (20.3%). Table 4-1 shows the proportions of oxides identified through XRF analysis.

Table 4-1: XRF: Analysed percentage grades of hardened cement pastes (HCP)

Element/compound	Hardened cement paste		
	PC	CAC	GP
	%	%	%
Fe_2O_3	1.806	10.083	1.470
SiO_2	17.765	4.064	44.057
Al_2O_3	3.725	32.750	20.330
K_2O	0.084	0.035	3.064
P	0.020	0.059	0.196
Mn_3O_4	0.519	0.216	0.147
CaO	53.730	32.896	11.615
MgO	2.201	0.528	2.402
TiO_2	0.242	1.479	1.143
Na_2O	0.014	<0.010	4.668
V_2O_5	<0.004	0.077	0.010
BaO	0.023	<0.006	0.118
Cr_2O_3	0.032	0.126	0.017
SrO	0.021	0.023	0.178
ZrO_2	0.025	0.053	0.049
MnO	0.374	0.156	0.106
SO_3	2.318	0.140	0.920
LOI	16.118	13.935	8.964
Total (XRF)	99.499	100.923	100.388

4.2.1.2 XRF of Aggregates

Five aggregate types were analysed using XRF. Dolomite was the most calcium-rich aggregate (23%) followed by dolerite (10.62%) and Andesite (7.9%). Furthermore, dolomite aggregate had a significant amount of magnesium oxide (15.6%). Granite and ferro-quartz had low calcium content with contents of 1.5% and .023% respectively. Ferro-quartz was the most silica-rich aggregate with 96% of the aggregate composed of SiO_2. Table 4-2 provides a comprehensive breakdown of major oxides identified by XRF analysis.

Table 4-2: XRF: Analysed percentage grades of aggregates

Element	Aggregate type				
	Dolomite %	Ferro-quartz %	Dolerite %	Andesite %	Granite %
Fe_2O_3	0.595	1.074	12.810	11.699	2.062
SiO_2	24.715	95.968	51.862	55.047	72.248
Al_2O_3	0.851	1.759	14.646	14.273	14.003
K_2O	0.259	0.432	0.703	0.957	4.201
P_2O_5	<0.007	0.017	0.177	0.123	0.086
Mn_3O_4	0.392	<0.008	0.214	0.157	0.038
CaO	23.031	0.023	10.615	7.897	1.535
MgO	15.645	0.155	6.029	4.300	0.572
TiO_2	0.020	0.085	1.145	0.870	0.247
Na_2O	<0.010	<0.010	2.419	3.319	3.974
V_2O_5	<0.004	0.007	0.053	0.036	0.005
BaO	<0.009	0.012	0.030	0.029	0.059
Cr_2O_3	<0.010	0.053	0.024	0.020	0.030
SrO	0.003	0.004	0.019	0.024	0.021
ZrO_2	0.006	0.023	0.023	0.021	0.028
MnO	0.365	<0.007	0.199	0.146	0.036
LOI	34.839	0.318	-0.168	1.738	0.706
Total (XRF)	100.357	99.932	100.602	100.511	99.815

4.2.2 X-ray diffraction (XRD)

Quantitative X-ray diffraction analysis was conducted on milled hardened cement paste and aggregates (95% smaller than 75 microns). X-ray diffraction was conducted between 5 and 90 degrees of 2θ. Mineral acid solubility data for each mineral type was obtained from an open-source online mineral database compiled by Crawford (n.d). XRD diffractograms for each HCP and aggregate sample are presented in Chapter 0 (Appendix A).

4.2.2.1 XRD of Hardened Cement Pastes

XRD data of the hardened cement pastes indicates that all three binder systems are mainly amorphous. The amorphous content of Portland cement was 79%, calcium aluminate cement was 70.1% and the amorphous content of fly ash-based geopolymer cement was 72 %. Therefore, it is likely that the amorphous phases of these binders have a significant bearing on their acid resistance.

Table 4-3: Mineralogy of hydrated PC paste obtained by quantitate XRD analysis

Mineral	**Percentage**	**Chemical formula**	**HCl Solubility**	**H_2SO_4 solubility**
Quartz	0.5%	SiO_2	Insoluble	Insoluble
Mullite	0.7%	$3Al_2O_3 \cdot 2SiO_2$	Insoluble	Insoluble
Calcite*	2.0%	$CaCO_3$	Soluble	Soluble
Portlandite*	6.3%	$Ca(OH)_2$	Soluble	Soluble
Hatrurite *	11%	$Ca_3(SiO_4)O$	(No data)	(No data)
Gypsum	0.5%	$CaSO_4$	Soluble	Insoluble
Amorphous	79%			

In Portland cement hydrated paste, calcium bearing minerals such as calcite, Portlandite and Hatrurite are soluble in acids. The amorphous phases are likely to be calcium silicate hydrates (C-S-H). X-ray diffraction graphs of Portland cement paste typically exhibit very broad bands due to their low crystallinity.

Table 4-4: Mineralogy of hydrated CAC paste obtained by quantitate XRD analysis

Mineral	**Percentage**	**Chemical formula**	**HCl solubility**	**H_2SO_4 solubility**
Cristobalite	0.5%	SiO_2	Insoluble	Insoluble
Quartz	0.3%	SiO_2	Insoluble	Insoluble
Magnetite*	0.2%	$FeO \cdot Fe_2O_3$	Soluble	Insoluble
Katoite**	6.7%	$Ca_3Al_2(SiO_4)(OH)_8$	(no data)	(no data)
Dolomite*	1.4%	$CaMg(CO_3)_2$	Soluble (if heated)	Insoluble
Srebrodolskite	7.1%	$Ca_2Fe^{3+}{}_2O_5$	(no data)	(no data)
Hedenbergite	0.1%	$CaFe^{2+}Si_2O_6$	Insoluble	(no data)
Krotite*	12.8%	$CaAl_2O_4$	(no data)	(no data)
Chromite*	1.2%	$FeCr_2O_4$	Insoluble	Insoluble
Amorphous	70.1%			

Hydrated CAC pastes also have a high proportion of amorphous content. Krotite (12.8%), Srebrodolskite (7.1%) and Katoite (6.7%) make up the bulk 29.9% of crystalline content.

Table 4-5: Mineralogy of hardened geopolymer cement paste obtained by quantitate XRD analysis

Mineral	Percentage	Chemical formula	HCl solubility	H_2SO_4 solubility
Quartz	8.7%	SiO_2	Insoluble	Insoluble
Mullite	13.9%	$3Al_2O_3{\cdot}2SiO_2$	Insoluble	Insoluble
Hematite*	0.9%	Fe_2O_3	Soluble	Insoluble
Sillimanite	3.5%	Al_2SiO_5	Insoluble	Insoluble
Calcite*	1.0%	$CaCO_3$	Soluble	Soluble
Amorphous content	72.0%			

The geopolymer had 72% amorphous content and 28% crystalline phases. Mullite (13.9%), quartz (8.7%) and sillimanite are insoluble in mineral acids. In their characterisation of selected South African fly ashes, Aphane et al. (2015) found mullite, accounted for greater 28.5% of fly ash mineralogy. In attempting to extract alumina from fly ash by leaching using sulfuric acid, it was observed that crystalline mullite was acid-insoluble. Furthermore, Aphane et al. (2015) found that quartz, another insoluble mineral accounted for 7.2% of fly ash mineralogy. The most likely reason for the high proportion of mullite and quartz in the geopolymer, is that these minerals originate from the fly ash precursor constituting the geopolymer cement.

4.2.2.2 XRD of Aggregates

Ferro-quartz XRD results show a high proportion of quartz the mineral with minute quantities of hematite and biotite. Quartz has high chemical stability and thus can be considered fully resistant to acid attack. Biotite and hematite are both soluble in concentrated acids however, their contribution to total acid resistance is negligible as they constitute only 1% of the mineralogy of the ferro-quartz aggregate.

Table 4-6: Mineralogy of ferro-quartz aggregate obtained by quantitative XRD analysis

Mineral	Percentage	Chemical formula	HCl solubility	H_2SO_4 solubility
Quartz	99%	SiO_2	Insoluble	Insoluble
Hematite	0.1%	Fe_2O_3	Soluble	Insoluble
Biotite	0.9%	$K(Mg,Fe)_3AlSi_3O_{10}(OH)2$	Insoluble	Soluble

The mineralogy of dolomite is mainly constituted by dolomite mineral crystals (75%) and quartz (24.1%). This aggregate, therefore, has high acid solubility as quartz constitutes only a quarter of its mineral composition.

Table 4-7: Mineralogy of dolomite aggregate obtained by quantitative XRD analysis

Mineral	Percentage	Chemical formula	HCl solubility	H_2SO_4 solubility
Quartz	24.1%	SiO_2	Insoluble	Insoluble
Dolomite	75.7%	$CaMg(CO_3)_2$	Soluble	Soluble
Biotite	0.3%	$K(Mg,Fe)_3AlSi_3O_{10}(OH)2$	Soluble	Soluble

Labradorite is the main mineral found in dolerite aggregate at 58.5%. This feldspar mineral is soluble in HCl and H_2SO_4. The reaction of labradorite feldspar with aqueous solutions at pH = 1 and 2.0 produce a surface which is depleted in calcium and aluminium and is enriched in silicon (Casey et al. 1989).

Table 4-8: Mineralogy of dolerite aggregate obtained by quantitative XRD analysis

Mineral	Percentage	Chemical formula	HCl solubility	H_2SO_4 solubility
Quartz	3.7%	SiO_2	Insoluble	Insoluble
Augite	16.8%	$(Ca,Na)(Mg,Fe,Al,Ti)(Si,Al)_2O_6$	Insoluble	Insoluble
Smectite 14	6.9%	$A_{0.3}D_{2-3}[T_4O_{10}]Z_2 \cdot nH_2O$	Insoluble	(no data)
Labradorite	58.5%	$((Ca, Na)(Al, Si)_4O_8)$	Soluble	Soluble
Muscovite	1.4%	$KAl_2(AlSi_3O_{10})(F,OH)_2$	Insoluble	Insoluble
Enstatite, ferroan	12.7%	$Mg_2Si_2O_6$	Insoluble	Insoluble

Andesite aggregate has two minerals regarded as being acid-soluble, clinochlore and clinozoisite. They constitute 13% and 5.8% of andesite's mineralogy respectively. Clinochlore, a mineral belonging to the chlorite group of minerals is soluble in acids is reported to be soluble in HCl by Ross (1969).

Table 4-9: Mineralogy of andesite aggregate obtained by quantitative XRD analysis

Mineral	Percentage	Chemical formula	HCl solubility	H_2SO_4 solubility
Microcline	3.1%	$KAlSi_3O_8$	Insoluble	Insoluble
Quartz	11.9%	SiO_2	Insoluble	Insoluble
Clinochlore	13%	$Mg_5Al(AlSi_3O_{10})(OH)_8$	Soluble	Soluble
Actinolite	18.1%	$Ca_2(Mg,Fe)_5Si_8O_{22}(OH)_2$	Soluble	(no data)
Diopside, ferroan	6.1%	$CaMgSi_2\ O_6$	Insoluble	Insoluble
Albite	42.1%	$Na(AlSi_3O_8)$	Insoluble	Insoluble
Clinozoisite	5.8%	$\{Ca_2\}\{Al_3\}(Si_2O_7)(SiO_4)O(OH)$	Soluble	Insoluble

The mineralogy of granite aggregate is largely made up of acid-insoluble minerals. The major minerals detected by XRF are albite (48.3%), microcline (15.9%) and quartz (32.7%). Small amounts of soluble minerals are also present in the form of clinochlore and actinolite.

Table 4-10: Mineralogy of granite aggregate obtained by quantitative XRD analysis

Mineral	Percentage	Chemical formula	Acid solubility	H_2SO_4 solubility
Albite	48.3%	$Na(AlSi_3O_8)$	Insoluble	Insoluble
Biotite	2.4%	$K(Mg,Fe)_3AlSi_3O_{10}(OH)2$	Insoluble	Soluble
Microcline	15.9%	$KAlSi_3O_8$	Insoluble	Insoluble
Quartz	32.7%	SiO_2	Insoluble	Insoluble
Clinochlore llb-2	0.6%	$Mg_5Al(AlSi_3O_{10})(OH)_8$	Soluble	Soluble
Actinolite	0.1%	$Ca_2(Mg,Fe)5Si_8O_{22}(OH)_2$	Insoluble	(no data)

4.2.3 pH of hardened cement pastes and milled aggregate

Measurements of the pH of milled aggregate and HCPs show that the un-corroded pH of all the HCPs are alkaline with PC HCP having the highest measured pH at 13.28, GP HCP equal to 12.73 and CAC HCP equal to 12.2

The aggregates all had relatively neutral pH values ranging from pH 7 to pH 9, with dolomite being the most basic aggregate at pH 9.21 and ferro-quartz having the lowest pH at 7.02. Furthermore the variation in the pH of the HCP's was substantially lower than the variation in pH measurements from the aggregates (Figure 4-2).

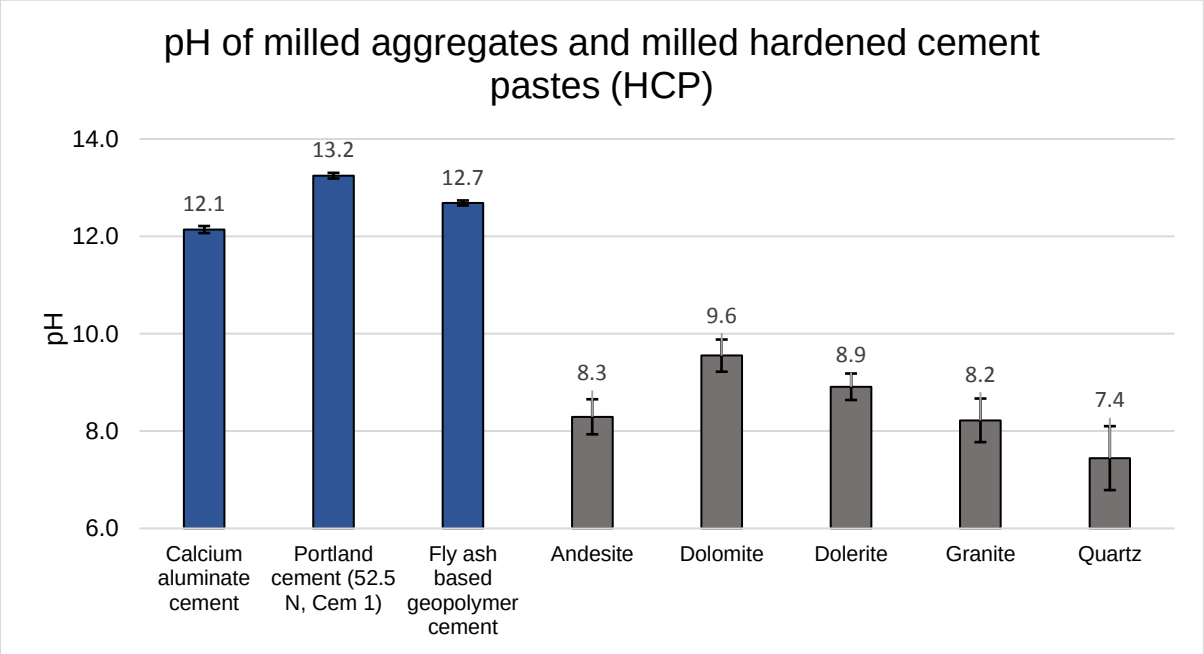

Figure 4-2: pH of milled hardened cement pastes and aggregates

Figure 4-2 provides some insight into the differences in pH between binders and aggregates. The pH of the binders range from 12.2-13.28 while the pH of the aggregates range from 7.02-9.21.

4.3 Acid performance tests

Seven (7) different cement aggregate combinations were tested under static and dynamic tests. Presentation of the results is organised firstly by the type of test (static or dynamic acid test) and secondly by a material grouping (calcareous aggregate concretes or GP concrete with siliceous aggregates). The results are presented in this way to maintain a reasonable resolution in the graphical representation of the data because the performance across all the different mixes varied significantly.

4.3.1 Static acid tests

4.3.1.1 Static HCl testing of concretes with calcareous aggregates

Corrosion was measured in terms of the mass loss in specimens. The first set of concretes to be tested was a geopolymer-dolomite with control mixes of CAC and PC paired with dolomite aggregate. The test was conducted over 800 hours, in hydrochloric acid maintained at pH 1. The test was conducted according to the method described in Chapter 3.6.3.

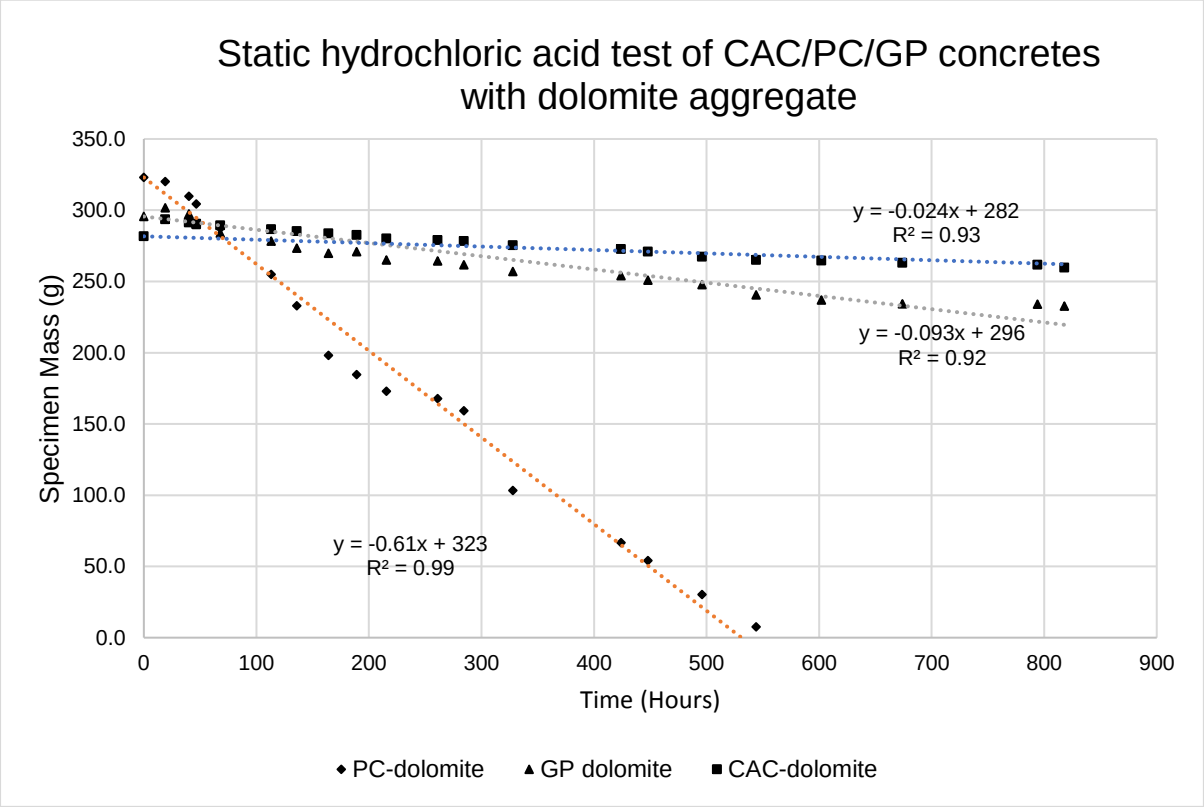

Figure 4-3: Mass loss of calcareous aggregate concretes in the static hydrochloric acid test

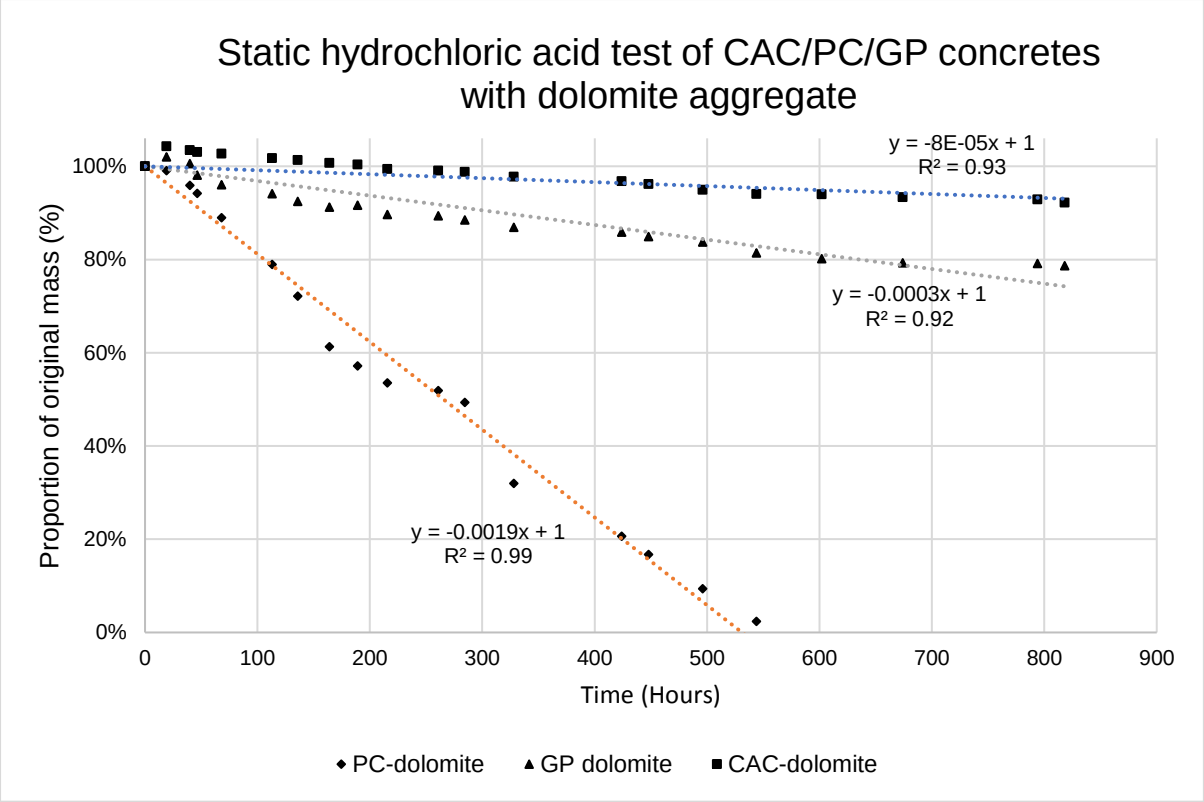

Figure 4-4: Proportion (%) of the original mass change of calcareous aggregate concretes in the static hydrochloric acid test

Table 4-11: Calculated corrosion rates of calcareous aggregate concretes in the static HCl test.

	GP-dolomite	PC-dolomite	CAC-dolomite
Initial specimen surface area (cm^2)	150	150	150
Change in mass (g/hr)	0.09	0.51	0.02
*Surface corrosion rate ($mg/cm^2/hr$)	0.62	3.37	0.16
Remaining proportion (%) of specimen at 819 hours.	79%	0%	92%

The surface corrosion rate is calculated by dividing the average rate of mass loss (g/hr) obtained by linear regression of the data for duration of the test, by the initial surface area of the specimen and then dividing this value by the duration of the test to get an averaged corrosion rate with units ($mg/cm^2/hr$). The corrosion rate formula expressed in Equation 4-1 below carried through for all the subsequent corrosion rate calculations reported in this chapter.

$$Surface\ corrosion\ rate = \frac{\left(Rate\ of\ mass\ loss\ (\frac{mg}{hr})\right)}{Initial\ surface\ area(cm2)} \qquad (4\text{-}1)$$

*It should be noted that the formula above can be shown to mathematically yield corrosion units of ($mg/cm^2/hr$).

$$\frac{\left((\frac{mg}{hr})\right)}{(cm2)} = \frac{\left((\frac{mg}{hr})\right) * hr}{(cm2) * hr} = \frac{(mg)}{(cm2) * hr} = \frac{(mg)}{(cm2) * hr} * hr = \frac{(mg)}{(cm2)} \qquad (4\text{-}2)$$

Under static hydrochloric acid testing over 800 hours, all specimens exhibited relatively linear rate of mass loss. Linear regression lines are plotted to provide a linear relationship between mass and time in Figure 4-3. CAC-dolomite concrete showed the lowest rate of corrosion (0.16 mg/cm^2/hr). The rate of GP-dolomite corrosion is 4 times higher than that of CAC-dolomite concrete (0.62 mg/cm^2/hr) while PC-dolomite exhibited the highest rate of mass loss at 3.37 gm/cm^2/hr, nearly 7 times higher than CAC-dol.

Figure 4-5: CAC-dolomite after 350 hours of immersion in pH 1, hydrochloric acid

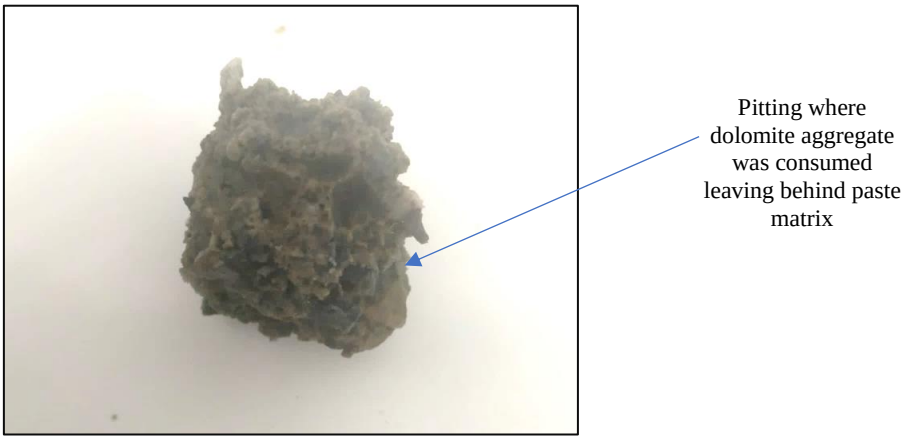

Figure 4-6: PC-dolomite after 350 hours of immersion in pH 1, hydrochloric acid

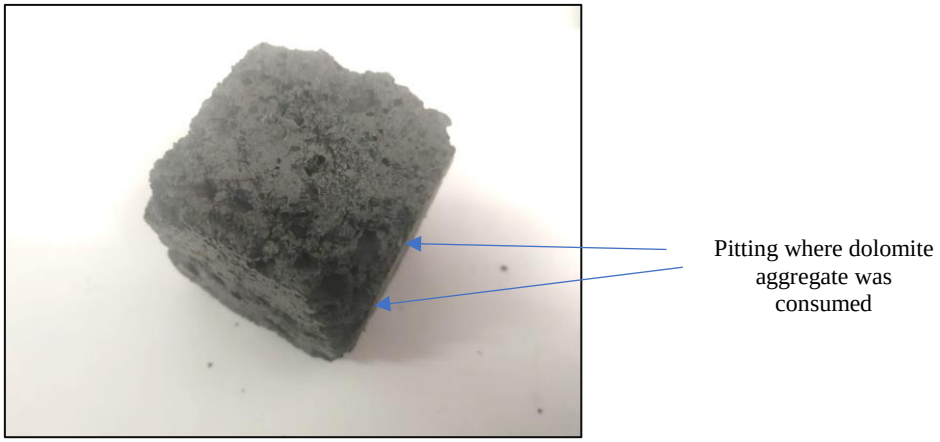

Figure 4-7: GP-dolomite after 350 hours of immersion in pH 1, hydrochloric acid

Figure 4-5, Figure 4-6 and Figure 4-7 show images of CAC-dolomite, PC-dolomite and GP-dolomite specimens after 350 hours of immersion in HCl. Visually, the CAC-dolomite specimens were the most uniform, with little variation in the corrosion of the paste and aggregate, i.e. the surface was fairly smooth. The GP-dolomite specimen displayed preferential corrosion of the aggregates with the geopolymer paste "standing proud". The PC-dolomite specimen was the most severely corroded, both paste and aggregate display a high degree of corrosion, however, the dolomite aggregate appeared to be more severely corroded. Given that the concrete mix designs were constituted by 23% cement paste and 77% aggregates, an interesting observation is that the dolomite aggregates in the CAC-dolomite concrete specimens did not display the same corrosion behaviour as they did in the PC and GP specimens. This indicates the existence of a protective mechanism that protects both paste and aggregate from acid attack.

4.3.1.2 Static HCl testing of GP concretes with siliceous aggregates

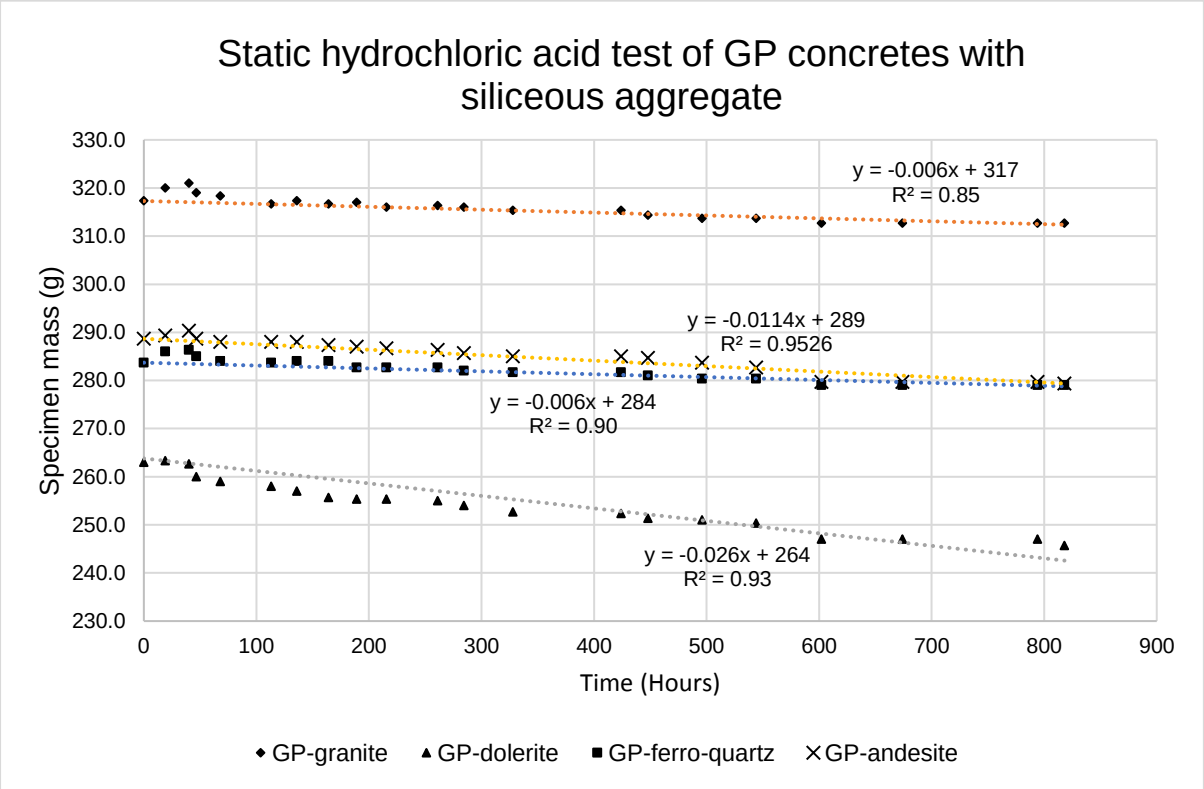

Figure 4-8: Mass change of siliceous aggregate concretes in the static hydrochloric acid test

The mass-loss rates of the four siliceous aggregate geopolymer concretes in hydrochloric were approximately linear. Figure 4-9 and Figure 4-11 show that over 818 hours in submersion in hydrochloric acid, the geopolymer specimens using siliceous aggregates had lower mass loss when compared to calcareous concrete. GP-dolerite specimens had the highest corrosion rate (0,1626 mg/cm^2/hour) followed by GP-andesite (0.0757 mg/cm^2/hour). GP-granite and GP-ferro-quartz. GP-ferro-quartz concrete exhibited the lowest rates of corrosion (0.0396 mg/cm^2/hr and 0,0406 mg/cm^2/hr respectively) of all the concretes tested under the static hydrochloric acid test (see Table 4-12).

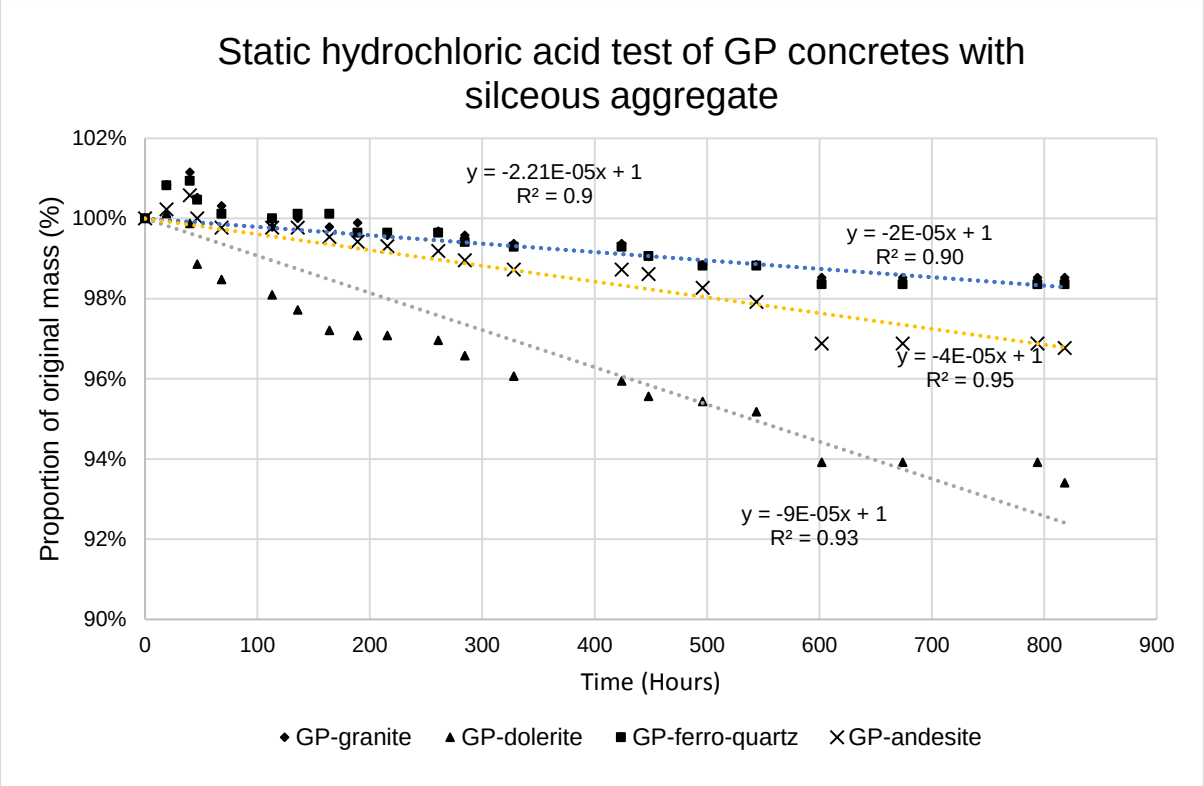

Figure 4-9: Proportion (%) of original mass evolution of siliceous aggregate concretes in the static hydrochloric acid test

Table 4-12 shows provides a tabulated summary of the corrosion data displayed in the figures above. The mass loss of the geopolymer specimens are significantly lower than the mass losses in the CAC-dolomite, PC-dolomite and GP-dolomite specimens reported provided section 4.3.1.1 of this chapter. Over the same test duration and acidic conditions the worst performing geopolymer specimen (GP-dolerite) only lost 7% of its mass whereas the GP-dolomite, CAC-dolomite and PC-dolomite specimens 21%, 8% and 100% of their original mass respectively.

Table 4-12: Calculated surface corrosion rates of calcareous aggregate concretes in the static hydrochloric acid test.

	GP-ferro-quartz	GP-andesite	GP-dolerite	GP-granite
Initial specimen surface area (cm^2)	150	150	150	150
Change in mass (g/hr)	0.0059	0.0114	0.0244	0.0061
Surface corrosion rate ($mg/cm^2/hr$)	0.0396	0.0757	0.1626	0.0406
Remaining mass proportion (%) of specimen at 819 hours.	98.35%	96.77%	93.41%	98.53%

*GP-ferro-quartz

*GP-andesite

*GP-dolerite

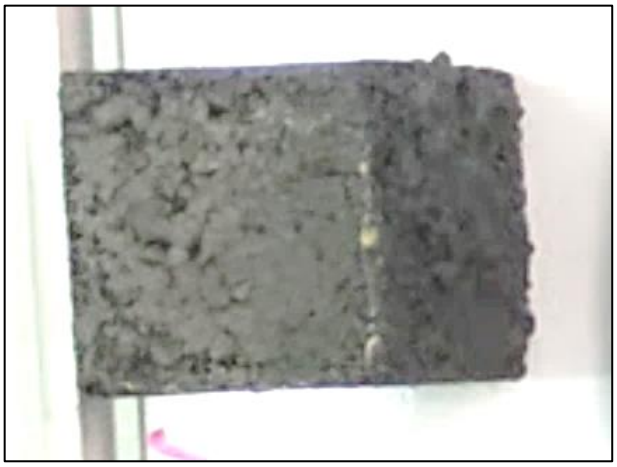

*GP-granite

Figure 4-10: GP-ferro-quartz, GP-andesite, GP-dolerite and GP-granite specimens after 700 hours of immersion in pH 1, hydrochloric acid (Respectively from left to right)

Apart from the GP-dolerite specimens, which displayed slight pitting on the surface of exposed aggregates, very little corrosion was visible on the geopolymer/siliceous aggregate set of concretes after 820 hours of immersion in HCl at pH 1. This was due to the relatively low rates of corrosion experienced by geopolymer specimens during the static hydrochloric acid test.

4.3.2 Dynamic acid tests

4.3.2.1 Dynamic HCl testing of concretes with calcareous aggregates

The detailed rationale for using hydrochloric acid is provided in chapter 3.6.3 of this study. In brief, HCl is used in this test because the corrosion of calcium-rich concretes in H_2SO_4 produces gypsum which quickly saturates the solution and causes corrosion to stall (Fourie 2007). However, HCl produces soluble calcium chloride and thus the acidic solution does not become saturated with precipitates salts. The corrosion reaction thus proceeds unencumbered.

The dynamic HCl test results of PC, CAC and GP concrete using dolomitic aggregates are presented below. Dynamic testing includes abrasive action of PVC bristles on the rotating surface of the cylindrical concrete specimen. This test was conducted for 25 hours.

It should be appreciated that abrasion in the context of the dynamic acid test does not refer to damage or removal of sound concrete but instead it refers to the removal of mechanically "weak" corrosion products deposited on the surface of the concrete specimen during corrosion. Figure 4-11 shows the mass loss over time of CAC, PC and GP concretes using dolomite subjected to the dynamic HCl test. Over a period of 25 hours, the data shows a highly correlated linear relationship between residual mass and time in the dynamic HCl test, with R^2 values of 0.99 or more for all three concretes.

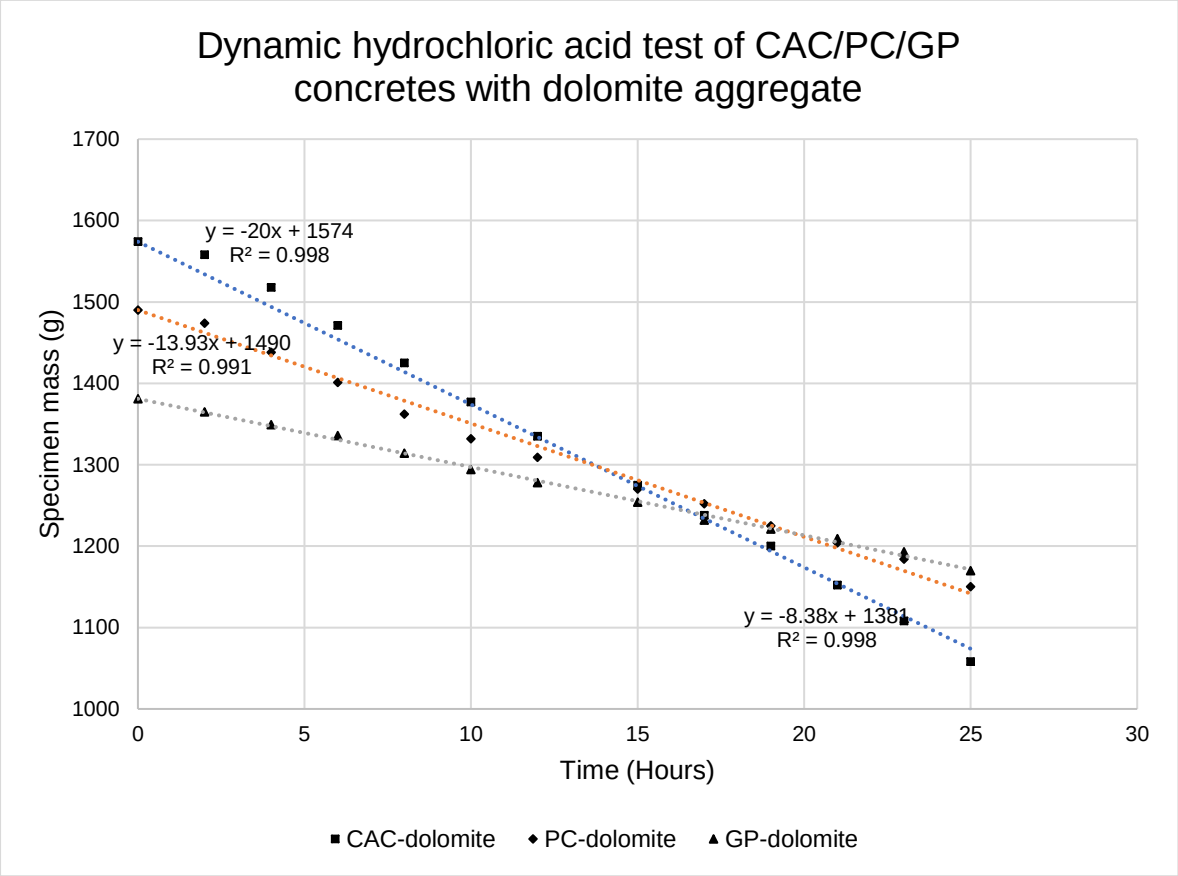

Figure 4-11: Mass change of calcareous aggregate concretes in the dynamic HCl test

All three dolomite aggregate concrete mixes exhibited a relatively steady rate of mass loss over the 25-hour test period. Unlike the results obtained from the static hydrochloric acid test, the CAC-dolomite concrete exhibited the highest surface corrosion rate (49.55 mg/cm^2/hr). The PC-dolomite specimens had corrosion rate of 34.98 mg/cm^2/hr, while the GP-dolomite specimen had the lowest surface corrosion rate (20.96 mg/cm^2/hr). It is important to note that under this test, the CAC-dolomite concrete exhibited lower acid resistance than PC-dolomite specimens and this result is in agreement with experimental results obtained by Fourie (2007) and Motsieloa (2012), where CAC and PC mixed with dolomite aggregates were tested.

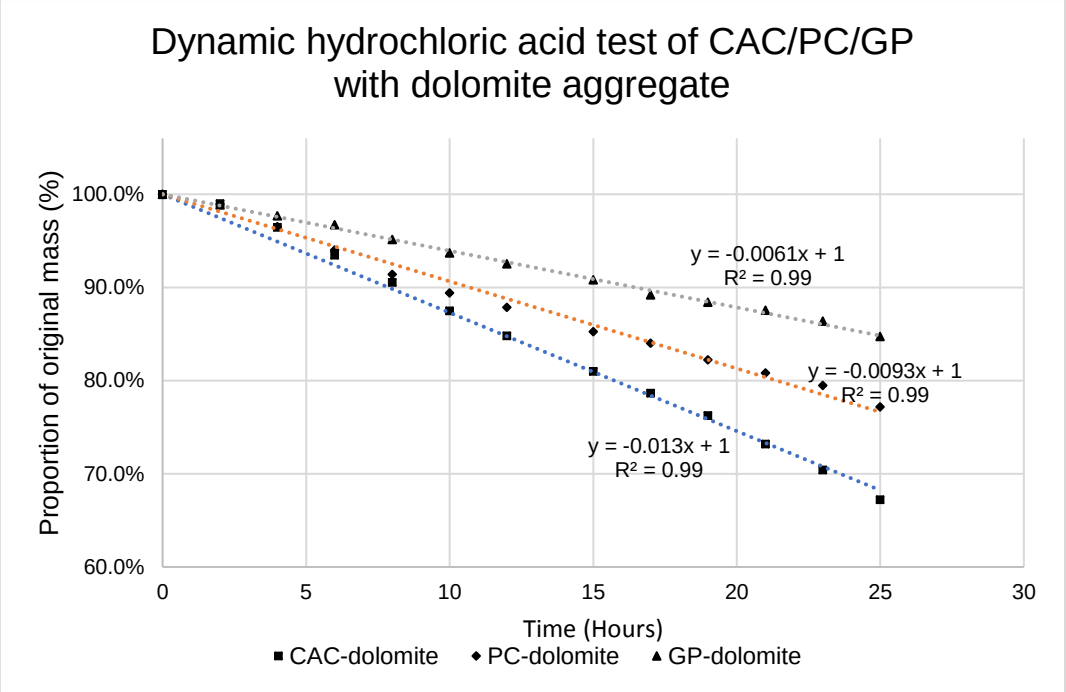

Figure 4-12: Mass proportion (%) change of calcareous aggregate concretes in the dynamic HCl test

Table 4-13: Corrosion data of CAC, GP and PC-dolomite concretes tested in the dynamic HCl test

	CAC-dolomite	PC-dolomite	GP-dolomite
Diameter (cm)	7.80	7.80	7.80
Length (cm)	12.58	12.35	12.43
Specimen surface area (cm2)	403.71	398.20	400.03
Change in mass (g/hr)	20.00	13.93	8.38
Surface corrosion rate (mg/cm^2/hr)	49.55	34.98	20.96
Remaining mass proportion (%) of concrete at 25 hours.	0.67	0.77	0.85

A visual assessment of the specimens after 25 hours in the dynamic HCl test provides some insight into the effect of acid attack on the specimens. CAC-dolomite specimens displayed a high degree of preferential corrosion of paste compared to the dolomite aggregate. The same can be said of the PC-dolomite specimens, however not to the same extent the CAC-dolomite. The GP-dolomite specimens exhibited the opposite pattern, with higher visible corrosion of the aggregate compared to the paste. Corrosion of the GP-dolomite specimens exhibited “cavities” on the surface of specimens where dolomitic aggregate had been dislodged or dissolved from the geopolymer matrix.

Figure 4-13: a) CAC-dolomite, b)OPC-dolomite and c) GP-dolomite specimens after 25 hours testing in the dynamic HCl rig at pH 1 (Respectively from left to right)

4.3.2.2 Dynamic HCl testing of GP concretes with siliceous aggregates

Under dynamic testing with hydrochloric acid, concrete mixes constituted by geopolymer cement and siliceous aggregates exhibited high resistance to acid attack. The hydrochloric acid tests were planned for 48 hours, however, due to power outages on two specific days, GP-dolerite and GP-granite specimens were tested over 24 hours instead of 48 hours. However, the data collected were sufficient to establish trends in the corrosion responses of these concretes. The most resistant concrete was GP-ferro-quartz concrete, followed by GP-granite concrete and the GP-andesite concrete. These three concretes had surface corrosion rates lower than 1 mg/cm^2/hr. GP-dolerite had the highest surface corrosion rate (4.51 mg/cm^2/hr) which is approximately 10 times higher than the other three siliceous aggregate specimens.

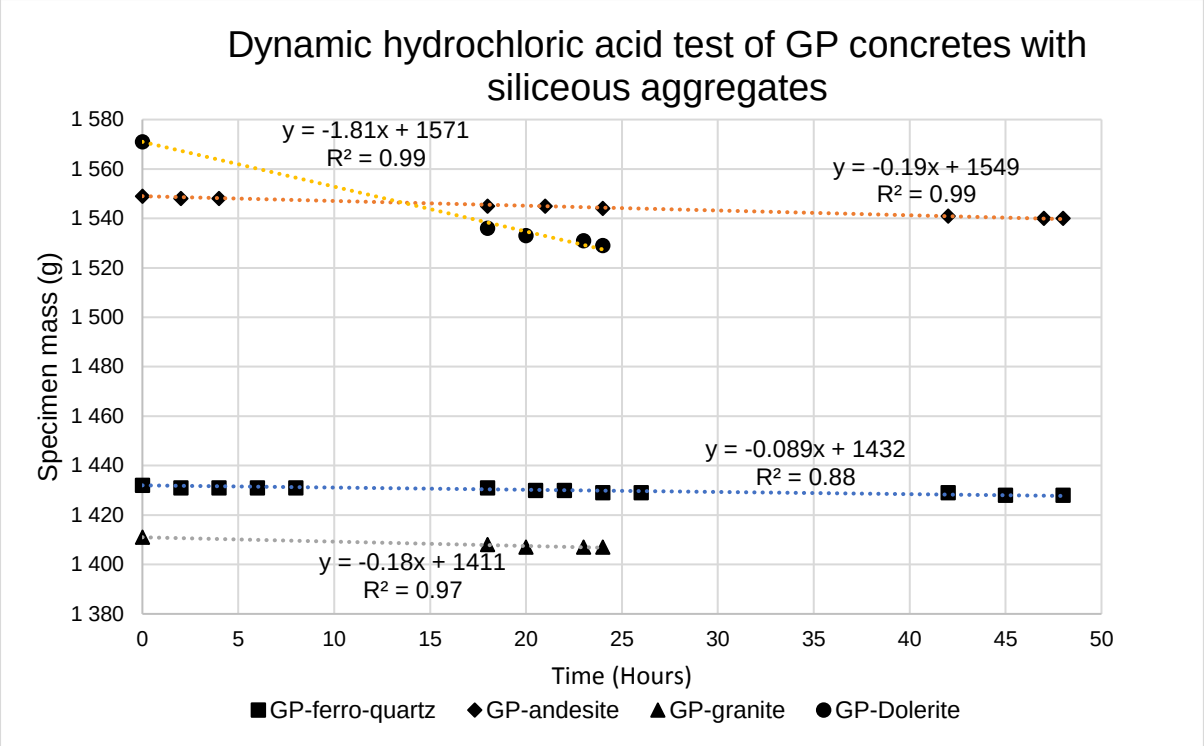

Figure 4-14: Mass change of siliceous aggregate concretes in the dynamic HCl test

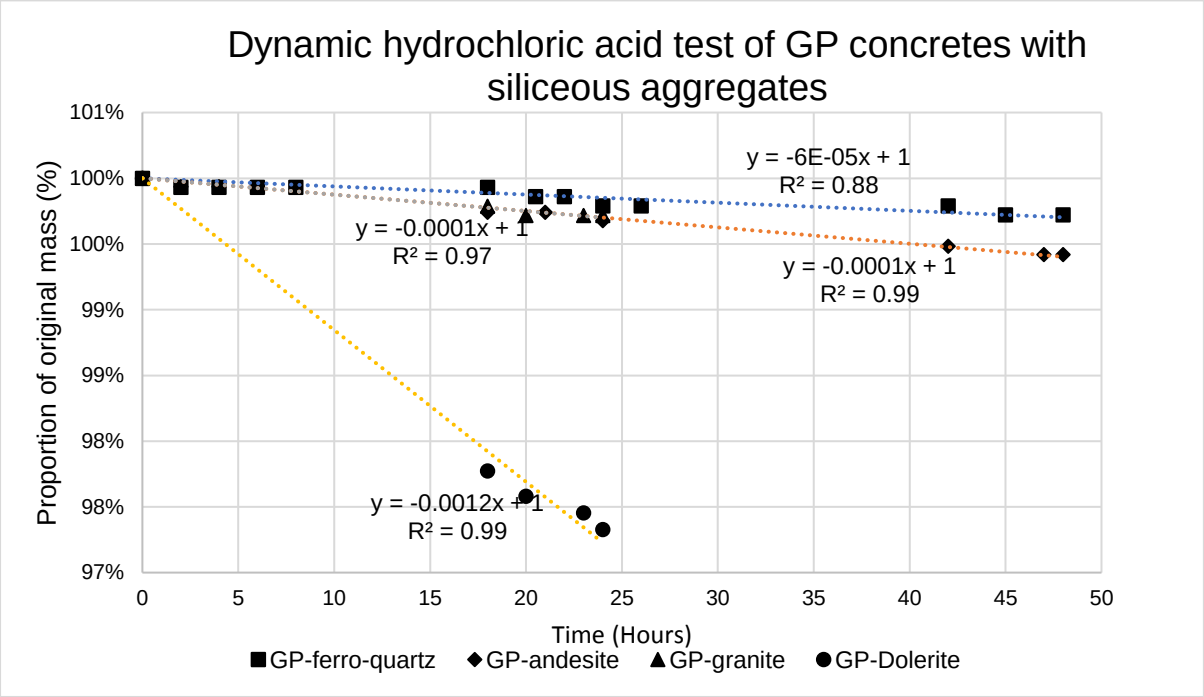

Figure 4-15: Proportion (%) of the original mass change of siliceous aggregate concretes in the dynamic HCl test

Table 4-14: Corrosion data of GP-Siliceous aggregate concretes tested in the dynamic HCl test

	GP-ferro quartz	GP-andesite	GP-dolerite	GP-granite
Diameter (cm)	7.8	7.8	7.8	7.8
Length (cm)	12.18	12.33	12.50	12.23
Specimen surface area (cm^2)	393.91	397.58	401.87	395.13
Change in mass (g/hr)	0.09	0.19	1.81	0.18
Surface corrosion rate ($mg/cm^2/hr$)	0.23	0.49	4.51	0.45
Remaining mass proportion (%) of concrete at 24 hours.	1.00	0.99	0.97	1.00

Visually, the condition of concrete specimens after testing showed slight to moderate deterioration amongst the geopolymer-siliceous aggregate specimens. Very little corrosion was visible on the GP-ferro-quartz and GP-granite specimens and it was not possible to identify whether corrosion was preferential on the aggregates or the paste. The GP-andesite specimen showed slight preferential corrosion of the paste while GP-dolerite specimen showed higher corrosion of the paste (see Figure 4-16).

a) GP-ferro-quartz b) GP-andesite c) GP-granite

d) GP-dolerite

Figure 4-16: Geopolymer-siliceous aggregate concrete specimens after testing in the dynamic HCl test.

4.3.2.3 Dynamic H_2SO_4 testing of GP concretes with siliceous aggregates

Geopolymer concretes consisting of ferro-quartz, andesite and granite aggregates showed the highest durability in both the static and dynamic hydrochloric tests. Since the chemical composition of ferro-quartz, granite and andesite aggregate had the lowest quantities of CaO (0.023%, 1.53% and 7.9% respectively) the undesirable precipitation of gypsum in the dynamic sulfuric acid test as described by Fourie (2007), which has the effect of halting the acidic reaction, was not likely. These siliceous aggregates paired with geopolymer binder allowed for sulfuric acid to be used in the dynamic acid test, which is the acid species found in microbially-induced corrosion. Furthermore, testing these three siliceous aggregate-geopolymer concrete mixes using both HCl and H_2SO_4 allowed for comparison of degradation by the two acid types.

This test was conducted over a period of 147 hours to assess whether the corrosion rates could potentially be influenced by aggregate fall-out in the case of the geopolymer paste being preferentially corroded.

The mass change of the three concretes is shown in Figure 4-17. Because the relative density of the aggregates ranges between 2.65 and 3.0, Figure 4-18 shows the proportion of mass change as in percentage of the original mass.

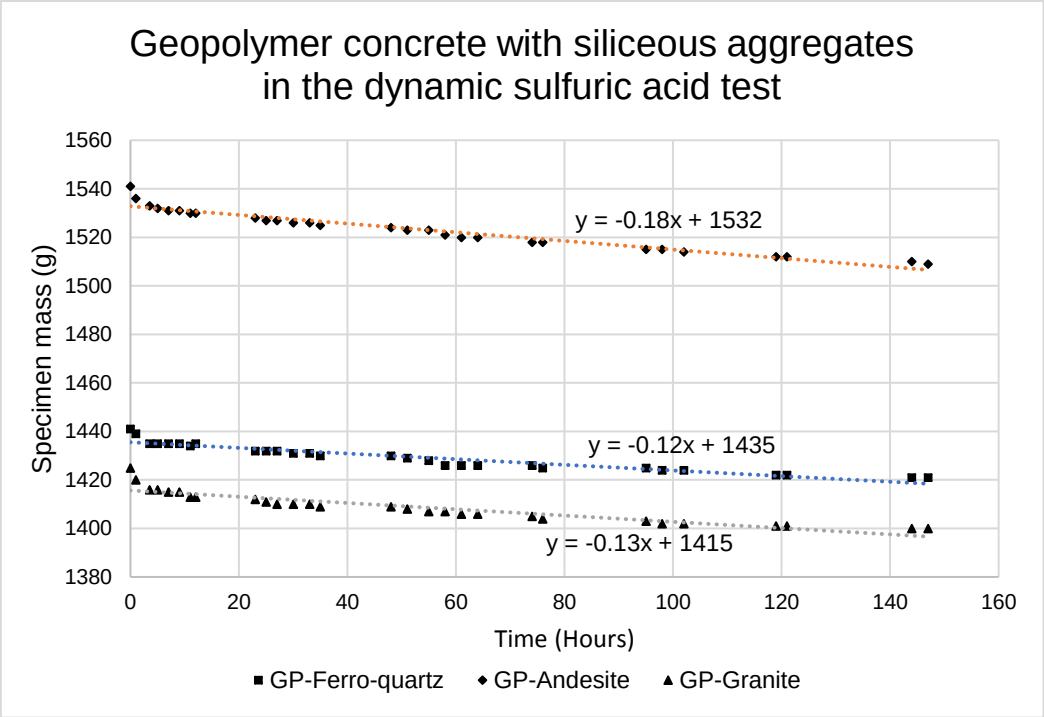

Figure 4-17: Mass change of siliceous aggregate concretes in the dynamic sulfuric acid test

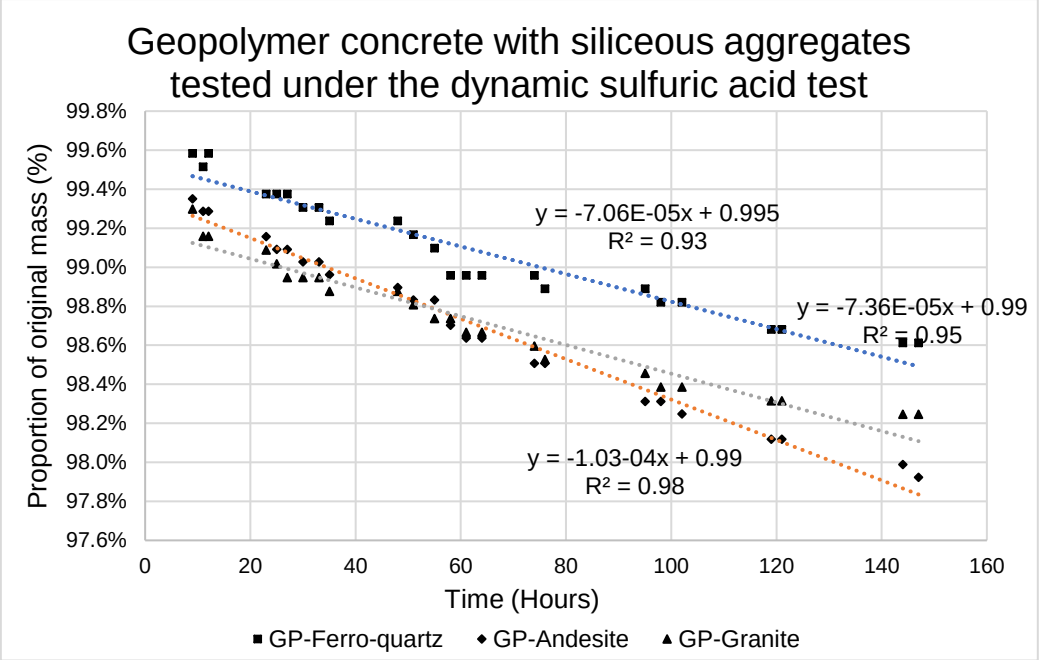

Figure 4-18: Proportion (%) of the original mass of siliceous aggregate concretes in the dynamic sulfuric acid test

Table 4-15: Corrosion data of GP-Siliceous aggregate concretes tested in the dynamic sulfuric acid test

Test parameter	GP-ferro quartz	GP-andesite	GP-granite
Specimen Diameter (cm)	7.80	7.80	7.80
Specimen Length (cm)	12.18	12.33	12.23
Specimen surface area (cm2)	393.91	397.58	395.13
Change in mass (g/hr)	0.12	0.18	0.13
Surface corrosion rate (mg/cm^2/hr)	0.30	0.45	0.33
Remaining mass proportion (%) of concrete at 147 hours.	98.6%	97.9%	98.2%

All three mixes exhibited relatively constant corrosion rates over the 147 hour test period. Specimens exhibited the same order of resistance to sulfuric acid as they did in the static hydrochloric acid test and dynamic HCl test. A significant result is that thee corrosion rates measured in the dynamic H_2SO_4 test were close to those measured in the dynamic HCl test.

4.3.2.4 Summary of acid performance test results

Results from the static acid tests are presented in two parts, firstly, the static HCl corrosion results from GP, CAC and GP concretes paired with dolomite aggregate and the secondly the static HCl corrosion results from GP mixes paired with siliceous aggregates. While GP specimens paired with siliceous aggregates exhibited little visual evidence of corrosion, a steady, yet low rate of mass loss was measured throughout the test indicating continuous corrosion of the GP concrete specimens.

The CAC-dolomite specimens exhibited a relatively smooth surface (i.e. no preferential corrosion of paste or binder) even though dolomite aggregate was preferentially corroded in the GP-dolomite and PC-dolomite mixes. The GP-dolomite mix showed clear preferential corrosion of the dolomite aggregate indicating that the GP paste had higher resistance to acid than dolomite aggregate. Details of the data used in producing these results is presented in chapter 0 (Appendix D) of this study.

Similar to the static acid test results, geopolymer mixes exhibited significantly higher resistance than PC and CAC concretes in the dynamic HCl test. Furthermore, CAC-dolomite concrete mixes' resistances differed significantly between the static and dynamic HCl test. In the static HCl test, CAC corrosion behaviour was characterised by high resistance (relative to PC-dolomite) and uniform corrosion (of aggregate and paste). However, in the dynamic HCl test CAC-dolomite mixes exhibited the highest rate of mass loss and the highest degree of preferential corrosion (of the paste). These observations are discussed in further detail in the chapter 4.5.

Given the low quantities of CaO content in GP HCP, ferro-quartz, granite and andesite aggregate, these mixes were also subjected to H_2SO_4 which allowed for comparisons of corrosion performance between these two acids in the dynamic acid test. Table 4-16 and Figure 4-19 provide a comparison of the corrosion rates of GP-ferro-quartz, GP-granite and GP-andesite tested using HCl and H_2SO_4 in the dynamic acid test.

Table 4-16: Comparison of corrosion rates measured for 3 geopolymer mixes in the dynamic HCl and H_2SO_4 test

Concrete mix	Corrosion rate dynamic HCl test ($mg/cm^2/hr$)	Corrosion rate dynamic H_2SO_4 test ($mg/cm^2/hr$)	Difference in corrosion rate ($mg/cm^2/hr$) between HCl and H_2SO_4
GP-ferro-quartz	0.225	0.295	0.070
GP-granite	0.446	0.328	0.118
GP-andesite	0.485	0.449	0.036

The corrosion rates measured for these siliceous GP mixes are low, relative to the corrosion rates exhibited by PC, CAC and concrete mixes containing dolomite aggregates, which are orders of magnitude higher. Furthermore the differences in the rate of corrosion between HCl and H_2SO_4 for the 3 geopolymer-siliceous aggregate mixes tested in both acids are minute (0.036- 0.118 $mg/cm^2/hr$).

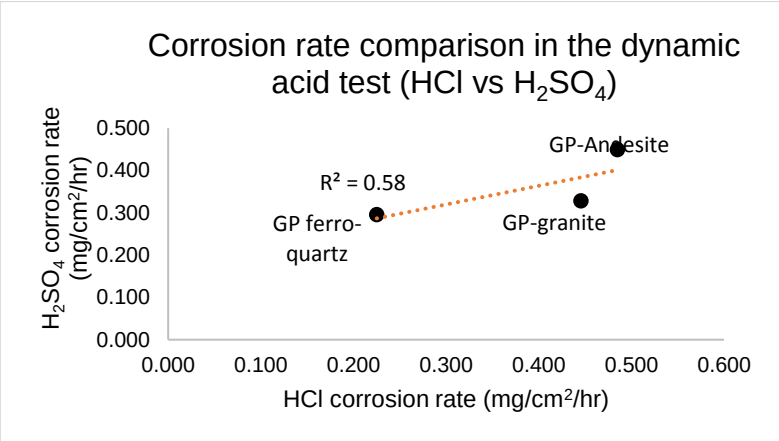

Figure 4-19: Comparison of corrosion rates measured in HCl and H_2SO_4 in the dynamic test

This result, if taken in the context of the finding that the dissolution phase of the corrosion of cementitious materials is dependent mainly on the prevailing pH of the solution and not the acid type (Gay et al. 2016), then the close rates of corrosion obtained from the HCl and H_2SO_4 are to be expected. What the dynamic acid test results presented in this chapter indicate is that the dynamic acid test may provide an indication of the rate of the dissolution phase of the corrosion process for different cement types, and that this rate is independent of acid type as long as the pH is kept constant. However, the dynamic acid test does not provide information related to the precipitation phase of corrosion.

4.3.3 Scanning electron microscopy (SEM)

SEM images of all pastes were taken both prior and after acidic corrosion. The specimens analysed after corrosion where subjected to hydrochloric acid in the dynamic HCl test. A larger catalogue of SEM images depicting corroded and un-corroded HCP specimens is presented in Appendix B (heading 0).

4.3.3.1 SEM: Fly ash based geopolymer cement

Kriven (2003) states that the nano-structure of geopolymers consists of geopolymer micelles which range from 5 nm to 20 nm in size. A characteristic of the geopolymer matrix is that the micelles form nano-channels and pores (Davidovits, 2017). Figure 4-20 shows a fracture surface, where the geopolymer micelle matrix is in contact with a fly ash sphere from an un-corroded geopolymer paste specimen. Figure 4-21 to Figure 4-23 shows the effect of HCl acid on fly ash spheres embedded in the geopolymer matrix.

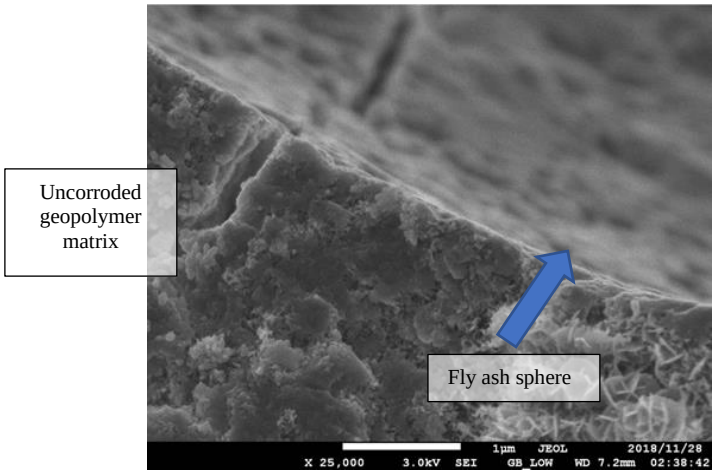

Figure 4-20: Fly ash sphere in contact with geopolymer micelle matrix

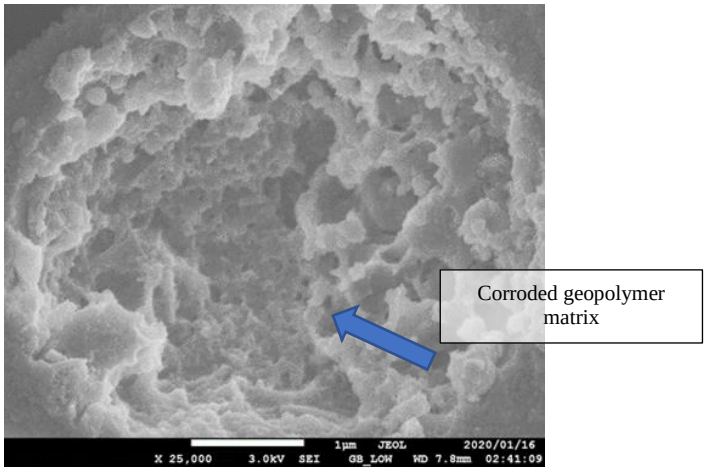

Figure 4-21: HCl Corroded specimen: cavity whereas FA sphere was embedded within the geopolymer micelle matrix

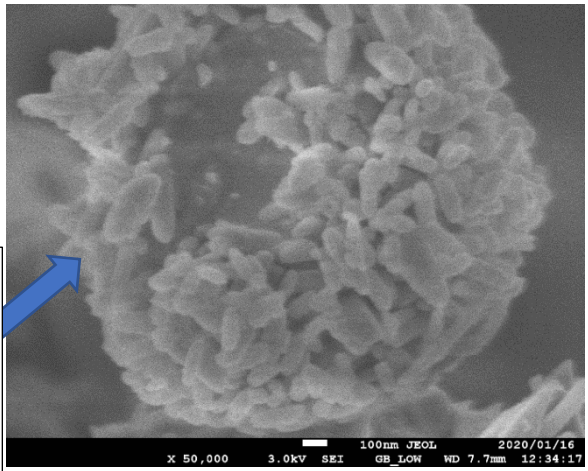

Figure 4-22: Corroded fly ash sphere enveloped by geopolymer matrix after exposure to the dynamic HCl test

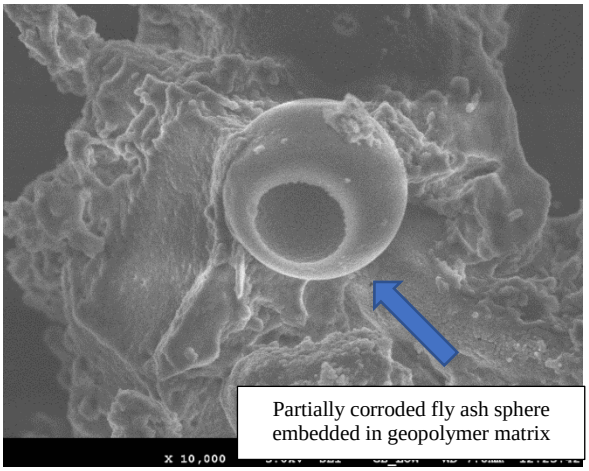

Figure 4-23: Partially corroded fly ash sphere enveloped by geopolymer matrix after exposure to the dynamic sulfuric acid test

What Figure 4-21 to Figure 4-23 show is that the fly ash spheres are preferentially corroded by hydrochloric and sulfuric acid, this is observation is in line with findings by Grengg (2018) which state that unreacted precursor materials such as fly ash are subject to dissolution under acid attack.

Figure 4-22 shows what seems to be a geopolymer matrix shell, which, before corrosion was covering an embedded fly ash sphere. Figure 4-23 shows a partially damaged fly ash sphere, with a circular opening at one end. The damaged sphere is embedded within the geopolymer matrix. This indicates that GP matrices at the micro and nanoscale exhibit preferential corrosion of some microstructures while others are dissolved in HCl.

4.3.3.2 SEM Portland cement:

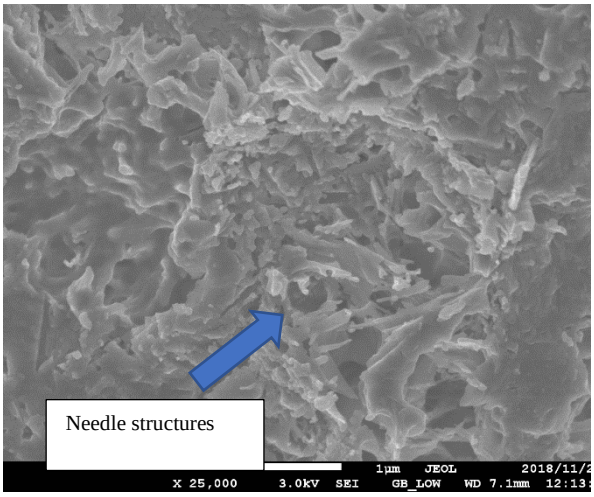

Figure 4-24: Un-corroded PC paste image (25000 x magnification)

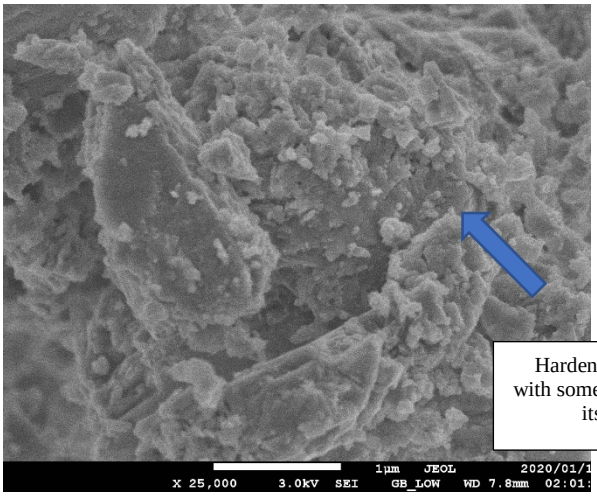

Figure 4-25: PC paste after exposure to the dynamic HCl test (25000 x magnification)

Un-corroded Portland HCP fracture surfaces display dense microstructure consisting of grain and needle structures. Figure 4-26 depicts images of HCP grains after exposure to hydrochloric acid. These grains are rougher and coarser than images collected from the un-corroded Portland cement HCP specimens. XRD results show that

6 % of the hydrated Portland cement paste is CH (Portlandite), which forms soluble calcium chloride ($CaCl_2$) and water when reacted with hydrochloric acid.

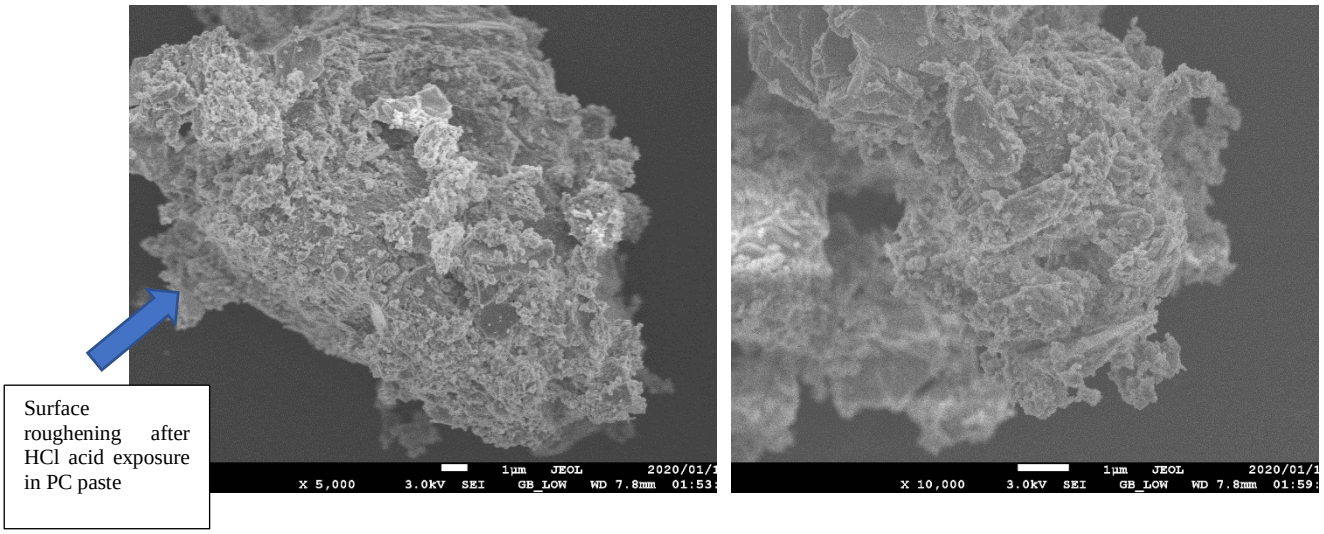

Figure 4-26: PC paste after exposure to the dynamic HCl test

SEM: CAC- dolomite

CAC specimens tested under the dynamic hydrochloric test do not display significant changes in morphology. This may be due to the high solubility of calcium aluminate cement hydrates. Due to limitations in time afforded to this study in the SEM, there is a possibility that the surfaces assumed to be corroded below, were actually un-corroded surfaces located on the chips taken off the surface of specimens which were subjected to the dynamic HCl test.

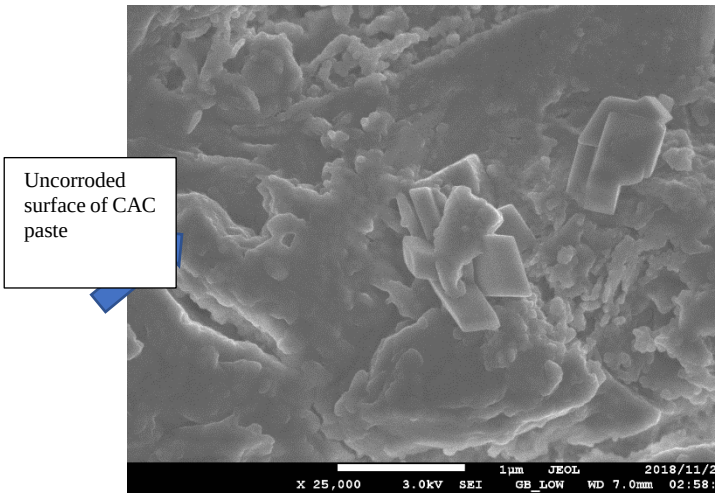

Figure 4-27: Un-corroded CAC hardened cement paste

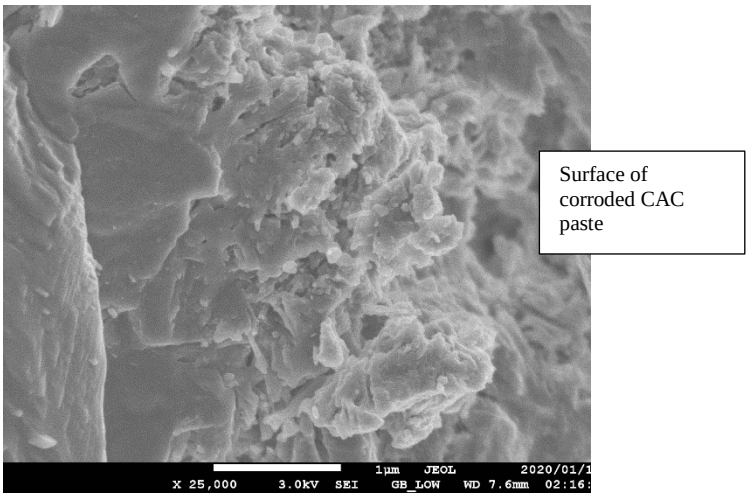

Figure 4-28: Corroded CAC hardened cement paste

4.3.3.3 Summary of SEM analysis findings

Geopolymer concretes exhibited interesting surface morphology after corrosion. In particular the corrosion surfaces of GP HCP were characterised by partially corroded and fully consumed fly ash spheres encased in the geopolymer matrix. This indicates that the GP matrix, is itself constituted by materials with varying resistance to

acids at the micro and nano scale. This may also suggest that corrosion in GP HCP is not necessarily concentrated at the surface that damage to the geopolymer structure may occur deeper into the surface of a corroding specimen where H^+ are transported via diffusion into the matrix.

In contrast PC-dolomite images and CAC dolomite did not exhibit marked differences in morphology after corrosion in the dynamic HCl test. The corroded surface of PC HCP was characterised by what appears as a slight roughening of the surface, while the images collected from CAC specimens before and after corrosion were relatively indistinguishable. In the case of CAC concretes, this raises the possibility that the fracture surfaces observed under SEM were chipped off sound concrete on the surface of the corroded specimen. This serves only to reinforce the suggestion that HCl corrosion of CAC-dolomite and PC-dolomite specimens in the dynamic acid test is largely dominated by surface acid attack, where diffusion of H^+ ions into the HCP matrix is negligible.

4.4 Compressive strength of concretes

The compressive strengths of the geopolymer specimens are presented in Figure 4-29 below and tabulated in Appendix E (Section 0). After curing at 60 degrees for 4 hours the strengths of geopolymer concrete exceeded 15 MPa strength threshold required by pipe manufactures for handleability (van Burick, personal communications 2019).

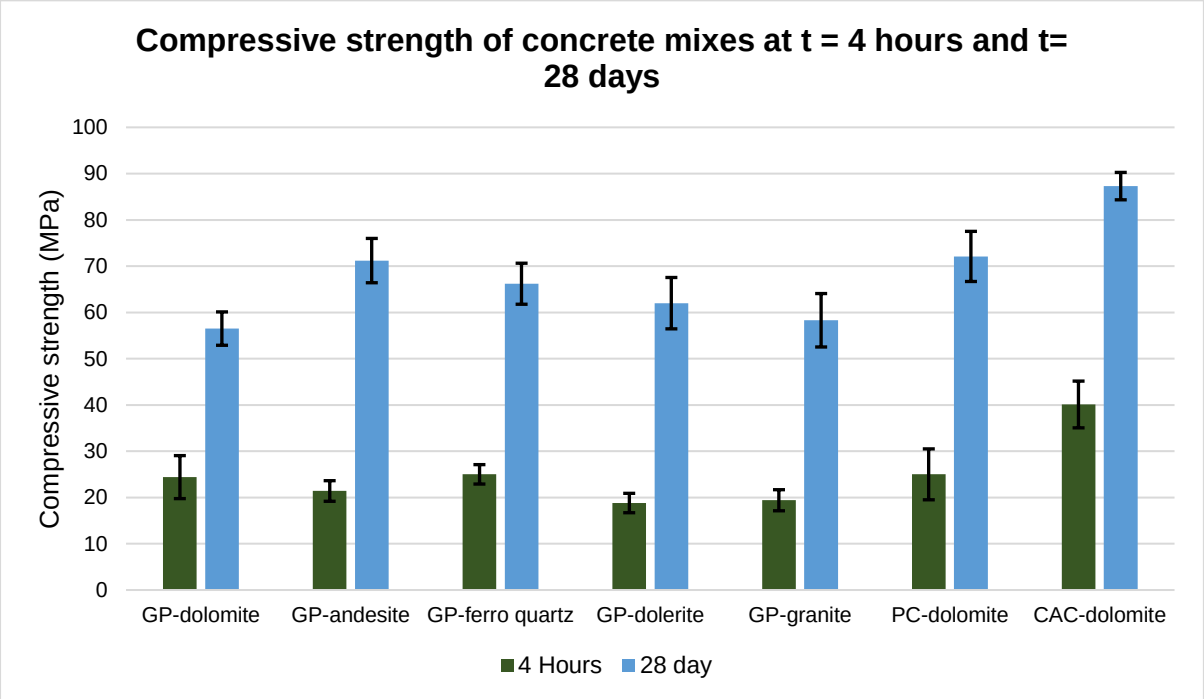

Figure 4-29: Compressive strength of concrete mixes at 4 hours and at 28 days after casting

The compressive strengths attained for all the geopolymer concrete specimens were suitable for both handling and 28-day compressive strength. The results shown above indicate that GP specimens attain more strength as they cure, in the same fashion as PC and CAC concretes develop strength over their curing period. Geopolymer concretes exhibited relatively similar strengths ranging between 19 and 25 MPa after 4 hours of curing and ranging between 56 and 72 MPa after 28 days of curing. CAC concretes had the highest mechanical strength with 40 MPa after 4 hours of elevated temperature curing and 87 MPa after 28 day-water bath curing.

4.5 Discussion

4.5.1 Static and dynamic acid test results of GP, PC and CAC concretes

One objective of this study was to determine whether the subject concretes have similar corrosion rates in the static test and dynamic test, and whether these two tests are relatable. Chapter 3.6.3 provides detail on the design two performance tests. Because the pH of the acid solutions was maintained at 1, and relatively constant rates of corrosion were observed throughout the duration of each test. With this trend observed, and the maintenance of pH a 1, and the replenishment of acids at intervals (see Chapter 3.6.3) it is suggested that the corrosion reactions in both the dynamic and static tests would, if given enough time, go to completion and thus the experiment is not encumbered by reaction stalling effects such the common ion effect.

Because the most significant difference between the static test and the dynamic test is the abrasive effect of the PVC bristles on the concrete, whereby corroded material is continuously removed, it is of interest to see what effect the removal of corrosion products in acidic media has on the corrosion rate. However, in the sewer environment, the exposure condition is erosion-corrosion and not necessarily abrasion-corrosion. Therefore, if the abrasive conditions in the dynamic acid test are to be linked to erosion corrosion in the sewer requires these two forms of degradation need to be related.

Abrasive wear occurs when a hard rough surface slides across a softer surface. Abrasion is defined as the loss of material due to hard particles or hard protuberances that are forced against and move along a solid surface (Affatato and Traina 2011).

In the dynamic HCl test it is suggested that the PVC bristles of the brush are hard enough to remove soft, loose corrosion products on the surface of the concrete, but not hard enough to remove un-damaged or sound concrete. Therefore the term abrasion in this study does not apply to mechanically sound or un-corroded concrete, but to corrosion products located on the surface of sound concrete.

Erosion is defined as a gravity-driven process that moves solids (sediment, soil, rock and other particles) in the natural environment or their source and deposits them elsewhere usually occurring due to transport by wind, water, or ice under the force of gravity (Affatato and Traina 2011).

What is common between abrasion in the dynamic HCl test and erosion in the sewer environment is that loose materials, which are not bound strongly to sound (un-corroded) concrete are transported from site of corrosion. While erosion requires fluids flowing under gravity to achieve this movement, abrasion in the dynamic acid test uses the test specimen's angular rotation and the resistance of the brush's PVC bristles to remove loose material from the surface of the concrete specimen. Since the condition in the dynamic acid test involves complete immersion in pH 1 and continuous brushing, it is reasonable to conclude that the test conditions are harsher than the erosive-corrosive conditions in the sewer. It is therefore suggested that the brushing (abrasive) in the dynamic acid test should be considered as an intensified form of erosion.

For this purpose, a parameter, the "abrasion factor", which is equal to the surface corrosion rate in the dynamic acid test divided by the surface corrosion rate in the static test for each concrete type is used. This parameter

provides a quantifiable measure of the effect of abrasion on concretes in acidic media that can be used as a basis for comparing different concretes subjected to the dynamic and static acid tests.

Higher values indicate that abrasion in acidic media has a severe effect while lower values indicate a minor effect. For a parameter such as the abrasion factor to be used in predictive corrosion models, many factors, such as the nature of the test, the stiffness of the bristles and the rate of rotation of the concrete specimen in the dynamic test would have to be calibrated to real MIC exposure conditions (Alexander 2020, personal communication, 6 August). For now, the abrasion factor serves only as a tool to compare the performance of different concrete types.

Table 4-17, shows the rates of corrosion measured in static and dynamic HCl tests for GP, CAC and PC concretes with dolomite aggregate. When comparing the three calcareous aggregate concretes it is clear that abrasion has a severe effect on the CAC-dolomite concrete because its abrasion factor is 310, this value being approximately 10 times higher than the abrasion factor in GP -dolomite concrete (33.8) and 31 times higher than PC-dolomite (10.4) concrete.

Table 4-17: Static hydrochloric test related to the dynamic HCl test (calcareous aggregate concretes)

	Static HCl test corrosion rate ($mg/cm^2/hr$)	Dynamic HCl test corrosion rate ($mg/cm^2/hr$)	Abrasion factor
GP-dolomite	0.620	21.0	33.8
PC-dolomite	3.369	35.0	10.4
CAC-dolomite	0.160	49.5	310.6

Table 4-18 shows the abrasion factors calculated from geopolymer concretes with siliceous aggregates. Abrasion, factors range from as low as 5.69 (GP-ferro-quartz) to 27.75 (GP-dolerite). GP-dolerite had the highest surface corrosion rate in both static and dynamic conditions for the set of GP-specimens with siliceous aggregates, the abrasion factor for this specimen was also 2 to 5 times higher than the other specimens in this set.

Table 4-18: Static hydrochloric test related to the dynamic HCl test (Geopolymer-siliceous aggregate concretes)

	Static HCl test corrosion rate ($mg/cm^2/hr$)	Dynamic HCl test corrosion rate ($mg/cm^2/hr$)	Abrasion factor
GP-ferro-quartz	0.04	0.23	5.69
GP-andesite	0.08	0.49	6.41
GP-dolerite	0.16	4.51	27.75
GP-granite	0.04	0.45	10.98

Table 4-19: Static hydrochloric test related to the dynamic sulfuric acid test (geopolymer-siliceous aggregate concretes)

	Static HCl test corrosion rate ($mg/cm^2/hr$)	Dynamic H_2SO_4 test corrosion rate ($mg/cm^2/hr$)	Abrasion factor
GP-ferro-quartz	0.04	0.30	7.46
GP-andesite	0.08	0.45	5.93
GP-granite	0.04	0.33	8.07

The three most resistant geopolymer concretes display similar abrasion factors (Table 4-18). These data provided are useful on a comparative basis, however, it is suggested that small differences in the corrosion rates and calculated factors could benefit from further verification and measurement since the test durations did not allow for these concretes to be tested for long enough to corrode them as severely as the PC and CAC dolomite concrete mixes.

GP-dolerite and GP-dolomite concretes had similar abrasion factors of 27.75 and 33.8 respectively. Because a higher abrasion factor indicates a form of protection that is less effective in the dynamic HCl test than in the static HCl test, the relatively high abrasion factors (compared to GP-ferro-quartz and GP-andesite) calculated for these two specimens are interesting because there is no evidence of a corrosion products providing a protective barrier similar to the AH_3 gel in CAC concretes. The AH_3 gel as reported by Letourneux and Scrivener (1999), forms a protective barrier around CAC concretes.

However, if the higher abrasion factors of GP-dolerite and GP-dolomite are thought about in terms of the effects of preferential corrosion, Figure 4-34 that these two mixes also happen to exhibit preferential corrosion of the aggregate.

Therefore a potential explanation for the higher GP-dolomite and GP-dolerite abrasion factors is that the aggregate at the surface of the GP-dolerite and GP-dolomite specimens dissolve more rapidly than the geopolymer paste in HCl, and as corrosion progresses, the connected GP-paste matrix increasingly makes up more and more of the exposed surface of the specimen which may have the effect of a physical corrosion barrier to vulnerable dolomite or dolerite aggregate embedded within the GP-paste. However, the GP HCP matrix is not inert and is also continuously corroding (at a lower rate compared to the aggregate) and thus losing mechanical strength, which makes it more vulnerable to the brushing effects of the PVC bristles in the dynamic HCl test. Therefore it is suggested that the protective mechanism causing higher abrasion factors in GP-dolerite and GP-dolomite concretes is the protection of the GP paste matrix which is more stable under static corrosion conditions than under the combined effects of abrasion and corrosion.

Conversely, in concrete mixes where the aggregate is not preferentially corroded and does not benefit from precipitates or gels emanating from HCl corrosion (CAC concretes), the abrasion factor values are relatively low, ranging between 6.4 (GP-ferro-quartz) and 10.4 (PC-dolomite). It should be borne in mind that this analysis is incomplete because HCl instead of H_2SO_4 was used in the static acid test and thus, the calculated abrasion factors are expected to change where H_2SO_4 was used in the static and dynamic acid tests of all the specimens.

4.5.2 Effect of CaO content on static and dynamic corrosion

Chemical composition of paste and binder components has a significant effect on the corrosion behaviour of concrete. Bertron (2014) suggestes that the calcium content of cementitious systems depends primarily on the initial calcium content of the cement matrix.

Therefore, this section of the study aims to assess the impact of calcium oxide (CaO) content, as determined by XRF analysis, on the corrosion rates of PC, CAC, and GP concrete. The calcium oxide content of each concrete

specimen type was calculated using data obtained from XRF analysis. The following formula applies to the calculation of CaO content for each concrete specimen.

$$CaO(\%)_{\text{concrete specimen}} = (CaO_{HCP} \times \text{binder } \%) + (CaO_{\text{aggregate}} \times \text{aggregate}\%) \quad (4\text{-}3)$$

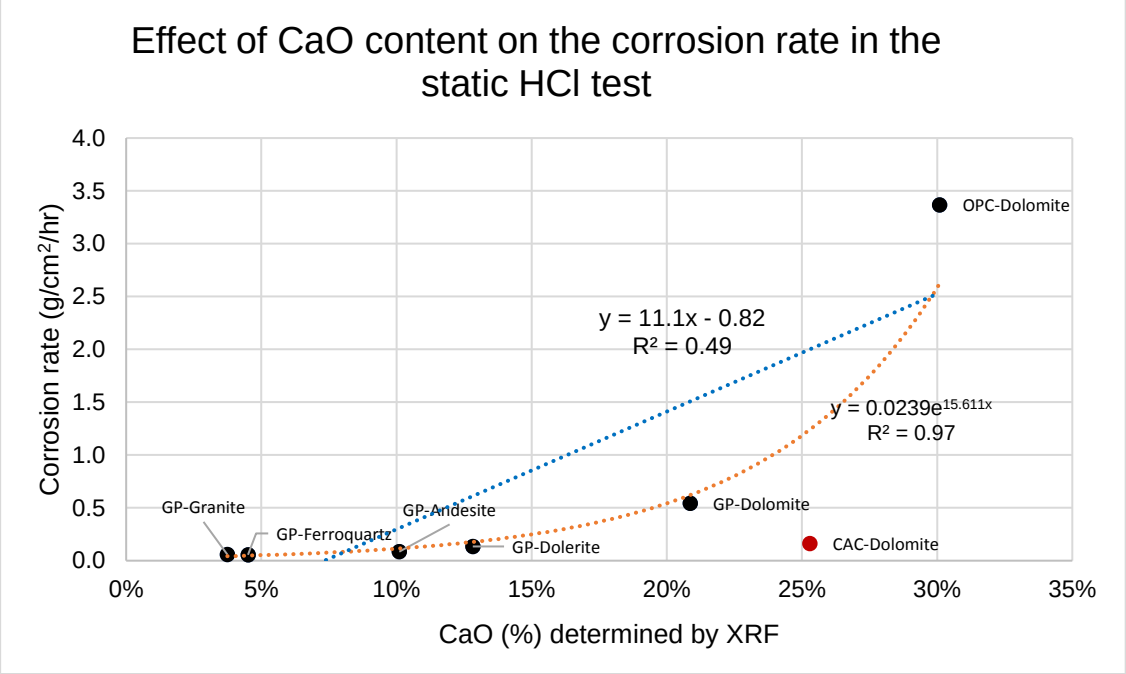

Figure 4-30: Comparison between the surface corrosion rate (static hydrochloric acid test) and CaO content.

Comparison of the corrosion rates of specimens subjected to the static HCl test for the most part, provide a trend, where increasing CaO content in the concretes is associated with a higher corrosion rate. Geopolymer concrete specimens had comparatively lower CaO contents compared to CAC and PC concretes and this corresponded to their lower corrosion rates in the static HCl test. The variation in CaO content in the five geopolymer mixes is attributed to the CaO content in the aggregate. The trend observed therefore, suggests that increasing CaO content in the geopolymer concrete specimens produces an increase in the rate of corrosion observed in the static HCl test. The PC-dolomite mix also follows the trend too, however, the corrosion rate is significantly higher.

Figure 4-30 shows two trend lines extrapolated from the data, the first is a linear trend which considers all data points (all mixes). This best fit line (in blue) has an R^2 value of 0.49 which indicates a poor correlation. If the result from the calcium aluminate cement is excluded from the data set, then a best fit line (exponential) with a higher correlation (R^2= 0.97) is achieved. This trend suggests that the relationship between CaO and the corrosion rate in the static test is non-linear.

However, this trend is contradicted by CAC-dolomite concrete. An explanation for this is provided by Herrison and Saucier (2015) and Letourneux and Scrivener (1999), where it is suggested that alumina hydrate gel (AH_3) serves as an acid resistance mechanism, by enveloping CAC concrete specimens subjected to acid attack. While CAC cements are understood to possess two other resistance mechanisms, the bacterio-static cannot affect the static HCl test because the acid is not generated microbially. The other resistance mechanism provided by CAC

cements is that they have 40% higher capacity to neutralise acid when compared to Portland cement (Herrison and Saucier 2015, Letourneux and Scrivener 1999).

While neutralisation capacity may account for some of the extra acid resistance observed in the static HCl test, the upper limit of neutralisation is only 40% higher, whereas the corrosion of the CAC-dolomite (0.3 g/cm^2) concrete is an order of magnitude lower than PC-dolomite (3.8 g/cm^2). Secondly the rate of a corrosion reaction is related to reaction kinetics and not necessarily neutralisation capacity.

Given that, the only variable between the CAC-dolomite and PC-dolomite corrosion result is the cement type (CAC vs PC), and the fact that the only other known resistance mechanism of CAC concretes to acid attack is the alumina hydrate gel (AH_3) protection, it follows that this drastic reduction in the corrosion rate must largely emanate from the protective layer of alumina gel, AH_3 formed around the CAC concrete specimens in the static HCl test.

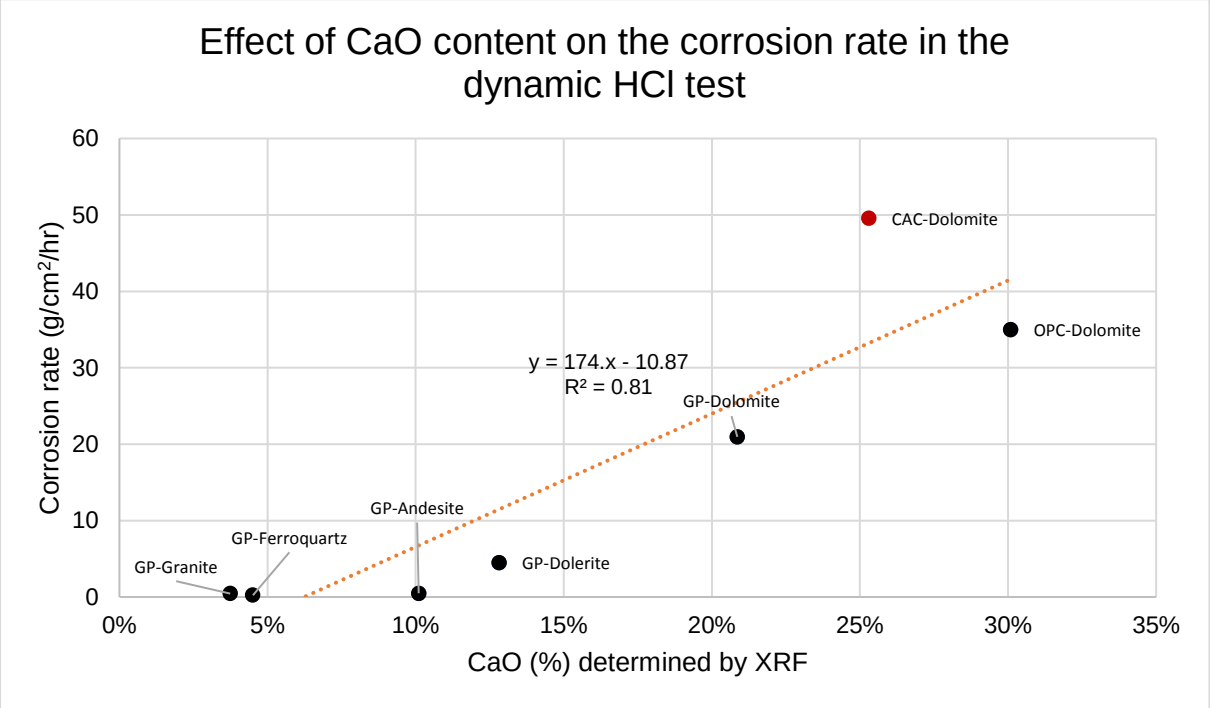

Figure 4-31: Comparison between the surface corrosion rate (dynamic HCl test) and CaO content.

In the dynamic HCl tests results shown in Figure 4-31, the R^2 value (of 0.81) does not indicate a strong correlation between CaO content and the corrosion rate. However, CaO content of concretes tested under dynamic HCl conditions provide the same general trend as the static test, where increasing CaO content in concrete specimens produces generally higher surface corrosion rates.

Once more, the CAC-dolomite specimen is an outlier. Under the dynamic HCl test, CAC has the highest surface corrosion rate, even though PC-dolomite concrete has higher CaO content.

These empirical relationships show that CaO content is linked to the surface corrosion rate on specimens in both static and dynamic conditions, however, the behaviour of CAC-dolomite specimens stand out as outliers in both cases.

4.5.3 Acidic and basic oxides

Related to the corrosion potential of a material is the nature of the oxides of which it consists. This study included XRF analysis to characterise and quantify the chemical composition of the HCPs and aggregates. XRD, therefore, provides us with the data needed to determine the quantity of basic and acidic oxides in a material. A brief review of basic and acidic oxide theory is therefore required to proceed.

Oxides can be categorised as basic, acidic, amphoteric, or neutral depending on the nature of the ions formed in solution. An acidic oxide is an oxide which when combined with water gives an acidic solution and likewise, a basic oxide is an oxide which, when dissolved with water produces a basic solution. When an oxide reacts chemically, both as a base or acid it is termed amphoteric. A neutral oxide is one which neither has an acidic characteristic or a basic one (Kurushkin and Kurushkin .2018)

For example, sulphur dioxide (SO_2), sulphur trioxide (SO_3), and carbon dioxide (CO_2) are acidic oxides that form sulfurous acid, sulfuric acid and carbonic acid respectively when added to water. Likewise, calcium oxide reacts (CaO) with water to produce calcium hydroxide (CaOH), which dissociates in solution to form Ca^{2+} and OH^- ions.

For the purpose of identifying the nature of oxides, chemists have mapped regions in the s and p blocks of the periodic table that can be used to identify whether an element produces an acidic oxide, amphoteric oxide or a basic oxide (see Table 4-20).

Table 4-20: Properties of *s*- and *p*-block elements in the periodic table (Periodic trends and oxides, 2020)

Li	Be	B	C	N	O	F
Na	Mg	Al	Si	P	S	Cl
K	Ca	Ga	Ge	As	Se	Br
Rb	Sr	In	Sn	Sb	Te	I
Cs	Ba	Tl	Pb	Bi	Po	At
Basic Oxides			Amphoteric Oxides		Acidic Oxides	

A few trends are important in identifying the nature of an oxide in solution from the periodic table. As elements become more electronegative (i.e. positioned toward the right-hand side of the periodic table) the more acidic the oxides become. Fluorine and Chlorine are found on the extreme right of the table, oxides of which form hydrofluoric acid and hydrochloric acid when mixed with water to form very strong acids.

Similarly, the more electropositive the element the stronger the basic oxide that is formed, Na_2O mixed with water forms NaOH which is a very strong base. Elements forming amphoteric oxides are found in the middle of the table and consequently, the strength of the acids and bases formed from oxides in this region is not high. The most abundant oxides of the cementitious systems being studied are CaO, SiO_2 and Al_2O_3. CaO is a basic oxide, SiO_2 is an acidic oxide while Al_2O_3 is amphoteric (Kurushkin and Kurushkin .2018). The quantities of these oxides in the aggregates and HCP is therefore used in the basicity calculation in the following section.

4.5.4 Relationship between the basicity value and corrosion

Basicity is a unitless number that quantifies the ratio of basic oxides to acidic oxides in a material. This calculated value is used widely as a signifier of the reactivity of metallurgical slags such as GGBS when used as an extender in Portland cement concretes. In Britain, BS EN 197-1:2011 prescribes that for GGBS, the basicity ratio by mass shown below must exceed 1 for use as an extender in Portland cement (Ogirigbo, 2016). A similar formula is found in SANS 50197-1, however the term "basicity" is neglected in this standard.

$$\text{Basicity} = \frac{\text{CaO (\%)} + \text{MgO (\%)}}{\text{SiO}_2\ (\%)} \qquad (4\text{-}4)$$

The intended purpose of the basicity ratio in this study is to quantify the ratio of basic oxides to acidic oxides in concrete components in their reacted (final) state, whereas the standard use of this parameter is intended for raw materials (slags). Furthermore, the formula used for basicity calculation in this study is kept consistent with the formula prescribed by SANS 50197-1 and BS EN 197-1:2011 because it includes the major acidic oxides and basic oxides found in cementitious materials.

Determination of the basicity value was determined from XRF results provided in Table 4-1 and Table 4-2 for HCPs and aggregates respectively.

Table 4-21: Calculated basicity of hardened cement pastes (HCP)

Binder (Hardened paste)	**Calculated basicity ($CaO+MgO/SiO_2$)**
PC	3.13
CAC	8.69
GP	0.27

Table 4-22: Calculated basicity of aggregates

Aggregate	**Calculated basicity ($CaO+MgO/SiO_2$)**
Dolomite	1.60
Ferro-quartz	0.044
Dolerite	0.60
andesite	0.48
Granite	0.22

Since concrete is a composite material consisting of aggregate embedded in a matrix of hardened cement paste, determination of concrete basicity requires that its component parts (hardened cement paste and aggregate) be calculated according to their mass proportions. The following formula was used for this purpose.

$$\text{Basicity}_{\text{concrete specimen}} = (\text{Basicity}_{\text{HCP}} \times \text{binder \%}) + (\text{Basicity}_{\text{Aggregate}} \times \text{aggregate \%}) \qquad (4\text{-}5)$$

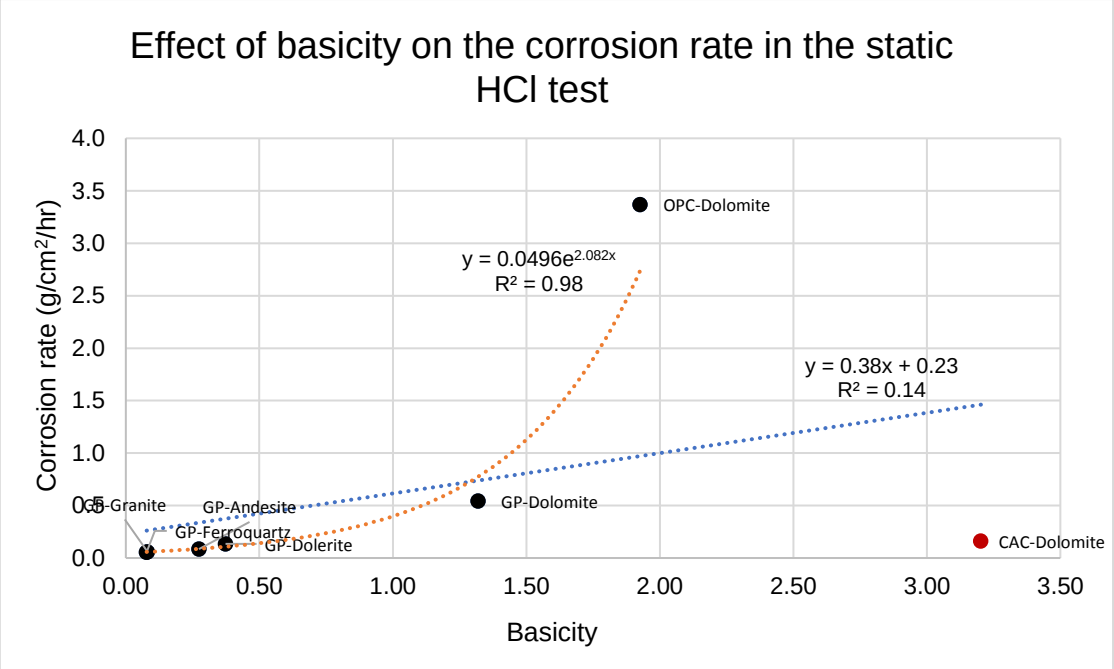

Figure 4-32: Basicity of concrete compared to the static corrosion rate

Under static hydrochloric acid testing the trend on the graph (Figure 4-32) is similar to that of presented in the comparison between CaO content and mass loss rate (Figure 4-31), with CAC-dolomite concrete specimens falling outside of the general trend observed with the rest of the concrete specimens. Once again, if the CAC-dolomite result is ignored, a highly correlated non-linear trend is observed (R^2= 0.98), however if CAC-dolomite data point is included, the correlation is poor (R^2= 0.15).

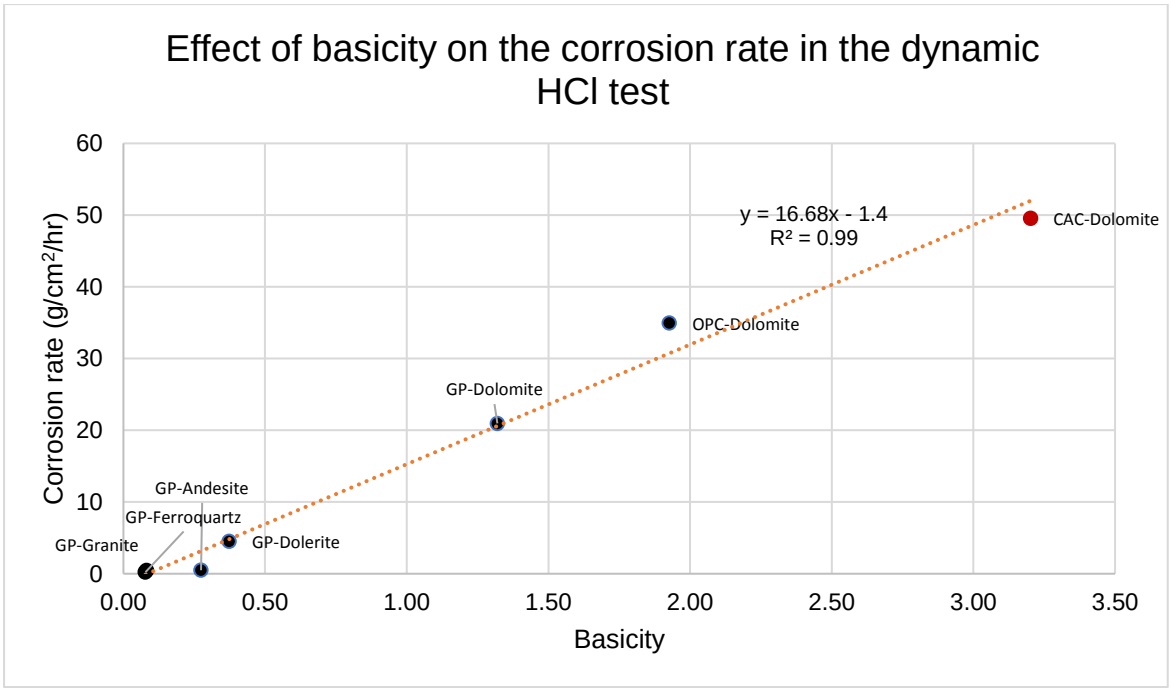

Figure 4-33: Relationship between basicity and the dynamic HCl corrosion rate

Where the basicity of concretes was compared to surface corrosion rate in the dynamic HCl test, a clear trend is observed. While this study considered a total of 7 concrete mix designs, all seven displayed a strongly proportional relationship between basicity and the surface corrosion rate in the dynamic test. Of key interest is that CAC-dolomite specimen now follows the established trend.

The differences in performance observed in the corrosion of the CAC-dolomite in the static and dynamic tests is attributed to the removal of the protective alumina gel layer (AH_3) in the dynamic test. Given that the solution pH in both static and dynamic tests was maintained at 1 and that AH_3 gel is stated to be a stable compound down to a threshold pH of 3.5-4 (Saucier and Kaitano 2018, Letourneux and Scrivener 1999), it is deduced that the abrasive conditions in the dynamic HCl test accelerated the decomposition of the protective alumina gel layer which enabled the HCl to continuously attack fresh concrete surfaces.

4.5.4.1 Effect of basicity on hardened cement paste and aggregate pairing

SANS 677:2010 makes a recommendation for acid solubility of aggregate by limiting aggregate insolubility to 25% by mass for concrete pipes in sewer applications. Concrete may be thought of as a combination of aggregates bound together by the HCP matrix.

Therefore, it would be ideal to determine the static and dynamic corrosion rates for hardened cement pastes and aggregate separately. In principle, this would require homogenous cubes and cylinders of hardened cement paste and aggregate to be subjected the static and dynamic acid tests respectively. Such a test would enable the quantification of the aggregate and paste corrosion rates separately, thereby providing a basis by which aggregate, and HCPs can be paired to minimise preferential corrosion of either binder or paste.

If basicity can be used to reliably predict the corrosion rate as is shown in Figure 4-33, it follows that the lower differences in the basicity between aggregate and paste for a particular concrete will, in turn, diminish preferential corrosion of either paste or binder. Figure 4-34 gives the difference between the basicity of aggregate and hardened cement pastes values for the combinations of aggregate and binder used in this study. The basicity values of hardened cement pastes and aggregates are taken from Table 4-21 and Table 4-22 respectively.

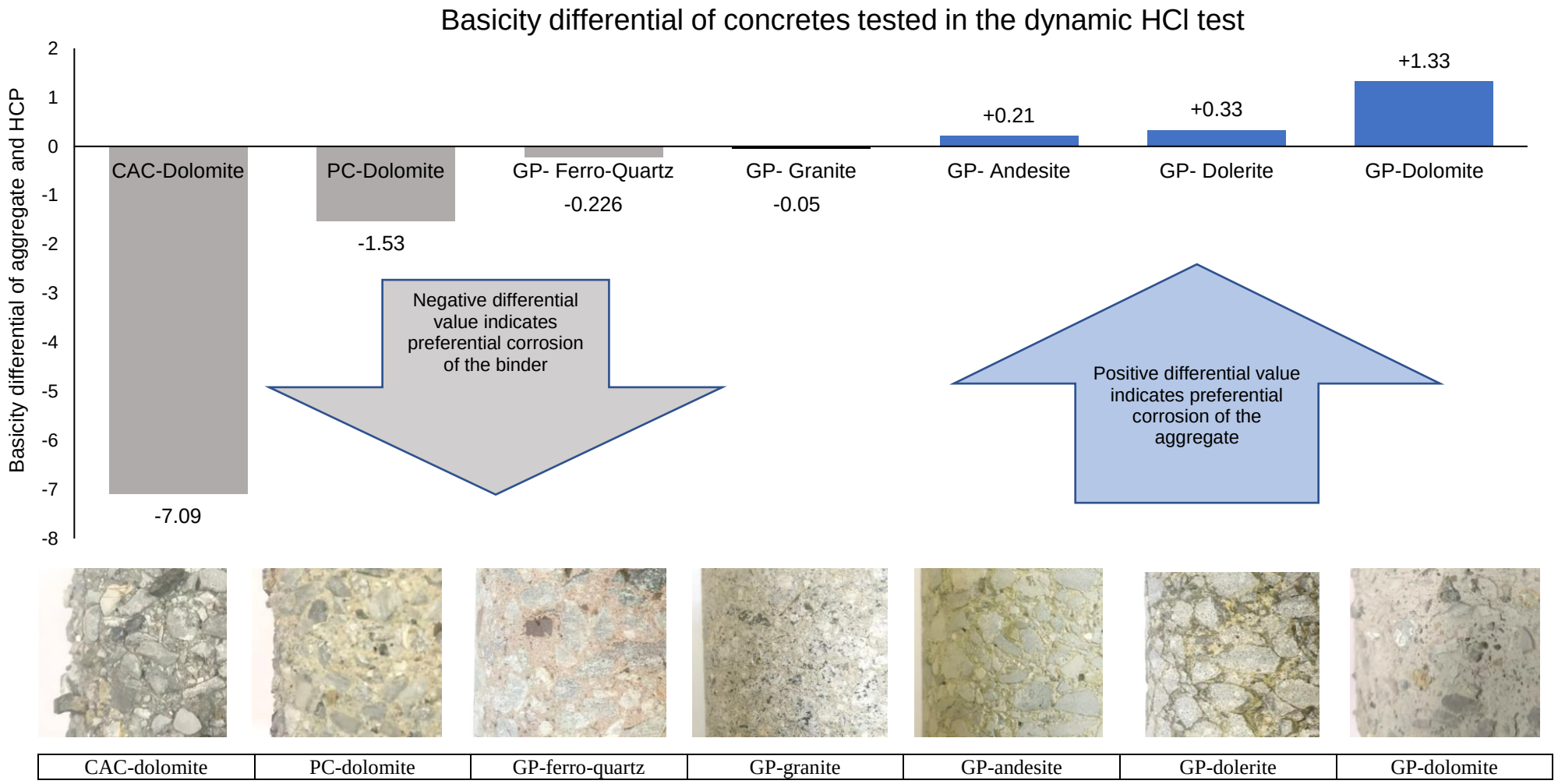

Figure 4-34: Ranked basicity differential between aggregate and hardened cement paste (Basicity $_{aggregate}$ − Basicity $_{HCP}$) with corresponding image of specimens tested in the dynamic HCl test

A negative value of basicity differential should indicate preferential corrosion of the paste component (i.e. aggregate standing proud) while a positive basicity differential should indicate preferential corrosion of the aggregate.

A qualitative estimation of preferential corrosion of the binder or aggregate component of concrete can be made by visually observing specimens tested in the dynamic HCl test. Figure 4-13 and Figure 4-16 provide enlarged images of the test specimens after testing the dynamic HCl test.

If the corroded specimen surfaces are scrutinised closely, the basicity differentials shown in Figure 4-34 correctly indicate which concrete component (aggregate or paste) is preferentially corroded. As can be seen in Figure 4-13 and Figure 4-34, the paste components in the CAC-dolomite and PC-dolomite specimens were both preferentially corroded (i.e. aggregate standing proud) while the PC-dolomite specimen displayed preferential corrosion of the aggregate. These visual observations correspond to the calculated basicity differentials of -1.53, -7.09 and 1.33 of PC-dolomite, CAC-dolomite and GP-dolomite respectively.

The same assessment can be made with the set of geopolymer mixes paired with siliceous aggregates. A prominent difference between the GP concretes and PC and CAC systems is that the basicity differentials are smaller in concrete specimens with siliceous aggregates. The calculated differentials indicate that granite (-0.05) and ferro-quartz (-0.22) GP specimens will experience preferential corrosion of the HCP component whereas andesite (0.21), dolerite (0.33) and dolomite (1.33) will experience preferential corrosion of the aggregate.

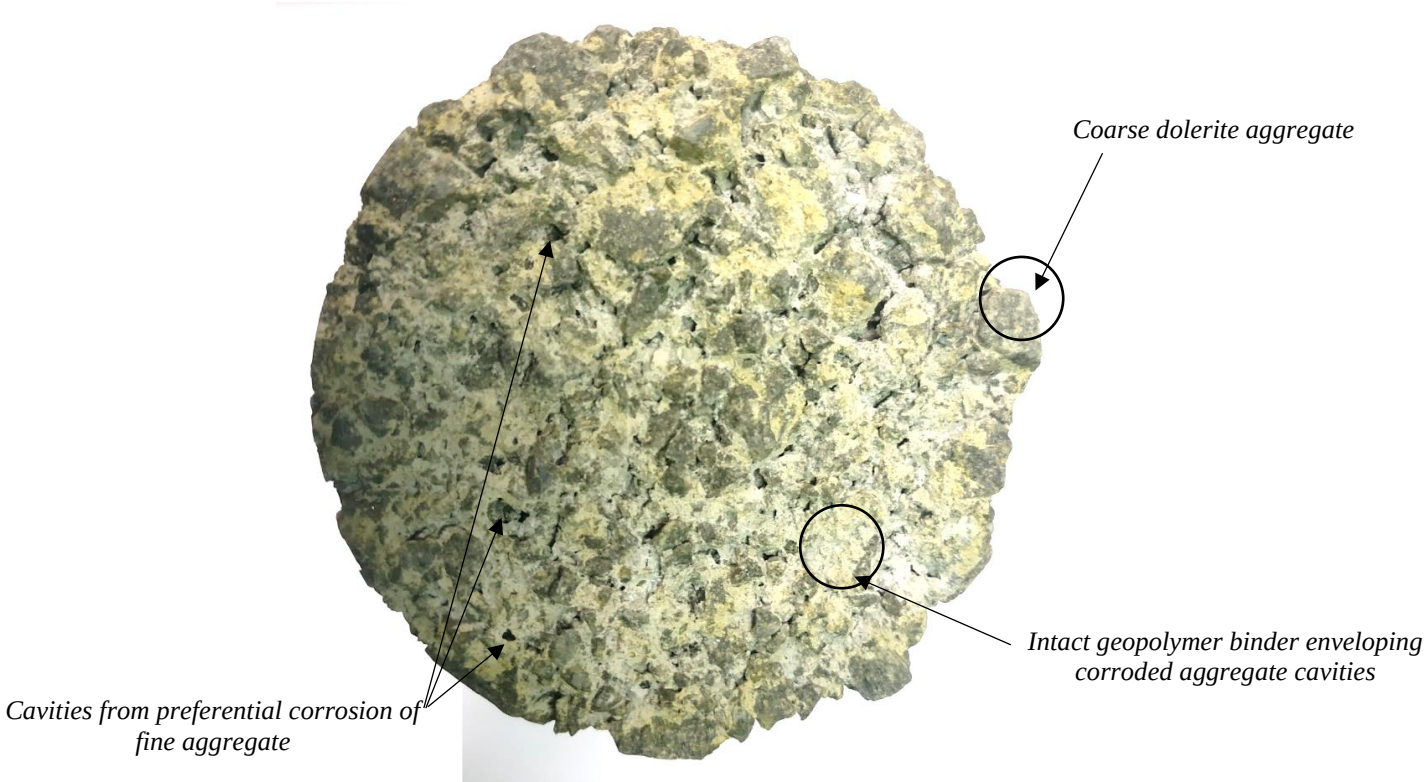

Figure 4-35: Top face of the GP-dolerite specimen displaying preferential corrosion of the aggregate

Concerning the GP-dolerite specimen, the image shown in Figure 4-34, which is taken from the side of the cylindrical specimen seems to indicate preferential corrosion of the paste. It is the opinion of the writer that the

image actually shows preferential corrosion of the fine fraction of dolerite aggregate. The top of the specimen clearly shows preferential corrosion of the aggregate with the paste matrix standing proud (see Figure 4-35).

Furthermore, the magnitude of the basicity differential may be used to estimate the degree of preferential corrosion in concrete. The three concretes with the lowest basicity differential (closest to zero) are GP-granite, GP-ferro-quartz and GP-andesite and these specimens display the least visible evidence of preferential corrosion. Therefore, the specimen images in Figure 4-16 show that the basicity differential values are consistent with the surface morphology.

The assessment of preferential corrosion could be translated from a qualitative one to a quantitative one by measuring the roughness of the corroded concrete specimen, where higher roughness would indicate higher preferential corrosion of either HCP or aggregate components.

4.5.5 Effect of mineralogy of hardened cement paste and aggregate on corrosion (XRD)

XRD analysis of the hardened cement pastes indicates that the 3 binder systems (PC, CAC and GP) are composed mainly of amorphous phases. The crystalline phases of GP HCP mainly consist of acid-resistant mullite and quartz. These acid-resistant crystalline phases partly explain GP HCP's resistance to HCl. However, 72% of GP HCP is constituted by amorphous phase materials. Analysing the structure of the amorphous phases falls outside the scope of this study.

4.5.6 Relevance of mineral acid testing to MIC of concrete in sewers

Numerous researchers have emphasised the point that mineral acid tests cannot be considered as representative of the conditions in a real sewer where acids are microbially generated. Kiliswa (2016) states that this determination is supported, in part, by test results related to CAC concretes being outperformed by OPC concretes in the dynamic HCl tests conducted by Fourie (2007) and Motsieloa (2012), whereas the performance of CAC concretes measured in the live sewer (VES) is significantly better than PC concretes. However, this determination requires an examination with the following points in mind.

4.5.6.1 Concrete mineral acid resistance dependency on test exposure conditions

There are clear differences in the corrosion behaviour of the concretes tested in this study under static and dynamic conditions. Where CAC and PC concrete were subjected to dynamic HCl testing, CAC concretes had the lower acid resistance compared to PC concretes, however, under static testing, the order of resistance is reversed with CAC concretes exhibiting significantly higher acid resistance than PC concretes.

4.5.6.2 MIC resistance of concrete is dependent on the exposure condition

The majority of measurements of corrosion (mass loss) in previous studies such as the VES, were primarily taken in the vicinity of the crown of the pipe. The concrete components measured (section 2.5.6) consist of pipe lids cut from a 120-degree segment at the top of the pipe, and core specimens suspended in a cage from the crown of the pipe. Because of this configuration, these measurements largely represent MIC of concrete in the gaseous atmosphere (i.e. the headspace) of the sewer pipe (i.e. above the tidal range of flow).

Multiple investigations of corrosion in sewers in numerous countries including, South Africa, France, Germany, Italy, United Kingdom, Netherlands, Denmark, Japan, Singapore, Kuwait, Venezuela, Brazil and Australia found that the most corroded areas on the concrete pipes were around the daily sewage flow level and at the that the most corroded sections in the sewers coincided with sites which had turbulent effluent flows (Kiliswa 2016). These findings point towards the exposure conditions at the effluent line being much more severe than the exposure conditions at the crown of the sewer pipe.

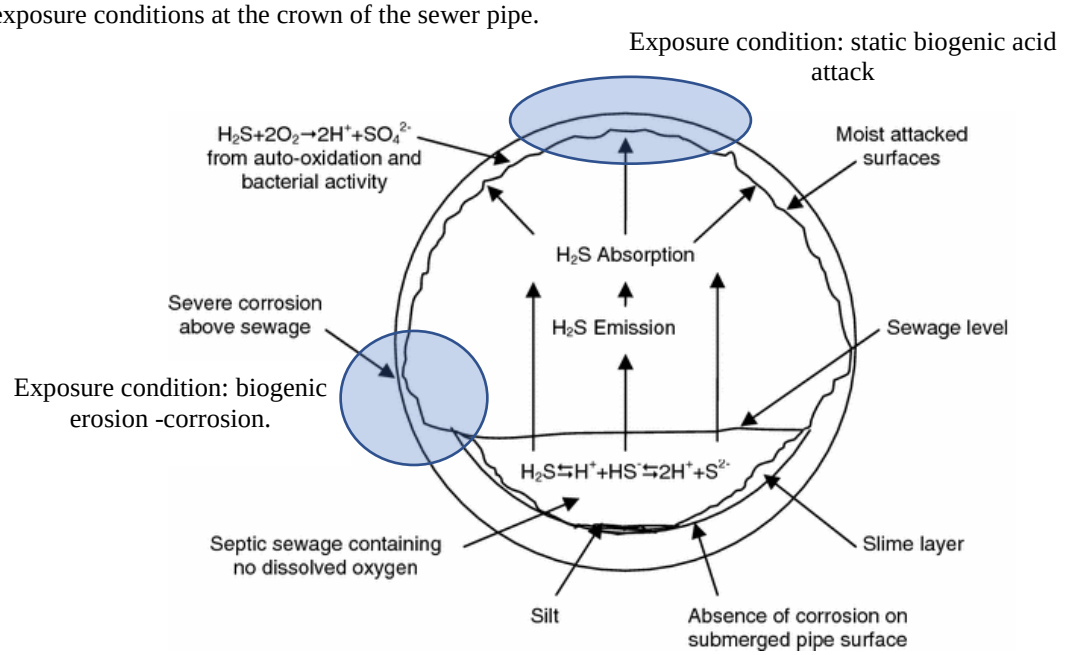

Figure 4-36: Schematic of a cross-section of a sewer pipe undergoing MIC showing regions where static biogenic corrosion is the dominant exposure condition and where erosion-corrosion is the dominant exposure condition. Adapted from Alexander and Fourie (2011).

4.5.6.3 Relating mineral acid tests to exposure conditions in the sewer

Design typically requires that the most adverse combinations of loading or environmental exposure condition be taken into consideration. Given that the exposure conditions across a pipe section differ significantly enough for them to be considered separately it is suggested that two exposure conditions be considered in designing a sewer pipe against MIC. Figure 4-36 shows the two types of exposure condition. The exposure condition at the crown of the sewer pipe is labelled as static biogenic acid attack, while the exposure condition at the effluent line is labelled as static corrosion.

Furthermore, the differences these materials exhibit under static immersion conditions and dynamic acid testing raise questions related to where in the pipe relatively static acidic conditions are likely and where erosive corrosive (dynamic) conditions are likely. Fourie (2007) states that the dynamic HCl test could be used to evaluate concrete mixes based on the conditions present at the waterline (effluent line).

It, therefore, follows that criteria for sewer concrete components exposed to the most aggressive sites, should include the capacity to resist the erosion-corrosion exposure condition. As is demonstrated in the results of this study, high resistance under static conditions cannot be extended to mean high resistance in erosive-corrosive conditions.

Table 4-23 shows the process involved in MIC of concrete sequentially from left to right. Below the sequence of processes are the test methods reviewed in Chapter 2 of this study. These methods range in complexity, and in the number of MIC processes they attempt to mimic.

Table 4-23: Checklist of individual MIC processes assessed in test methods

MIC Process	1. Hydrogen Sulfide gas production		2. Colonisation of concrete by SOB		3. Sulfuric acid production		4. Static acid attack		5. Erosion-corrosion	
Origin of process used in the test method	Biogenic	Artificial	Biogenic	Artificial	Biogenic	Artificial	Biogenic	Artificial	Biogenic	Artificial
Virginia Sewer Experiment (VES)	✓	✗	✓	✗	✓	✗	✓	✗	✗	✗
Hamburg chamber	✗	✓	✗	✓	✓	✗	✓	✗	✗	✗
Accelerated test for biodeterioration of cementitious materials	✗	✓	✗	✓	✓	✗	✓	✗	✗	✗
TAP (Testing apparatus for accelerated concrete degradation)	✗	✗	✗	✗	✗	✓	✗	✗	✗	✓
Dynamic hydrochloric/sulfuric acid test	✗	✗	✗	✗	✗	✓	✗	✗	✗	✓
Static immersion test	✗	✗	✗	✗	✗	✓	✗	✓	✗	✗

Test information sources: VES: Goyns (2013) and Kiliswa (2016), Hamburg chamber: Herrison and Saucier (2015), Accelerated test for biodetoriation of cementitious materials: Lavigne (2015), TAP, Dynamic hydrochloric acid test (Fourie, 2007), Static immersion test Bakhaerv (2005) and Song (2005).

The most representative test would include all 5 MIC steps wherein the origin of corrosion is biogenic. The closest assessment method to this ideal test, is the VES which meets all these requirements, except for erosion-corrosion (see Figure 4-36), where data related to this deterioration mechanism was not collected. Therefore, this assessment falls one process short of a comprehensive assessment of MIC of concrete in sewers. The Hamburg chamber and the "accelerated test for the biodegradation of cementitious materials" both make compromises in that they artificially dose micro bacteria on the surface of concretes being tested, the production of H_2SO_4 is consequently microbially controlled, however, these tests also do not include the erosive-corrosive conditions at the tidal line shown in Figure 4-36.

The TAP and the dynamic hydrochloric/sulfuric acid test include abrasive/erosive effects in addition to acid corrosion. Since these tests involve submerging test specimens in mineral acid solutions at pH 1, these test conditions are characterised by excess hydrogen ions, a condition unlikely to be representative of the MIC of

concrete where H^+ is likely to be neutralised by the concrete immediately. Similarly, the static HCl test is more aggressive than the static biogenic attack encountered at the crown of a sewer pipe.

Tests such as the static HCl test and the dynamic HCl test could be useful for comparing the resistance of competing concrete materials where the dominant MIC exposure conditions are known to be either static biogenic corrosion or erosion-corrosion.

Because the exposure condition where corrosion measurements of PC-dolomite and CAC-dolomite were taken in the VES are categorised in this study as being static biogenic corrosion, these data are thus compared to results from the static HCl test in this study (Table 4-24).

While dynamic mineral acid tests corrosion data are available, corrosion measurements near the waterline (zone erosion-corrosion exposure conditions) for real sewers are not available, therefore conducting a comparison of corrosion rates similar to Table 4-24 for erosion-corrosion was not possible.

Table 4-24: PC-dolomite and CAC-dolomite, static HCl test corrosion rate compared to VES corrosion rates

Concrete (23% binder: 77% Aggregate)	**Static HCl test corrosion rate ($mg/cm^2/hr$)**	**(mm/yr.)****	**Mean VES corrosion rate (mm/yr.)-**	**Ratio of static HCl test/VES corrosion rates**
PC-dolomite	3.84	114.2	1.475	77.4
CAC-dolomite	0.27	6.22	0.365	17.0
GP-ferro-quartz	0.056	1.53	Not tested*	

*GP concretes have not been tested in the VES as yet.

** Conversion of the static acid corrosion rate from mass to depth of corrosion was undertaken using the initial concrete densities calculated for specimens subjected to static HCl test.

For ease of comparison, Figure 4-37 provides a comparison between the corrosion rates of PC-dolomite and CAC-dolomite in the static HCl test and in VES, where the static HCl test corrosion rates have been normalised in favour of the PC-dolomite concrete mix which is given a value of unity.

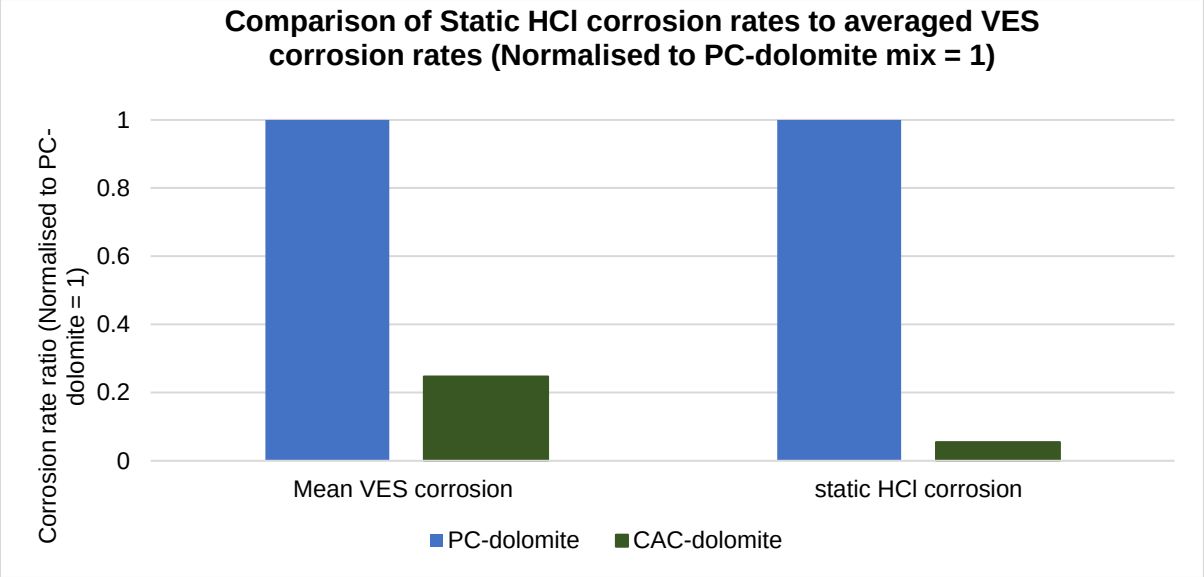

Figure 4-37: Corrosion rates (normalised to PC-dolomite VES corrosion rate) of the static HCl test and CAC-dolomite, static HCl test corrosion rate compared to averaged VES corrosion rates

If the corrosion rates measured in the dynamic test are converted into mm/year units by taking into account the density of concrete and calculating the volume of material per unit area to get the depth of corrosion (see Table 4-24), it is clear that the static HCl test much more aggressive than the biogenic corrosion conditions at the VES. This is to be expected as the PC-dolomite concrete in the static HCl test does not benefit from the protective effects of gypsum ($CaSO_4$), whereas in the VES, gypsum precipitating from sulfuric acid corrosion provides some degree of protection to the concrete (Alexander, personal communications, August 2020).

The calculated annual corrosion rate from the static HCl test indicates the rate of corrosion is 77 times higher than the VES for Portland cement-dolomite mixes. The same comparison for CAC-dolomite gives a surprisingly smaller ratio, with the corrosion rate in the static test only 17 times higher than in the VES.

While only two concretes types are compared, the static HCl immersion test provides the correct ranking in the order of resistance to corrosion when compared to VES measurements. A major criticism of the dynamic HCl test was that results from that test ranked PC-dolomite systems above CAC-dolomite systems in terms of acid resistance (mass loss and H^+ consumption), which was at odds with measurements from live sewer studies and biogenic corrosion chamber experiments.

However, the magnitude of the difference in the corrosion rate between CAC-dolomite and PC-dolomite mixes in the static test was much higher than the corrosion rate difference between the same two mixes in the VES. Under the static HCl test CAC-dolomite 18.36 times more resistant than PC-dolomite systems, the calculated difference in resistance between CAC-dolomite and PC-dolomite systems as reported by Kiliswa (2016) in the VES ranges between 2.9 and 5.3 times. This is attributed to the conditions in the static test being significantly more aggressive than the conditions at the crown of the pipe during MIC in the sewer environment.

4.5.6.4 Treatment of exposure conditions in MIC design methods

There has been a noticeable gap in research and design attention focused on exposure conditions of biogenic erosion-corrosion in sewer infrastructure. Instead, much attention has been placed on the rate of sulfide flux from effluent, which to a significant extent depends on hydraulic conditions. These hydraulic conditions are considered in design methods such as the Life Factor Method (LFM). In the LFM, the effects of turbulent flows are catered for by the use of the turbulence corrosion factor (TCF). According to Kiliswa (2016), the TCF ranges from 1.0 to 2.5 for areas with typical turbulent flow conditions and 5 to 10 for turbulent junctions. The TCF is used to calculate the maximum annual corrosion rate in using the following formula:

$$c_{max} = c_{avg} \times TCF$$

It is important to note that the original LFM is calibrated for PC concretes. An improved LFM was developed by Kiliswa (2016), where this model was adapted to include binder systems such as CAC and blends of PC with GGBS and silica fume (SF). The significant differences in the static corrosion and erosion-corrosion performance of specimens such as the CAC-dolomite concrete measured in this study require further development of the LFM.

4.5.7 Acid resistance of GP concretes compared to PC and CAC concretes

GP-ferro-quartz and GP granite were measured to be the best performing mixes. For simplicity, GP-ferro-quartz, the specimen with the lowest measured corrosion rates is used in the comparison. It should be noted that GP-granite and GP-andesite specimens had similar resistances to GP-ferro-quartz as the corrosion rates of these two specimens were marginally higher. Table 4-25 shows the magnitude in improvement of GP-ferro quartz concretes in both tests when compared to the PC-dolomite concrete mix, which is used an experimental control.

Table 4-25: Magnitude of resistance improvement of GP-ferro-quartz concretes when compared to PC-dolomite concrete (control)

	Control mix	Factor of resistance improvement/reduction	
Performance test	PC-dolomite (Control)	CAC-dolomite	GP-ferro-quartz
Dynamic HCl test	1	0.7	155
Static HCl test	1	21.1	85

Table 4-26: Magnitude of resistance improvement of GP-ferro-quartz concretes when compared to CAC-Dolomite concrete (control)

Performance test	CAC-dolomite (Control)	Magnitude resistance improvement calculated for GP-ferro-quartz
Dynamic HCl test	1	220
Static HCl test	1	4

The order in resistance to corrosion in the dynamic HCl test is GP-ferro-quartz>PC-dolomite>CAC-dolomite. Where GP-ferro-quartz concrete provides a 155-fold increase in resistance when compared to PC-dolomite and a 220-fold increase when compared to CAC-dolomite. As discussed in

Under the static HCl test, the order in performance is GP-ferro-quartz>CAC-dolomite>PC-dolomite. Where GP-ferro-quartz concrete provides a 85-fold resistance increase compared to PC-dolomite and CAC-dolomite provides a 21.1-fold increase in resistance compared to PC-dolomite. The resistance of CAC-dolomite in the static test is attributed to the protective alumina gel (AH_3) layer formed around the specimen when CAC concrete reacts with acid.

Table 4-25and Table 4-26 summarise the magnitude of by which of geopolymer concretes were more resistant under acid attack compared to Portland cement and calcium aluminate cement concretes. As discussed in chapter 3.2 of this study, it is suggested the dynamic acid test is useful for indicating the rate of dissolution of concrete in acidic solutions where the rate of dissolution is related to the kinetics of corrosion. Therefore, it is suggested that the fly ash based geopolymer possesses a higher resistance to dissolution resulting in a slower rate of degradation in acidic solutions compared to PC and CAC concretes. However, it must be reiterated that the dynamic acid test does not provide an indication of the rate of precipitation nor does it indicate the effect of precipitates on MIC resistance.

4.6 Chapter summary

In broad terms this chapter provides a comparison of binders (GP, PC, and CAC) aggregates (dolomite, dolerite, granite, ferro-quartz, and andesite) and concrete mixes of selected aggregate-binder combinations in terms of their performance under mineral acid testing and their chemical, mineralogical and mechanical characteristics.

Mineral acid testing yielded consistent trends in the performance of concrete mixes. Geopolymer concretes exhibited high resistance to both static and dynamic acid tests. PC-dolomite and CAC-dolomite mixes, while intended to be controls to GP concrete mixes, also exhibited interesting behaviour under acid testing. The CAC-dolomite exhibited relatively high resistance in the static HCl test and low resistance in the dynamic HCl test. PC-dolomite mixes exhibited low resistances in both tests.

Given the differences in performance observed in the static and dynamic tests, a parameter intended to quantify these performance differences called the abrasion factor was proposed. The term “abrasion” is related to the brushing (abrasive) action of the PVC bristles on the rotating concrete specimen in the dynamic acid test.

It is suggested that the abrasion factor is useful for quantifying corrosion protection mechanisms that are effective under static exposure conditions but less effective under erosive-corrosive exposure conditions. The material property that affects the abrasion factor value most significantly was shown to be the formation of protective corrosion products such as AH_3 gel in CAC cements. Furthermore, the abrasion factor was observed to be relatively higher in mixes where the aggregates were preferentially corroded (i.e. the hardened cement paste matrix was more resistant to acid attack).

SEM analysis of corroded (from the dynamic HCl test) and uncorroded HCP indicated that for PC and CAC-mixes, corrosion in the dynamic HCl test is largely a surface phenomenon, whereas corroded GP mixes exhibited

preferential corrosion of specific micro and nano-structures (including fly ash spheres). This indicates that the HCl corrosion behaviour of GP HCP's may not just be a surface phenomenon and may involve the movement of H^+ ions through transport mechanisms such as diffusion. Further research is required to test this hypothesis.

The hardened cement pastes and aggregates were characterised separately using x-ray diffraction and x-ray fluorescence analysis. Through XRD analysis the structure of the hardened cement pastes was found to consist mainly of amorphous phases (>70%) for all three paste types. However, the mineralogy of the crystalline phases showed that the GP hardened cement paste was largely characterised by acid insoluble minerals. The crystalline phase PC hardened cement paste were largely made up of soluble minerals such as Portlandite. XRD of the aggregates was much more comprehensive as all the aggregate types were of crystalline character, and thus allowed for the identification of the minerals and their proportions. As a means to gauge the solubility of the aggregates in acids, the solubility of all the minerals from which the aggregates are formed were reported.

XRF analysis provided the elemental composition of the aggregates and hardened cement pastes. Since previous investigators had stressed the importance of the Ca/Si ratio in the corrosion of Portland cement concretes (Yuan, 2013) the relationship between CaO content and the corrosion rate (mass loss rate) was plotted for each concrete mix. The general trend observed was that an increase in CaO content in the concrete was matched with higher corrosion rates in the static HCl test and the dynamic HCl test. However, CAC-dolomite corrosion rates tended to be outliers in both acid tests.

It was posited that the nature of chemical oxides, which can be classified as basic or acidic, play an important role in corrosion reactions. Therefore, a chemical parameter "the basicity value" was used to establish the proportions of major basic oxides to major acidic oxides in the HCP, aggregate and the concrete mixes. The basicity value was then compared to corrosion performance of specimens in the static and dynamic acid tests. While the relationship between basicity and corrosion performance in the static HCl test was not remarkable, a highly correlated relationship between the basicity value and the corrosion rate in the dynamic HCl test was observed.

Given that the basicity value was highly correlated to the corrosion rate in the dynamic HCl test and that the basicity value can be calculated for HCP and aggregates separately it was postulated that the basicity value may be of use in determining extent and bias of preferential corrosion in concrete specimens. Another parameter, the "basicity differential" was proposed to quantify the difference in the basicity value between the HCP and the aggregate components of the concrete mix while taking into account the relative proportions of aggregate and HCP in the mix design. By visually assessing specimens from the dynamic HCl test comparing nature of preferential corrosion to the concrete mixes "basicity differential" it was observed that the basicity differential was a good predictor of the extent and direction of preferential corrosion of the concrete mixes. CAC-dolomite had the highest observed preferential corrosion of the paste, which corresponded to a negative "basicity differential" of (-7.09) while GP-dolomite had the highest observed preferential corrosion of the aggregate with a corresponding "basicity differential of (1.33). GP-andesite, GP-granite and GP-ferro-quartz mixes presented relatively uniform corrosion, and this corresponded to their "basicity differential" values being close to zero.

Lastly, an attempt to relate corrosion mineral acid testing performance of concrete mixes to data extrapolated from VES reports by Goyns (2013) and Kiliswa (2016). Since VES corrosion data was largely collected from the crown of the corroding sewer, it was suggested that the live sewer exposure condition be classified as static biogenic

corrosion which was then related to the corrosive conditions in the static HCl test. Comparisons of the corrosion rates measured in the VES and the static HCl test for CAC-dolomite and PC-dolomite mixes produced agreement in the order of corrosion resistance of PC-dolomite vs CAC-dolomite. It is speculated that this finding indicates that there is potential for the development of calibrated durability models which could utilise results from performance based tests such as the static and dynamic HCl test as input parameters for the design concrete infrastructure subjected to MIC.

4.7 References

Affatato, S., Traina, F. 2011. “Bio and medical tribology”. Tribology for Engineers, 243

Alexander, M.G., Fourie, C.W. 2011. “Performance of sewer pipe concrete mixtures with Portland and calcium aluminate cements subject to mineral and biogenic acid attack”. Materials and Structures. Vol. 44.

Alsadig, D.Y., Wagialla KM. 2018. “Effect of local steel slag on compressive strength of cement mortars”. Journal of advanced chemical engineering.

Aphane, M.E., van der Merwe, E.M., Doucet, F.J., Petrik, L. 2015. “The effect of sulfuric acid concentration on the removal of reactive aluminium from South African coal fly ash”. World of coal ash conference, Nashville TN.

Bertron, A. 2014. “Understanding interactions between cementitious materials and microorganisms: a key to sustainable and safe concrete structures in various contexts”.

British standards institute (BSI). 2011. “BS EN 197 Cement. Composition, specificantions and conformity criteria for common cements”

Casey, W. H., Westrich, H.R, Arnold, W. Banfield, J.F. 1989. “The surface chemistry of dissolving Labadorite feldspar”. Geochimica et Cosmochimica. Vol 53.

Crawford, J. n.d. “Solubility data on 646 common and not so common minerals”. Viewed 20 January, 2020.<https://www.mindat.org/article.php/553/Solubility+Data+on+646+Common+and+Not+So+Common+Minerals>

Gay, H., Meynet, T., Combani, J. 2016. “Local study of the corrosion kinetics of hardened Portland cement under acid attack”. Cement and concrete research.

Goyns, A. M. 2013. Design manual for concrete pipe outfall sewers. Midrand: Concrete Manufacturers Association.

Kiliswa, M. W. 2016. “Composition and microstructure of concrete mixtures subjected to biogenic acid corrosion and their role in corrosion prediction of concrete outfall sewers.” PhD thesis, University of Cape Town.

Kurushkin, M., & Kurushkin, D. 2018. “Acid–Base Behavior of 100 Element Oxides: Visual and Mathematical Representations”.

Kushkin, D. Kurushkin, M. 2018. “Acid-Base behaviour of 100 element oxides: Visual and Mathematical representations”.

Letourneux, R., Scirvener, K. 1999. “The resistance of calcium aluminate cements to acid corrosion in wastewater applications”. Lafarge, France.

Malmstrom, M., Banwart, S. 1997. “Biotite dissolution at 25o CK The pH dependence on dissolution rate and stoichiometry”. Geochimica et Cosmochimica. Vol 61.

Martin-Garrido, M., Martinez-Ramirez, S., Perez, G., Guerroro, A. 2016. “Calcium silicate hydrate characterization by spectroscopic techniques”.

Motsieloa, N. 2012. “Acid resistance of sewer pipe concrete.” MSc thesis, University of Cape Town.

Ogirigbo, O.R. 2016. “Influence of Slag Composition and Temperature on the Hydration and Performance of Slag Blends in Chloride Environments”. PhD dissertation, University of Leeds.

People.wou.edu. 2020. “Periodic Trends And Oxides.” [online] Available at: <https://people.wou.edu/~courtna/ch412/oxides.html?ref=binfind.com/web> [Accessed 24 September 2020]

Ross, G.J. 1969. “Acid dissolution of Chlorites: release of magnesium iron and aluminium and mode of acid attack”. Clays and Clay Minerals. Vol 17.

Schneemann, K. 2000. “Abrasion and Erosion”. Ullmann’s Encyclopedia of Industrial Chemistry.

South African bureau of standards (SABS). 2006. “SANS 50197-1:2013: Concrete tests, Part 3: Making and curing of test specimens”.

5 Conclusions and recommendations

5.1 Conclusions

5.1.1 Concrete resistance to MIC

A general conclusion reached by this study is that the resistance of concrete to microbially-induced corrosion is a multifaceted concept and thus requires an examination of its parts. This is especially true when considered in the context of durability design of concrete structures. In this context, a material that is resistant to MIC need not necessarily be highly chemically resistant to acid attack. Instead, MIC resistance is attributed to a materials ability to remain serviceable for the duration of its planned life while being subjected to sewer conditions that promote biogenic acid production. Since sulfur-oxidizing bacteria are essential to the production sulfuric of acid (H_2SO_4), sewer pipe materials which inhibit bacterial activity are also reported to be MIC resistance regardless of their resistance to acid attack. Furthermore, resistance need not only emanate from un-corroded material, MIC resistance also consists of the protective physical and biological mechanisms emanating from corrosion products. Therefore, the MIC resistance of a material could be thought of as the net effect of numerous MIC resistance components. As is shown in Figure 5-1, these resistance components can be categorised into physical, chemical, and biological groupings.

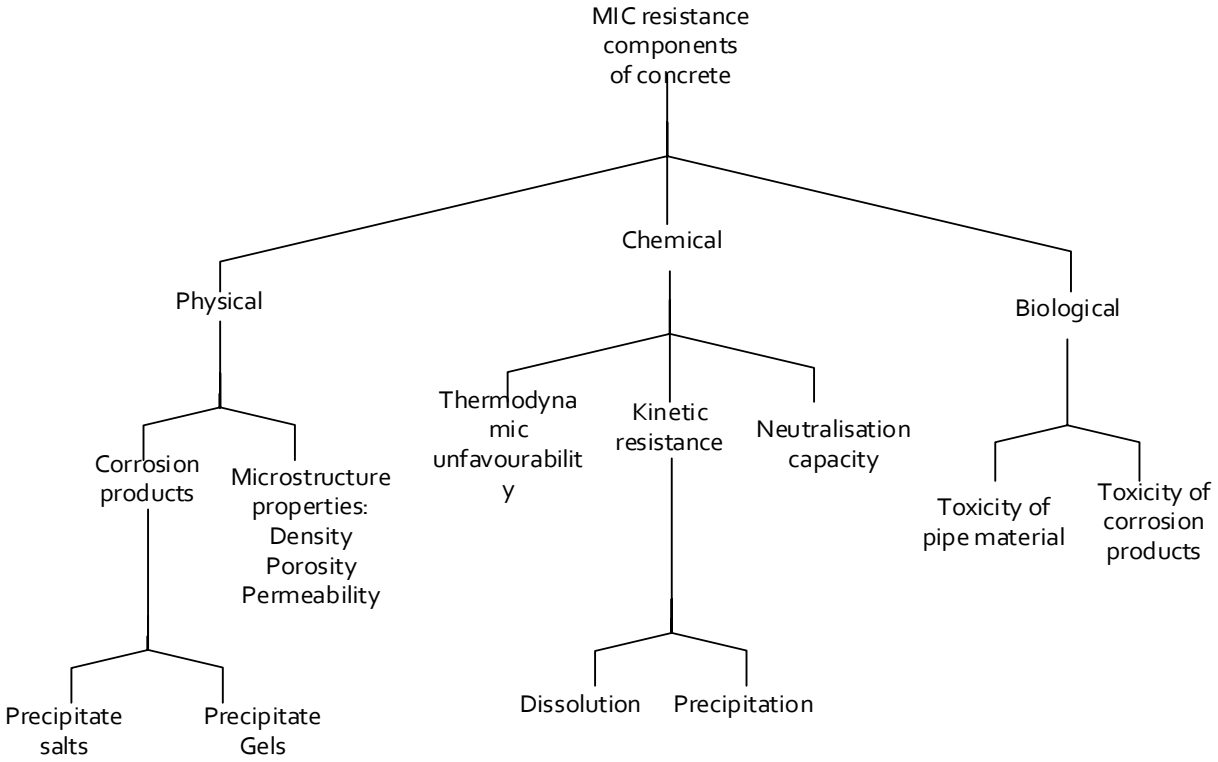

Figure 5-1: Categories of MIC resistance components

A second conclusion regarding the MIC resistance components identified above is that it is likely that they contribute to the net MIC resistance of a material in different magnitudes. Another useful way to categorise MIC

resistance components relates to what stage in the sequence of MIC processes that resistance component is effective. It may be plain to say that damage to concrete begins upon the commencement of a corrosion reaction, and more specifically, at the dissolution stage of the corrosion reaction. Therefore, MIC resistance components that are effective before the point at which damage commences (dissolution) stage are to be prized. However, as reported numerous investigators, the efficacy of various concrete materials to inhibit bacterial activity sufficiently enough to halt the production of sulfuric acid before the onset of corrosion has not been demonstrated even where concrete has been dosed with highly toxic materials such as heavy metals (Alexander and Fourie 2011, Druga et al. 2019).

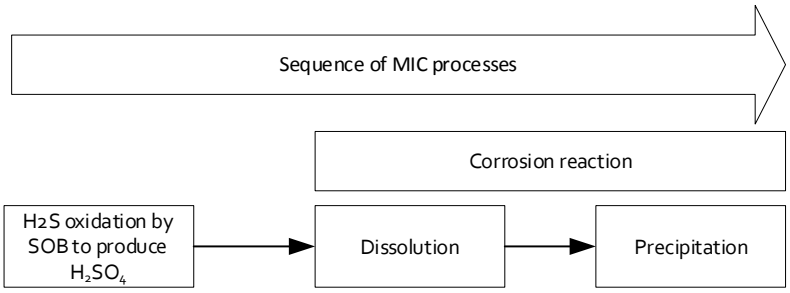

Figure 5-2: Sequence of MIC processes

5.1.2 Description of MIC exposure conditions

This study suggests that the significance of an MIC resistance component to the net MIC resistance of concrete is highly dependent on the environmental exposure conditions under which MIC occurs. The effect of different MIC exposure conditions on concrete degradation in the has been observed in long term sewer condition studies worldwide and, in particular, the exposure condition at the sewer line has been reported to be more aggressive than the exposure at the crown of the sewer pipe for Portland cement-based concrete pipes (Kiliswa, 2016).

Thus, an attempt is made by the researcher to describe the exposure conditions at these two locations of a corroding pipe's cross-section. These exposure descriptions are intended to aide durability design, and are by necessity, simplifications of real MIC conditions. However, it is hoped that the dominant causes of degradation are captured by the suggested exposure descriptions. Furthermore, it is certain that more types of exposure condition exist in real sewers or other infrastructure where MIC of concrete occurs. These two descriptions are thus not exhaustive.

MIC occurs at both locations (crown and effluent line), the condition at the effluent line is characterised as being a combination of erosion and biogenic corrosion (biogenic erosion-corrosion) while the condition at the crown of the sewer is described as static biogenic corrosion. The erosive component, at the effluent line emanates from the erosive effects of effluent flow. The term static, in the static biogenic corrosion conditions is meant to indicate that no other significant degrading effects, other than biogenic corrosion of the concrete are present.

5.1.3 Relating MIC exposure conditions, MIC resistance components and performance tests

If exposure conditions have an effect on the efficacy of concrete's MIC resistance components, and it is accepted that simplified simulations of each exposure condition can be performed through laboratory tests, then there exists

a conceptual link between MIC exposure condition, concrete MIC resistance components and performance tests. Table 5-1

Table 5-1: Suggested links between performance test, MIC resistance component and MIC exposure condition.

Performance tests	MIC resistance component(s)	MIC exposure condition	Example in sewer
Dynamic acid test (HCl or H_2SO_4)	Kinetic resistance to dissolution	Corrosion erosion	Corrosion at the effluent line
Static HCl test	resistance due to precipitates and gels	Static biogenic corrosion	Corrosion at the crown of the pipe

5.1.3.1 Dynamic acid test conclusions

According to this scheme, a conclusion reached by this study is that the dynamic acid test is well suited to assessing the combined kinetic resistance to dissolution of concrete. This test's suitability for the measurement of this parameter, is that the conditions present in that test effectively eliminate the physical and biological categories of the MIC resistance components listed in Figure 5-1. This is effect is enabled by continuous brushing of the corroding concrete specimen, which eliminates the protection from any corrosion products formed at the surface. Furthermore, 3 geopolymer mixes (GP-andesite, GP-ferro-quartz and GP-granite) has sufficiently low quantities of CaO to test under H_2SO_4 without the acidic solution becoming saturated with $CaSO_4$ and stalling corrosion reaction through the common ion effect. This effect was described by Fourie (2007) when testing PC and CAC concretes in the dynamic acid test using H_2SO_4. This study established that for these three concretes, no significant difference was observed in the corrosion rates when tested under HCl or H_2SO_4. This finding is in line with previous work conducted by Gay et al. (2016) who state that the dissolution phase of the corrosion reaction is not affected by the type of acid, but instead the rate of dissolution is a function of pH. Given that the pH of all acid tests conducted in this study was maintained at 1, it follows that the dynamic acid test may be used to determine the rate of dissolution of a corroding concrete specimen.

This study links kinetic resistance (to dissolution) to the erosion-corrosion exposure condition, which is exemplified by concrete corrosion degradation at the effluent line. This link is at the moment, relatively speculative as limited study has been directed toward MIC of corrosion at the effluent line in real sewers. However, it is widely accepted that degradation due to MIC at the effluent line is typically worse than the crown of the pipe (Kiliswa, 2016). This indicates harsh exposure conditions at that location. This conclusion agrees with postulations made by researchers regarding the conditions at the effluent line. Fourie (2007) for instance posited that concrete at the effluent line is subject to the harsh conditions of erosion-corrosion (dynamic conditions) and suggested the use of the dynamic test as a means to test concrete resistance against the harsh conditions at the effluent line.

HCl is the preferred acid for use in the dynamic test. In summary, the choice was necessitated by problems related to the insolubility of $CaSO_4$ where calcium-rich binders are tested in H_2SO_4. Justification for this choice is given by Alexander and Fourie (2011) and is restated in section 2.5.2 of this study.

GP-ferro-quartz, GP-granite and GP-andesite were tested in both HCl and H_2SO_4. The corrosion behaviour of these geopolymer/siliceous-aggregate concretes did not differ significantly when tested using HCl or H_2SO_4. This is most likely due to of the chemical structure of geopolymers.

5.1.3.2 Static HCl test conclusions

An acknowledged shortcoming of this study is that H_2SO_4 was not used for the static test. Instead, HCl was used whereas it would have been very beneficial to have used both acid types. This shortcoming was due to the need for consistency, and since HCl was to be used in the dynamic acid test, this would require HCl be used in the static acid test as well.

Nonetheless, valuable and data have been drawn from the static HCl test. As is shown in Table 5-1, the static HCl test is linked to MIC resistance components related to the protective effects of precipitates and gels. Out of the three cementitious systems (CAC, PC and GP) considered in this study, CAC concretes tested in the static HCl, were observed to significantly benefit from the existence of a protective gel enveloping the concrete specimen. This gel is suspected to be alumina gel (AH_3), a corrosion product that forms from both HCl and H_2SO_4 corrosion of CAC HCP (Gay et al. 2018).

A useful consequence of conducting both static and dynamic acid tests is that the corrosion rates between the two test conditions could be compared. Since the main difference between the two test regimes is the abrasion (removal) of corrosion products by the PVC bristles in the dynamic acid test, a quantity, termed the abrasion factor, equal to the corrosion rate in the dynamic test divided by the corrosion rate in the static test, could be used to quantify the degree to which corrosion products provide protection. A higher abrasion factor indicates the presence of a protective mechanism, effective in the static exposure condition (static acid test), that is not as effective in the erosive-corrosive exposure condition (dynamic acid test).

Static HCl corrosion test results were compared to long term data from the VES and it was shown that the order of resistance performance of OPC-dolomite and CAC-dolomite was in agreement in both assessments. As expected, because the static HCl test can only assess the MIC resistance component of concrete attained from HCl-concrete corrosion products, the static HCl test does not produce results which are directly proportional to measured corrosion rates in the at the crown of the sewer in the VES (static biogenic corrosion exposure condition). However, it is hoped that this rapid performance test results such as those from the static and dynamic tests could be built into a calibrated model suitable for predicting the durability of concretes.

5.1.4 Performance of GP, PC and CAC concretes under mineral acid test

Even though this study was focused on geopolymers, the control specimens also exhibited noteworthy behaviours. The results from the dynamic acid test showed that the resistance fly ash-based GP concretes under erosion-corrosion is significantly higher than both CAC and PC concretes. Under the dynamic HCl/H_2SO_4 test, the best performing fly ash-based GP concrete (GP-ferro-quartz) provided up to a 180-fold improvement in resistance when compared to PC-dolomite concretes, and up to a 275-fold improvement in resistance when compared to CAC-dolomite concretes. This finding is interpreted in terms of the kinetic resistance to dissolution MIC resistance component shows us that the corrosion of geopolymers is drastically slower at the dissolution phase,

than PC and CAC concretes. The order of the seven concrete mixes tested is provided below. It is suggested that the table gives the order and ranking in terms of the concrete mixes' resistance to dissolution during MIC.

Table: 5-2: Ranked performance of GP/PC/CAC concrete mixes tested in the dynamic HCl test

Rank in resistance	Concrete mix	Corrosion rate ($mg/cm^2/hr$)
1	GP-ferro-quartz	0.19
2	GP-granite	0.44
3	GP-andesite	0.46
4	GP-dolerite	4.43
5	GP-dolomite	21.1
6	PC-dolomite	34.12
7	CAC-dolomite	52.1

Under the static HCl test, the most resistant fly ash-based GP concretes (GP-ferro-quartz) provided a 69-fold improvement in acid corrosion resistance when compared to PC-dolomite concretes and a 4.82 fold improvement in acid corrosion resistance when compared to CAC-dolomite concretes.

CAC-dolomite concrete was found to have the highest difference in performance between erosion-corrosion (under the dynamic HCl test) and static corrosion (under the Static HCl test) testing which were quantified by the abrasion factor described referred to in 5.1.3.2

Table 5-3: Ranked performance of GP/PC/CAC concrete mixes tested in the static HCl test

Rank in resistance	Concrete mix	Corrosion rate ($mg/cm^2/hr$)	Abrasion factor
1	GP-ferro-quartz	0.056	3.3
2	GP-granite	0.0587	7.5
3	GP-andesite	0.086	5.4
4	GP-dolerite	0.14	32.9
5	CAC-dolomite	0.27	196
6	GP-dolomite	0.54	39
7	PC-dolomite	3.85	8.8

CAC-dolomite concrete had a calculated abrasion factor of 195. In comparison, the abrasion factor of OPC-dolomite concrete was calculated to be 8.8, and the abrasion factor of the most resistant GP concrete (GP-ferro-quartz) was calculated to be 3.3.

The comparatively high resistance of CAC-dolomite concrete in the static HCl test is attributed to the protective effect of alumina gel (AH_3) which forms from both H_2SO_4 and HCl corrosion reactions. During corrosion AH_3 (alumina gel) coats the concrete and acts as a barrier to acid attack in the static HCl test. This finding is in agreement with findings on the protective effects of AH_3 by Herrison and Suacier (2015) Letourneux and Scrivener (1999).

Given that the abrasion factor is a quantification of the protective effects of corrosion products, high values, such as the abrasion factor calculated for CAC-dolomite mixes indicate that CAC concretes benefit significantly from

the physical protection of corrosion products (gels and precipitates). On the other hand, the geopolymer concretes tested in this study have a low abrasion factors and thus it is inferred that they do not benefit significantly from protection from corrosion products. However, this finding is only partially complete because H_2SO_4 was not used in the static test and it is known that insoluble sulfate salts offer some protection to concrete undergoing MIC. Therefore, the static test and abrasion factor in this case assesses the protective effects of corrosion products that are common to both HCl and H_2SO4 corrosion reactions. Therefore, it is anticipated that under H_2SO_4 static testing, the precipitation of gypsum will increase the relatively low abrasion factor of PC-dolomite mixes will be increased.

5.1.5 Effect of material properties on corrosion

Part of this study was focused on identifying the properties of concrete and its components that have a strong bearing on corrosion resistance. Because of the complexity brought about by concrete being a heterogeneous material, hardened cement pastes and aggregates were characterised separately. These materials were then subjected to X-ray diffraction analysis, X-ray fluorescence analysis, and pH measurements. Thereafter data from these tests were correlated to the corrosion performance tests described in Chapter 3.

5.1.5.1 Mineralogy of GP, CAC and PC hardened cement pastes

XRD analysis showed that the three binders consisted of mostly amorphous phases. The amorphous content of Portland cement was 79%, calcium aluminate cement 70.1% and the amorphous content of geopolymer cement was 72 Thus, only the mineralogy of the crystalline phases was characterised. Of significance was that the fly ash-based geopolymer's mineralogy consisted of acid-insoluble minerals (under ambient temperature and pressure). Mullite (13.9%) and quartz (8.7%) were the main insoluble minerals in geopolymer hardened cement paste. Much of the insoluble mullite was attributed to fly ash used in the geopolymer binder.

The crystalline phase Portland hardened cement pastes consisted mainly of Portlandite (6.3%) and haurite (11%), which are acid-soluble minerals. The crystalline phase of calcium aluminate cement hardened paste was found to consist mainly of krotite (12.8%) and katoite (6.7%) and the solubility of these minerals was not established.

On the other hand, the mineralogy of aggregates was analysed to consist of crystalline phases (99% or more). The 5 aggregates chosen to be used in the concrete mixes (dolomite, dolerite, andesite, ferro-quartz and granite)

It should be noted that the mineralogy of cementitious materials is a highly complex field of study. The objective of using these methods was to obtain a reasonable measure of the mineralogical character of these pastes, and thus these findings are not suggested to be definitive.

5.1.5.2 Effect of concrete basicity on kinetic resistance to dissolution

X-ray fluorescence analysis enabled the identification and the quantification of oxides and their proportions in the hardened cement paste samples. Previous investigators have stressed the importance of calcium bearing compounds to concrete corrosion resistance. For instance, the Life Factor Method (LFM) requires quantification of the proportion of $CaCO_3$ in concrete to estimate corrosion resistance. Furthermore, the rate at which Portland cement concrete is decalcified under biogenic corrosion has been suggested to be a function of Ca/Si ratio (Yuan 2013). However, in this study relating CaO content to corrosion performance in the static and dynamic test did

not yield strong correlations. This was due to corrosion rates from CAC-dolomite mixes which contradicted the prevailing trends in the data.

The basicity parameter ($CaO+MgO)/SiO_2$) which provides the ratio of the major basic and acidic oxides when related to the corrosion rate from the dynamic HCl test, yielded strong linear relationship where all the concrete mixes were results were used (R^2 = 99.4%). Low basicity values corresponded to low corrosion rates and high basicity values corresponded to high corrosion rates.

This study relates the corrosion mechanism in the dynamic HCl test to the dissolution rate of concrete materials in acidic solutions. Thus the conclusion reached is that, in acidic media, concretes with low basicity values dissolve slower rates when compared to concretes with high basicity values. This comparison showed that geopolymer concretes paired with siliceous aggregates had the lowest corrosion rates in the dynamic test and thus had the highest kinetic resistance to dissolution, and therefore corrosion. On the other hand, the CAC-dolomite mixes had the highest basicity values and also displayed the highest corrosion rates in the dynamic HCl test.

The reason behind the high (99.7%) correlation between basicity and the corrosion rate measured in the dynamic HCl test is not fully understood, nor has the consistency in the observed linear relationship between the two parameters been verified extensively. Thus as a first step, the reliability of the basicity-corrosion rate (in the dynamic acid test) has to be tested with more binder/aggregate concrete mix combinations. The effect of acidic and basic oxides on the corrosion properties of cementitious materials requires further study. However, the evidence from this study suggests that basicity value determined via XRF may be used to assess the rate of dissolution, which is the first phase of the corrosion reaction. If this relationship holds, the value of this relationship is applicable not just to MIC problems but to acid corrosion of concrete in general.

5.1.5.3 Effect of HCP and aggregate basicity on preferential corrosion

Early investigations found that Portland cement paired with siliceous aggregates degraded very quickly (CSIR, 1959). It was recognised that preferential corrosion of the paste component in concrete was undesirable, therefore compatibility of HCP and aggregate components was serious design concern. However, not much attention has been given to this specific corrosion problem, instead accept/reject rules related to the solubility of aggregates in acid have been adopted in concrete sewer pipe mix design codes and manuals such as SANS 677.

If the basicity value and dynamic acid corrosion rate correlations found in this study are accepted, and it is accepted that the corrosion rates measured in the dynamic acid test are a measure of the dissolution rate of concrete materials under acid attack, then it follows that difference in the basicity value between the HCP and aggregate can be used to estimate the extent of differential corrosion between the HCP and aggregate. Basicity differential values were compared visually to the corroded specimens. The corroded specimens with the lowest basicity differentials were GP-andesite (-0.05) and GP-ferro-quartz (0.21), visually these specimens did not exhibit preferential corrosion. At the extremes, CAC-dolomite corroded specimens, which had a calculated basicity value of -7.09, exhibited high degree of preferential corrosion of the paste, while GP-dolomite corroded specimens, which had a basicity value of 1.33, exhibited a high degree of corrosion of the aggregate. Therefore, the basicity differential is an improved method by which the compatibility of aggregate and paste may be paired.

While preferential corrosion measurements were not taken in the VES, it could be argued that concrete mixes with high basicity values such as CAC and siliceous aggregate mixes reported by Goyns (2013) and Kiliswa (2016) performed better than a PC-dolomite mix in the real sewer condition. However, the basicity differential is a measure related to dissolution and does not take into account the effect of precipitates. In the case CAC-siliceous aggregate undergoing corrosion, the protective AH_3 gel has been found to envelop both aggregate and paste in a protective film thereby creating a physical barrier between acid and HCP and aggregate (Letourneux and Scrivener, 1999). These protective effects are better quantified, as mentioned above, by the abrasion factor.

5.1.5.4 Properties of geopolymers that enable resistance to dissolution

This study suggests that the primary property of geopolymers that enables high resistance to acid attack is the kinetic resistance to the dissolution phase of the corrosion reaction. Furthermore there is little evidence from the tests undertaken in this study suggesting that products resulting from HCl or H_2SO_4 corrosion of geopolymer concretes provide any significant protection to geopolymers.

However, geopolymer concretes do corrode albeit at a rate slower than PC and CAC concretes. A visual assessment of HCl and H_2SO_4 corroded geopolymer HCPs was undertaken via SEM.

High magnification imaging of corroded GP HCP showed fly ash spheres embedded within the geopolymer matrix had been corroded leaving behind the geopolymer micelle matrix. This finding is important because it indicates that the geopolymeric structure is more resistant than fly ash spheres, which themselves are constituted by relatively insoluble minerals such as mullite. The high acid resistance of the hardened cement GP paste matrix agreement with previous work by Grengg (2017) who state that acid corrosion on GP mortars leaches out alkali ions, but the binder aluminosilicate network structure remains stable, dissolving significantly lower amounts of Si and Al compared to PC and CAC systems.

Furthermore, 28% of the analysed GP HCPs is crystalline and constituted mainly by acid-resistant minerals such as mullite and quartz. Researchers working on MIC on GP concrete attribute the high acid resistance to a low CaO/SiO_2 ratio (Bernal and Provis, 2014). This finding was confirmed by this study and further developed by comparison of the basicity and surface corrosion rate

5.1.5.5 Properties of CAC concretes that increase MIC resistance

If only the dynamic acid test results of the seven concrete mixes in this study are considered, then it appears that the CAC-dolomite concrete mix has poor resistance to dynamic acid attack. However, the opposite is true for the static acid test, where CAC showed much higher resistance to static HCl corrosion than PC. Therefore, it is suggested that the performance of CAC concretes under acid attack are highly dependent on the prevailing exposure conditions. Results from the static and dynamic HCl tests, when interpreted in terms of MIC resistance components proposed by this study, indicate that CAC concrete mixes had low resistance to dissolution, but benefit from high resistance from corrosion products. If these findings are applied to sewer conditions it could be posited that CAC concretes are better suited for exposure conditions in the sewer where physical weathering effects such as erosion and abrasion from flowing water are minimal, and that CAC concretes may be unsuitable for sewer structures where acid corrosion occurs simultaneously with erosion and abrasion, such as pipe sections where turbulent flows are present.

5.1.5.6 Properties of PC concretes that enable MIC resistance

Under HCl both mineral acid tests regimes, PC concrete generally exhibited poor corrosion resistance. A fair criticism to this study would be that the protective physical barrier caused by gypsum ($CaSO_4$) precipitating in the sewer was not assessed. This shortcoming due to the use of HCl in the static test is acknowledged and should be included in future study. However, the resistance of PC concretes to dissolution should hold true despite of the use of HCl instead of H_2SO_4 (Gay et al. 2016). This study can conclude that the resistance to dissolution of the PC-dolomite concrete is low compared to the geopolymer concrete mixes. However, without testing in H_2SO_4 (in the static acid test), a conclusion related to the degree to which corrosion products provide a physical barrier to resist MIC in the PC-dolomite mixes cannot be reached.

5.2 Recommendations

5.2.1 Live sewer testing of geopolymer concretes

It is recommended that the set of geopolymer concrete specimens tested in this study be tested in a live sewer to so that corrosion data from a real sewer environment is obtained for geopolymers. Corrosion measurements should ideally be collected from samples placed in varied sewer exposure conditions, which include, static biogenic corrosion (crown) and biogenic erosion-corrosion (effluent line).

5.2.2 Recommendations to performance test

This study used mass loss as a measure of concrete degradation due to corrosion. If the view that MIC is a surface degradation problem, then this measure may suffice. However, the geopolymer concrete mixes tested in this study have displayed high resistances to dissolution in acidic solutions and therefore there exists the possibility that H^+ ions can diffuse into the concrete matrix while the surface concrete remains relatively sound. Thus, it is suggested that mechanical properties such as strength and the dynamic modulus of elasticity are also included to measure degradation.

Furthermore, it may be worthwhile to vary the value of the pH solution in both the static and dynamic acid tests because it has been suggested that the protective AH_3 gel is attacked at pH values lower than 3.5 (Letourneux and Scrivener 1999). Therefore, it is of interest to investigate whether the protective effects of AH_3 gel are more pronounced in less acidic solutions than used in this study (i.e. higher pH values).

5.2.2.1 Improvements to the static acid test

It is recommended that the static acid test should be conducted using H_2SO_4 and HCl. It is posited that using testing concrete materials using both acids separately could provide insight into the protective effects of precipitates. For instance, where CAC mixes are to be tested, both gypsum and alumina gel will precipitate under H_2SO_4 testing, however, under HCl testing, the corresponding salt is $CaCl_2$ which is soluble. Therefore, by comparing the corrosion rates in both these tests it may be possible to quantify the relative contributions of AH_3 gels and gypsum to corrosion protection.

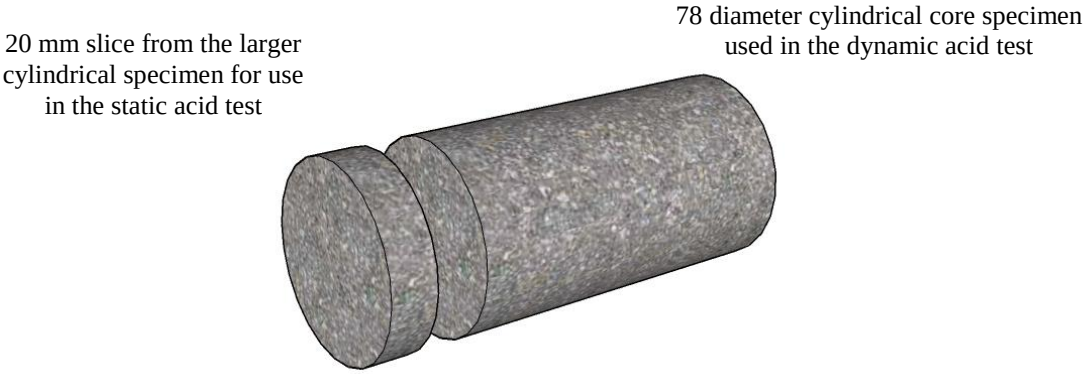

Figure 5-3: Proposed test specimens for the dynamic and static acid tests.

It is further recommended that for static tests, a 20 mm thick slice of the cylindrical concrete specimen test is used in the static test (Figure 5-3). This will ensure that the specimen preparation for both tests is identical thus reducing unwanted variability.

5.2.2.2 Improvements to the dynamic acid test

Despite, the findings by Gay et al. (2016) and the relatively similar corrosion rates obtained using HCl and H_2SO_4 in the dynamic acid test in this study which indicate that the dissolution rate of concrete is independent of acid type, to promote the representativeness mineral acid tests to MIC, it is suggested concretes tested in the dynamic acid test be subjected to H_2SO_4 as well as HCl.

Given tendency of precipitating salts such as gypsum to stall corrosion in where calcium rich concretes were tested in H_2SO_4 (Fourie 2007), it is recommended that the dynamic acid test rig be modified to enable the use of H_2SO_4.

To avoid the corrosion stalling effects of the common ion effect in the dynamic H_2SO_4 test where calcium based concretes are the subject of testing, it is recommended that the solution be drained and replenished frequently enough to avoid saturation of the solution with precipitating salts while maintaining the pH at the required value of 1. This may be achieved by tapping the solution from the bottom of the while simultaneously replenishing the acid in the tank.

It is further recommended that this test be coupled with surface-roughness measurements of the corroded specimens to quantify the degree of preferential corrosion of paste or aggregate on the specimen. Measurements similar to “Testing apparatus for accelerated concrete degradation” (TAP) which utilise laser sensors to measure changes in geometry on the surface of corroded concrete specimens are possible highlighted as possible.

5.2.3 Accelerated performance testing of MIC resisting properties of concrete

This study showed that the order in corrosion resistance of competing concretes types strongly depends on the damaging mechanisms present in the test and the MIC resisting property (MIC resistance component) of the concrete being tested. Furthermore, the most representative biogenic corrosion tests for concrete currently available typically require long periods before a result is available. For instance, in the Hamburg chamber, specimens are typically monitored for 12 months, while live sewer experiments such as the VES require periods longer than 5 years for appreciable trends to be established. These lengthy evaluation periods are not desirable, as

engineers typically require short periods for performance and quality testing for the purposes of design and quality assurance.

As a consequence, it is recommended that the MIC resistance of concrete be broken down into performance-measurable MIC resistance components which can be tested rapidly. Thereafter, with the development of predictive models, these performance data could be used as input parameters to a calibrated durability model related to the service life of structure subjected to MIC. The key MIC resisting properties and the recommended tests are provided below.

5.2.3.1 Kinetic resistance to dissolution tested through the dynamic acid test

This type of resistance is not dependent on corrosion products that may have a protective effect on concrete by shielding it from acid attack. Tests such as the dynamic HCl test is a suitable performance test that is capable of providing results within 48 hours.

5.2.3.2 Resistance due to corrosion products tested through the static acid test

Static corrosion resistance includes the protective effects of corrosion products. The type acid selected is dependent on the anticipated type of corrosion. In the case of MIC, where researchers such as Grengg (2017) and Monteny et al. (2000) suggest that $CaSO_4$ precipitated in the corrosion of calcium-based concrete systems does not provide a protective barrier to acid attack. It is therefore recommended that HCl, which forms soluble salts is used instead.

5.2.3.3 Neutralisation capacity tested through acid base titration

Higher acid neutralisation capacity thought to enable a material to tolerate aggressive (acid) environment for longer periods (Espinosa et al. 1996). The principle of a material's acid neutralisation capacity is based on the quantity of acid necessary to destroy a given quantity of material. Therefore, neutralisation capacity (NC) can be defined as the quantity of acid H^+ ions (in Moles (M)) necessary to neutralise a given quantity of material (in grams) (Kiliswa, 2016).

There are numerous methods and standards by which the acid neutralisation capacity can be determined through testing. The test method described by Kiliswa (2016) and Letourneux and Scrivener (1999) requires a known quantity of concrete material to be fully reacted with an excess solution of a strong acid such as HCl of standard molarity. The rate of the reaction is accelerated by milling the sample to a powdered form to increase its surface area and heating the acidic solution. Thereafter a known quantity of NaOH is titrated into the solution until it's pH is a neutral 7. By measuring the quantity of NaOH consumed in the titration, the amount of HCl consumed in by neutralisation of the test-material can be calculated.

5.2.3.4 Resistance due to the bacteriostatic effect through testing

The bacterio-static effect is defined as the capability of a substance to inhibit the growth or reproduction of bacteria. In concrete materials, this effect manifests in two ways. The first way is through the inclusion of a material that is toxic to bacteria in the concrete mix. Materials with toxic effects on bacteria such as heavy metals have been included in a few studies with varied success in attaining statistically significant results (Alexander and Fourie 2011; Druga et al. 2018).

In its second form, the bacterio-static effect is observed during corrosion and is caused by the liberation of materials which are toxic to bacteria and come about as products of ongoing corrosion reactions. In CAC concrete subjected to MIC, Herrison and Saucier (2015) state this resistance type comes into effect when aluminium ions are liberated from the decomposition of alumina gel (AH_3) at pH values ranging between 3 and 4.

Furthermore, the corrosion products of cementitious materials can either promote or deter bacterial growth. For example, the porous, moist and pulpy characteristics of $CaSO_4$ gypsum formed in biogenic corrosion of PC concretes is thought to promote the growth sulfur-oxidizing bacteria thereby increasing the rate of biogenic H_2SO_4 generation (De Belie et al 2002) whereas the inclusion of biocides such as toxic heavy metal ions is thought to deter bacterial growth. These complexities make the bacterio-static effect the most ambiguous type of resistance to quantify. It is recommended that research be undertaken into a suitable method of conducting performance tests to measure this form of resistance.

5.2.3.5 Resistance due to physical microstructural properties of concrete tested

The physical properties of concrete may also play a significant role in resisting MIC. While it has been established that microstructural properties do affect corrosion, the extent to which they do has not been assessed in comparison to the other resistance properties. It is therefore suggested that concrete mixes should have their corrosion performance tested by varying the quality of their microstructure. To this end, the oxygen permeability index (OPI) performance test can be used as a means measure permeability. Similarly, sorptivity can be used to measure the absorption properties of the concretes. These parameters can then be compared to corrosion (degradation) parameters such as hydrogen consumption, mass loss and surface roughness.

5.2.4 Effect of carbonation on geopolymer concretes

While this is not directly an MIC problem, the literature reviewed in chapter 2 of this study indicates that geopolymer concretes do carbonate, which is accompanied by a reduction in the pH of the concrete substrate. Given that the pH measurements of un-corroded HCPs found that the pH of GP concretes was substantially lower than those of OPC carbonation of geopolymer concretes may potentially pick up speed colonisation by sulfur oxidizing bacteria. In addition, concrete sewer pipes are typically reinforced with steel, it is important to establish whether carbonation induced corrosion may be a significant durability concern in the sewer environment.

5.2.4.1 End.

Testing a material for each component of MIC resistance separately provides a clearer assessment of the capability of material to resist MIC compared to a test that measures the combined resistance of multiple resistance types at once. Furthermore, understanding each resistance type in isolation could enable the development of resistance models relating to the varying exposure conditions that exist in the sewer and other concrete infrastructure exposed to acidic conditions.

5.3 References

Alexander, M.G., Fourie, C.W. 2011. Performance of sewer pipe concrete mixtures with Portland and calcium aluminate cements subject to mineral and biogenic acid attack. Materials and Structures. Volume 44

De Belie, N., Monteny, J, Taerwe L. 2002. "Apparatus for accelerated degradation testing of concrete specimens". Materials and Structures vol 35.

Druga, M., Ukrainczyk, N., Weise, K., Lackner, S. 2018. "Interaction between wastewater microorganisms and geopolymer on cementitious materials: Biofilm characterization and deterioration characteristics of mortars". International Biodeterioration & Biodegradation, Volume 134.

Espinosa, B., Letourneux, R., & Marcdargent, S. 1996. Acid attack of hydraulic cement-bound materials: Corrosion kinetics and neutralisation capacity. Proceedings of the 13th International Corrosion Congress. November 25 – 29. Melbourne. 494 – 503.

Gay, H., Meynet, T., Combani, J. 2016. "Local study of the corrosion kinetics of hardened Portland cement under acid attack". Cement and concrete research.

Grengg, C., Mittermary, F., Ukrainczyk, N., Koraimann, G., Kienesberger, S., Dietzel, M. 2018. "Advances in concrete materials for sewer systems affected by microbially induced concrete corrosion: A review."

Herrison. J., Saucier. F. 2015. Use of Calcium Aluminate Cements in H2S Biogenic Environment. Institute of Concrete Technology. 2015-2016 Yearbook.

Kiliswa, M. W. 2016. "Composition and microstructure of concrete mixtures subjected to biogenic acid corrosion and their role in corrosion prediction of concrete outfall sewers." PhD thesis, University of Cape Town.

Letourneux, R., Scirvener, K. 1999. "The resistance of calcium aluminate cements to acid corrosion in wastewater applications". Lafarge, France.

Appendices

Appendix A. X-ray diffractograms

A.1 Hardened cement pastes

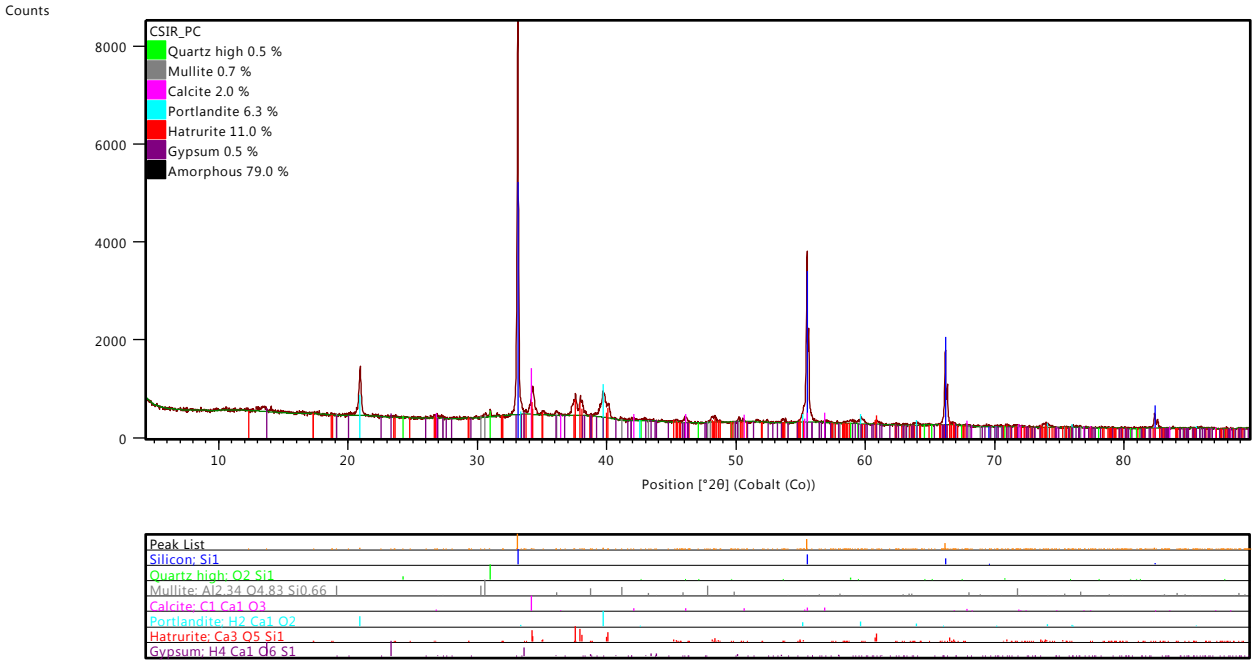

Figure A 1: XRD of Portland cement hardened paste

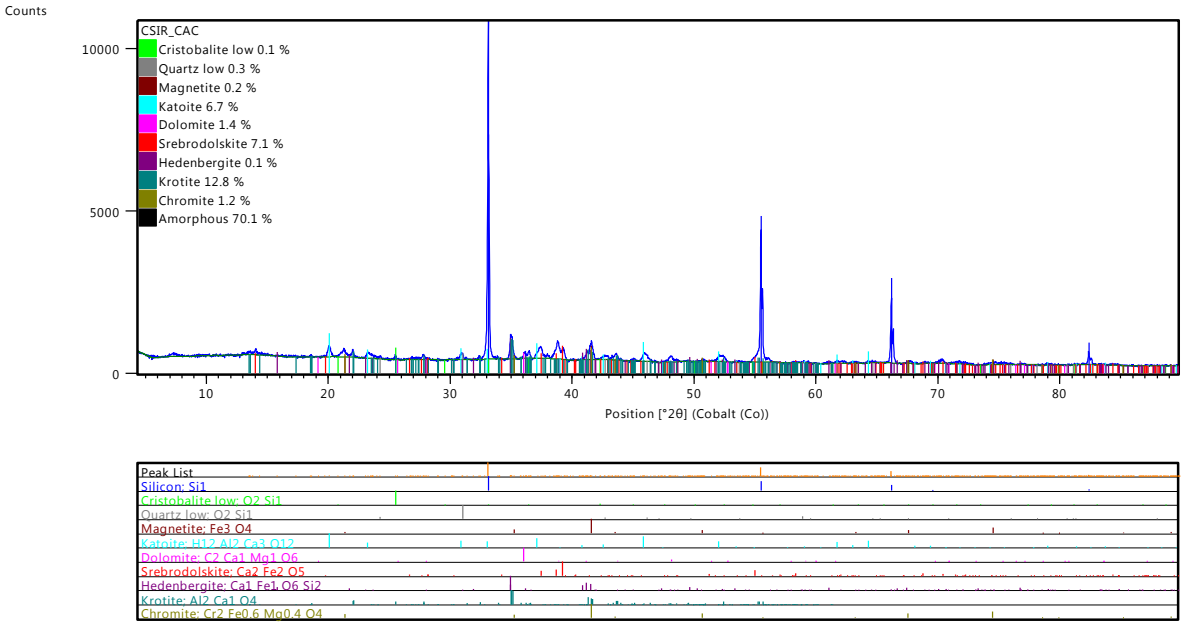

FigureA-2: XRD of calcium aluminate cement hardened paste

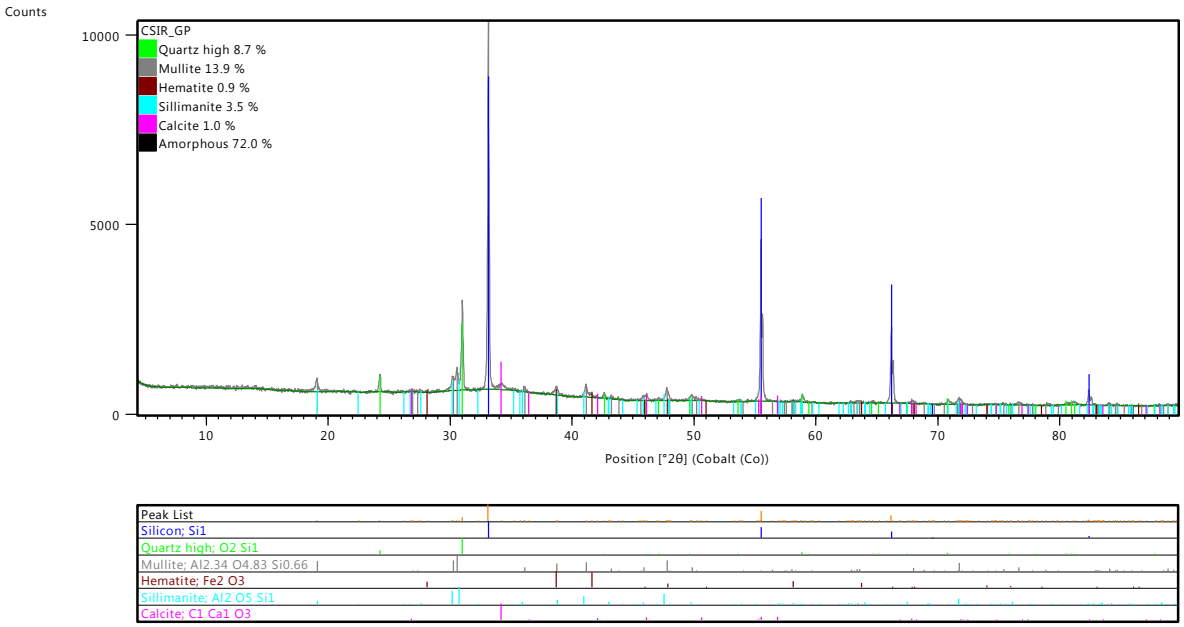

FigureA-3: XRD of geopolymer cement hardened paste

A.2 Aggregates

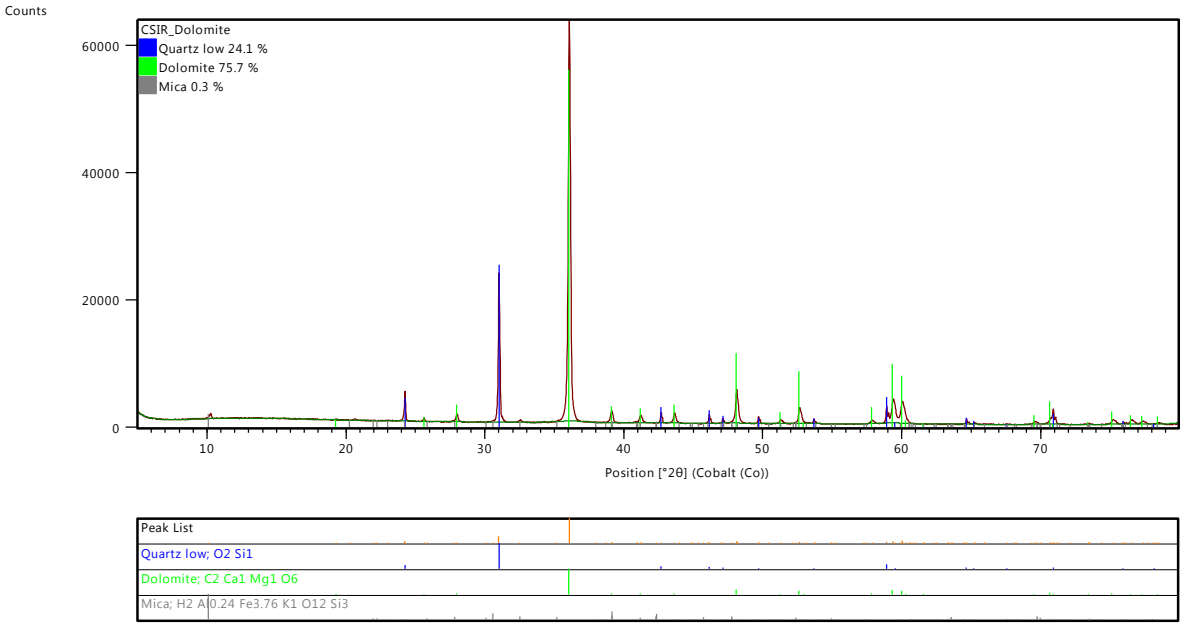

FigureA-4: XRD of Dolomite aggregate

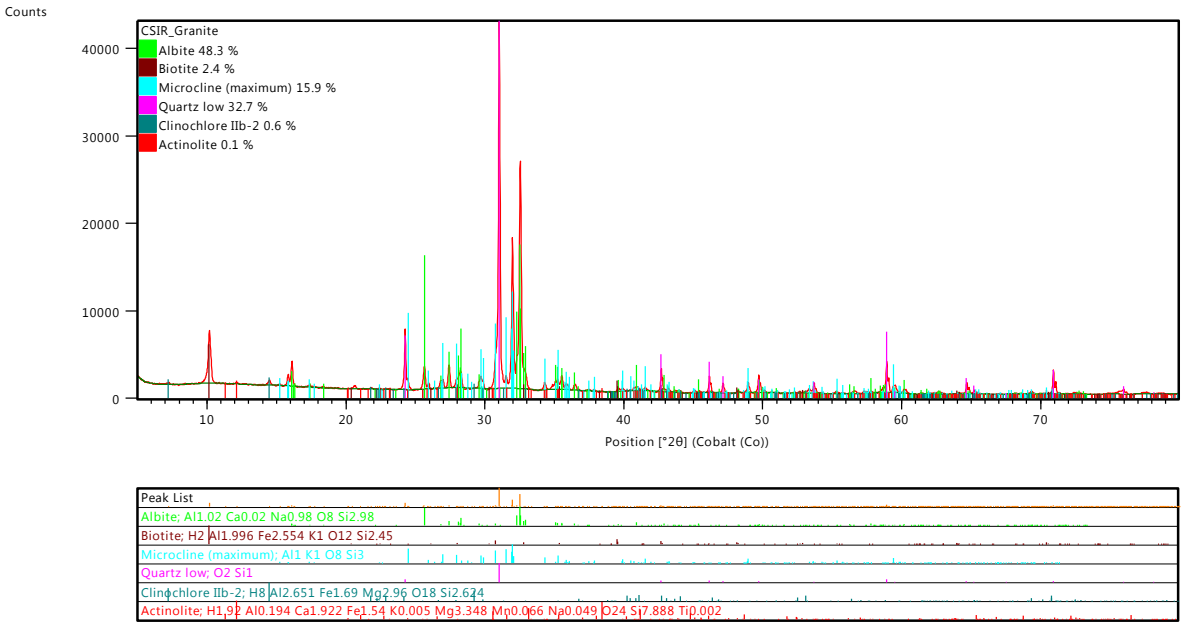

FigureA-5: XRD of granite aggregate

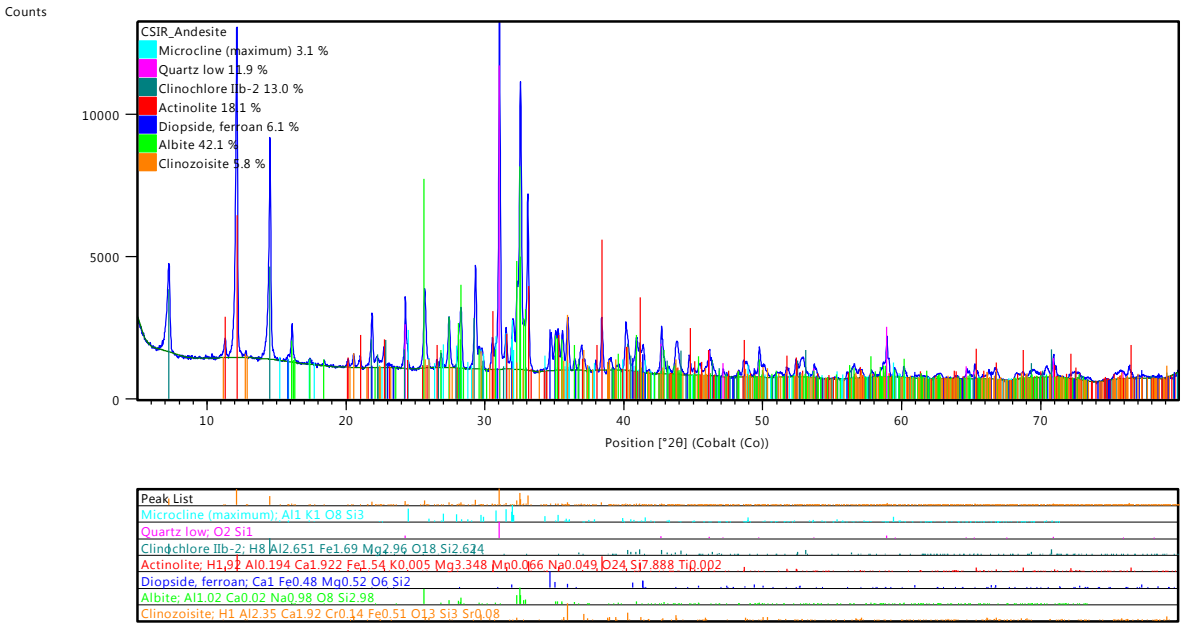

FigureA-6: XRD of andesite aggregate

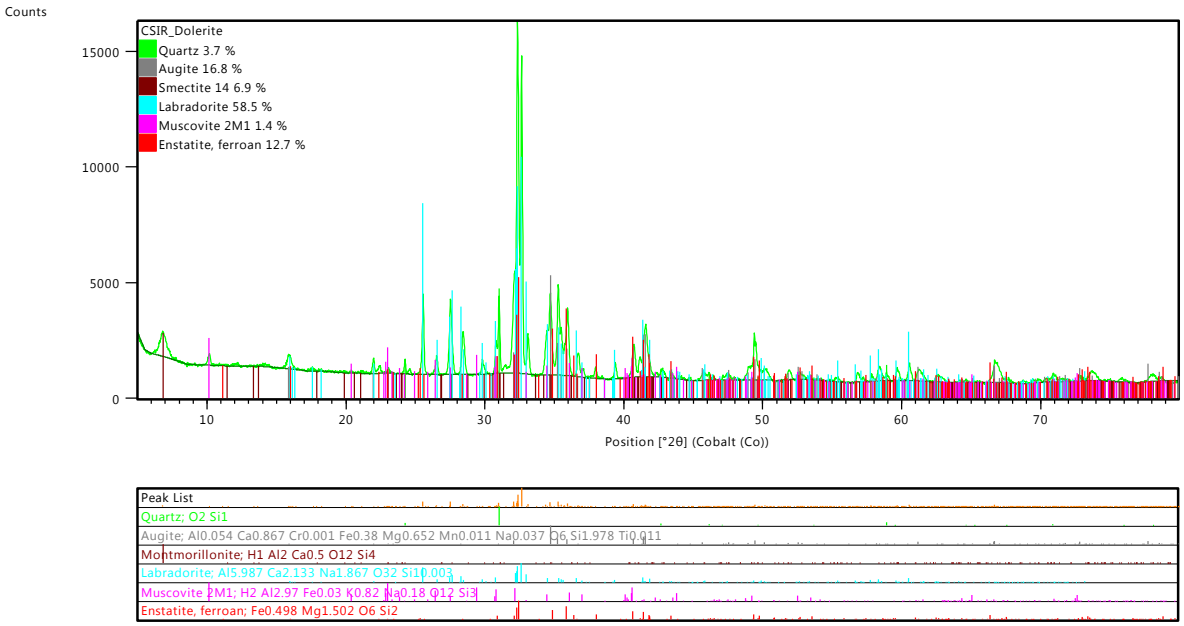

Figure A-7: XRD of dolerite aggregate

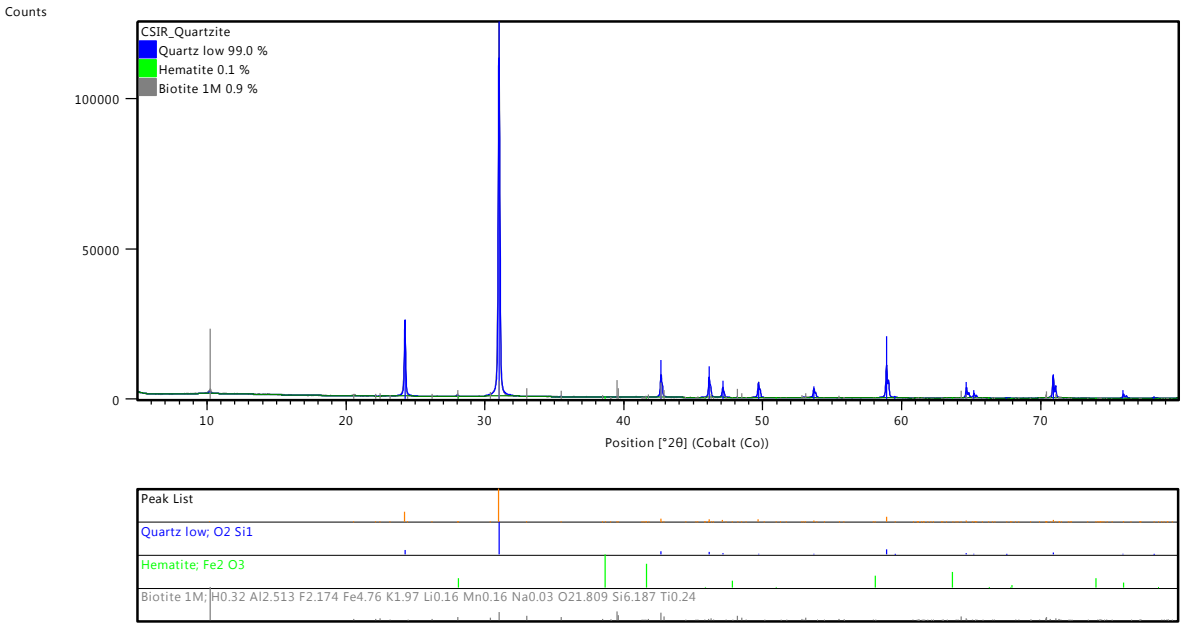

FigureA-8: XRD ferro-quartz aggregate

Appendix B: SEM images of geopolymers

B.1 GP HCP (Un-corroded specimens)

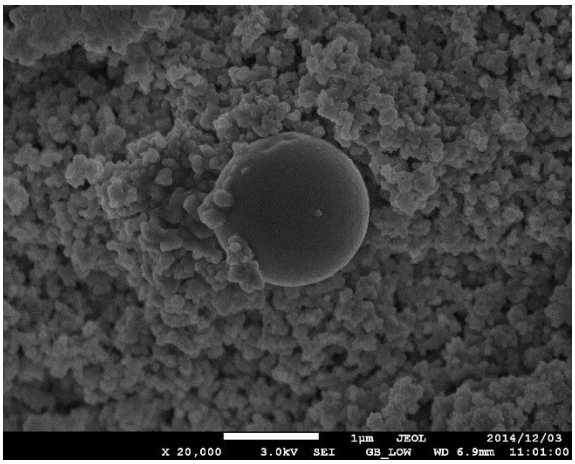

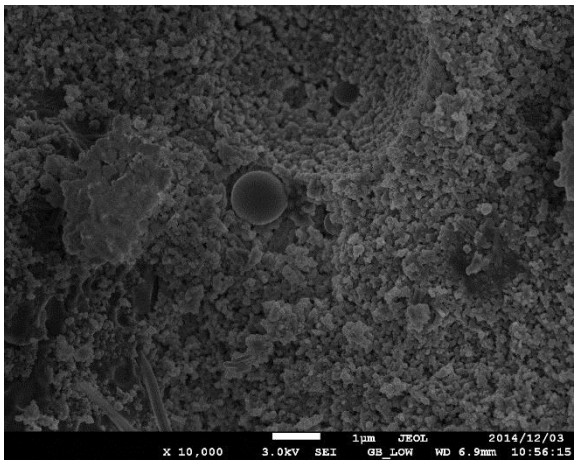

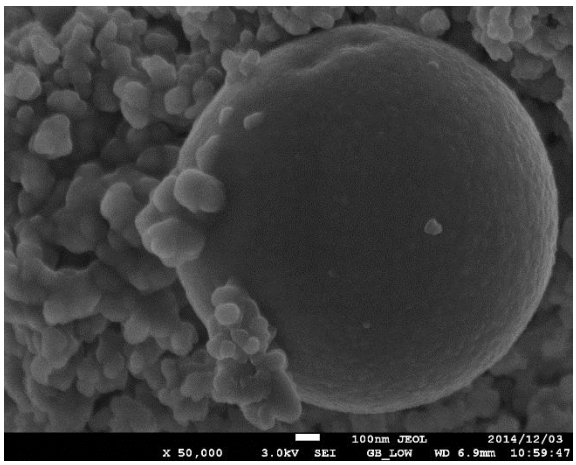

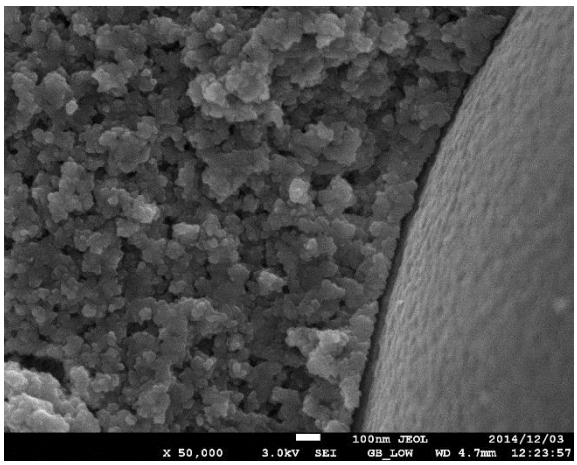

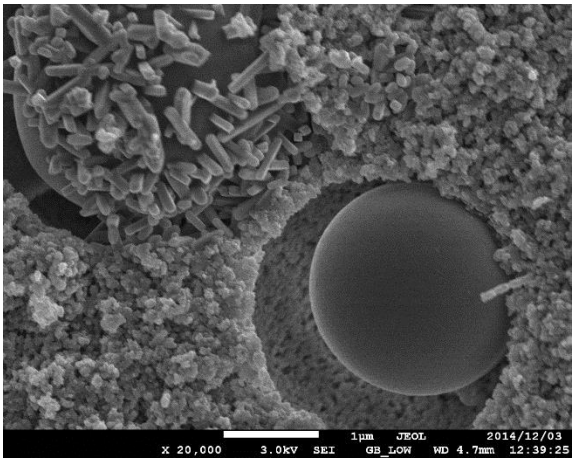

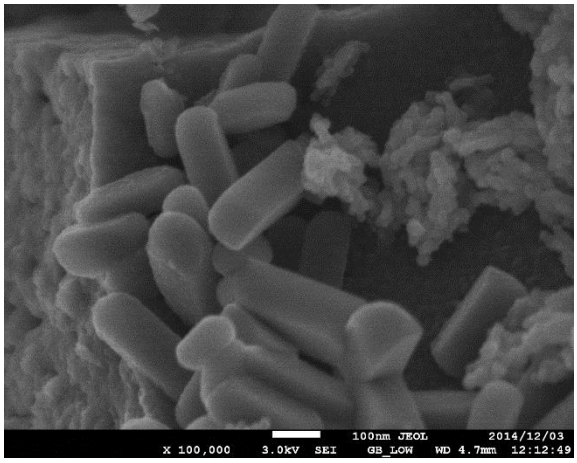

B.2. GP HCP after exposure to H_2SO_4

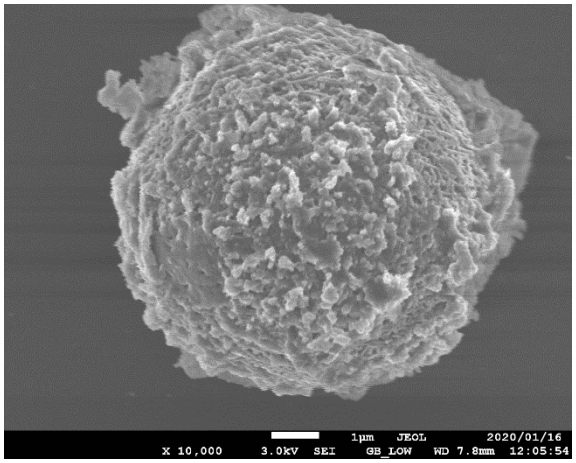

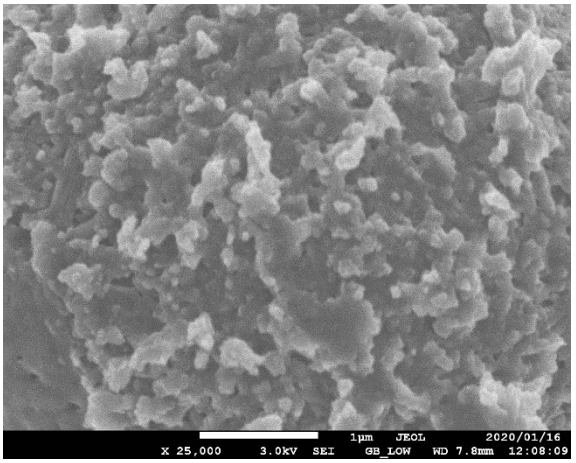

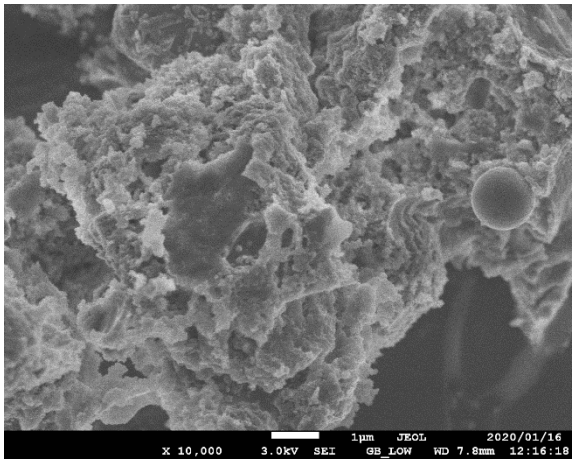

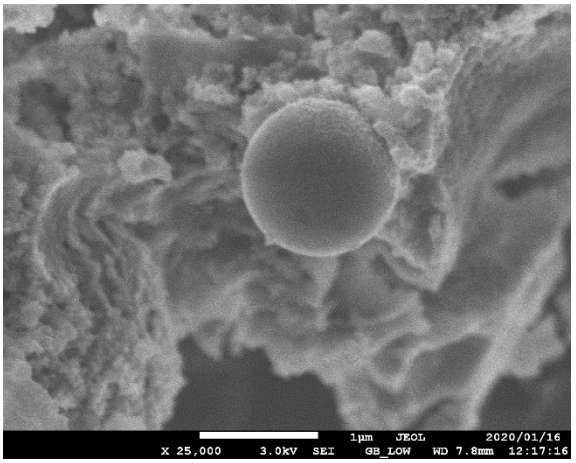

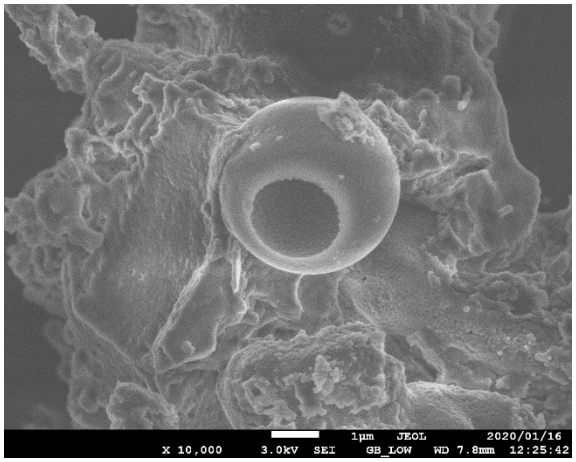

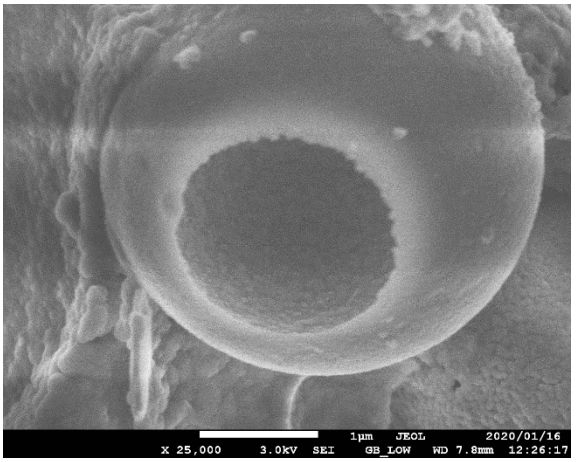

B.3 GP HCP after exposure to HCl

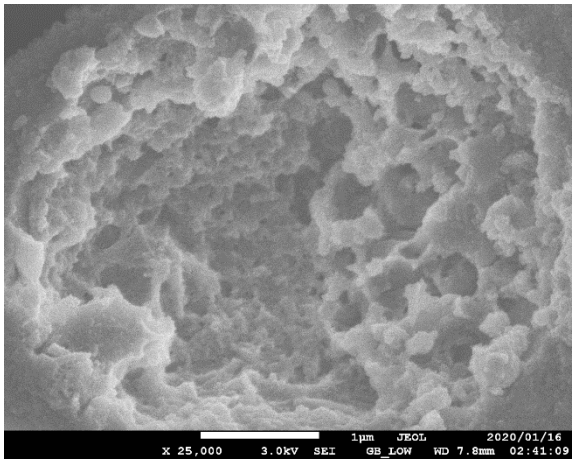

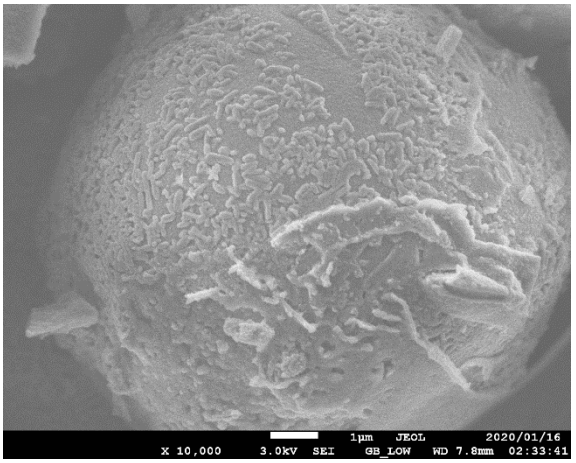

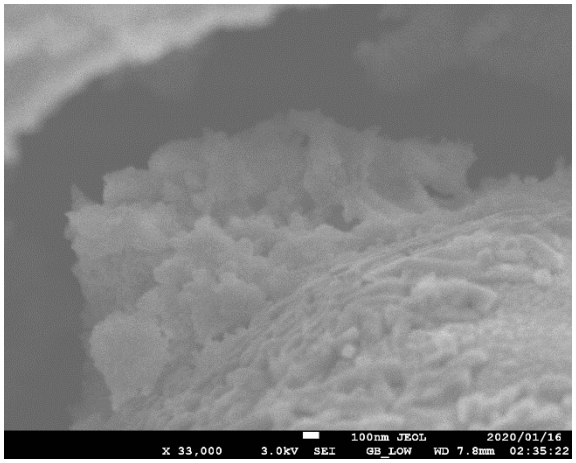

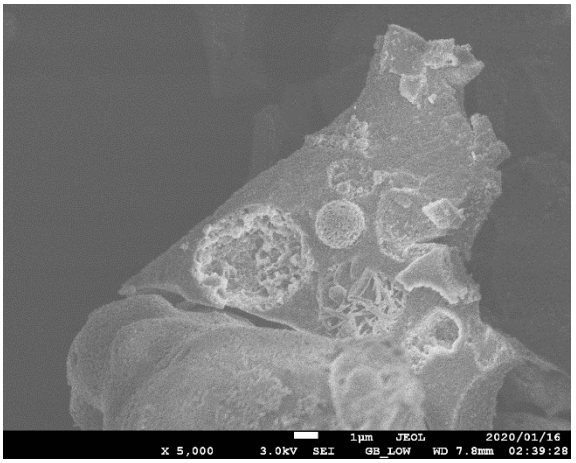

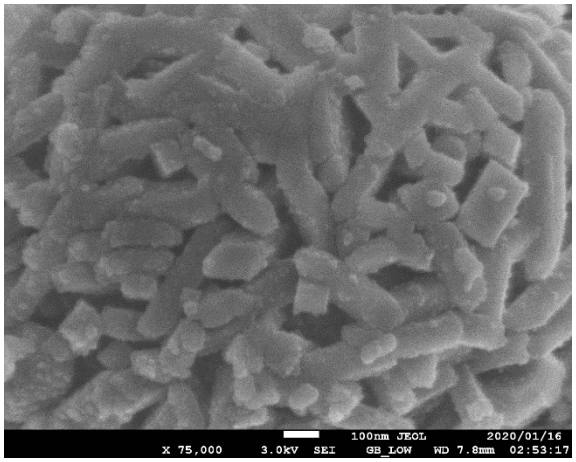

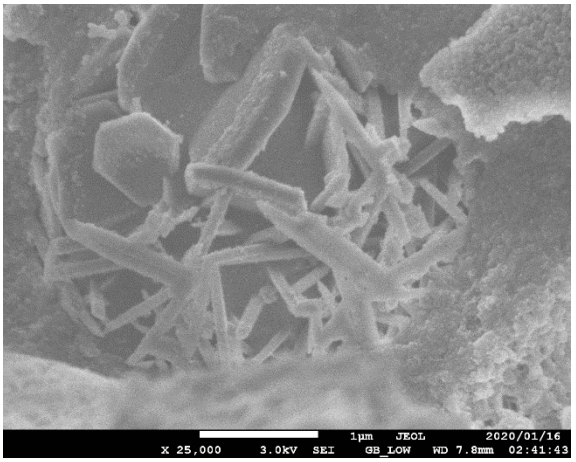

Appendix C: Aggregate grading data

C.1 Andesite aggregate

Fine aggregate (crusher sand)			
Sieve size (mm)	Mass retained (g)	Retaine (%)	Passing (%)
0.075	15	3%	6%
0.18	29	6%	9%
0.3	14	3%	15%
0.425	28	6%	18%
0.6	29	6%	23%
0.85	42	8%	29%
1.18	54	11%	38%
1.7	67	13%	48%
2.36	90	18%	62%
3.35	86	17%	80%
4.75	15	3%	97%
6.75	0	0%	100%

Coarse aggregate (stone)			
Sieve size (mm)	Mass retained (g)	Retained (%)	Passing (%)
4.75	66	13%	0%
6.75	360	72%	13%
9.5	74	15%	85%
13.2	0	0%	100%

Coarse + Fine aggregate grading	
Sieve size (mm)	Passing (%)
0.075	3%
0.18	4%
0.3	6%
0.425	8%
0.6	10%
0.85	13%
1.18	16%
1.7	21%
2.36	27%
3.35	34%
4.75	42%
6.7	50%
9.5	92%
13.2	100%

Fineness modulus (FM)	4.99

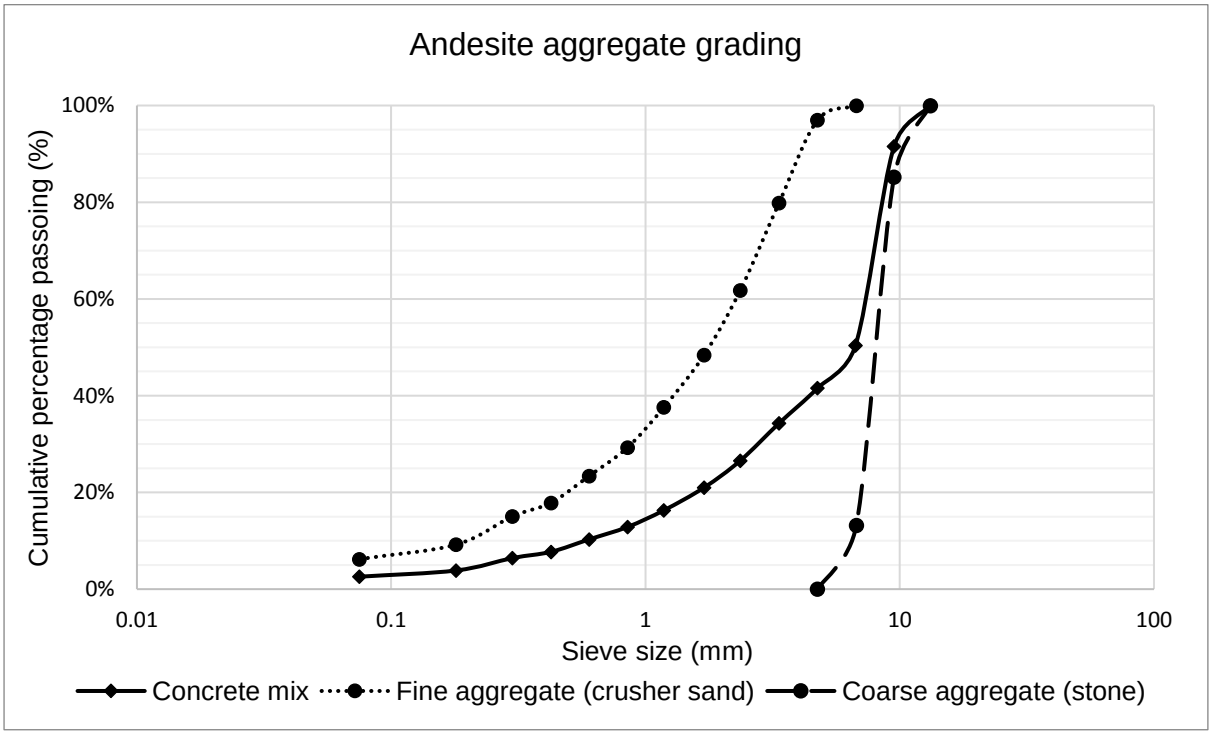

C.2 Granite aggregate

Fine aggregate (crusher sand)			
Sieve size (mm)	Mass retained (g)	Retaine (%)	Passing (%)
0.075	57	12%	3%
0.18	28	6%	15%
0.26	54	11%	21%
0.425	51	10%	32%
0.6	49	10%	42%
0.85	53	11%	52%
1.18	53	11%	62%
1.7	49	10%	73%
2.36	51	10%	83%
3.35	32	6%	93%
4.75	1	0%	100%
6.7	0	0%	100%

Coarse aggregate (stone)			
Sieve size (mm)	Mass retained (g)	Retained (%)	Passing (%)
4.75	66	13%	0%
6.75	368	74%	13%
9.5	55	11%	87%
13.2	11	2%	98%

Coarse + Fine aggregate grading	
Sieve size (mm)	Passing (%)
0.075	2%
0.18	7%
0.3	9%
0.425	14%
0.6	18%
0.85	22%
1.18	27%
1.7	32%
2.36	36%
3.35	40%
4.75	43%
6.7	51%
9.5	93%
13.2	99%

Fineness modulus (FM)	4.65

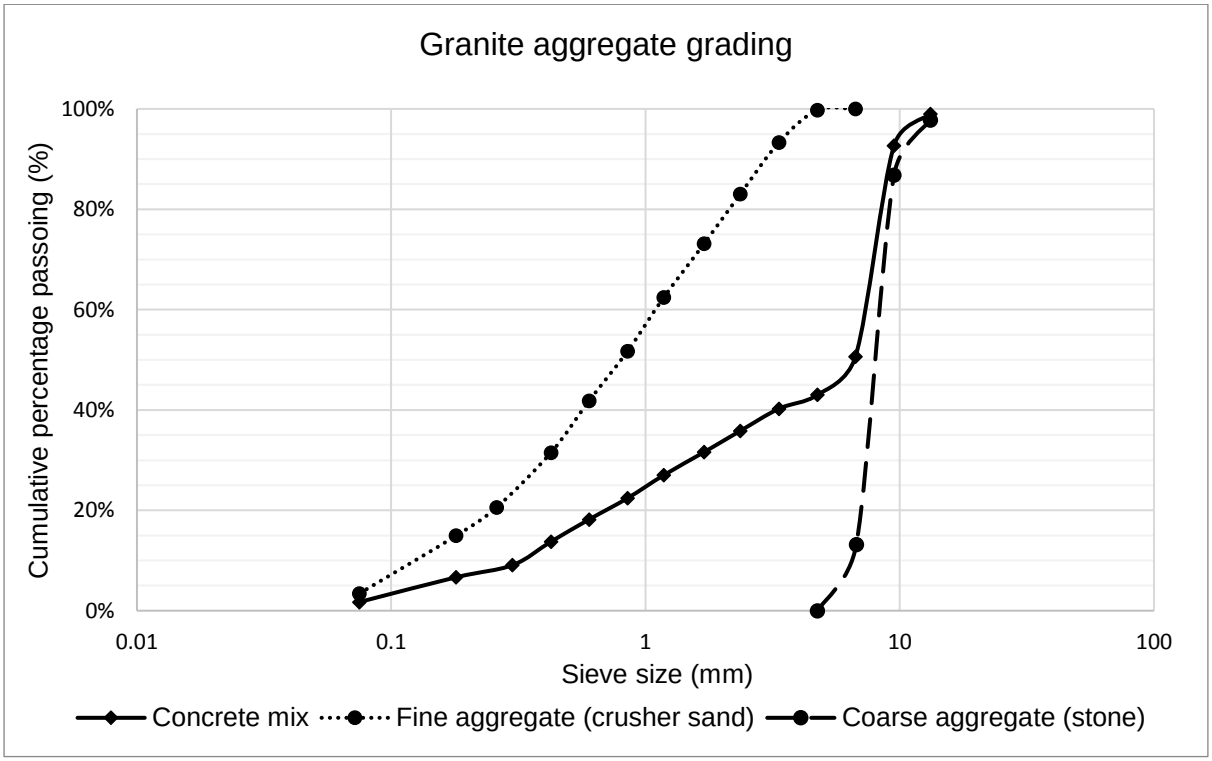

C.3 Ferro-quartz aggregate

Fine aggregate (crusher sand)			
Sieve size (mm)	Mass retained (g)	Retaine (%)	Passing (%)
0.075	55	11%	7%
0.18	22	4%	18%
0.26	38	8%	22%
0.425	26	5%	30%
0.6	33	7%	35%
0.85	40	8%	42%
1.18	51	10%	50%
1.7	53	11%	60%
2.36	64	13%	71%
3.35	58	12%	84%
4.75	19	4%	96%
6.7	0	0%	100%

Coarse aggregate (stone)			
Sieve size (mm)	Mass retained (g)	Retained (%)	Passing (%)
4.75	19	4%	0%
6.75	348	70%	4%
9.5	133	27%	73%
13.2	0	0%	100%

Coarse + Fine aggregate grading	
Sieve size (mm)	Passing (%)
0.075	3%
0.18	8%
0.3	10%
0.425	13%
0.6	15%
0.85	18%
1.18	21%
1.7	26%
2.36	31%
3.35	36%
4.75	41%
6.7	45%
9.5	85%
13.2	100%

Fineness modulus (FM)	4.79

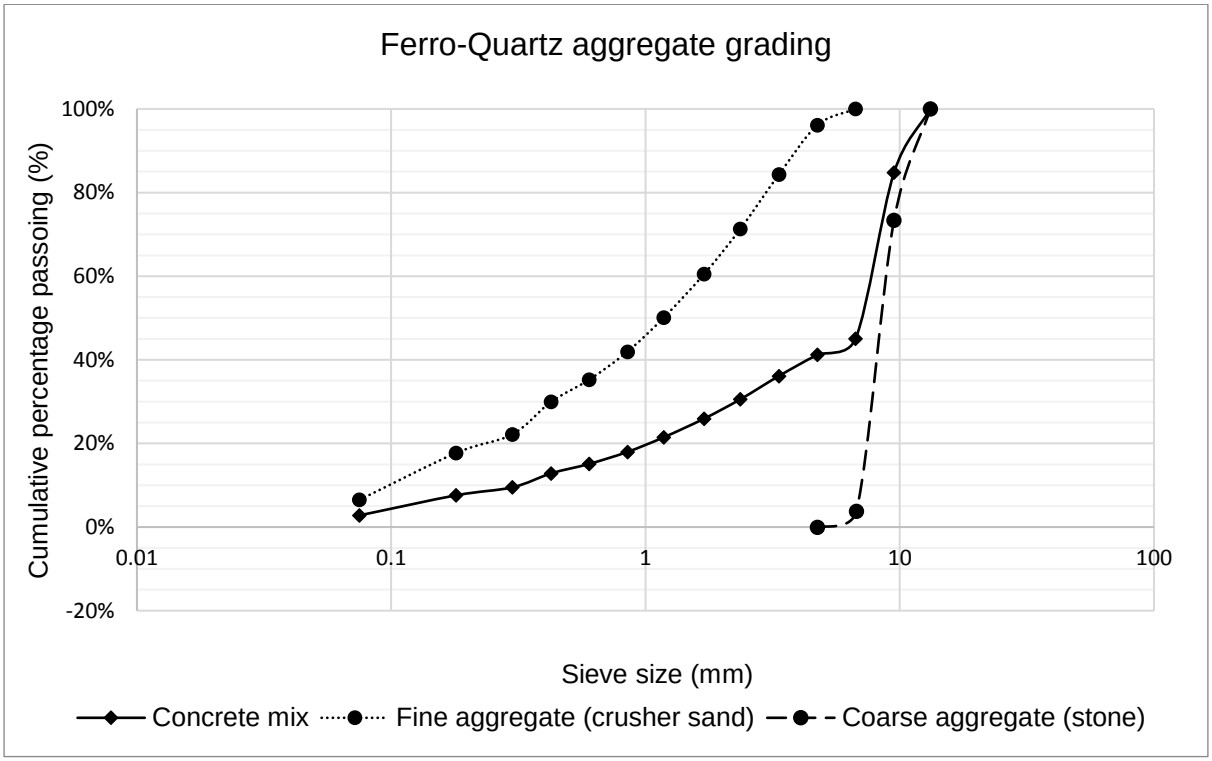

C.4 Dolomite aggregate

Fine aggregate (crusher sand)			
Sieve size (mm)	Mass retained (g)	Retaine (%)	Passing (%)
0.075	27	4%	10%
0.18	18	3%	14%
0.26	26	4%	16%
0.425	27	4%	20%
0.6	29	4%	24%
0.85	38	6%	28%
1.18	51	7%	34%
1.7	65	9%	41%
2.36	84	12%	51%
3.35	111	16%	63%
4.75	144	21%	79%
6.7	48	7%	100%

Coarse aggregate (stone)			
Sieve size (mm)	Mass retained (g)	Retained (%)	Passing (%)
4.75	19	4%	0%
6.75	348	70%	4%
9.5	133	27%	73%
13.2	0	0%	100%

Coarse + Fine aggregate grading	
Sieve size (mm)	Passing (%)
0.075	1%
0.18	3%
0.3	4%
0.425	6%
0.6	7%
0.85	9%
1.18	11%
1.7	15%
2.36	19%
3.35	24%
4.75	31%
6.7	42%
9.5	85%
13.2	100%

Fineness modulus (FM)	5.27

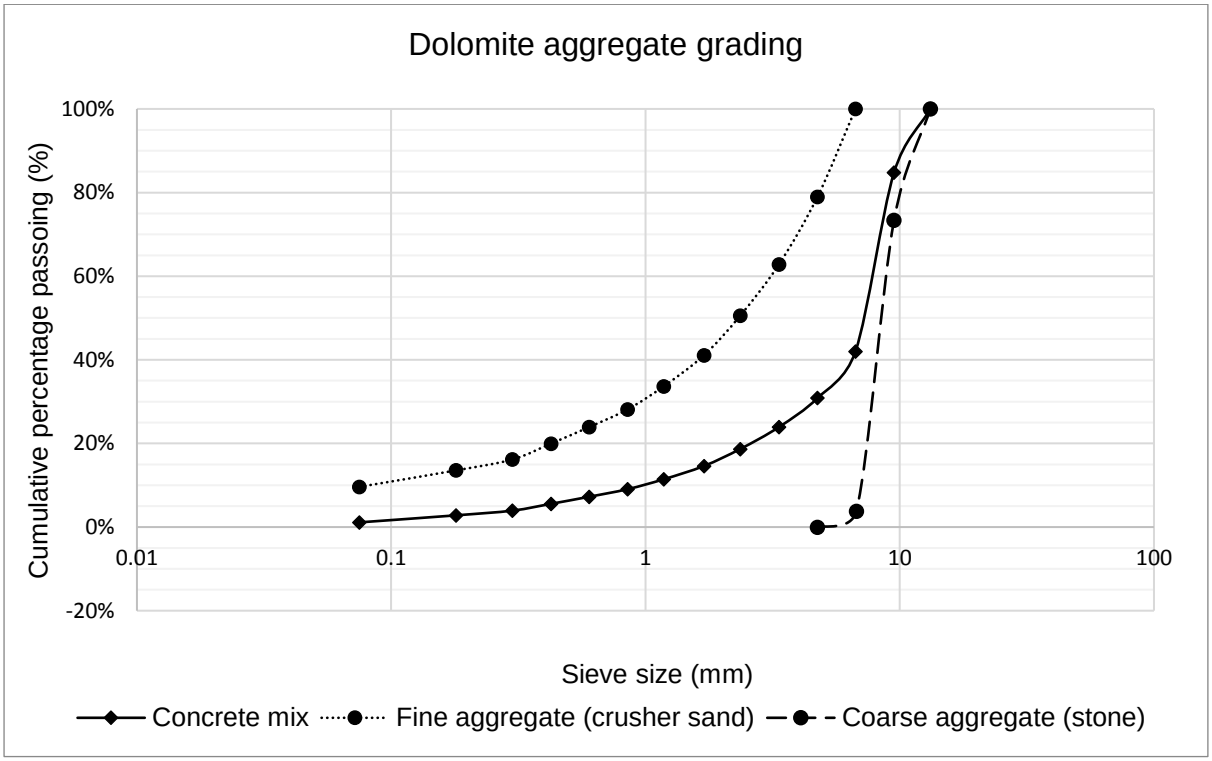

C.5 Dolerite aggregate

Fine aggregate (crusher sand)			
Sieve size (mm)	Mass retained (g)	Retaine (%)	Passing (%)
0.075	105	8%	1%
0.18	57	4%	9%
0.26	84	6%	14%
0.425	73	5%	20%
0.6	104	8%	25%
0.85	116	9%	33%
1.18	160	12%	42%
1.7	203	15%	53%
2.36	235	17%	69%
3.35	169	13%	86%
4.75	18	1%	99%
6.7	0	0%	100%

Coarse aggregate (stone)			
Sieve size (mm)	Mass retained (g)	Retained (%)	Passing (%)
4.75	35	7%	0%
6.75	370	74%	7%
9.5	95	19%	81%
13.2	0	0%	100%

Coarse + Fine aggregate grading	
Sieve size (mm)	Passing (%)
0.075	1%
0.18	4%
0.3	6%
0.425	8%
0.6	11%
0.85	14%
1.18	18%
1.7	23%
2.36	29%
3.35	37%
4.75	42%
6.7	47%
9.5	89%
13.2	100%

Fineness modulus (FM)	4.95

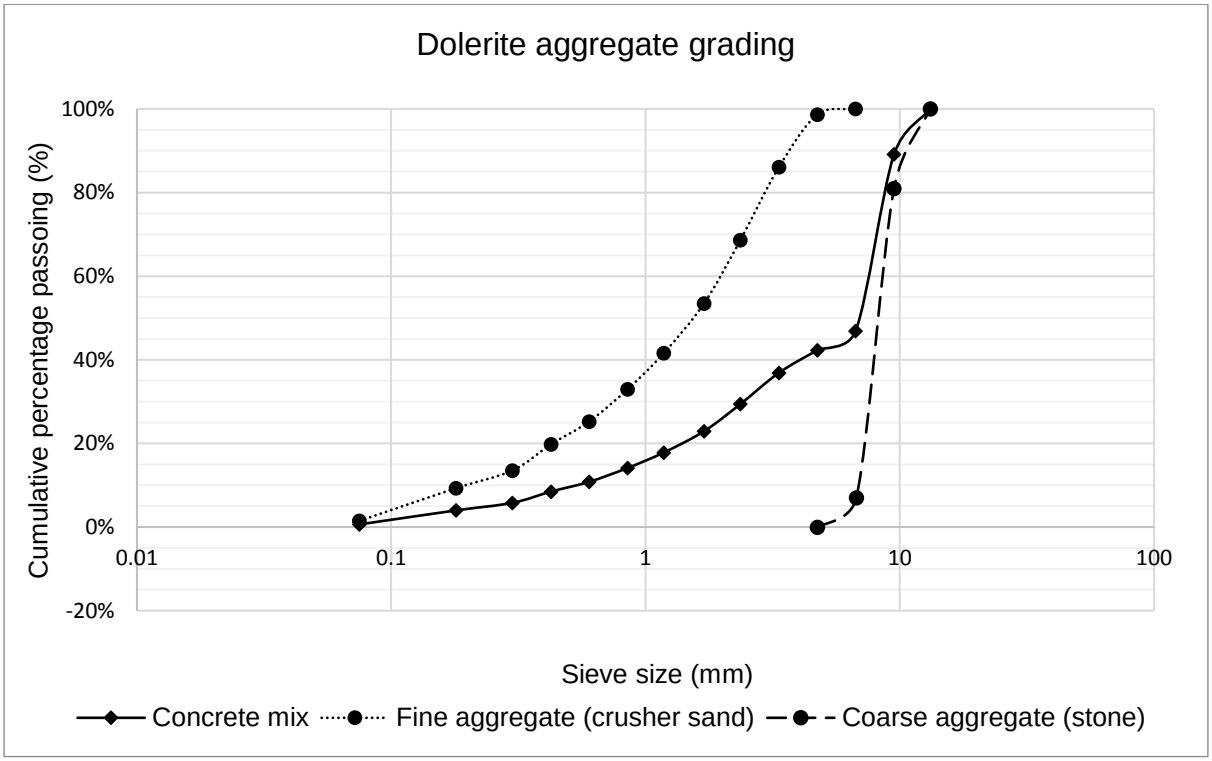

Appendix D: Acid testing data

D.1 Dynamic HCl test data

Dolomite aggregate concretes-Dynamic HCl acid test			
	CAC-dolomite	PC-dolomite	GP-dolomite
Time (Hours)	Mass (g)		
0	1574	1490	1381
2	1558	1474	1365
4	1518	1438	1349
6	1471	1401	1336
8	1425	1362	1314
10	1377	1332	1294
12	1335	1309	1278
15	1275	1270	1254
17	1238	1252	1232
19	1200	1225	1221
21	1152	1204	1209
23	1108	1184	1193
25	1058	1150	1170

Dolomite aggregate concretes-Dynamic HCl acid test			
	CAC-dolomite	PC-dolomite	GP-dolomite
Time (Hours)	% of original mass		
0	100.0%	100.0%	100.0%
2	99.0%	98.9%	98.8%
4	96.4%	96.5%	97.7%
6	93.5%	94.0%	96.7%
8	90.5%	91.4%	95.1%
10	87.5%	89.4%	93.7%
12	84.8%	87.9%	92.5%
15	81.0%	85.2%	90.8%
17	78.7%	84.0%	89.2%
19	76.2%	82.2%	88.4%
21	73.2%	80.8%	87.5%
23	70.4%	79.5%	86.4%
25	67.2%	77.2%	84.7%

GP-Siliceous aggregate concretes-Dynamic hydrochloric acid test (mass vs time)

GP-ferro-quartz		GP-andesite		GP-granite		GP-Dolerite	
t (hours)	Mass (g)	t (hours)	Mass (g)	t (hours)	Mass (g)	t (hours)	Mass (g)
0	1432	0	1549	0	1411	0	1571
2	1431	2	1548	18	1408	18	1536
4	1431	4	1548	20	1407	20	1533
6	1431	18	1545	23	1407	23	1531
8	1431	21	1545	24	1407	24	1529
18	1431	24	1544				
20.5	1430	42	1541				
22	1430	47	1540				
24	1429	48	1540				
26	1429						
42	1429						
45	1428						
48	1428						

GP-Siliceous aggregate concretes-Dynamic hydrochloric acid test (% of original mass vs time)

GP-ferro-quartz		GP-andesite		GP-granite		GP-Dolerite	
t (hours)	Mass (g)	t (hours)	Mass (g)	t (hours)	Mass (g)	t (hours)	Mass (g)
0	100.00%	0	100.00%	0	100.00%	0	100.00%
2	99.93%	2	99.94%	18	99.79%	18	97.77%
4	99.93%	4	99.94%	20	99.72%	20	97.58%
6	99.93%	18	99.74%	23	99.72%	23	97.45%
8	99.93%	21	99.74%	24	99.72%	24	97.33%
18	99.93%	24	99.68%				
20.5	99.86%	42	99.48%				
22	99.86%	47	99.42%				
24	99.79%	48	99.42%				
26	99.79%						
42	99.79%						
45	99.72%						
48	99.72%						

D.2 Static HCl test data

CAC-dolomite						
Specimen mass (g) data						
Time (hrs)	Sample 1	Sample 2	Sample 3	Mean value	Std. Dev	% of mass
0	279	283	283	281.7	2.3	100%
19	292	294	295	293.7	1.5	104%
40	290	293	291	291.3	1.5	103%
46.5	290	291	290	290.3	0.6	103%
68	288	290	290	289.3	1.2	103%
113	286	288	286	286.7	1.2	102%
136	285	286	285	285.3	0.6	101%
164	283	285	283	283.7	1.2	101%
189	282	284	282	282.7	1.2	100%
215.5	280	282	278	280.0	2.0	99%
261	278	281	278	279.0	1.7	99%
284.5	278	280	277	278.3	1.5	99%
328	277	276	273	275.3	2.1	98%
424	275	273	270	272.7	2.5	97%
448	272	272	269	271.0	1.7	96%
496	270	270	262	267.3	4.6	95%
544	267	266	262	265.0	2.6	94%
602	267	264	263	264.7	2.1	94%
674	265	262	262	263.0	1.7	93%
794	264	261	260	261.7	2.1	93%
818	263	258	258	259.7	2.9	92%

PC-dolomite						
Specimen mass (g) data						
Time (hrs)	Sample 1	Sample 2	Sample 3	Mean value	Std. Dev	% of mass
0	316	325	328	323.0	6.2	100%
19	312	322	326	320.0	7.2	99%
40	302	312	315	309.7	6.8	96%
46.5	298	308	307	304.3	5.5	94%
68	282	290	290	287.3	4.6	89%
113	254	259	252	255.0	3.6	79%
136	227	236	236	233.0	5.2	72%
164	191	202	201	198.0	6.1	61%
189	182	185	187	184.7	2.5	57%
215.5	173	173	173	173.0	0.0	54%
261	164	169	170	167.7	3.2	52%
284.5	139	169	170	159.3	17.6	49%
328	113	103	94	103.3	9.5	32%
424	64	73	63	66.7	5.5	21%
448	52	53	57	54.0	2.6	17%
496	25	34	32	30.3	4.7	9%
544	3	10	10	7.7	4.0	2%
602	0	0	0	0.0	0.0	0%
674	0	0	0	0.0	0.0	0%
794	0	0	0	0.0	0.0	0%
818	0	0	0	0.0	0.0	0%

GP Dolomite

Specimen mass (g) data

Time (hrs)	Sample 1	Sample 2	Sample 3	Mean value	Std. dev	% of mass
0	305	296	286	295.7	9.50	100%
19	311	303	291	301.7	10.07	102%
40	305	296	291	297.3	7.09	101%
46.5	301	292	277	290.0	12.12	98%
68	295	286	271	284.0	12.12	96%
113	290	281	264	278.3	13.20	94%
136	285	276	259	273.3	13.20	92%
164	281	272	256	269.7	12.66	91%
189	289	271	253	271.0	18.00	92%
215.5	277	268	250	265.0	13.75	90%
261	276	267	250	264.3	13.20	89%
284.5	273	265	247	261.7	13.32	89%
328	268	260	243	257.0	12.77	87%
424	265	257	240	254.0	12.77	86%
448	262	254	237	251.0	12.77	85%
496	258	251	234	247.7	12.34	84%
544	252	238	232	240.7	10.26	81%
602	248	238	225	237.0	11.53	80%
674	243	238	222	234.3	10.97	79%
794	243	238	221	234.0	11.53	79%
818	240	238	220	232.7	11.02	79%
			Slope	-0.0930497	0	

GP-ferro-quartz

Specimen mass (g) data

Time (hrs)	Sample 1	Sample 2	Sample 3	Mean value	Std. Dev	% of mass
0	285	278	288	283.7	5.1	100%
19	285	281	292	286.0	5.6	101%
40	285	282	292	286.3	5.1	101%
46.5	284	281	290	285.0	4.6	100%
68	283	280	289	284.0	4.6	100%
113	283	279	289	283.7	5.0	100%
136	283	280	289	284.0	4.6	100%
164	283	279	290	284.0	5.6	100%
189	282	278	288	282.7	5.0	100%
215.5	282	278	288	282.7	5.0	100%
261	282	278	288	282.7	5.0	100%
284.5	281	278	287	282.0	4.6	99%
328	281	277	287	281.7	5.0	99%
424	281	277	287	281.7	5.0	99%
448	280	277	286	281.0	4.6	99%
496	279	276	286	280.3	5.1	99%
544	279	276	286	280.3	5.1	99%
602	278	274	285	279.0	5.6	98%
674	278	274	285	279.0	5.6	98%
794	278	274	285	279.0	5.6	98%
818	278	274	285	279.0	5.6	98%

GP-granite

Specimen mass (g) data

Time (hrs)	Sample 1	Sample 2	Sample 3	Mean value	Std. Dev	% of mass
0	318	308	326	317.3	9.0	100%
19	320	309	331	320.0	11.0	101%
40	322	311	330	321.0	9.5	101%
46.5	320	309	328	319.0	9.5	101%
68	319	308	328	318.3	10.0	100%
113	318	308	324	316.7	8.1	100%
136	318	307	327	317.3	10.0	100%
164	317	307	326	316.7	9.5	100%
189	317	307	327	317.0	10.0	100%
215.5	317	306	325	316.0	9.5	100%
261	317	307	325	316.3	9.0	100%
284.5	317	306	325	316.0	9.5	100%
328	316	306	324	315.3	9.0	99%
424	316	306	324	315.3	9.0	99%
448	315	305	323	314.3	9.0	99%
496	315	304	322	313.7	9.1	99%
544	315	304	322	313.7	9.1	99%
602	313	303	322	312.7	9.5	99%
674	313	303	322	312.7	9.5	99%
794	313	303	322	312.7	9.5	99%
818	313	303	322	312.7	9.5	99%

GP-dolerite

Specimen mass (g) data

Time (hrs)	Sample 1	Sample 2	Sample 3	Mean value	Std. dev	% of mass
0	262	263	264	263.0	1.00	100%
19	264	263	263	263.3	0.58	100%
40	264	262	262	262.7	1.15	100%
46.5	261	260	259	260.0	1.00	99%
68	260	259	258	259.0	1.00	98%
113	259	258	257	258.0	1.00	98%
136	258	257	256	257.0	1.00	98%
164	256	255	256	255.7	0.58	97%
189	256	255	255	255.3	0.58	97%
215.5	256	255	255	255.3	0.58	97%
261	256	255	254	255.0	1.00	97%
284.5	254	254	254	254.0	0.00	97%
328	253	252	253	252.7	0.58	96%
424	253	252	252	252.3	0.58	96%
448	252	251	251	251.3	0.58	96%
496	252	251	250	251.0	1.00	95%
544	251	250	250	250.3	0.58	95%
602	247	247	247	247.0	0.00	94%
674	247	247	247	247.0	0.00	94%
794	247	247	247	247.0	0.00	94%
818	245	246	246	245.7	0.58	93%

GP-andesite						
Specimen mass (g) data						
Time (hrs)	Sample 1	Sample 2	Sample 3	Mean value	Std. dev	% of mass
0	293	289	284	288.67	4.51	100.0%
19	293	292	283	289.33	5.51	100.2%
40	294	295	282	290.33	7.23	100.6%
46.5	292	293	281	288.67	6.66	100.0%
68	291	292	281	288.00	6.08	99.8%
113	291	291	282	288.00	5.20	99.8%
136	292	291	281	288.00	6.08	99.8%
164	290	291	281	287.33	5.51	99.5%
189	290	291	280	287.00	6.08	99.4%
215.5	290	290	280	286.67	5.77	99.3%
261	290	290	279	286.33	6.35	99.2%
284.5	289	289	279	285.67	5.77	99.0%
328	288	289	278	285.00	6.08	98.7%
424	288	289	278	285.00	6.08	98.7%
448	288	288	278	284.67	5.77	98.6%
496	288	287	276	283.67	6.66	98.3%
544	285	287	276	282.67	5.86	97.9%
602	283	282	274	279.67	4.93	96.9%
674	283	282	274	279.67	4.93	96.9%
794	283	282	274	279.67	4.93	96.9%
818	283	282	273	279.33	5.51	96.8%

Appendix E: Compressive strengths of specimens

4 hour unconfined compressive strengths of 100mm cubes

Concrete mix	Mean strength (MPa)	Specimen number			St.dev
		1	2	3	
GP-dolomite	24.40	21.42	22.03	29.76	4.65
GP-andesite	21.40	20.94	23.82	19.44	2.23
GP-ferro quartz	25.00	24.33	23.32	27.35	2.10
GP-dolerite	18.80	20.94	18.71	16.75	2.10
GP-granite	19.40	17.81	22.01	18.38	2.28
PC-dolomite	25.00	27.91	28.44	18.66	5.50
CAC-dolomite	40.10	38.13	36.33	45.84	5.05

28 day unconfined compressive strengths of 100mm cubes

Concrete mix	Mean strength (MPa)	Specimen number			St.dev
		1	2	3	
GP-dolomite	56.50	54.72	54.13	60.65	3.61
GP-andesite	71.20	69.22	67.72	76.66	4.79
GP-ferro quartz	66.20	66.42	70.52	61.66	4.43
GP-dolerite	62.00	64.30	66.03	55.67	5.55
GP-granite	58.30	56.82	53.41	64.67	5.77
PC-dolomite	72.10	74.44	65.91	75.96	5.42
CAC-dolomite	87.30	87.22	90.30	84.38	2.96

Appendix F: Basicity value computation

Basicity values of hardened cement pastes				
HCP type	CaO (%)	MgO (%)	SiO2 (%)	Basicity
PC	53.7%	2.01%	17.77%	3.138
CAC	32.9%	2.40%	4.06%	8.686
GP	11.6%	0.53%	44.06%	0.276

Basicity values of aggregates				
Aggregate type	CaO (%)	MgO (%)	SiO2 (%)	Basicity
Dolomite	23%	16%	25%	1.565
Ferro-Quartz	2%	0%	96%	0.026
Dolerite	11%	6%	52%	0.321
Andesite	8%	4%	55%	0.222
Granite	2%	1%	72%	0.029

Static and dynamic HCl corrosion rates vs concrete CaO (%) conctent and Concrete basicity				
	Dynamic corrosion rate (HCl)	Static surface corrosion rate (HCl)	Concrete CaO%	Concrete Basicity
OPC-Dolomite	34.98	3.369	30%	1.93
CAC-Dolomite	49.55	0.160	25%	3.20
GP-Dolomite	20.96	0.543	21%	1.32
GP-Ferroquartz	0.23	0.056	5%	0.08
GP-Andesite	0.49	0.085	10%	0.27
GP-Dolerite	4.51	0.135	13%	0.37
GP-Granite	0.45	0.059	4%	0.08